

Mapping plant communities and understanding the landscape structure of  
coastal barrens using an unmanned aerial vehicle

by

Michael Buckland-Nicks

A Thesis Submitted to Saint Mary's University, Halifax, Nova Scotia,  
in Partial Fulfillment of the Requirements for the  
Degree of Master of Science in Applied Science

April 20<sup>th</sup>, 2018, Halifax, Nova Scotia

Copyright Michael Buckland-Nicks, 2018

Approved: Dr. Jeremy Lundholm  
Supervisor  
Department of Biology

Approved: Dr. Danika Van Proosdij  
External Examiner  
Department of Geography  
Saint Mary's University

Approved: Dr. Karen Harper  
Supervisory Committee Member  
Department of Biology

Approved: Dr. Jeff Barrell  
Supervisory Committee Member  
Department of Fisheries and Oceans,  
Government of Canada

Approved: Dr. Sam Veres  
Chair of Thesis Defence  
Faculty of Graduate Studies and  
Research

Date: April 20<sup>th</sup>, 2018

# Mapping plant communities and understanding the landscape structure of coastal barrens using an unmanned aerial vehicle

by Michael A. Buckland-Nicks

## Abstract

Coastal barrens are landscape mosaics - patchworks of plant communities that exist in harsh environmental conditions created by land-sea interactions and shallow soils. Many rare and uncommon species inhabit these ecosystems, making them a high priority for conservation. In Nova Scotia, coastal barrens are abundant along the coastline of the Halifax region. Little is known of the spatial distributions of plant communities that inhabit them and their overall landscape structure. The purpose of this study was to investigate the use of a UAV to map plant communities and to quantify the landscape structure of coastal barrens. First, high-resolution multispectral UAV imagery was evaluated to discriminate plant communities from three classification levels across three coastal barrens sites in Halifax, Nova Scotia: Chebucto Head, Prospect Bay, and Polly's Cove. All plant communities were discriminated with 95% confidence except for one pair, showing that plant communities in the coastal barrens could be discriminated with a high level of confidence using UAV imagery. Next, UAV imagery was classified to produce detailed maps of plant communities for the three coastal barrens landscapes. Environmental factors, such as elevation, stream networks and wind exposure were also mapped to help understand landscape structure. Sites were dominated by shrublands and dwarf heath; however, many other types of communities co-occurred on these landscapes, including bogs, salt marshes, and tree islands. The most common plant community across the three sites was *Gaylussacia baccata* shrubland. Plant community patches varied in

size, shape, abundance, and spatial distribution from one plant community type to another and in many cases from one site to another. Landscape patterns were driven by various combinations of environmental factors, including slope position, proximity to stream networks, elevation, and distance to coastline. Overall differences in landscape structure could be mostly explained by the degree of topographic heterogeneity of each landscape. UAVs are an excellent tool for mapping plant communities and quantifying landscape structure and this information is critical for informing land managers, conservation planners, and policy makers.

## **Acknowledgements**

First, I would like to thank my supervisor Dr. Jeremy Lundholm. Jeremy has been an incredible mentor for me and was so supportive of my interests in geographic information systems. Thank you also to my supervisory committee Dr. Karen Harper and Dr. Jeff Barrell for offering their time in giving valuable feedback and helping steer me towards the finish line. I am also very grateful for the assistance I received from my fellow graduate students, lab mates, and field assistants who have helped me to collect my field data, assisted me with flying the drone, and offered their amazing advice, knowledge, and expertise: Hughstin Grimshaw-Surette, Maddie Clarke, Amy Heim, Emily Walker, Logan Gray, Jasmine Jamieson, and Graeme Matheson. I would like to thank Greg Baker for always making the time to share his infinite wisdom on geographic information systems and advice on flying the drone. I would also like to acknowledge my uncle, Trevor Hart, for offering his time and help for the statistical analysis of this project. I am indebted to Caitlin Porter for all her time and help with classifying plant communities and helping me to plan this study. I express my gratitude to the teams at MPSPARC and CBWES for sharing knowledge and collaborating on using drones as research tools. Lastly, I am eternally grateful for my supportive friends and family who have kept me positive, motivated, and have offered advice and encouragement when I needed it.

# Table of Contents

Abstract .....	i
Acknowledgements .....	iii
Table of Contents .....	iv
List of Tables .....	v
List of Figures .....	viii
Chapter 1: Introduction .....	1
Chapter 2: Evaluating Multispectral Imagery from an Unmanned Aerial Vehicle for Discriminating Plant Communities in the Coastal Barrens of Halifax, Nova Scotia ..	26
Chapter 3: Landscape Patterns of Plant Communities in the Coastal Barrens of Halifax, Nova Scotia .....	85
Chapter 4: Synthesis .....	169
Appendix I .....	177
Appendix II .....	236

## List of Tables

### Chapter 2

**Table 2.1.** Acquisition results of RGB imagery at the study sites and root-mean-square error of the georeferenced models based on ground control points.

**Table 2.2.** Spectral indices derived by UAV imagery.

**Table 2.3.** Structural indices derived by analysis of 3D point clouds and subsequent 10 cm digital elevation models computed from structure from motion photogrammetric processing of UAV imagery.

**Table 2.4.** The number of field plots of types I, II and III sampled at Chebucto Head, Prospect Bay, and Polly's Cove.

**Table 2.5.** The top 10 most frequent plant species identified from field plot sampling across all sites.

**Table 2.6.** List of classes from the association level plant community classification from field plot sampling across all three sites. Plant communities with less than three field plots were removed and not used for statistical analysis.

**Table 2.7.** List of classes from the formation class plant community classification from field plot sampling across all three sites. Plant communities with less than three field plots were removed and not used for statistical analysis.

**Table 2.8.** Top 10 indices sorted by their "score" of importance in relation to their contribution to the linear discriminant analysis (LDA) model for each plant community classification. The score was determined by summing the weighted contributions of each index for each discriminatory axis from the LDA model.

### Chapter 3

**Table 3.1.** Landscape-level metrics used to describe landscape composition.

**Table 3.2.** Class-level metrics used to describe the spatial configurations of plant community patches within a landscape.

**Table 3.3.** Environmental factors computed for plant community patches.

**Table 3.4.** Classification accuracies of mapped plant communities from the broadened association level classification at Chebucto Head.

**Table 3.5.** Summary of the spatial configurations of plant community patches at Chebucto Head. \*AW = Area-weighted.

**Table 3.6.** The top three most common neighbors of each plant community type at Chebucto Head.

**Table 3.7.** Environmental factors for plant communities at Chebucto Head. \*AW = Area-weighted; C.I = Area-weighted 95% confidence interval.

**Table 3.8.** Classification accuracies of mapped plant communities from the broadened association level classification at Prospect Bay.

**Table 3.9.** Summary of the spatial configurations of plant community patches at Prospect Bay. \*AW = Area-weighted.

**Table 3.10.** The top three most common neighbors of each plant community type at Prospect Bay.

**Table 3.11.** Environmental factors for plant communities at Prospect Bay. \*AW = Area-weighted; C.I = Area-weighted 95% confidence interval.

**Table 3.12.** Classification accuracies of mapped plant communities from the broadened association level classification at Polly's Cove.

**Table 3.13.** Summary of the spatial configurations of plant community patches at Polly's Cove. \*AW = Area-weighted.

**Table 3.14.** The top three most common neighbors of each plant community type at Polly's Cove.

**Table 3.15.** Environmental factors for plant communities at Polly's Cove. \*AW = Area-weighted; C.I = Area-weighted 95% confidence interval.

## **Appendix I**

**Table A1.1.** Specifications of the unmanned aerial vehicle used in this study.

**Table A1.2.** Flight times and conditions for UAV surveys from May to August in 2016.

**Table A1.3.** Full list of indices extracted from UAV imagery and the 3D point cloud.

**Table A1.4.** Final list of indices after redundant and multicollinear indices were identified and removed using variance inflation factor (VIF) analysis.

**Table A1.5.** List of plant species identified and their frequencies from field plot sampling.

**Table A1.6.** Full list of classes from the association level plant community classification across all three sites from field plot sampling.

**Table A1.7.** Plant community groupings for the association level classification, broadened association level classification, and formation class classification.

**Table A1.8.** Full list of indices sorted by their “score” of importance in relation to their contribution to the linear discriminant analysis (LDA) model for each plant community classification. The score was determined by summing the weighted contributions of each index for each discriminatory axis from the LDA model.

**Table A1.9.** Classification accuracies of the linear discriminant analysis (LDA) model for the association level plant community classification.

**Table A1.10.** Classification accuracies of the linear discriminant analysis (LDA) model for the broadened association level plant community classification.

**Table A1.11.** Classification accuracies of the linear discriminant analysis (LDA) model for the formation class plant community classification.

## **Appendix II**

**Table A2.1.** List of spectral and structural indices derived from UAV imagery and the 3D point cloud to classify plant communities.

**Table A2.2.** Confusion matrix of plant communities from the broadened association level classification at Chebucto Head.

**Table A2.3.** Confusion matrix of plant communities from the broadened association level classification at Prospect Bay.

**Table A2.4.** Confusion matrix of plant communities from the broadened association level classification at Polly’s Cove.



# List of Figures

## Chapter 2

**Figure 2.1.** Coastal barrens sites selected for this study: Chebucto Head, Prospect Bay, and Polly's Cove. All three sites are located in the Halifax region of Nova Scotia, Canada.

**Figure 2.2.** An RGB orthomosaic of the Chebucto Head study site in Halifax, Nova Scotia. Aerial imagery was captured from a UAV in May 2016 at 90 m altitude, providing 4 cm ground resolution.

**Figure 2.3.** An RGB orthomosaic of the Prospect Bay study site in Halifax, Nova Scotia. Aerial imagery was captured from a UAV in May 2016 at 90 m altitude, providing 4 cm ground resolution.

**Figure 2.4.** An RGB orthomosaic of the Polly's Cove study site in Halifax, Nova Scotia. Aerial imagery was captured from a UAV in May 2016 at 90 m altitude, providing 4 cm ground resolution.

**Figure 2.5.** Flowchart illustrating the methodology used to extract spectral and structural information from multispectral UAV imagery to discriminate plant communities identified from field plot sampling in the coastal barrens of Halifax, Nova Scotia.

**Figure 2.6.** DJI Phantom 3 Professional quadcopter used to collect high-resolution multispectral aerial imagery. The aircraft was equipped with a 12-megapixel RGB camera on a rotating gimbal and a fixed Sentera single Near-Infrared sensor.

**Figure 2.7.** A grid mission in the Pix4DCapture flight planning mobile application. Pix4DCapture was used to autonomously fly the unmanned aerial vehicle to collect sequential high-resolution multispectral aerial imagery of the three study sites.

**Figure 2.8.** An illustration of a tree at Polly's Cove as a 3D point cloud computed from structure from motion photogrammetry.

**Figure 2.9.** Plant communities from the formation class classification projected in the first three dimensions of the linear discriminant analysis model. Linear discriminant analysis projects variables into fewer dimensions while maximizing the separation of a class.

**Figure 2.10.** An example of the opposition surge in UAV imagery, also known as the hot-spot effect or opposition effect (A and B). A) was captured in May of 2016 at Prospect Bay and shows no opposition surge because the angle of insolation in the spring is relatively low; B) was captured in July of 2016 and shows the opposition surge manifested in the eastern part of the image as a bright hue. The optical phenomenon

occurs when the phase angle, the angle between the observer and the light source, approaches  $0^\circ$ .

### Chapter 3

**Figure 3.1.** Three coastal barrens landscapes selected as study sites in the Halifax region of Nova Scotia, Canada: Polly's Cove (A), Prospect Bay (B), and Chebucto Head (C).

**Figure 3.2.** Flowchart illustrating the image classification workflow used in this study to derive plant community maps from UAV imagery.

**Figure 3.3.** A) color imagery of the Polly's Cove study site and the barrier island near the site. B) A digital elevation model of the Polly's Cove study site and the barrier island near the site. It was hypothesized that the barrier island may shelter parts of the site and consequently influence the landscape patterns of the plant communities.

**Figure 3.4.** Mapped plant communities from the broadened association level classification at Chebucto Head, Nova Scotia.

**Figure 3.5.** Landscape composition of Chebucto Head: A) Coarse classification of plant communities; B) Stream networks; C) Vegetation cover; and D) Slope classification.

**Figure 3.6.** Mapped plant communities from the broadened association level classification at Prospect Bay, Nova Scotia.

**Figure 3.7.** Landscape composition of Prospect Bay: A) Coarse classification of plant communities; B) Stream networks; C) Vegetation cover; and D) Slope classification.

**Figure 3.8.** Mapped plant communities from the broadened association level classification at Polly's Cove, Nova Scotia.

**Figure 3.9.** Landscape composition of Polly's Cove: A) Coarse classification of plant communities; B) Stream networks; C) Vegetation cover; and D) Slope classification.

### Appendix I

**Figure A1.1.** 95% confidence intervals for the mean linear discriminant analysis (LDA) scores of plant communities from the association level classification for each discriminatory axis.

**Figure A1.2.** 95% confidence intervals for the mean linear discriminant analysis (LDA) scores of plant communities from the broadened association level classification for each discriminatory axis.

**Figure A1.3.** 95% confidence intervals for the mean linear discriminant analysis (LDA) scores of plant communities from the formation class classification for each discriminatory axis.

## **Appendix II**

**Figure A2.1.** Elevation above sea-level at A) Chebucto Head, B) Prospect Bay, and C) Polly's Cove.

**Figure A2.2.** Distance from the coastline at A) Chebucto Head, B) Prospect Bay, and C) Polly's Cove.

**Figure A2.3.** Wind exposure at A) Chebucto Head, B) Prospect Bay, and C) Polly's Cove.

**Figure A2.4.** Stream orders of stream networks at A) Chebucto Head, B) Prospect Bay, and C) Polly's Cove.

**Figure A2.5.** Incoming solar radiation at A) Chebucto Head, B) Prospect Bay, and C) Polly's Cove.

**Figure A2.6.** Slope positions at A) Chebucto Head, B) Prospect Bay, and C) Polly's Cove.

**Figure A2.7.** Local surface ruggedness at A) Chebucto Head, B) Prospect Bay, and C) Polly's Cove.

**Figure A2.8.** Global surface ruggedness at A) Chebucto Head, B) Prospect Bay, and C) Polly's Cove.

**Figure A2.9.** 95% confidence intervals for the area-weighted mean elevation of plant communities at Chebucto Head.

**Figure A2.10.** 95% confidence intervals for the area-weighted mean distance from the coastline for plant communities at Chebucto Head.

**Figure A2.11.** 95% confidence intervals for the area-weighted mean wind exposure of plant communities at Chebucto Head.

**Figure A2.12.** Most frequent (area-weighted) stream order for plant communities at Chebucto Head.

**Figure A2.13.** 95% confidence intervals for the area-weighted mean incoming solar radiation received by plant communities at Chebucto Head.

**Figure A2.14.** Most frequent (area-weighted) slope position classifications for plant communities at Chebucto Head.

**Figure A2.15.** 95% confidence intervals for the area-weighted mean local surface ruggedness of plant communities at Chebucto Head.

**Figure A2.16.** 95% confidence intervals for the area-weighted mean global surface ruggedness of plant communities at Chebucto Head.

**Figure A2.17.** 95% confidence intervals for the area-weighted mean elevation of plant communities at Prospect Bay.

**Figure A2.18.** 95% confidence intervals for the area-weighted mean distance from the coastline for plant communities at Prospect Bay.

**Figure A2.19.** 95% confidence intervals for area-weighted the mean wind exposure of plant communities at Prospect Bay.

**Figure A2.20.** Most frequent (area-weighted) stream order for plant communities at Prospect Bay.

**Figure A2.21.** 95% confidence intervals for the area-weighted mean incoming solar radiation received by plant communities at Prospect Bay.

**Figure A2.22.** Most frequent (area-weighted) slope position classifications for plant communities at Prospect Bay.

**Figure A2.23.** 95% confidence intervals for the area-weighted mean local surface ruggedness of plant communities at Prospect Bay.

**Figure A2.24.** 95% confidence intervals for the area-weighted mean global surface ruggedness of plant communities at Prospect Bay.

**Figure A2.25.** 95% confidence intervals for the area-weighted mean elevation of plant communities at Polly's Cove.

**Figure A2.26.** 95% confidence intervals for the area-weighted mean distance from the coastline for plant communities at Polly's Cove.

**Figure A2.27.** 95% confidence intervals for the area-weighted mean wind exposure of plant communities at Polly's Cove.

**Figure A2.28.** Most frequent (area-weighted) stream order for plant communities at Polly's Cove.

**Figure A2.29.** 95% confidence intervals for the area-weighted mean incoming solar radiation received by plant communities at Polly's Cove.

**Figure A2.30.** Most frequent (area-weighted) slope position classifications for plant communities at Polly's Cove.

**Figure A2.31.** 95% confidence intervals for the area-weighted mean local surface ruggedness of plant communities at Polly's Cove.

**Figure A2.32.** 95% confidence intervals for the area-weighted mean global surface ruggedness of plant communities at Polly's Cove.

# 1

## Introduction



*Island viewed from a UAV off Polly's Cove, Nova Scotia*

Ecosystems and their biodiversity are globally threatened by human activities (Mckee et al., 2004; Brooks et al., 2006). Biodiverse ecosystems are intrinsically valuable to human society and the ecosystem services they provide are irreplaceable (Edwards and Abivardi, 1998). Coastal environments are of particular concern, since more than forty percent of the global population live in coastal areas (UN Atlas of the Oceans, 2015). High population densities primarily threaten coastal environments due to land use activities, such as coastal development, timber harvesting, burning, agriculture, and tourism traffic. The pressures exhibited on coastal environments suggest a deep need to study coastal ecosystems and their biodiversity to inform land managers, conservation planners, and policy makers on how to protect these areas for long-term conservation.

Coastal barrens are open habitats that are dominated by low-growing vegetation such as grasses and ericaceous woody shrubs (Rodwell, 1991; Oberndorfer and Lundholm, 2009; Burley and Lundholm, 2010; Porter, 2013). They occur in coastal areas all over the world (Williams and Ashton, 1987; Rodwell, 1991; Anderson et al., 1999; Webb, 1998; Porter, 2013). Coastal barrens are often described as landscape mosaics – patchworks of plant communities that exist in harsh environmental conditions created by land-sea interactions and shallow soils (Oberndorfer and Lundholm, 2009; Burley and Lundholm, 2010; Porter, 2013). Despite what the name implies, coastal barrens can support a large range of habitat types including wetlands, shrublands, dwarf heaths, and trees islands and can contain high levels of biodiversity and many rare species (Oberndorfer and Lundholm, 2009; Burley and Lundholm, 2010; Porter, 2013).

In Nova Scotia, Canada, coastal barrens are scattered along the coastlines. Some of the most iconic sites are found in the Halifax region. The province of Nova Scotia has

recognized the importance of protecting the coastal barrens and previous studies have documented their species and communities (Oberndorfer and Lundholm, 2009; Burley and Lundholm, 2010; Cameron and Bondrup-Nielsen, 2013; Porter, 2013). There is still much to learn about these ecosystems, including the spatial distributions and spatial patterns of species and communities, their overall landscape composition and structure, and the biotic and abiotic processes that form and change them. These aspects of landscape ecology are critical for improving our knowledge of coastal barrens and informing conservation managers how to protect and manage these ecosystems.

### **Characteristics of Coastal Barrens**

Geographically, coastal barrens are widespread. In North America, they are particularly abundant along the northeastern coast of the United States and Atlantic Canada (Motzkin and Foster, 2002; Griffiths and Orians, 2004; Oberndorfer and Lundholm, 2009; Porter, 2013). They are less abundant in South America, although McCulloch et al. (2000) reported the presence of coastal heathlands from palaeoecological data. They are prominent in Britain, the Netherlands, and other coastal European countries (Rodwell, 1991; Webb, 1998; Piessens et al., 2005; Saure et al., 2013). In Europe, they are considered to be ‘cultural landscapes’, since historically coastal barrens were used for farming and sheep grazing (Webb, 1998; von Oheimb et al., 2008). Coastal barrens are also documented in Australia (Williams and Ashton, 1987; Martin and Catterall, 2001) and Africa (Boucher, 1983; Milewski, 1983).

The environmental conditions for coastal barrens are often harsh for both plants and animals. Soil properties are among the most important factors for plant survival



(Smith et al., 2012). Plants require soil not only for anchoring themselves, but also for receiving nutrients, minerals, and water for their vital functioning (Chapin III, 1980; Barber, 1995). In general, edaphic conditions for coastal barrens are relatively poor for plants due to their acidic, nutrient-poor, and often shallow nature (Webb, 1998; Oberndorfer and Lundholm, 2009; Porter, 2013). Acidic soils are problematic for vegetation because they can make vital nutrients unavailable due to leaching and can cause increases in toxic metals such as aluminum, which is detrimental for root development and can cause the yellowing of plant leaves (De Graaf et al., 1997). When soils become too acidic, species diversity and richness generally decrease (Roem and Berendse, 2000). Studies by Oberndorfer and Lundholm (2009) and Porter (2013) both found that nutrient availability in coastal barrens in Nova Scotia can vary significantly, which can be stressful for plants. Variability in nutrient availability can promote species and habitat diversity by creating multiple niches, which may partly explain the high levels of diversity and rare species found in coastal barrens (Oberndorfer and Lundholm, 2009; Cameron and Bondrup-Nielsen, 2013; Porter, 2013).

High winds are characteristic of coastal environments. Sea breezes form due to temperature differences between the land and the sea (Simpson, 1994). Temperature differences creates differences in pressure, resulting in a sea breeze moving from the ocean towards the land. High winds can be stressful for plants. The turbulent and drag forces of wind can cause damage to plant tissues such as tearing, stripping, and abrasion (Cleugh et al., 1998). Sometimes strong winds can uproot plants (De Langre, 2008). Winds can also cause erosion and remove topsoil, exposing plant roots, further increasing the risk of uprooting and reducing available soil for root exploration. Winds can also

speed up the evaporation of water, which can reduce the amount of available water for plants (Cleugh et al., 1998). Lastly, wind also can influence other environmental factors, such as precipitation patterns and salt spray (Baker et al., 2001). Some studies have suggested wind exposure is one of the most important factors driving the structure and composition of vegetation in the coastal barrens (Oberndorfer and Lundholm, 2009, Burley and Lundholm, 2010, Porter, 2013), although wind models have not yet been made to test this assumption.

The three-dimensional shape of a landscape influences the amount of exposure an area receives to wind and other environmental factors (Sebastiá, 2004; Mikita and Klimánek, 2010). Topographic heterogeneity can result in a mosaic of habitat patches depending on the degree and scale of topographic variability (Vivian-Smith, 1996; Sebastiá, 2004; Warren II, 2008). In a study on alvars, a type of barren ecosystem, Stark et al. (2004) found that microtopography was possibly the most important factor determining alvar succession by forest. Furthermore, elevation gradients can affect the distribution and structure of plant communities (Choler et al., 2001; Lomolino, 2001). Coastal barrens are highly variable in their topographic ruggedness (Heikens and Robertson, 1994) and the extent of ruggedness and differences in elevation likely plays an important role in defining the occurrence, distribution, and persistence of coastal barren vegetation (Burley and Lundholm, 2010; Porter, 2013).

Salt spray is common in coastal areas and typically occurs when ocean waves strike the surface of rocks or cliff faces. This causes salt water to be sprayed into the air, often blowing across the nearby landscape. Salt spray coupled with high winds can cause physical injury to plant tissues, and high salt content accumulated on plant leaves and in

the soil can inhibit water uptake and even cause osmotic injury at the cellular level (Bernstein and Hayward, 1958; Dirr, 1976). Oberndorfer and Lundholm (2009) found that in some coastal barren sites in Nova Scotia, there was a direct correlation between sodium content in the soil and proximity to the coast, providing evidence of this effect. Griffiths and Orians (2004) hypothesized that salt spray may be an important factor for preventing forest encroachment on coastal barrens, since salt spray can inhibit plant growth by inducing water stress, affect plant physiology, and inhibit the uptake of certain nutrients. In one of their experiments, a common tree species, *Pinus rigida*, was transplanted at different distances from a coastline in Massachusetts; it was found that although salt spray didn't cause direct mortality, there were significant signs of growth inhibition caused by the salt (Griffiths and Orians, 2004), providing evidence that the salt spray may prevent or slow tree encroachment on coastal barrens. Although the significance of salt spray will vary from one region to another, it is likely an important factor that influences plant community composition and distribution in the coastal barrens.

Water is essential for the structure and function of plants (Taiz and Zeiger, 2006). It is required for important physiological processes like photosynthesis, creating turgor pressure for cell rigidity, and the transportation of vital materials across the plant. The availability of water across a landscape is dependent on many factors. Since coastal barrens occur in coastal areas, they are often cool in the growing season compared to inland areas, and can experience relatively high levels of humidity, fog, and precipitation (Bakun, 1990). Precipitation patterns are typically stable and constant in coastal areas due to two main atmospheric processes: orographic and convectional uplifting. Orographic

uplift occurs when an air mass encounters an elevated surface and becomes physically uplifted (Wu et al., 2006). This is common when a sea-breeze forms from the ocean and travels inland where the landscape is elevated above the ocean. If the landscape topography is quite variable, then precipitation regimes will be affected. Convective uplift happens when a cool air mass travels over a warmer surface and rises due to increasing in temperature. Sea-breezes are cool because they are generated from the ocean and when they travel inland where it is warmer, convective uplift occurs. Uplifting will cause air to become cooler and denser, approaching the saturation level for water vapor in which precipitation will take place (Wu et al., 2006). Interestingly, Baker et al. (2001) found that coastline curvature can also impact precipitation regimes, where convex coastlines are associated with heavier rainfall. Despite regular precipitation regimes, coastal barrens can still exhibit drought-like conditions due to their combination of shallow soil and high winds, which can increase evaporation. Landscape topography also plays a key role in water regimes, since conditions tend to be wetter in valleys and dryer on slopes and ridges. Salt spray can also induce water-stress by inhibiting water absorption in plant roots (Bernstein and Hayward, 1958). As such, water availability in coastal barrens can be highly variable, providing opportunities for plants that reside on either end of the water-tolerance spectrum to establish in these ecosystems (Rodwell, 1991; Oberndorfer and Lundholm, 2009; Porter, 2013).

The family Ericaceae is the most common family of plants observed in coastal barrens (Rodwell, 1991; Webb, 1998; Tybirk et al., 2000; Oberndorfer and Lundholm, 2009; Porter, 2013). They are a very diverse group of woody flowering plants that are thought to have originated in North America during the time it belonged to the

supercontinent Laurasia, approximately 200-300 million years ago (Kron and Luteyn, 2005). Ericoids are now found in all parts of the world and many are adapted for shallow soil conditions, high wind exposure, and drought (Llorens et al., 2004). In Nova Scotia, an ericoid called *Empetrum nigrum*, commonly known as black crowberry, is the most dominant plant species on the coastal barrens (Oberndorfer and Lundholm, 2009; Hill et al., 2012; Porter, 2013). In Europe, it is also very prominent (Bell and Tallis, 1973; De Shmidt, 1977; Rodwell, 1991; Tybirk et al., 2000) and it is often accompanied by another ericoid shrub *Calluna vulgaris*, known as common heather, which is the most dominant heathland plant in Europe (Sedláková and Chytrý, 1999; Calvo et al., 2002).

Coastal barrens are diverse ecosystems that can be hot spots for uncommon and rare species. Oberndorfer and Lundholm (2009) surveyed six coastal barren sites in Nova Scotia using field plots and recorded 105 species of vascular plants, 41 species of macrolichens, and 27 species of mosses. Furthermore, 11 species were provincially rare. Interestingly, of the 173 species identified during the study, only 15 were found across all sites, suggesting that floristic compositions of coastal barrens can be geographically variable, which should be an important consideration for conservation management. The study concluded that the plant species and communities observed in the coastal barrens were similar to those observed in other coastal barrens around the world, particularly in Europe and New England. In a similar study, Porter (2013) collected field plot data on plant species abundances for 49 coastal barren sites in Nova Scotia to classify coastal barren plant communities. Over 253 species of vascular plants, mosses, and lichens were observed and 13 were found to be rare. Most vascular plant species belonged to the family Ericaceae; however, many other species belonged to Rosaceae, Asteraceae, and

Poaceae (true grasses). These studies show that coastal barrens can contain high amounts of biodiversity and are often home to rare flora, highlighting their importance for conservation (Anderson et al., 1999; Latham, 2003).

### **Classification of Vegetation**

In the natural world, there have been two main views about how vegetation exists: as discrete units or patches, in the form of plant communities or associations (Clements, 1916), or continuous variation of individual species along environmental gradients (Gleason, 1926). The modern synthesis of these two views assumes that plant species are distributed individualistically but can form associations or communities that are in discrete and recognizable units (van der Maarel and Franklin, 2013; Porter, 2013). A plant community will be defined as “a relatively uniform piece of vegetation in a uniform environment, with a recognizable floristic composition and structure that is relatively distinct from the surrounding vegetation” (van der Maarel and Franklin, 2013). Although classifications of plant communities are human constructs, it is still valuable to classify vegetation. It seeks to simplify the multiple-species continuum, helping to understand ecological patterns and processes in a manageable way (Grossman et al., 1994; NPS, 2011). Doing so can help simplify and communicate ecological information to land managers, conservation planners, and policy makers.

The Canadian National Vegetation Classification (CNVC, 2013) is a vegetation classification system that consists of an 8-level taxonomic hierarchy. It uses a physiognomic-floristic approach to classifying vegetation at different levels in the hierarchy and is consistent with the United States National Vegetation Classification

(USNVC) and the International Vegetation Classification (IVC) (Grossman et al., 1998). In this hierarchy, the “association” is the finest level of classification and is based primarily on floristic criteria (e.g. *Empetrum nigrum* – *Juniperus communis* dwarf heath). The “formation class” is the coarsest level of classification and is based primarily on physiognomy (e.g. shrubland). All classification levels are valuable to use and offer important ecological information at different scales of interest.

### **Landscape Ecology**

Landscape ecology is the study of interacting organisms and their distributions across landscapes. A landscape generally refers to a landform or surface of a region and its associated habitats (Turner, 1989). Landscapes are scale-dependent and so are the landscape patches (Wiens, 1976). A widely held view of landscapes is the patch-corridor-matrix model (Forman, 1995), which describes landscapes as mosaics consisting of patches, corridors, and a background matrix. The distribution and degree of patchiness across landscapes can influence the distributions of organisms, their interactions, and their adaptations (Wiens, 1976). Furthermore, the size, shape, and distribution of patches, i.e., their spatial configuration, can influence patterns of species abundance in animals such as birds (Turner, 1989). A great deal can be learned by studying the interactions and distributions of organisms across landscapes, and this knowledge can be applied to many disciplines, such as integrating land-use planning and decision making (Turner, 1989).

There are three important characteristics of landscapes that interest landscape ecologists: landscape structure, function, and change (McGarigal and Marks, 1995). Landscape structure refers to the composition (global) and spatial configuration (local) of

landscape features and patches that make up a landscape. It also refers to the spatial heterogeneity of a landscape, including the heterogeneity of habitat patches, geological features, and environmental conditions. Landscape function refers to interactions of landscape patches or elements and the flow of energy, materials, and organisms across landscapes. Landscape change is the alteration of landscape structure and function over time. To understand landscape function or change, landscape structure must be known (McGarigal and Marks, 1995). Landscape structure can be quantified using land cover maps and computing various kinds of landscape metrics using geographic information systems (GIS) (McGarigal et al., 2009). Land cover maps display the distributions of landscape features and species or communities and GIS provides the ability to analyze and quantify the spatial patterns and interrelationships within a map, for example calculating the total area occupied by a mapping class. Making accurate land cover maps can be challenging depending on the scale of study and level of detail desired; however, recent advances in remote sensing technology have made map-making more feasible.

### **Remote Sensing**

Remote sensing is the science of obtaining information from objects at a distance. Many different platforms can be used to do remote sensing including satellites, manned aircraft, and more recently unmanned aerial vehicles (UAVs) (Ustin and Gamon, 2010). Global landcover maps have been made using the SPOT4-VEGETATION satellite with a 1 km pixel resolution and the Landsat ETM+ satellite with a 30 m pixel resolution (Xie et al., 2008). The Worldview-2 Satellite has one of the finest resolutions for satellite imagery to date with 2 m pixel resolution; however, this resolution is still insufficient to



resolve important details of vegetation for mapping at the fine scale (Adam et al., 2010; Cruzan et al., 2016). Vegetation has also been successfully mapped using manned aircraft, which can collect both spectral and 3D structural data using a variety of sensors, such as hyperspectral sensors and LIDAR (light detection and ranging) (Hill and Thomson, 2005; Asner et al., 2015; Burai et al., 2015), at even higher resolutions than satellites. Although the resolution is greater, the cost of collecting remotely sensed data with a manned aircraft is very high and not practical for studies requiring frequent surveys.

Mapping remotely sensed data can be useful in many research areas and disciplines, particularly in plant ecology. Remote sensing has been used to map biophysical parameters of vegetation, such as stress levels, chlorophyll, leaf water content, leaf area index (LAI), and biomass (Adam et al., 2010; Mathews and Jensen, 2013; Aasen et al., 2015; Galidaki et al., 2017). Disturbance regimes can also be detected by remote sensors; for example, Minařík and Langhammer (2016) used a UAV to model disturbance dynamics of a forest and response of individual trees to the bark beetle. Remote sensing can also be used to map the distribution of organisms. Baldeck et al. (2014) collected airborne LIDAR and hyperspectral imagery from a savanna in Kruger National Park, South Africa to map over 500,000 tree and shrub crowns across a 144 km<sup>2</sup> landscape. Producing the map revealed complex landscape patterns of woody plant communities, which would not have been observable using field-based methods alone. In another example, Chastain et al. (2008) used a combination of field data, remote sensing data, and topographic data to map plant communities based on the USNVC (United States National Vegetation Classification) in Ozark National Scenic Riverways, Missouri.

Interestingly, their initial map of 49 associations had less accuracy and was not as useful to resource managers as compared to their revised map containing 33 associations.

Many challenges still exist to collect remote sensing data in a cost-effective, time-efficient manner, and at the desired resolution for the investigation. To map plant communities in the coastal barrens, a very high resolution of remotely sensed data would be required because coastal barrens are patchy at very fine scales. This fine-scale patchiness would have important implications for how organisms interact, how they are distributed, and the overall structure and function of coastal barrens landscapes. In some cases, patches can be very small ( $< 1$  m), such as a patch of lichen, and transitions from one patch to another can be abrupt (Burley and Lundholm, 2010). Additionally, differences in the 3D structure of vegetation canopies could be useful for discriminating plant community types and their physiognomic forms, such as tree islands compared to shrublands. This would require very high-resolution 3D remote sensing data to detect structural differences. Conventional remote sensing techniques are likely inadequate for achieving the level of detail required to discriminate plant community patches at the fine-scale and accurately map the distributions of plant communities in the coastal barrens.

### **Unmanned Aerial Vehicles**

More recently, commercial UAVs, which are synonymous with unmanned aircraft systems (UAS), can capture very high-resolution aerial imagery with pixel sizes in the low centimeters (e.g. Puttock et al., 2015). At this level of detail, vegetation stands can easily be differentiated, and researchers have begun to construct highly detailed vegetation maps that are giving the field of landscape ecology a whole new perspective

(Gonçalves et al., 2015; Guillot and Pouget, 2015; Sturdivant et al., 2017). UAVs are also receiving a lot of attention due to their low-cost and ability to cover large regions in a relatively short amount of time. They have the potential to repeatedly survey areas, providing not only a good spatial resolution, but a good temporal resolution as well – an aspect that has often limited the use of satellite imagery and manned aircraft.

Furthermore, UAVs can collect high-resolution data about the environment by being equipped with specialized sensors for hyperspectral imagery, thermal imagery, and even LIDAR, like manned aircraft (Klemas, 2015). They can also be equipped with cameras that capture light in the NIR (near-infrared) spectrum, which is very useful for differentiating vegetation characteristics (Ustin and Gamon, 2010). UAVs can capture sequential overlapping aerial imagery, making it possible to compute high-resolution 3D information of vegetation canopies and landscape features using structure from motion (SfM) photogrammetry (Micheletti et al., 2015), providing an unprecedented level of 3D detail at regional scales (Remondino et al., 2011).

Already UAVs have been used to produce highly detailed distributional maps of vegetation across landscapes. Zweig et al. (2015) used a UAV to map wetland communities in a 1 km area in Florida. In a mountainous heathland in Portugal, Gonçalves et al. (2015) derived spectral indices from UAV imagery to classify heathland communities. Fraser et al. (2016) used a UAV to collect sub-centimeter aerial imagery and computed ultradense 3D point clouds with a 1 cm resolution to quantify shrub heights in the low-Arctic. In an application of UAVs in a coastal environment, Sturdivant et al. (2017) produced accurate landcover maps of beach vegetation consisting of foredunes, marshes, shrubs, and herbaceous vegetation. These applications demonstrate

that UAVs can collect high-resolution spectral and 3D structural data across landscapes, offering a promising solution to map plant community patches in the coastal barrens at the fine-scale.

## **Study Sites**

Coastal barrens are abundant in Atlantic Canada and some of the most iconic sites are found in the Halifax region of Nova Scotia, including Chebucto Head, Prospect Bay, and Polly's Cove. The climate of Halifax, Nova Scotia is cool and mild with annual rainfall amounts of 1200 mm, annual snowfall amounts of 221 cm, and an average annual temperature of 6.6°C (ECCC, 2018). The spring and summer growing season tends to run from May to September with average monthly temperatures above 10°C, while the fall and winter months extend from October to April with temperatures below freezing. Annual wind speeds are 16.5 km/h and average wind direction is south during the spring and summer and northwest during the fall and winter (ECCC, 2018). The surficial geology of the Halifax region is largely composed of granitoid rock from the Devonian-Carboniferous period (MacDonald et al., 1992). Weathering and erosion of granite is very slow (Oosting and Anderson, 1939), which may explain the abundance and persistence of coastal barrens in the Halifax Region.

### **Chebucto Head**

Chebucto Head, located at N 44.51008 W 63.52659, is approximately 25 km southeast of Halifax. It is part of the Duncan's Cove Nature Reserve and is frequently visited by tourists for its hiking trails and its iconic light house. The site is characterised

by its tall granite cliffs, exposed rock outcrops and dwarf heath along the coastline. The terrain is very rugged, with many hills and valleys. Many species and communities have been documented at the site including various types of bogs, shrublands, dwarf heath, and tree islands (Oberndorfer and Lundholm, 2009; Burley and Lundholm, 2010; Porter, 2013).

### **Prospect Bay**

Prospect Bay, located at N 44.47444, W 63.80156, is southwest of the city of Halifax, Nova Scotia and is situated next to a small fishing community known as Prospect Village. Part of the site is owned by the Nature Conservancy of Canada (NCC) and the other part by a private landowner. Although little research has been done in the area to document its flora, it is frequently visited for its hiking trails. The terrain is simple and consists mostly of rolling hills and granite rocks along the coastline. Hill et al. (2012) describe the area as being dominated by *Empetrum nigrum* dwarf heath.

### **Polly's Cove**

Polly's Cove is 45 km southwest of Halifax and is located at approximately N 44.49088, W 63.88388 within a few kilometers of one of the most iconic coastal barrens sites around the world – Peggy's Cove. It is part of the West Dover Provincial Park and is stewarded by the Nova Scotia Department of Natural Resources (NSDNR). Like Chebucto Head, the site has rugged terrain with exposed rocky ridges, deep valleys, and granite cliffs along the coastline. It is also frequently visited by tourists for its hiking trails along the coastline. Like Prospect Bay, few studies have documented the site's

flora. Dwarf heath is generally observed along the coastline and further inland are tree islands, bogs, and shrublands.

## **Purpose of Study**

The purpose of this study is to investigate the use of a UAV to map plant communities and understand the landscape structure of the coastal barrens in Halifax, Nova Scotia. The research questions of this study are as follows:

- 1) Can multispectral UAV imagery be used to discriminate plant community types in the coastal barrens?
- 2) What are the landscape patterns of plant communities in the coastal barrens of Halifax, Nova Scotia?
- 3) How do the landscape patterns of plant communities relate to environmental factors?
- 4) What is the overall landscape structure of coastal barrens in Halifax, Nova Scotia and how does it compare between sites?

## References

- Aasen, H., Burkart, A., Bolten, A., & Bareth, G. (2015). Generating 3D hyperspectral information with lightweight UAV snapshot cameras for vegetation monitoring: from camera calibration to quality assurance. *ISPRS Journal of Photogrammetry and Remote Sensing*, *108*, 245-259.
- Adam, E., Mutanga, O., & Rugege, D. (2010). Multispectral and hyperspectral remote sensing for identification and mapping of wetland vegetation: a review. *Wetlands Ecology and Management*, *18*(3), 281-296.
- Anderson, R. C., Fralish, J. S. & Baskin, J. M. (1999). Savannas, barrens, and rock outcrop plant communities of North America. Cambridge University Press, Cambridge, UK.
- Asner, G. P., Ustin, S. L., Townsend, P. A., Martin, R. E., & Chadwick, K. D. (2015). Forest biophysical and biochemical properties from hyperspectral and LiDAR remote sensing. *Land resources monitoring, modeling and mapping with remote sensing*. CRC Press, Taylor & Francis Group, 429-448.
- Baker, R. D., Lynn, B. H., Boone, A., Tao, W. K., & Simpson, J. (2001). The influence of soil moisture, coastline curvature, and land-breeze circulations on sea-breeze-initiated precipitation. *Journal of Hydrometeorology*, *2*(2), 193-211.
- Bakun, A. (1990). Global climate change and intensification of coastal ocean upwelling. *Science*, *247*(4939), 198-201.
- Baldeck, C. A., Colgan, M. S., Féret, J. B., Levick, S. R., Martin, R. E., & Asner, G. P. (2014). Landscape-scale variation in plant community composition of an African savanna from airborne species mapping. *Ecological Applications*, *24*(1), 84-93.
- Barber, S. A. (1995). Soil nutrient bioavailability: a mechanistic approach. John Wiley & Sons.
- Bell, J. N. B., & Tallis, J. H. (1973). *Empetrum Nigrum* L. *Journal of Ecology*, 289-305.
- Bernstein, L., & Hayward, H. E. (1958). Physiology of salt tolerance. *Annual Review of Plant Physiology*, *9*(1), 25-46.
- Boucher, C. (1983). Floristic and structural features of the coastal foreland vegetation south of the Berg River, western Cape Province, South Africa. *Bothalia*, *14*(3 & 4), 669-674.

- Brooks, T. M., Mittermeier, R. A., da Fonseca, G. A., Gerlach, J., Hoffmann, M., Lamoreux, J. F., ... & Rodrigues, A. S. (2006). Global biodiversity conservation priorities. *Science*, *313*(5783), 58-61.
- Burai, P., Deák, B., Valkó, O., & Tomor, T. (2015). Classification of herbaceous vegetation using airborne hyperspectral imagery. *Remote Sensing*, *7*(2), 2046-2066.
- Burley, S. T., & Lundholm, J. T. (2010). Environmental predictors of forest expansion on open coastal barrens. *Biodiversity and conservation*, *19*(11), 3269-3285.
- Calvo, L., Tarrega, R., & Luis, E. D. (2002). Regeneration patterns in a *Calluna vulgaris* heathland in the Cantabrian mountains (NW Spain): effects of burning, cutting and ploughing. *Acta Oecologica*, *23*(2), 81-90.
- Cameron, R. P., & Bondrup-Nielsen, S. (2013). Plant Communities within Atlantic Coastal Heathlands in Nova Scotia. *Northeastern Naturalist*, *20*(4).
- Canadian National Vegetation Classification (CNVC) [online] 2013. Sault Ste. Marie, ON, Canada. Accessed 2015. Accessed on October 08, 2017 from: <http://cnvc-cnvc.ca>.
- Chapin III, F. S. (1980). The mineral nutrition of wild plants. *Annual review of ecology and systematics*, 233-260.
- Chastain, R. A., Struckhoff, M. A., He, H. S., & Larsen, D. R. (2008). Mapping vegetation communities using statistical data fusion in the Ozark National Scenic Riverways, Missouri, USA. *Photogrammetric Engineering & Remote Sensing*, *74*(2), 247-264.
- Choler, P., Michalet, R., & Callaway, R. M. (2001). Facilitation and competition on gradients in alpine plant communities. *Ecology*, *82*(12), 3295-3308.
- Clements, F. (1916). Plant succession: An analysis of the development of vegetation. Washington, DC: Carnegie Institute of Washington Publication.
- Cleugh, H. A., Miller, J. M., & Böhm, M. (1998). Direct mechanical effects of wind on crops. *Agroforestry Systems*, *41*(1), 85-112.
- Cruzan, M. B., Weinstein, B. G., Grasty, M. R., Kohn, B. F., Hendrickson, E. C., Arredondo, T. M., & Thompson, P. G. (2016). Small unmanned aerial vehicles (micro-UAVs, drones) in plant ecology. *Applications in Plant Sciences*, *4*(9), 1600041.
- De Graaf, M. C., Bobbink, R., Verbeek, P. J., & Roleofs, J. G. (1997). Aluminium toxicity and tolerance in three heathland species. *Water, air, and soil pollution*, *98*(3-4), 229-239.



- De Langre, E. (2008). Effects of wind on plants. *Annu. Rev. Fluid Mech.*, 40, 141-168.
- De Smidt, J. T. (1977). Heathland vegetation in the Netherlands. *Phytocoenologia*, 258-316.
- Dirr, M. A. (1976). Selection of trees for tolerance to salt injury. *Journal of Arboriculture*, 2(11), 209-216.
- Edwards, P. J., & Abivardi, C. (1998). The value of biodiversity: where ecology and economy blend. *Biological Conservation*, 83(3), 239-246.
- Environment and Climate Change Canada. (2018). Canadian Climate Normals 1981-2010 Station Data: Halifax Stanfield Int'l A. Retrieved April 25<sup>th</sup>, 2018 from [www.climate.weather.gc.ca/climate\\_normals](http://www.climate.weather.gc.ca/climate_normals)
- Forman, R. T. (1995). Some general principles of landscape and regional ecology. *Landscape ecology*, 10(3), 133-142.
- Fraser, R. H., Olthof, I., Lantz, T. C., & Schmitt, C. (2016). UAV photogrammetry for mapping vegetation in the low-Arctic. *Arctic Science*, 2(3), 79-102.
- Galidaki, G., Zianis, D., Gitas, I., Radoglou, K., Karathanassi, V., Tsakiri-Strati, M., ... & Mallinis, G. (2017). Vegetation biomass estimation with remote sensing: focus on forest and other wooded land over the Mediterranean ecosystem. *International Journal of Remote Sensing*, 38(7), 1940-1966.
- Gleason, H. A. (1926). The individualistic concept of the plant association. *Bulletin of the Torrey botanical club*, 7-26.
- Gonçalves, J., Henriques, R., Alves, P., Sousa-Silva, R., Monteiro, A. T., Lomba, Â., ... & Honrado, J. (2016). Evaluating an unmanned aerial vehicle-based approach for assessing habitat extent and condition in fine-scale early successional mountain mosaics. *Applied vegetation science*, 19(1), 132-146.
- Griffiths, M. E., & Orians, C. M. (2004). Salt spray effects on forest succession in rare coastal sandplain heathlands: evidence from field surveys and *Pinus rigida* transplant experiments. *Journal of the Torrey Botanical Society*, 23-31.
- Grossman, D. H., Goodin, K. L., Li, X., Faber-Langendoen, D., Anderson, M., Bourgeron, P., & Vaughn, R. (1994). Field Methods For Vegetation Mapping. NBS/NPS Vegetation Mapping Program. The Nature Conservancy, Arlington, VA, and Environmental Systems Research Institute, Redlands, CA.

Grossman, D. H., Faber-Langendoen, D., Weakley, A. S., Anderson, M., Bourgeron, P., Crawford, R., ... & Pyne, M. (1998). International classification of ecological communities: terrestrial vegetation of the United States. *The Nature Conservancy, Arlington, Virginia*.

Guillot, B., & Pouget, F. (2015). Uav Application in Coastal Environment, Example of the Oleron Island for Dunes and Dikes Survey. *The International Archives of Photogrammetry, Remote Sensing and Spatial Information Sciences*, 40(3), 321.

Heikens, A. L., & Robertson, P. A. (1994). Barrens of the Midwest: a review of the literature. *Castanea*, 184-194.

Hill, N. M., Vander Kloet, S. P., & Garbary, D. J. (2012). The regeneration ecology of *Empetrum nigrum*, the black crowberry, on coastal heathland in Nova Scotia. *Botany*, 90(5), 379-392.

Hill, R. A., & Thomson, A. G. (2005). Mapping woodland species composition and structure using airborne spectral and LiDAR data. *International Journal of Remote Sensing*, 26(17), 3763-3779.

Kerbiriou, C., Leviol, I., Jiguet, F., & Julliard, R. (2008). The impact of human frequentation on coastal vegetation in a biosphere reserve. *Journal of Environmental Management*, 88(4), 715-728.

Klemas, V. V. (2015). Coastal and environmental remote sensing from unmanned aerial vehicles: an overview. *Journal of Coastal Research*, 31(5), 1260-1267.

Kron, K. A., & Luteyn, J. L. (2005). Origins and biogeographic patterns in Ericaceae: new insights from recent phylogenetic analyses. *Biol Skr*, 55, 479-500.

Latham, R. E. (2003). Shrubland longevity and rare plant species in the northeastern United States. *Forest Ecology and Management*, 185(1), 21-39.

Llorens, L., Penuelas, J., Beier, C., Emmett, B., Estiarte, M., & Tietema, A. (2004). Effects of an experimental increase of temperature and drought on the photosynthetic performance of two ericaceous shrub species along a north-south European gradient. *Ecosystems*, 7(6), 613-624.

Lomolino, M. (2001). Elevation gradients of species-density: historical and prospective views. *Global Ecology and biogeography*, 10(1), 3-13.

MacDonald, M. A., Horne, R. J., Corey, M. C., & Ham, L. J. (1992). An overview of recent bedrock mapping and follow-up petrological studies of the South Mountain Batholith, southwestern Nova Scotia, Canada.

- Martin, T. G., & Catterall, C. P. (2001). Do fragmented coastal heathlands have habitat value to birds in eastern Australia?. *Wildlife Research*, 28(1), 17-31.
- Mathews, A. J., & Jensen, J. L. (2013). Visualizing and quantifying vineyard canopy LAI using an unmanned aerial vehicle (UAV) collected high density structure from motion point cloud. *Remote Sensing*, 5(5), 2164-2183.
- McCulloch, R. D., Bentley, M. J., Purves, R. S., Hulton, N. R. J., Sugden, D. E., & Clapperton, C. M. (2000). Climatic inferences from glacial and palaeoecological evidence at the last glacial termination, southern South America. *Journal of Quaternary Science*, 15(4), 409-417.
- McGarigal, K., & Marks, B. J. (1995). Spatial pattern analysis program for quantifying landscape structure. *Gen. Tech. Rep. PNW-GTR-351. US Department of Agriculture, Forest Service, Pacific Northwest Research Station.*
- McGarigal, K., Tagil, S., & Cushman, S. A. (2009). Surface metrics: an alternative to patch metrics for the quantification of landscape structure. *Landscape ecology*, 24(3), 433-450.
- McKee, J. K., Sciulli, P. W., Fooce, C. D., & Waite, T. A. (2004). Forecasting global biodiversity threats associated with human population growth. *Biological Conservation*, 115(1), 161-164.
- Micheletti, N., Chandler, J. H., & Lane, S. N. (2015). Structure from motion (SFM) photogrammetry. *Geomorphological Techniques*, Chap. 2, Sec. 2.2.
- Mikita, T., & Klimánek, M. (2010). Topographic exposure and its practical applications. *Journal of Landscape Ecology*, 3(1), 42-51.
- Milewski, A. V. (1983). A comparison of ecosystems in mediterranean Australia and southern Africa: nutrient-poor sites at the Barrens and the Caledon coast. *Annual Review of Ecology and Systematics*, 57-76.
- Minařík, R., & Langhammer, J. (2016). Use of a Multispectral UAV photogrammetry for detection and tracking of forest disturbance dynamics. *International Archives of the Photogrammetry, Remote Sensing & Spatial Information Sciences*, 41.
- Motzkin, G., & Foster, D. R. (2002). Grasslands, heathlands and shrublands in coastal New England: historical interpretations and approaches to conservation. *Journal of Biogeography*, 29(10-11), 1569-1590.
- National Park Service. (2011). *Vegetation Classification Guidelines: National Park Service Vegetation Inventory, Version 2.0.*

- Oberndorfer, E. C., & Lundholm, J. T. (2009). Species richness, abundance, rarity and environmental gradients in coastal barren vegetation. *Biodiversity and Conservation*, 18(6), 1523-1553.
- Oosting, H. J., & Anderson, L. E. (1939). Plant succession on granite rock in eastern North Carolina. *Botanical Gazette*, 100(4), 750-768.
- Piessens, K., Honnay, O., & Hermy, M. (2005). The role of fragment area and isolation in the conservation of heathland species. *Biological Conservation*, 122(1), 61-69.
- Porter, C. (2013). Classification of dwarf heath plant communities on the coastal barrens of Nova Scotia. Thesis. Master of Science. Saint Mary's University, Halifax, Nova Scotia.
- Puttock, A. K., Cunliffe, A. M., Anderson, K., & Brazier, R. E. (2015). Aerial photography collected with a multirotor drone reveals impact of Eurasian beaver reintroduction on ecosystem structure. *Journal of Unmanned Vehicle Systems*, 3(3), 123-130.
- Remondino, F., Barazzetti, L., Nex, F., Scaioni, M., & Sarazzi, D. (2011). UAV photogrammetry for mapping and 3d modeling—current status and future perspectives. *International Archives of the Photogrammetry, Remote Sensing and Spatial Information Sciences*, 38(1), C22.
- Rodwell, J. S. (1991). British plant communities (Vol. 5). Cambridge University Press.
- Roem, W. J., & Berendse, F. (2000). Soil acidity and nutrient supply ratio as possible factors determining changes in plant species diversity in grassland and heathland communities. *Biological Conservation*, 92(2), 151-161.
- Saure, H. I., Vandvik, V., Hassel, K., & Vetaas, O. R. (2013). Effects of invasion by introduced versus native conifers on coastal heathland vegetation. *Journal of Vegetation science*, 24(4), 744-754.
- Sebastiá, M. T. (2004). Role of topography and soils in grassland structuring at the landscape and community scales. *Basic and Applied Ecology*, 5(4), 331-346.
- Sedláková, I., & Chytrý, M. (1999). Regeneration patterns in a Central European dry heathland: effects of burning, sod-cutting and cutting. *Plant Ecology*, 143(1), 77-87.
- Simpson, J. E. (1994). Sea breeze and local winds. Cambridge University Press.
- Smith, D. S., Schweitzer, J. A., Turk, P., Bailey, J. K., Hart, S. C., Shuster, S. M., & Whitham, T. G. (2012). Soil-mediated local adaptation alters seedling survival and performance. *Plant and Soil*, 352(1-2), 243-251.

- Stark, K. E., Lundholm, J. T., & Larson, D. W. (2004). Arrested development of soil on alvars of Ontario, Canada: implications for conservation and restoration. *Natural Areas Journal*, 24(2), 95-100.
- Sturdivant, E. J., Lentz, E. E., Thieler, E. R., Farris, A. S., Weber, K. M., Remsen, D. P., ... & Henderson, R. E. (2017). UAS-SfM for Coastal Research: Geomorphic Feature Extraction and Land Cover Classification from High-Resolution Elevation and Optical Imagery. *Remote Sensing*, 9(10), 1020.
- Taiz, L., & Zeiger, E. (2006). *Plant Physiology* (4th ed., pp. 37-70). Sunderland: Sinauer Associates.
- Turner, M. G. (1989). Landscape ecology: the effect of pattern on process. *Annual review of ecology and systematics*, 20(1), 171-197.
- Tybirk, K., Nilsson, M. C., Michelsen, A., Kristensen, H. L., Shevtsova, A., Tune Strandberg, M., ... & Johnsen, I. (2000). Nordic Empetrum dominated ecosystems: function and susceptibility to environmental changes. *Journal of the Human Environment*, 29(2), 90-97.
- UN Atlas of the Oceans. (2015). Retrieved November 29, 2015, from [www.oceansatlas.org](http://www.oceansatlas.org)
- Ustin, S. L., & Gamon, J. A. (2010). Remote sensing of plant functional types. *New Phytologist*, 186(4), 795-816.
- van der Maarel, E., & Franklin, J. (2013). *Vegetation Ecology. Second Edition*. Wiley-Blackwell.
- Vivian-Smith, G. (1997). Microtopographic heterogeneity and floristic diversity in experimental wetland communities. *Journal of Ecology*, 71-82.
- Warren II, R. J. (2008). Mechanisms driving understory evergreen herb distributions across slope aspects: as derived from landscape position. *Plant Ecology*, 198(2), 297-308.
- Webb, N. R. (1998). The traditional management of European heathlands. *Journal of Applied Ecology*, 987-990.
- Wiens, J. A. (1976). Population responses to patchy environments. *Annual review of ecology and systematics*, 7(1), 81-120.
- Williams, R. J., & Ashton, D. H. (1987). The composition, structure and distribution of heathland and grassland communities in the subalpine tract of the Bogong High Plains, Victoria. *Australian journal of ecology*, 12(1), 57-71.

Wu, W., Hall, C., & Zhang, L. (2006). Predicting the temporal and spatial probability of orographic cloud cover in the Luquillo Experimental Forest in Puerto Rico using generalized linear (mixed) models. *Ecological modelling*, 192(3), 473-498.

Xie, Y., Sha, Z., & Yu, M. (2008). Remote sensing imagery in vegetation mapping: a review. *Journal of plant ecology*, 1(1), 9-23.

Zweig, C. L., Burgess, M. A., Percival, H. F., & Kitchens, W. M. (2015). Use of unmanned aircraft systems to delineate fine-scale wetland vegetation communities. *Wetlands*, 35(2), 303-309.

# 2

## **Evaluating Multispectral Imagery from an Unmanned Aerial Vehicle for Discriminating Plant Communities in the Coastal Barrens of Halifax, Nova Scotia**



*Patches of ferns, dwarf heath, shrublands, and tree islands at Prospect Bay, Nova Scotia*

## **Abstract**

In the coastal barrens of Halifax, Nova Scotia, plant communities are dispersed across landscapes like shattered glass: different vegetation types exhibit a range of patch sizes and spatial patterns. Maps have not yet been made of plant communities in the coastal barrens of Nova Scotia and consequently there is little known of their landscape patterns. Unmanned Aerial Vehicles (UAVs) are a promising tool to map coastal barrens vegetation, providing a cost-effective way to collect high-resolution spectral, temporal, and 3D information at regional scales. This study evaluated the use of a UAV with RGB and near-infrared sensors to discriminate plant communities at three coastal barrens sites in Halifax: Chebucto Head, Polly's Cove, and Prospect Bay. Three levels of plant community classification were evaluated from the Canadian National Vegetation Classification: the association level, based on floristic criteria, the broadened association level, and the formation class, based on physiognomy. Field sampling was conducted in the summer of 2016 and UAV imagery was collected in the spring and summer of 2016. Spectral and structural indices were extracted from the UAV imagery and were evaluated for discriminating plant communities using linear discriminant analysis. All plant communities from both classification levels were discriminated with 95% confidence except for one pair in the association level classification. Overall classification accuracy for the association level classification was lower (63%) than the formation class classification (92%); however, merging confused groups to form a broadened association level classification improved the accuracy to 83%. These results show that plant communities in the coastal barrens can be discriminated at different classification levels using a UAV.



## Introduction

Coastal barrens are terrestrial ecosystems that are scattered along coastlines around the world, particularly in Atlantic Canada and Europe. They typically occur within 500 m of the coastline and are predominantly occupied by low-growing ericaceous vegetation and few trees. In Nova Scotia, Canada, coastal barrens are abundant, and some of the most iconic sites occur in the Halifax region. The province of Nova Scotia has recognized the importance of protecting these areas and researchers have begun to document the species and communities that exist in the coastal barrens (Oberndorfer and Lundholm, 2009; Cameron and Bondrup-Nielsen, 2013; Porter, 2013). Still, their distributions, spatial patterns and interrelationships, and processes that form and change them are largely unknown. Maps can help to visualize spatial relationships and would improve our understanding of coastal barrens as an ecosystem, communicate the importance and value that these ecosystems hold, and better focus future research and conservation efforts.

Mapping the distributions of species and communities is valuable in many ways. Much of the field of ecology focuses on understanding the patterns and scales of the distributions and abundances of organisms, and this requires some level of distributional mapping (Turner, 1989). Maps can be used to manage habitats and restoration projects, assess regional biodiversity, design protected areas, assess risks of invasive species, and predict the impacts of climate change on species, communities and ecosystems (He et al., 2005; Tart et al., 2005; Adam et al., 2010; Franklin, 2010). There are many ways to create maps; however, creating detailed vegetation maps across large areas would require either intensive field work or the use of remote sensing technology. The challenge with

using remote sensing technology to map vegetation is obtaining the necessary spatial and spectral resolution needed to discriminate vegetation types with high confidence.

An important consideration for mapping vegetation is whether a classification system will be used to classify assemblages of plant species into discrete units or plant communities (Demers, 1991). A plant community is defined as “a relatively uniform piece of vegetation in a uniform environment, with a recognizable floristic composition and structure that is relatively distinct from the surrounding vegetation” (van der Maarel and Franklin, 2013). Grouping vegetation into more manageable units helps to simplify the multiple-species continuum (Ferrier, 2002; NPS, 2011; Faber-Langendoen et al., 2014). It also helps to communicate ecological information for landscape managers, conservation planners, and policy makers. Classifications for plant communities are scale-dependent and range from fine level to coarse level, with either end of the spectrum being valuable for ecologists and conservationists (Grossman et al., 1998). In Canada, the Canadian National Vegetation Classification (CNVC, 2013) uses a standardized 8-level taxonomic hierarchy to classify plant communities, which is based on the United States National Vegetation Classification (USNVC) and the International Vegetation Classification (IVC). Association is the finest level of classification and is based primarily on floristic criteria, including dominant species; formation class is the coarsest classification level and is based primarily on physiognomy.

Unmanned aerial vehicles (UAVs) offer a promising solution for mapping vegetation in the coastal barrens by offering a cost-effective method to obtain aerial imagery with sub-decimeter pixel resolutions, computing high-resolution 3D structural information, and having good temporal resolution (Remondino et al., 2011; Gonçalves et

al., 2015; Guillot and Pouget, 2015). UAVs have been used to map plant communities in different terrestrial ecosystems, such as wetlands (Zweig et al., 2015), low-arctic tundra (Fraser et al., 2016), and dunes (Sturdivant et al., 2017), but have yet to be used to map plant communities in the coastal barrens. Prior to using a remote sensing platform for mapping plant communities, the platform should be evaluated for its ability to discriminate the vegetation at the desired scale or classification level. If the remote sensing platform is not able to discriminate vegetation types at the desired classification level, then it is not justifiable to use it for mapping applications.

The aim of this study is to evaluate the use of a UAV equipped with RGB and NIR sensors for discriminating plant communities in the coastal barrens of Halifax, Nova Scotia. This will be achieved by the following objectives: 1) To assess the discriminatory power of multispectral UAV imagery for discriminating plant communities in the coastal barrens at three classification levels from the Canadian National Vegetation Classification: association level, broadened association level, and formation class; and, 2) To determine which indices extracted from UAV imagery explain the most variance of plant communities in the coastal barrens.

## Methods

### Study Area

Coastal barrens are scattered along the coastline of Atlantic Canada and northeastern United States. In the Halifax region of Nova Scotia, granite cliffs are abundant, forming numerous coastal barrens sites (Figure 2.1). Three coastal barrens sites in the Halifax region of Nova Scotia, Canada were selected for this study and systematically surveyed in 2016 by a UAV to collect high-resolution multispectral aerial imagery: Chebucto Head (N 44.51008 W 63.52659; Figure 2.2), Prospect Bay (N 44.47444, W 63.80156; Figure 2.3), and Polly's Cove (N 44.49088, W 63.88388; Figure 2.4). All three sites are similar due to their proximity, experience similar climatic conditions, and are well-documented in previous research (Oberndorfer and Lundholm, 2009; Burley et al., 2010; Porter, 2013). Each site measures approximately 500 meters across and 500 meters inland from the coastline, in the shape of a square. This equates to an approximate study area of 25 ha per site. These dimensions were chosen because previous research has suggested that coastal barrens typically occur within 500 meters of the coastline (Oberndorfer and Lundholm, 2009; Porter, 2013). Furthermore, a 25-hectare area represents a significant portion of a landscape, consisting of a large spectrum of environmental gradients, vegetation types and regional variation.

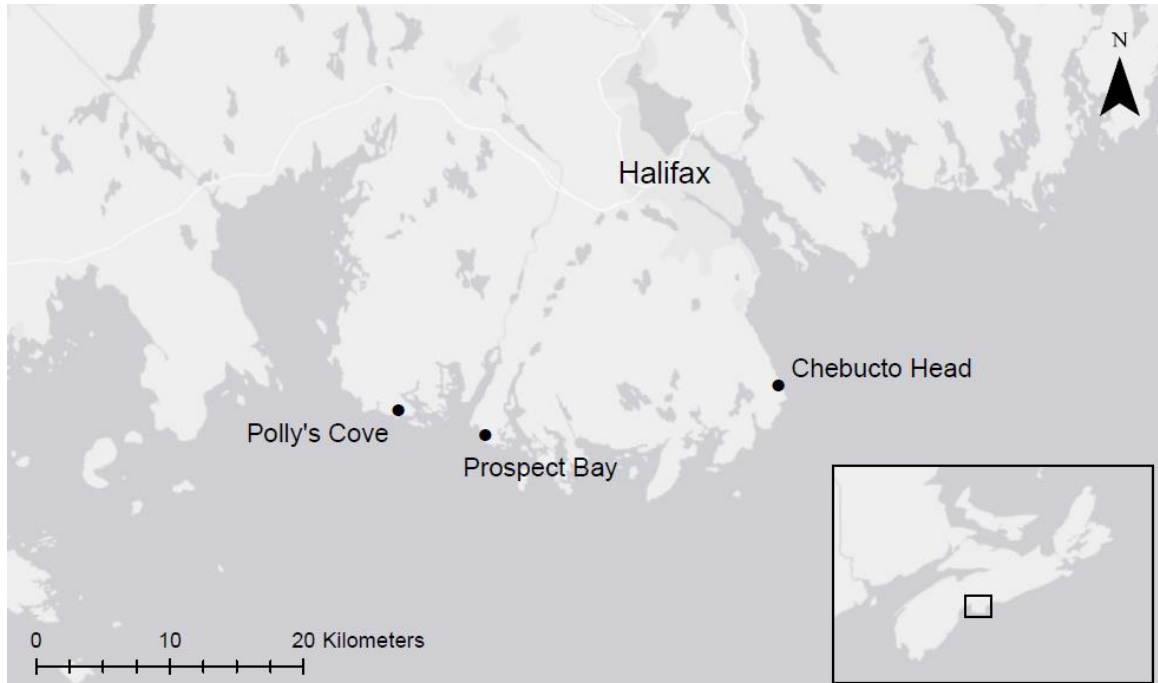


Figure 2.1. Coastal barrens sites selected for this study: Chebucto Head, Prospect Bay, and Polly's Cove. All three sites are located in the Halifax region of Nova Scotia, Canada.

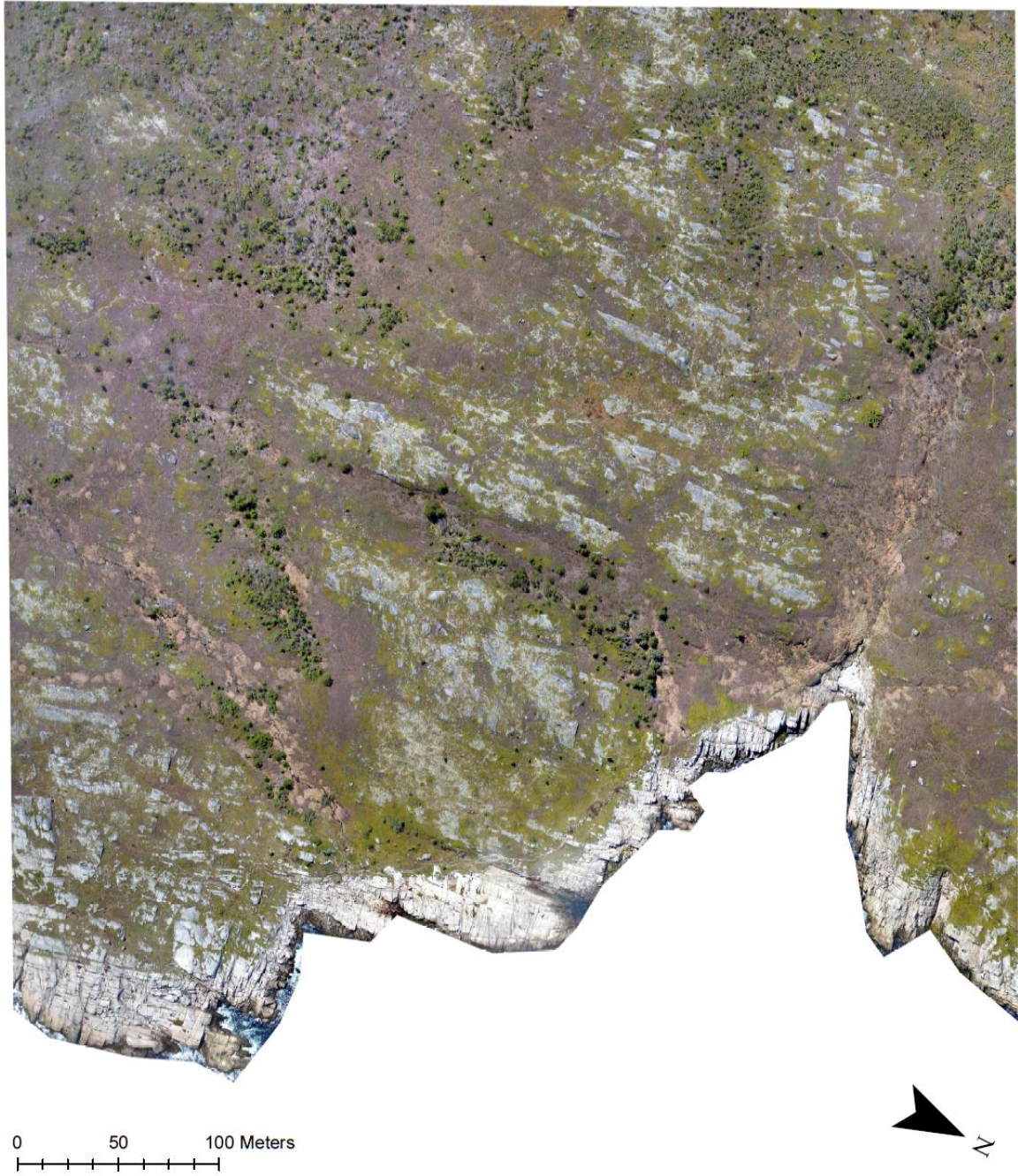


Figure 2.2. An RGB orthomosaic of the Chebucto Head study site in Halifax, Nova Scotia. Aerial imagery was captured from a UAV in May 2016 at 90 m altitude, providing 4 cm ground resolution.

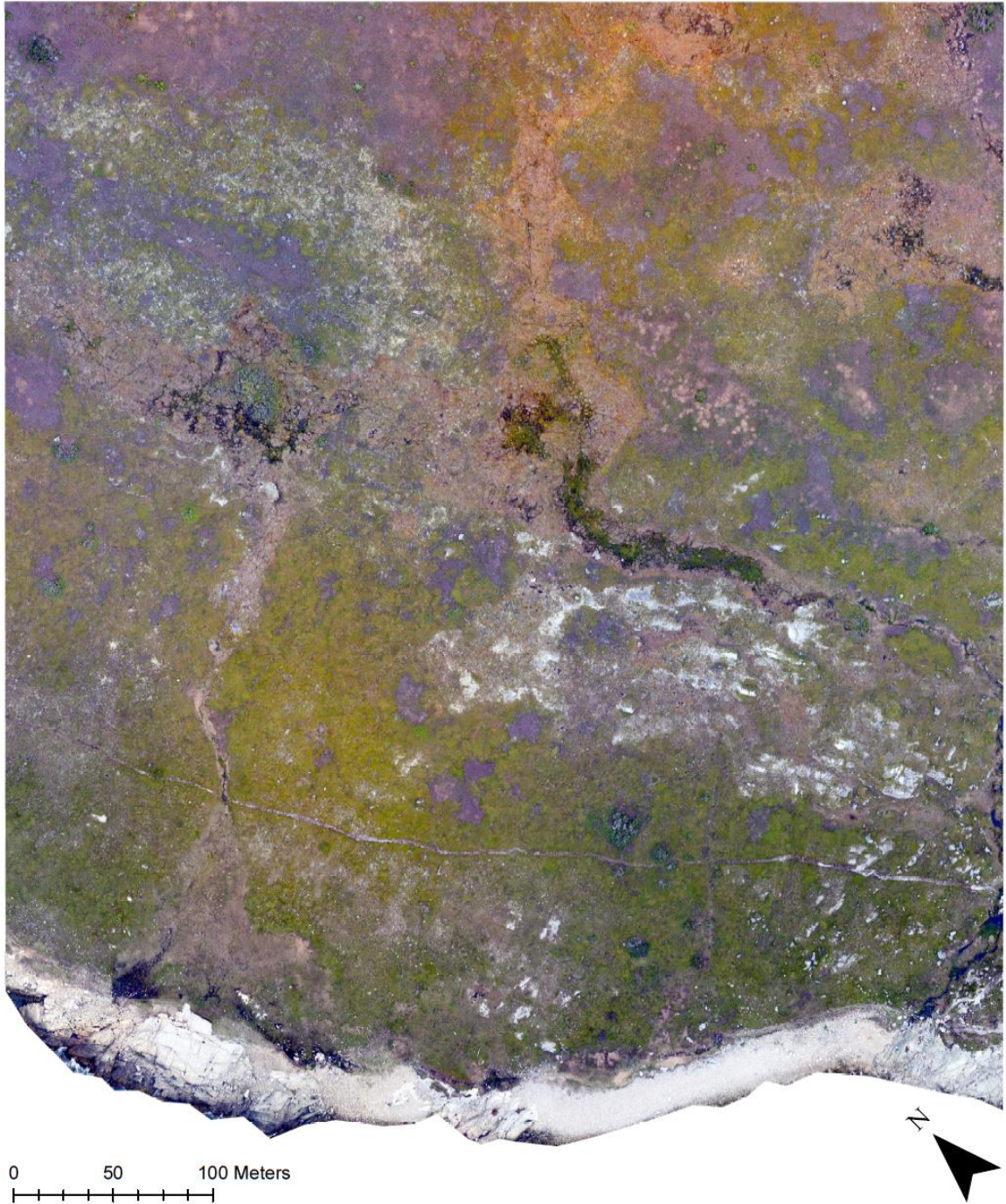


Figure 2.3. An RGB orthomosaic of the Prospect Bay study site in Halifax, Nova Scotia. Aerial imagery was captured from a UAV in May 2016 at 90 m altitude, providing 4 cm ground resolution.

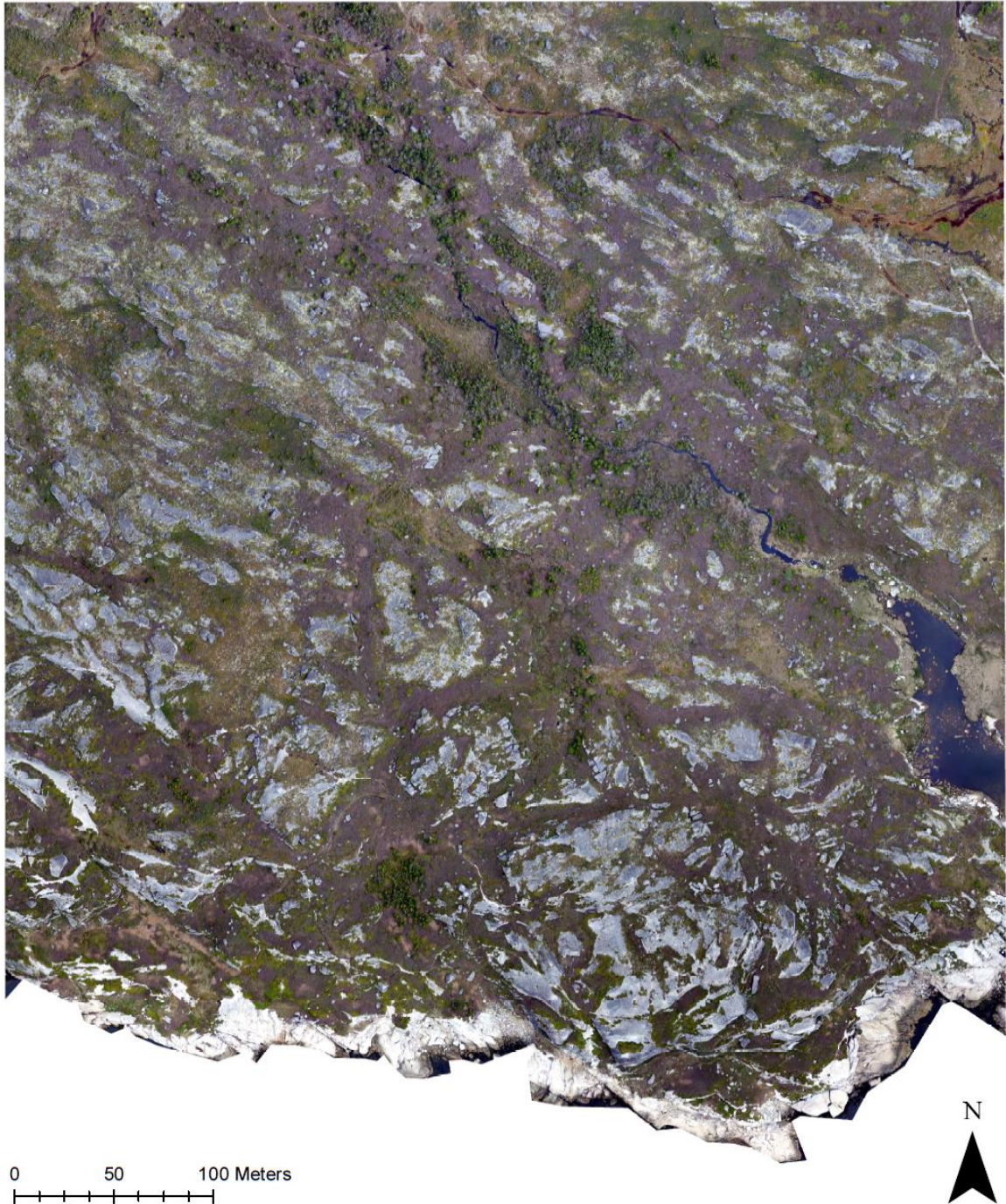


Figure 2.4. An RGB orthomosaic of the Polly's Cove study site in Halifax, Nova Scotia. Aerial imagery was captured from a UAV in May 2016 at 90 m altitude, providing 4 cm ground resolution.



## Data Collection and Processing

Multispectral UAV imagery was collected in the spring and summer of 2016 at each study site and was evaluated for discriminating plant communities based on ground truthing from field plot data (Figure 2.5). The UAV used for this study was a DJI Phantom 3 Professional quadcopter, equipped with a 12-megapixel RGB camera on a rotating gimbal and a fixed Sentera single Near-Infrared (NIR) sensor (Figure 2.6; see Table A1.1 in Appendix for aircraft specifications). The cameras are independent of one another and require separate microSD cards. The quadcopter weighs approximately 1.28 kg and uses lithium ion batteries, each providing a maximum flight time of 23 minutes.

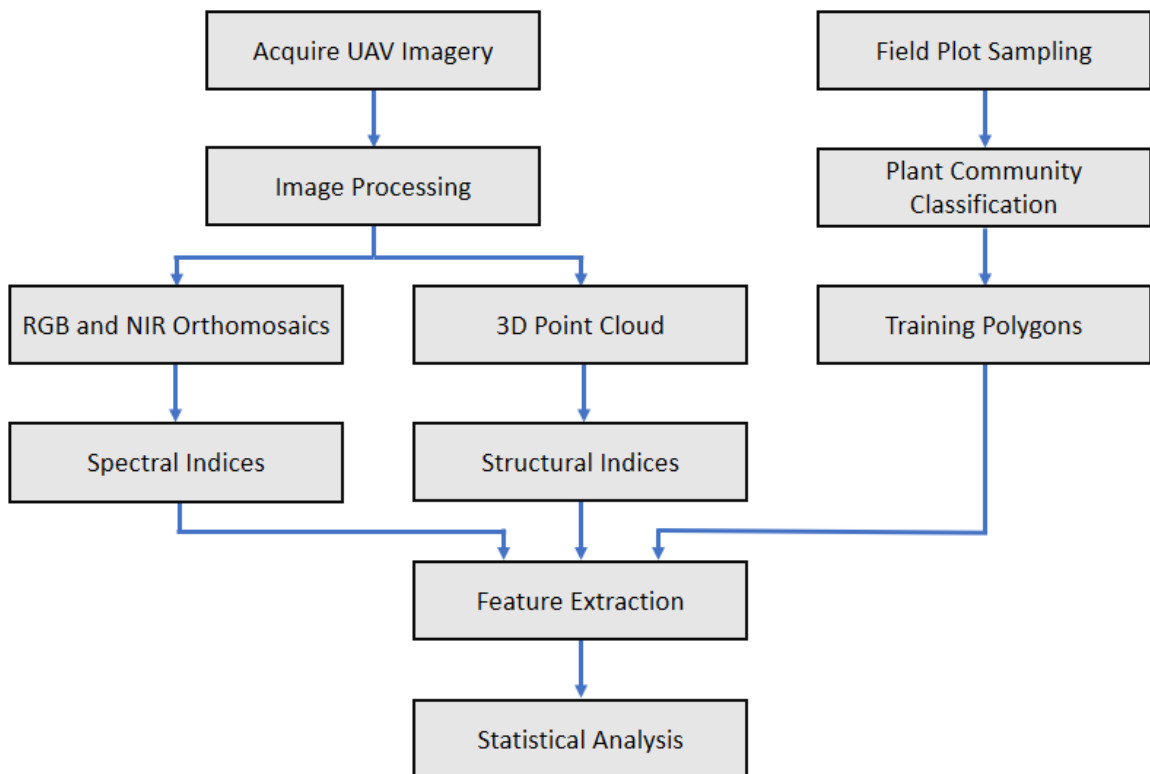


Figure 2.5. Flowchart illustrating the methodology used to extract spectral and structural information from multispectral UAV imagery to discriminate plant communities identified from field plot sampling in the coastal barrens of Halifax, Nova Scotia.



Figure 2.6. DJI Phantom 3 Professional quadcopter used to collect high-resolution multispectral aerial imagery. The aircraft was equipped with a 12-megapixel RGB camera on a rotating gimbal and a fixed Sentera single Near-Infrared sensor.

Pix4DCapture (Pix4D, Lausanne, Switzerland), a flight planning mobile application that can be downloaded for free on most smart phones and tablets that use IOS or Android, was used to create flight plans and autonomously control the UAV to collect sequential high-resolution aerial imagery at the study sites. Customizable grid missions were created within the application to delineate areas to map and to control flight parameters, such as image overlap and flight altitude (Figure 2.7). Flights were conducted with the camera facing downward (nadir), with overlap set at 80% and sidelap as 60%. In the spring, above-ground altitude was set to 90 m (resulting in 4 cm pixel resolution for the RGB camera; 8 cm pixel resolution for the NIR sensor) and in the summer, it was set to 50 m (resulting in 2 cm pixel resolution for the RGB camera; 4 cm pixel resolution for the NIR sensor) to have a better resolution for reconstructing the vegetation canopies in 3D. Since the UAV has two independent cameras, Pix4DCapture

controlled the RGB camera while the NIR sensor was set to take images at a two-second interval to achieve similar image overlap.

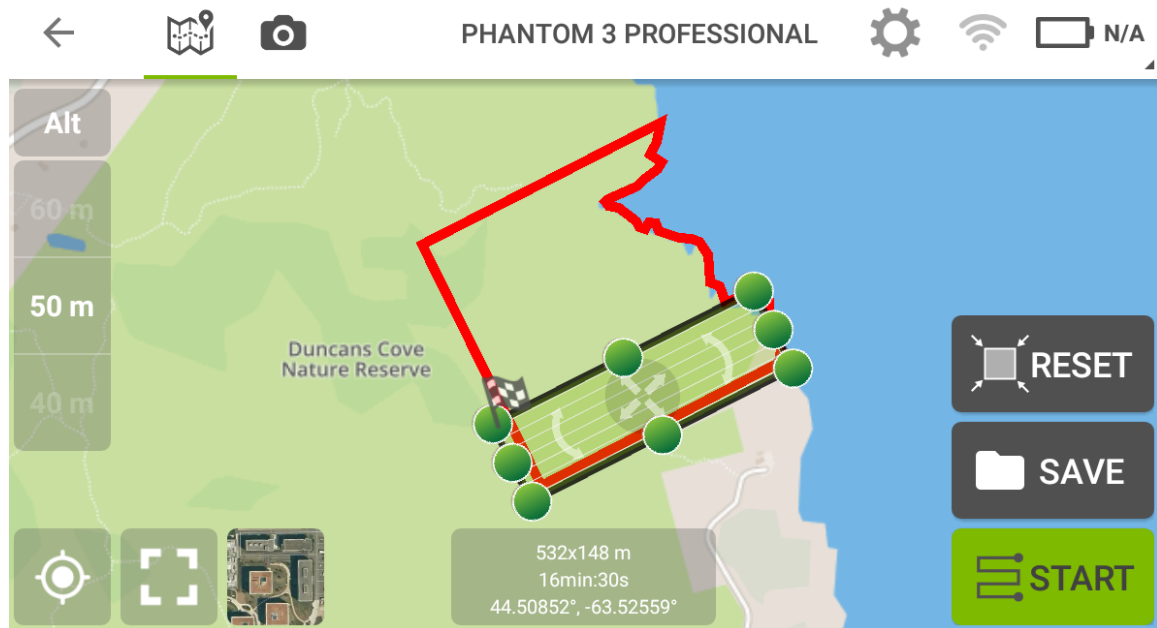


Figure 2.7. A grid mission in the Pix4DCapture flight planning mobile application. Pix4DCapture was used to autonomously fly the unmanned aerial vehicle to collect sequential high-resolution multispectral aerial imagery of the three study sites.

Many plant species found in the coastal barrens are deciduous shrubs or herbaceous perennials (Oberndorfer and Lundholm, 2009; Porter, 2013). The timing of aerial surveys for observing and discriminating plant communities is therefore crucial. In the fall, deciduous shrubs lose their leaves and herbaceous vegetation undergoes senescence, known as the leaf-off period. In the late spring and early summer of the following year, deciduous species regain their leaves and herbaceous perennial species re-emerge, known as the leaf-on period. Research has shown that seasonal phenologies, such as the leaf-on and leaf-off periods, have been useful for discriminating vegetation based on their spectral properties (Anderson, 1970; Gilmore et al., 2008; Dandois and Ellis, 2013; He et al., 2015). Further, some evergreen shrubs on Nova Scotia coastal

barrens exhibit distinct seasonal colour changes in their foliage. The timing of surveys was planned to capture this seasonal variation by collecting imagery at the end of May (leaf-off period) and beginning of August (leaf-on period) in 2016 (see Table A1.2 for details on survey dates).

To ensure that aerial surveys were geolocated on the earth's surface to sub-meter accuracy, ten to twelve ground control points (GCPs) were laid out across each site prior to image acquisition. A GCP is a visible target that is meant to be seen in aerial imagery and has known XYZ coordinates which can later be used during image processing to accurately georeference the models. GCPs consisted of 9-inch red plastic plates that were pinned to the ground with metal pegs. A Real-Time Kinematic (RTK) was used to acquire accurate geolocations of the center of each GCP in the field with horizontal accuracy of 1-2 cm and vertical accuracy 2-6 cm.

The goal of acquiring and processing UAV imagery for this study was to create two products: a single orthomosaic image of each site from May and August in 2016, and a 3D point cloud in August (leaf-on period) for each site. An orthomosaic is a mosaic of multiple images that have been stitched together and orthorectified to remove perspective distortions. Orthomosaics retain the high resolution and detail of the original images used to create them and are a great solution for image analysis and landscape mapping. A 3D point cloud is simply a mass of points containing XYZ coordinates, which can be used to create digital elevation models (DEM) and provide useful 3D information about a landscape and its vegetation, such as topographic variability and canopy structure.

Creating orthomosaics and 3D point clouds from multiple overlapping UAV images is possible through a technique known as structure from motion (SfM) photogrammetry. When multiple overlapping images are acquired, objects within the images are viewed from multiple angles or perspectives. The position and appearance of the objects may also change relative to their surroundings from one image to another. SfM software can use this information to reconstruct surfaces and compute 3D models (Micheletti et al., 2015) (Figure 2.8).

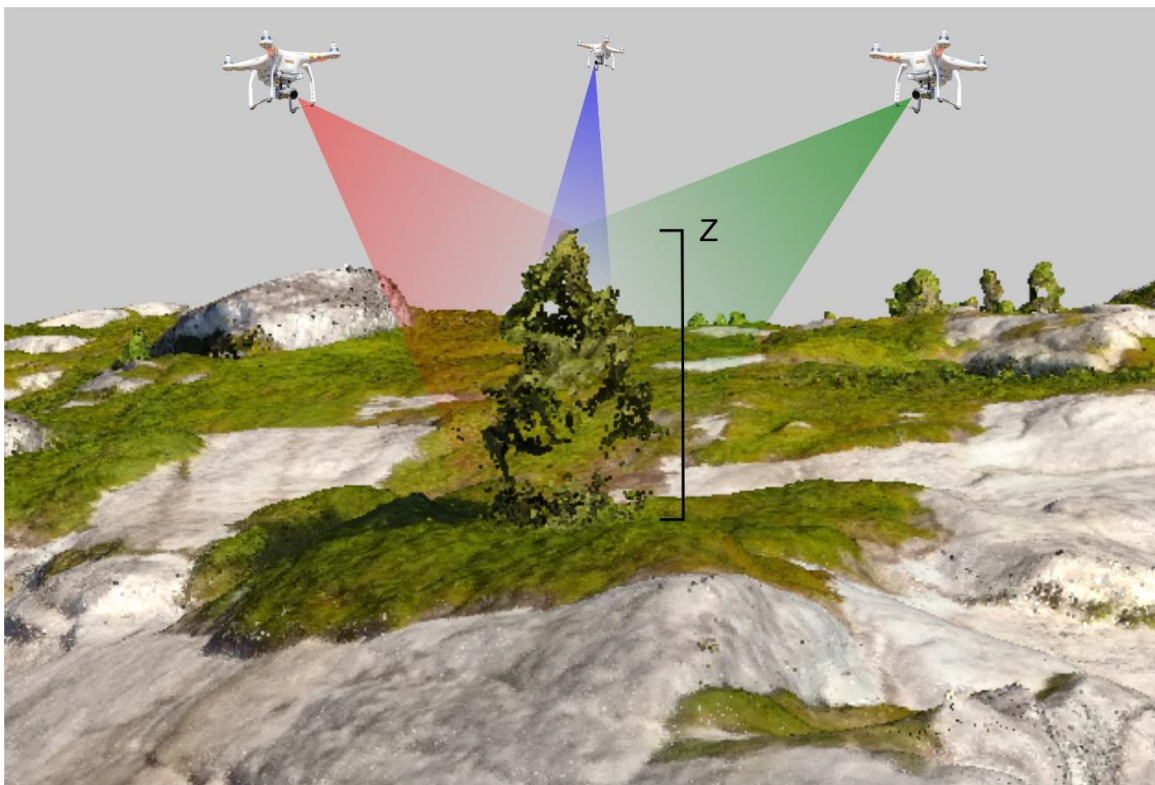


Figure 2.8. An illustration of a tree at Polly's Cove as a 3D point cloud computed from structure from motion photogrammetry.

Images were processed using the SfM software program Agisoft Photoscan Professional (v. 1.3.2, Agisoft LLC, St Petersburg, Russia). Images were first imported and aligned using the *Align Photos* tool and the following settings: *Accuracy* set as 'High', *Generic preselection* unchecked, *Reference preselection* checked, *Key point limit*

set at 40000, *Tie point limit* set at 4000, and *Adaptive camera model fitting* checked. This aligned the UAV imagery and created a preliminary *thin* 3D point cloud. Ground control points were then added to georeference the model, followed by running the *Optimize Cameras* command to update the geolocation of the model. To ensure surveys from the spring accurately overlaid with summer surveys, additional GCPs were created from the DEM of the summer surveys to georeference the spring surveys. Next, the *Build Dense Pointcloud* tool was run with the following settings: *Quality* set as ‘High’ and *Depth filtering* set as ‘Moderate’. The *Quality* setting determines how dense to build the point cloud; selecting ‘High’ means that the point density of the point cloud would be half the value of the pixel size of the original imagery. For example, if the pixel size was 2 cm (flight altitude of ~50 m above ground), the point density at ‘High’ would be roughly one point every 4 cm<sup>2</sup>. For sites with imagery flown at 50 m altitude, this produced point clouds with over 100 million 3D points. Next, the *Build DEM* tool was run with the following settings: *Source data* set as ‘Dense cloud’, *Interpolation* set as ‘Enabled (default)’, and *Resolution* set as the lowest possible value. Creating the DEM (digital elevation model) in the software is necessary to create an orthomosaic, since an elevation model is required to orthorectify the images. Alternatively, you can create a 3D triangulated mesh; however, this produced variable results. Lastly, the *Build Orthomosaic* tool was run with the following settings: *Surface* set as ‘DEM’, *Blending mode* set as ‘Mosaic’, *Enable color correction* unchecked, *Enable hole filling* checked, and *Pixel size (m)* set as the lowest possible value. The final products were then exported: the orthomosaic as a single TIFF file and the 3D point cloud as an LAS file, both of which

can be imported into other software programs for further analysis, such as ArcGIS.

Results from image acquisition and processing can be viewed in Table 2.1.

Table 2.1. Acquisition results of RGB imagery at the study sites and root-mean-square error of the georeferenced models based on ground control points.

<b>Aerial Survey</b>	<b>Ground Resolution (cm)</b>	<b>Number of Images</b>	<b>X error (cm)</b>	<b>Y error (cm)</b>	<b>Z error (cm)</b>	<b>Total error (cm)</b>
Chebucto Head RGB May	4.1	178	2.1	1.9	3.6	4.6
Chebucto Head RGB August	2.2	806	0.5	0.4	0.5	0.8
Prospect Bay RGB May	3.6	215	2.5	2.9	3.2	5
Prospect Bay RGB August	2	763	1	1.7	1.7	2.6
Polly's Cove RGB May	4.3	218	4.6	3.2	4.8	7.4
Polly's Cove RGB August	2.7	780	1.5	0.7	2.7	1.8



In total, 85 indices were extracted from the UAV imagery and 3D point cloud (see full list in Table A1.3). Among them, 60 were spectral indices (Table 2.2) and 25 were structural indices (Table 2.3). The spectral indices were chosen based on previous studies, which included the normalized difference of vegetation Index (NDVI) (Huete et al., 2002), color index of vegetation (CIVE) (Kataoka et al., 2003), hue, saturation, and intensity value (HSV) (Ford and Roberts, 1998; Zheng, Zhang, and Wang, 2009), and other mathematical combinations of red, green, blue, and near-infrared (NIR) channels (Gilmore et al., 2008; Gonçalves et al., 2015; Fraser et al., 2016). NDVI is a function of the NIR and the visible red part of the electromagnetic spectrum:  $(\text{NIR}-\text{R})/(\text{NIR}+\text{R})$ . Chlorophyll in plant leaves are highly reflective of NIR and are more absorbent of the red visible region of the electromagnetic spectrum whereas plants with less chlorophyll, such as unhealthy or stressed plants, show more equal reflectance of the two regions (Ackermann, 2011). Due to the unique responses of vegetation to NIR and r, NDVI has been shown to be very useful in many fields of research involving the mapping of vegetation (Huete et al., 2002). For example, Burai et al. (2015) measured NDVI across an alkali landscape and found that some species and communities could be discriminated solely based on NDVI.

Another potentially useful index for discriminating plant community types is CIVE, proposed by Kataoka et al. (2003):  $0.441*\text{R} - 0.881*\text{G} + 0.385*\text{B} + 18.78745$ . Zheng, Zhang, and Wang (2009) found that CIVE performed well to discriminate vegetation from its surroundings in photographs. Lastly, converting an image from RGB color space to HSV color space has been shown to provide useful information on the colors in an image (Zheng, Zhang, and Wang, 2009; see Table 2.2 for conversion

formulas). Hue describes color as an angle from 0° to 360°, where 0° is red, 120° is green, and 240° is blue (Ford and Roberts, 1998). Saturation refers to the degree to which a color is saturated in white, which measures from 0 to 1. Intensity value is a measure of lightness and darkness, where 0 is black and 1 is white (Ford and Roberts, 1998). Laliberte and Rango (2008) evaluated the use of HSV for mapping rangeland vegetation and found that it helped to produce the most accurate classification model and recommended HSV be used in other vegetation mapping applications.

Table 2.2. Spectral indices derived by UAV imagery.

Index	Description	Source
R	Mean, standard deviation and mean change of the red channel in May and August	Gonçalves et al., 2015
G	Mean, standard deviation and mean change of the green channel in May and August	Gonçalves et al., 2015
B	Mean, standard deviation and mean change of the blue channel in May and August	Gonçalves et al., 2015
R/B	Mean, standard deviation and mean change of the red channel divided by the blue channel in May and August	Gonçalves et al., 2015
R/G	Mean, standard deviation and mean change of the red channel divided by the green channel in May and August	Gonçalves et al., 2015
G/B	Mean, standard deviation and mean change of the green channel divided by the blue channel in May and August	Gonçalves et al., 2015
NIR	Mean, standard deviation and mean change of near-infrared channel in May and August	Gilmore et al., 2008
NDVI	Mean, standard deviation and mean change of normalized difference of vegetation index (NDVI) in May and August $NDVI = \frac{NIR-R}{NIR+R}$	Huete et al., 2002
CIVE	Mean, standard deviation and mean change of color index of vegetation (CIVE) in May and August $CIVE = 0.441 * R - 0.881 * G + 0.385 * B + 18.78745$	Kataoka et al., 2003
Hue	Mean, standard deviation and mean change of the hue in degrees (0-360°) in May and August $Hue = \cos^{-1} \frac{(0.5*(R-G)+(R-B))}{((R-G)^2+(R-B)(G-B))^{0.5}}$	Ford and Roberts, 1998
Saturation	Mean, standard deviation and mean change of the saturation in May and August $Saturation = 1 - \left( \frac{R+G+B}{3} \right) * a$ Where a is the minimum of R, G and B	Ford and Roberts, 1998
Intensity	Mean, standard deviation and mean change of the intensity value in May and August $Intensity = \frac{R+G+B}{3}$	Ford and Roberts, 1998

Structural indices included measures of vegetation height, topographic position index (TPI), curvature (concavity/convexity), slope (degrees), ratio of 3D surface area to the 2D planimetric area, and lastly point cloud density. All structural indices were derived from SfM photogrammetric processing of UAV imagery acquired in August 2016.

Canopy height measurements can be useful metrics for describing physiognomic forms of

plant communities, such as trees and shrubs. Fraser et al. (2016) found that 3D point clouds derived from UAV imagery were accurate in predicting actual canopy heights of arctic shrubs. TPI is a scale-dependent index and involves the use of a search window/neighborhood to determine the relative topographic position of a central point to its surroundings (De Reu et al., 2013). In a forested ecosystem, Zellweger et al. (2013) found that TPI was one of the best predictors for multi-species occurrences. A similar metric to TPI is the deviation from mean elevation (DEV), which is also described by De Reu et al. (2013). DEV normalizes TPI to local surface roughness by dividing TPI by the standard deviation of the neighborhood elevation values (TPI/SD). De Reu et al. (2013) recommended using both DEV and TPI for classification of landform and surface structure. Curvature is another common landscape metric to describe the concavity and convexity of an elevation model, where -1 to 0 is concave and 0 to +1 is convex. Gonçalves et al. (2015) used curvature as a metric to aid in the classification of heathland vegetation. Another useful metric for describing terrain ruggedness is the slope of the terrain, from 0° to 90° (McGarigal et al., 2009), which could be useful for the detection of abrupt edges and the ruggedness of vegetation canopies. Determining the ratio of 3D surface area to the 2D planimetric area of a neighborhood could give a direct measurement of the ruggedness of the terrain or vegetation canopy. Hoechstetter et al. (2008) describe a moving window algorithm to estimate the true 3D surface area, which involves the triangulation of a point cloud, summing the area of the triangles, and then dividing the 3D area by the 2D planar area; this method was used in this study. Lastly, point cloud density is yet another structural index that can potentially provide useful information about canopy structure, with the assumption that a more heterogeneous

surface will require more 3D points for reconstruction than a homogeneous surface. For example, Matthews and Jensen (2013) used point density of a 3D point cloud obtained from a UAV to help model leaf area index (LAI) in a vineyard.

Table 2.3. Structural indices derived by analysis of 3D point clouds and subsequent 10 cm digital elevation models computed from structure from motion photogrammetric processing of UAV imagery.

Index	Description	Source
Vegetation Height	Mean, max, and standard deviation of vegetation heights. Vegetation heights were calculated by subtracting the minimum from the maximum elevation value within a 50 cm search radius of each pixel using the 10 cm elevation model	Corcoran et al., 2015
Topographic Position Index (TPI)	Mean and standard deviation of topographic position index (TPI) from the 10 cm elevation model. Cell search windows included 5x5, 11x11, 33x33 and 111x111 $TPI = z_o - \bar{z}$ Where $z_o$ = elevation of central point, $\bar{z}$ = mean elevation of neighborhood	De Reu et al., 2013
Deviation from Mean Elevation (DEV)	Mean and standard deviation of the deviation from mean elevation (DEV) from the 10 cm elevation model. Cell search windows included 5x5, 11x11, 33x33 and 111x111 $DEV = \frac{z_o - \bar{z}}{SD}$ Where $z_o$ = elevation of central point, $\bar{z}$ = mean elevation of neighborhood, and SD = standard deviation of elevation values in the neighborhood	De Reu et al., 2013
Curvature	Mean and standard deviation of the curvature index (convexity/concavity) from 10 cm elevation model. Calculated using the <i>Curvature</i> tool from the DEM Surface Tools toolbox with <i>Profile</i> setting ( <a href="http://www.jennessent.com/arcgis/surface_area.htm">http://www.jennessent.com/arcgis/surface_area.htm</a> )	Gonçalves et al., 2015
Slope	Mean and standard deviation of the slope (degrees) from 10 cm elevation model. Calculated using the <i>Slope (Spatial Analyst)</i> tool in ArcGIS	McGarigal et al., 2009
3D Surface Area / Planimetric Area Ratio	The ratio of the 3D surface area of the triangulated point cloud and the 2D planimetric area	Hoechstetter et al., 2008
Point Cloud Density	Density of point cloud per m <sup>2</sup>	Ørka and Hauglin, 2016

The goal of the field sampling strategy was to achieve the greatest level of representation of plant community types across each site in a time-efficient and effective

way. Doing so reduced the time required in the field, which was necessary due to the time-constraints of sampling in a single field season, and also minimized impacts on the sites. To achieve this, locations of field plots were determined in three ways. Type I plot locations were determined by analyzing RGB and NIR orthomosaics from UAV imagery to identify distinct vegetation patches to sample in the field. Since the orthomosaics were georeferenced, geographic coordinates could be directly obtained in GIS and subsequently entered into a handheld global positioning service (GPS) with a horizontal accuracy of 5-10 m to find the locations in the field. To help pinpoint the actual location to sample in the field, a down-scaled RGB orthomosaic from the UAV imagery of each site was uploaded as the basemap of the handheld GPS. Type II plots were recorded when unique plant communities or communities that had insufficient sample sizes were encountered in the field. Lastly, Type III plot locations were determined by stratified random sampling. Sites were divided into four sections, followed by generating 6 random field plot locations in each section, a maximum 24 field plots per site. If plot locations did not contain any vegetation or were inaccessible (e.g. on the edge of a cliff), they were omitted from the study. In total, 374 field plots were sampled (Table 2.4).

Table 2.4. The number of field plots of types I, II and III sampled at Chebucto Head, Prospect Bay, and Polly's Cove.

<b>Site</b>	<b>Type I plots</b>	<b>Type II plots</b>	<b>Type III plots</b>
<b>Chebucto Head</b>	62	38	24
<b>Prospect Bay</b>	51	41	24
<b>Polly's Cove</b>	71	40	23
<b>Sum</b>	184	119	71
<b>Grand Total</b>	374		

Field plots were sampled within the three study sites from June to August in 2016. Plots generally measured 4 by 4 m (16 m<sup>2</sup>) except for when plant community patches

were sparse or irregularly shaped. The percent cover of each taxa was visually estimated. Also recorded from plots were photographs and a set of geographic coordinates of the plot center using a Garmin GPSMAP 64S,

Field plots were initially assigned two classifications based on the Canadian National Vegetation Classification (CNVC, 2013): the association level, which is the finest level of the 8-level hierarchy and is based primarily on floristic criteria such as dominant species; and, the formation class, the coarsest level of the 8-level hierarchy, which is based on physiognomy. After confused classes from the association level classification were identified, a third classification was formed: the broadened association level classification.

To extract spectral and structural indices for each plant community from the UAV imagery, plant community patches from field sampling were delineated by manually drawing training polygons in ArcGIS (v. 10.3.1, Environmental Research Systems Institute, Redlands, California). Training polygons are commonly used to extract and compile statistics for mapping classes and play an integral part in creating maps and providing accuracy assessments through ground truthing. Training polygons were drawn around homogeneous patches of vegetation with the help of the UAV imagery, plot photographs, field data sheets, and GPS coordinates from each plot location. Sizes of polygons were meant to represent the sampled areas from field plots, which were approximately 4 by 4 m (16 m<sup>2</sup>); however, in cases when sampled areas contained more than one community type or patches were sparse or irregularly shaped, smaller polygons were drawn. In cases when a plant community type was composed of multiple, smaller patches, multiple polygons were drawn and were treated as a subset.

To extract spectral and structural indices using the training polygons, polygons were first converted to raster zones using the *Polygon to Raster (Spatial Analyst)* tool in ArcGIS. Next, the *Zonal Statistics as Table (Spatial Analyst)* tool in ArcGIS computed statistics for each index within each raster zone/training polygon. Statistics for each index were merged to form a data table consisting of 60 spectral indices (Table 2.2), 25 structural indices (Table 2.3), and columns containing the plant community classification and training sample IDs. This table was later used for statistical analysis.

### **Statistical Analysis**

Statistical analyses were performed in R (v. 3.4.1; R Core Team, 2017). Data were preprocessed prior to data analysis. Only plant community types with a minimum of three field plots were analyzed. All indices were scaled, centered, and checked for normality by plotting histograms. Indices that appeared to be non-normal were transformed if possible. To remove redundant and collinear indices, indices with a greater correlation than  $r^2 = 0.95$  correlation with another index were first removed. Next, a backwards stepwise selection of indices was done using variance inflation factor (VIF) analysis, a common technique for assessing indices for multicollinearity (Mansfield and Helms, 1982). In each step, the index with the highest ‘score’ was removed until all indices had a score less than 10, which is commonly viewed as the cut-off value for indicating multicollinearity. After these indices were removed, the remaining dataset consisted of 36 indices (see Table A1.4).



To determine if there was evidence of spectral and structural differences between plant communities based on indices extracted from processed UAV imagery, linear discriminant analysis (LDA) was performed. LDA is a common classification and dimensionality reduction technique that looks for linear combinations of explanatory variables (the spectral and structural indices) to predict a categorical variable, in this case the plant community type (Fisher, 1936). Like principal components analysis (PCA), it projects the explanatory variables into a set of fewer dimensions/axes to best describe the variance of the variables, but at the same time maximizes class separation. Davidson et al. (2016) found that LDA performed well at classifying low-arctic vegetation and Salovaara et al. (2005) used LDA to classify four different types of tropical rainforest from LANDSAT ETM+ satellite imagery with promising results.

The discriminatory power of the LDA model was assessed in two ways: First, 95% confidence intervals were constructed about the mean ‘scores’ of each plant community type within each discriminatory axis. To determine if confidence intervals overlapped in each discriminatory dimension for every plant community comparison, a matrix was made. The matrix was used to evaluate the number of times each plant community comparison could be differentiated with 95% confidence in at least one of the discriminatory dimensions from the LDA. Plant community comparisons that always had overlapping confidence intervals were considered to be non-differentiable. In the second part of the analysis, the classification accuracy of the LDA model was evaluated using leave-one-out cross validation. Leave-one-out cross validation is a common technique in which one observation/sample is removed from the model training dataset at a time and then the model attempts to classify the unknown testing sample (Molinaro et al., 2005).

This was done for the entire dataset, providing an overall classification accuracy for the LDA model.

The relative importance of each index as it contributed to the LDA model was determined by taking the absolute value of the scalings (i.e., strength of contribution; similar to the loadings in a PCA) for each discriminatory dimension, weighting the scalings by the proportion of contribution of each discriminatory dimension to the LDA model, and lastly summing the weighted scalings from each discriminatory dimension for each index. The result is a relative, unitless “score” of the overall variance explained from each index for the discriminatory model.

Discriminatory analysis was performed on the association level plant community classification and the formation class classification based on field plot data. After confused classes from the association level plant community classification were identified, a broadened association level classification was formed by merging confused classes and was also evaluated.

## Results

Across all sites, a total of 121 plant species were identified from field plot sampling (Table A1.5). Sixty-seven species were found at all three sites. The greatest number of species identified was at Polly’s Cove (101), followed by Prospect Bay (93), then Chebucto Head (84). Polly’s Cove also had the greatest number of unique species to that site (14), followed by Prospect Bay (13), then Chebucto Head (4). The top 10 most frequent species are presented in Table 2.5

Table 2.5. The top 10 most frequent plant species identified from field plot sampling across all sites.

Plant Species Name	Common Name	Frequency (# plots)
<i>Kalmia angustifolia</i>	Sheep Laurel	188
<i>Juniperus communis</i>	Common Juniper	185
<i>Gaylussacia baccata</i>	Black Huckleberry	182
<i>Vaccinium angustifolium</i>	Late Lowbush Blueberry	140
<i>Cornus canadensis</i>	Bunchberry	132
<i>Empetrum nigrum</i>	Black Crowberry	131
<i>Morella pensylvanica</i>	Northern Bayberry	126
<i>Alnus viridis</i>	Green Alder	124
<i>Trientalis borealis</i>	Northern Starflower	119
<i>Pteridium aquilinum</i>	Bracken Fern	118

From the association level plant community classification, 60 plant communities were classified across all sites (Table A1.6). After plant communities with less than three field plots were removed, 33 plant communities remained and were used for statistical analysis (Table 2.6). Merging confused classes to form the broadened association level classification narrowed the list of plant communities to 16 (Table A1.7). Nine plant communities were classified based on the formation class classification: dwarf heath,

shrubland, tree island, bog, salt marsh, brackish marsh, seep, lichen, and other (Tables 2.7 and A1.7).

Table 2.6. List of classes from the association level plant community classification from field plot sampling across all three sites. Plant communities with less than three field plots were removed and not used for statistical analysis.

Association Level Classification	Frequency (# plots)
<i>Abies balsamea</i> tree island	5
<i>Acer rubrum</i> tree island	7
<i>Alnus viridis</i> shrubland	3
<i>Betula papyrifera</i> tree island	9
<i>Calamagrostis canadensis</i> coastal vegetation	3
<i>Carex exilis</i> - <i>Gaylussacia bigeloviana</i> bog	6
<i>Carex nigra</i> bog	13
<i>Cladonia</i> spp.	39
<i>Corema conradii</i> lithomorphic	5
<i>Empetrum nigrum</i> - <i>Juniperus communis</i> dwarf heath	40
<i>Empetrum nigrum</i> dwarf heath	14
<i>Gaylussacia baccata</i> shrub bog	4
<i>Gaylussacia baccata</i> shrubland	79
<i>Gaylussacia bigeloviana</i> shrub bog	9
<i>Gaylussacia bigeloviana</i> shrubland	7
<i>Gaylussacia</i> shrub bog	7
<i>Ilex glabra</i> shrubland	8
<i>Juncus balticus</i> brackish marsh	7
<i>Juniperus communis</i> - <i>Corema conradii</i> lithomorphic	25
<i>Juniperus communis</i> dwarf heath	18
<i>Juniperus horizontalis</i> dwarf heath	8
<i>Larix laricina</i> tree island	8
<i>Maianthemum trifolium</i> bog	3
Mixed tall shrubs	22
<i>Morella pensylvanica</i> shrubland	4
Open bog	13
<i>Osmunda cinnamomea</i> seep	13
<i>Picea glauca</i> tree island	5
<i>Picea mariana</i> tree island	26
<i>Rubus allegheniensis</i> - <i>Morella pensylvanica</i> coastal vegetation	4
<i>Spartina patens</i> salt marsh	4
<i>Spartina pectinata</i> brackish marsh	3
<i>Trichophorum caespitosum</i> bog	11

Table 2.7. List of classes from the formation class plant community classification from field plot sampling across all three sites. Plant communities with less than three field plots were removed and not used for statistical analysis.

Formation Class Classification	Frequency (# plots)
Bog	73
Brackish marsh	3
Dwarf heath	110
Lichen	39
Other	3
Salt marsh	4
Seep	13
Shrubland	127
Tree island	60

When 95% confidence intervals were constructed about the mean LDA scores for each discriminatory axis for classes from the association level plant community classification, only 1 pair (<1%) of 528 possible comparisons of plant communities could not be discriminated in any of the dimensions (see plots of confidence intervals in Figures A1.1A-AF). The pair that could not be discriminated was *Gaylussacia bigeloviana* shrub bog and *Gaylussacia baccata* shrub bog. The top 10 indices that explained the most variance of plant communities for the association level classification are summarized in Table 2.8 (see Table A1.3 for descriptions of indices; see Table A1.8 for complete list). The overall classification accuracy of the LDA model using leave-one-out cross validation for the association level plant community classification was 63%. Table A1.9 lists the plant community classifications in order from best to worst classification accuracy.

Table 2.8. Top 10 indices sorted by their “score” of importance in relation to their contribution to the linear discriminant analysis (LDA) model for each plant community classification. The score was determined by summing the weighted contributions of each index for each discriminatory axis from the LDA model.

Association Level Classification		Broadened Association Level Classification		Formation Class Classification	
Index	Score	Index	Score	Index	Score
R mean May	0.98	R mean May	1.10	R mean May	1.24
Slope SD	0.68	Slope SD	0.75	Slope SD	0.88
Saturation SD May	0.53	R/G mean May	0.51	R/G mean May	0.55
CIVE SD August	0.50	Saturation SD May	0.47	Change R mean	0.40
Change R mean	0.50	Change R mean	0.45	CIVE mean August	0.37
R/G mean May	0.50	TPI mean 5	0.44	CIVE SD August	0.37
Hue SD August	0.42	CIVE mean August	0.39	TPI mean 5	0.36
CIVE mean August	0.39	NIR mean May	0.35	R/B mean May	0.29
TPI mean 5	0.37	R/B mean May	0.33	TPI mean 111	0.28
R/B mean May	0.35	CIVE SD August	0.32	NIR mean May	0.28

Most misclassifications from the association level classification resulted from structurally similar plant communities (Table A1.9). For example, all three field plot locations of *Abies balsamea* tree island were misclassified as *Picea mariana* tree island, both of which are coniferous tree islands. Table A1.7 summarizes how plant community classifications from the association level were merged to form the broadened association level classification to improve classification accuracy.

When the LDA was repeated for the broadened association level plant community classification, all plant communities could be discriminated from each other when the 95% confidence intervals of the mean LDA scores in each discriminatory axis were compared (see Figures A1.2A-O). The top 10 indices that explained the most variance of plant communities for the broadened association level classification are summarized in

Table 2.8 (see Table A1.3 for descriptions of indices; see Table A1.8 for complete list). The overall classification accuracy of the LDA model improved to 83%. Table A1.10 lists plant community classifications from the broadened association level classification in order from best to worst.

In the final LDA, plant communities in the formation class classification could be discriminated from each other with 95% confidence when confidence intervals of the mean LDA scores in each discriminatory dimension were compared (see Figures A1.3A-H). Figure 2.9 illustrates the separation of plant communities from the formation class classification in 3D when the first three LDA dimensions are plotted. The top 10 indices that explained the most variance of plant communities for the formation class classification are summarized in Table 2.8 (see Table A1.3 for descriptions of indices; see Table A1.8 for complete list). The overall classification accuracy of the LDA model improved to 92%. Table A1.11 lists plant community classifications from the formation class classification in order from best to worst.



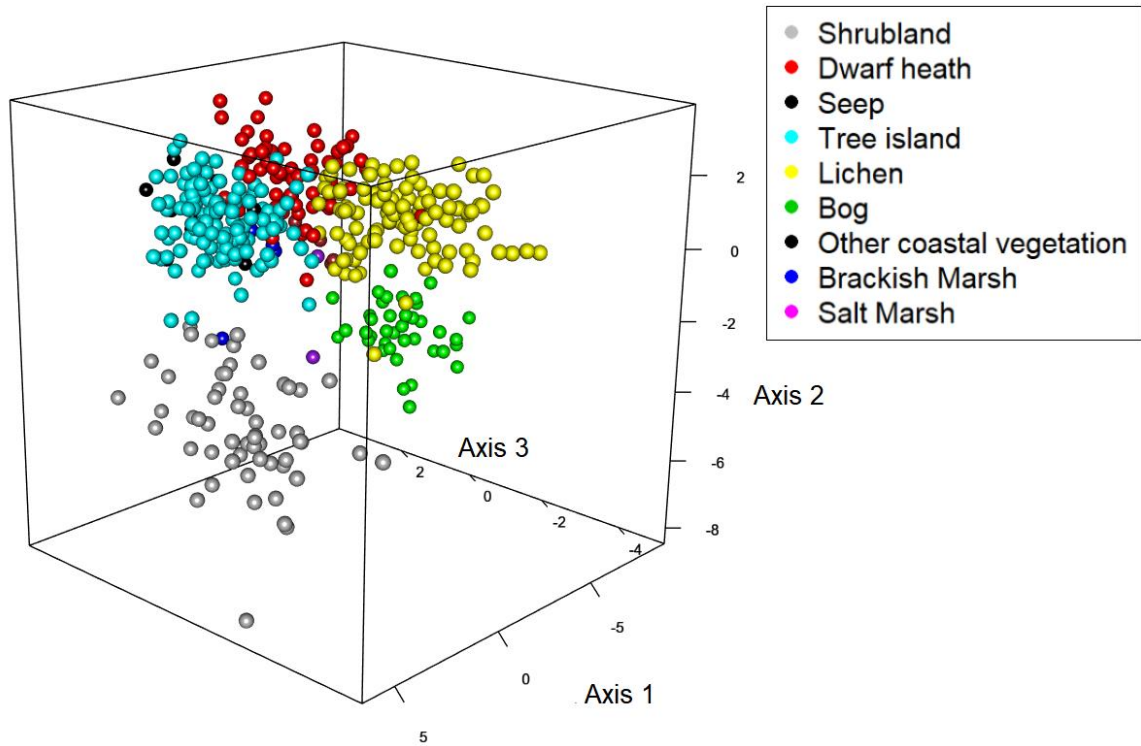


Figure 2.9. Plant communities from the formation class classification projected in the first three dimensions of the linear discriminant analysis model. Linear discriminant analysis projects variables into fewer dimensions while maximizing the separation of a class.

## Discussion

In this study, multispectral UAV imagery was evaluated for its ability to discriminate plant communities at three classification levels in the coastal barrens of Halifax, Nova Scotia. Over 99% of plant community comparisons in the association level plant community classification could be discriminated with 95% confidence. The only pair that could not be discriminated was *Gaylussacia bigeloviana* shrub bog and *Gaylussacia baccata* shrub bog. In most aspects, the shrub bogs appear identical, the only difference being that they were dominated by different species belonging to the same genus. Even in the field, the leaves needed to be closely examined to tell the difference between the two species, which explains why differences between the two communities were not detected using the UAV imagery. It is possible that the two species could be discriminated at a different time of the year, such as the late summer or fall, if they undergo senescence at different times. After the accuracy assessment and confused classes were merged to form the broadened association level classification, effectively reducing the number of classes from 33 to 16, all communities could be discriminated with 95% confidence. The same result was found for the formation class plant community classification. These findings suggest that UAV imagery can be used to discriminate plant communities at different classification levels with high confidence. This further suggests that it is possible to use a UAV to map the locations of plant communities in the coastal barrens at different classification levels, which has not previously been demonstrated.

Overall classification accuracy of the LDA model for the association level classification was moderate at 63%; however, broadening the association level

classification by merging ecologically similar groups that were causing misclassifications increased the overall accuracy to 83%. Overall classification accuracy rose to 92% for the formation class classification. Most misclassifications were found between plant communities that were structurally similar. Part of the reason for misclassifications in the association level classification could be due to the limitations in the spectral and structural indices chosen for the study to discriminate the plant communities. Another reason could be that initial misclassification was caused by uncertainty in assigning classifications to the field plot data. Lastly, differences in spatial resolution of aerial imagery from different surveys as well as the ge positioning error of the handheld GPS and RTK may have introduced error in extracting spectral and structural statistics from field plot locations.

Classifications were not always straightforward: many communities shared similar species but with varying cover, while other communities may not have had any species in common except for the dominant species. These gray areas in assigning classifications made it challenging to determine the appropriate classification names. One such community was *Rubus allegheniensis* - *Morella pensylvanica* coastal vegetation; initially, this community seemed to be an outlier, and there was uncertainty in whether to call it a shrubland or place it in the generic category of 'coastal vegetation'. Upon reviewing the UAV imagery and the spectral and structural characteristics of the plant community, it seemed apparent that the community better fit in the category of shrublands. A similar finding was made for *Carex exilis* - *Gaylussacia bigeloviana* bog; at first, the community was classified simply as a bog dominated by sedges and dwarf shrubs; however, when the community was analyzed with the UAV imagery, it became

clear that the community was most like shrub bogs rather than grass/sedge/open bogs. Utilizing the UAV imagery in this way can support the classification of plant communities, providing a bird's eye view of how the communities appear from above and offering information on their spectral and structural characteristics in high-resolution as another line of evidence for forming the classifications.

Sample size, i.e. the number of field plots sampled per community type, is another factor that may have impacted the classification results of the LDA model (Burley, 2009). Low sample size for vegetation sampling was unavoidable for finer classification levels; some plant community types may only have one occurrence within a site, and in other cases patches can go undetected when field sampling. A solution to this problem is merging classes with low sample sizes to form broader classes, which was done in the broad association level classification. One consequence of merging classes to form a broader class, however, is that within-class variance is increased, which may cause more misclassifications to occur between otherwise dissimilar plant communities.

The two indices that explained the most variance of the LDA models for the association level classification, the broadened association level classification and for the formation class classification were the red band from the May imagery and the standard deviation of the canopy's slopes, respectively. Other top indices included Saturation SD May, R/G mean May, and change in R mean. Most of the important indices were spectral indices from May imagery; however, some indices from August were important as well. This makes sense, because most of the vegetation in August appears in the imagery as a bright green color, while in May there is a much greater contrast between vegetation types: shrublands appear brown due to leafless branches being exposed, dwarf heaths are

different shades of green or yellow, coniferous trees are different shades of green and deciduous trees are without leaves and appear as brown or grey. However, some plant communities, such as herbaceous vegetation, may only be observable in the summer or fall and not in the spring. Another consideration that needs to be made is that imagery in the spring had slightly coarser spatial resolutions (4cm) compared to imagery in the summer (2cm), which may have also influenced classification accuracy. Furthermore, flight conditions in the spring at the three sites were in cloudy or partly cloudy conditions while all surveys in the summer were conducted in full sun, which may have further influenced the ability to discriminate vegetation. Although the springtime seems to be the most advantageous time to discriminate plant communities in the coastal barrens of Halifax, Nova Scotia, collecting imagery from more than one season may be necessary to observe and discriminate all plant community types depending on the level of classification.

Some studies have found NIR to be very useful for discriminating plant communities and even species (Anderson, 1970; Gilmore et al., 2008; Adam et al., 2010), since chlorophyll in plant leaves are highly reflective of the NIR region of the electromagnetic spectrum (Galidaki et al., 2017). In this study, indices derived from the NIR sensor of the UAV did not appear to be as important for discriminating the plant communities as anticipated. The index NIR mean May, however, was listed among the top 10 most important indices for discriminating plant communities for both the broadened association level classification and for the formation class classification. It is possible that the coarser spatial resolution of the NIR sensor (generally 2x coarser than the RGB sensor) reduced the ability of the NIR band to discriminate plant community

types, and that surveys should be conducted lower to the ground to detect greater statistical differences in the vegetation.

Interestingly, the standard deviation of the slope of the vegetation canopies was the second most important index for discriminating plant communities in all three classification levels. Also, the mean topographic position index calculated within a 5-pixel search window consistently scored in the top 10 most important indices for discriminating plant communities. Providing that SfM photogrammetry can accurately reconstruct the vegetation canopies in 3D as previous studies have found (Fraser et al., 2016), it is rational that some structural indices would be important for discriminating plant community types, especially plant communities in the formation class classification, which is based primarily on physiognomy. The finding that structural indices were important for discriminating plant communities across multiple classification levels highlights the value of collecting 3D structural information for discriminating vegetation.

One limitation with using hue as a spectral index is that it is circular. Values for hue range from 0 to 360°, where 0° is red, 120° is green, and 240° is blue (Ford and Roberts, 1998). Hue may be a useful index to discriminate vegetation types; however, computing linear statistics on a circular index would give misleading results and is most likely the reason hue was not found to be important in the linear discriminant analysis. In a similar case, Monk et al. (2011) converted aspect, a circular variable describing bearing or direction from 0 to 360°, to two linear variables: northness and eastness. Converting hue in a similar manner to two linear indices may solve this issue and should be explored in future studies.

Determining the flight altitude above ground is an important consideration for collecting UAV imagery. It directly correlates with the ground resolution/pixel size of each image. For example, if an image is captured at 90 m altitude relative to the ground, the ground resolution will be approximately 4 cm with the UAV's RGB camera and 8 cm with the NIR sensor compared to only 2 cm and 4 cm respectively if flown at 50 m altitude. Point clouds from 50 meters above ground had much greater structural detail than images captured at 90 meters. Furthermore, it was much easier to discern important details of the vegetation using imagery collected from lower flight altitudes. There are, however, some drawbacks with flying lower altitudes. One such consideration is wildlife: the lower an aircraft is flown, the more likely wildlife, such as birds, are to respond, become stressed, and become aggressive towards the aircraft (Ditmer et al., 2015; Vas et al., 2015; Lyons et al., 2017), which creates unsafe conditions due to risks of collision. In this study, there were two close encounters with sea gulls when the UAV was flown near their nesting sites. For surveying large areas, it may not be practical and safe to fly much lower than 50 m altitude above the ground. Another consideration is time: the lower the aircraft is flown to the ground, the more images are needed to be acquired to achieve enough image overlap to accurately mosaic images and compute 3D information by SfM photogrammetry, due to the reduced field of view as objects get closer to the sensor. To survey one of the sites in this study (each study occupied approximately 25 ha), it required 2 batteries and roughly 40 minutes of flight time when flown at 90 meters altitude compared to 3 batteries and over an hour to fly at 50 meters altitude. Although a high image overlap was programmed into the Pix4DCapture app for the surveys conducted in this study, some images from low altitude surveys were difficult to align

during image processing and needed manual tiepoints. It is recommended that if UAV surveys are conducted closer to the ground, ensure that there is enough image overlap and sidelap for each survey, preferably 80% and 60% respectively.

Choosing a higher altitude in the spring followed by a lower altitude in the summer was a limitation in this study. Imagery acquired at lower altitudes had inherently higher spatial resolution than the higher altitude imagery. The resulting differences in spatial resolution made the surveys not directly comparable for discriminating the plant communities. If multiple surveys are conducted for temporal analysis, it is advisable to choose one above-ground altitude for aerial surveys to achieve consistent spatial resolutions and allow the imagery to be directly comparable.

No matter the remote sensing platform, weather conditions will affect the quality and output of a sensor, with UAVs being no exception. During this study, many environmental factors and weather conditions were found to affect the quality of images acquired. Particularly in coastal areas, winds can be a challenge for operating a UAV. High winds can cause difficulties in controlling the aircraft, reducing battery life and consequently flight time, and can even cause some images to appear blurry due to shaking of the aircraft and sensor. To avoid high winds, UAV surveys were generally conducted in the mornings or early afternoons before winds got above 30 km/h. Another factor that should be considered is insolation and scene illumination. The intensity and angle of illumination of the sun changes constantly, and depends on the time of day, time of year, as well as atmospheric conditions such as cloud cover. One example of this is when images collected in the spring and the summer are compared: evergreen vegetation in the summer appeared much brighter in images compared to the same evergreen



vegetation in May, simply because the angle of insolation in May was lower than in the summer, causing less solar radiation to be reflected towards the sensor. Variability in insolation can alter the spectral statistics of an image, which can have consequences for image analysis and should be considered when comparing multiple surveys.

An observed effect of insolation in this study was the opposition surge, also known as the opposition effect or hot-spot effect. The opposition surge is an optical phenomenon that is caused when the phase angle, the angle between the observer and the light source, approaches  $0^\circ$  (Burratti, Hillier, and Wang, 1996). It can cause bright hues to appear in images and was observed in this study when UAV imagery was collected in the summer, when the insolation angle was at its peak (see Figure 2.10). Interestingly, the opposition surge was not observed in the spring imagery, likely since the angle of insolation was much lower. To avoid the effects of opposition surge, it is recommended to fly earlier in the day when the angle of the sun is lower, especially around summer solstice.

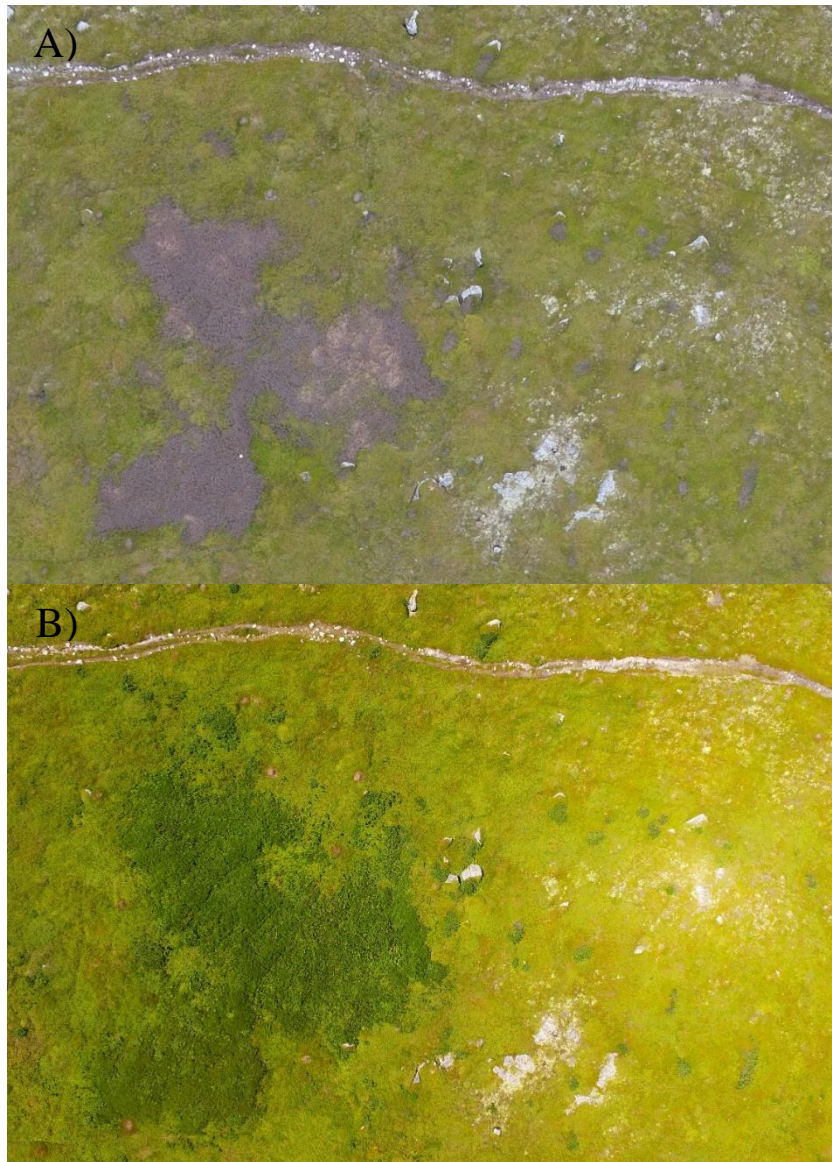


Figure 2.10. An example of the opposition surge in UAV imagery, also known as the hot-spot effect or opposition effect (A and B). A) was captured in May of 2016 at Prospect Bay and shows no opposition surge because the angle of insolation in the spring is relatively low; B) was captured in July of 2016 and shows the opposition surge manifested in the eastern part of the image as a bright hue. The optical phenomenon occurs when the phase angle, the angle between the observer and the light source, approaches  $0^\circ$ .

Aside from the opposition surge, most problems with varying intensity of illumination within and between surveys can be mitigated by configuring the settings of the sensor and through image post-processing. Fixing the white balance and exposure

settings to a constant value for an RGB camera will help to keep scene illumination constant (Dandois, 2014). An alternative is to collect only raw, unaltered images. The disadvantage with collecting raw images is that it is memory intensive and requires a lot of storage space, especially when capturing hundreds of images for a single survey. Although it was not done in this study, another option is to radiometrically calibrate the sensor before each survey. This can be done by capturing an image of a radiometrically calibrated target, and then correcting the values of all the images collected in that survey to the known radiometric values of the radiometrically calibrated target (Kelcey and Lucieer, 2012). If done for each survey, images from one survey to another would theoretically be radiometrically comparable, likely enhancing the ability of aerial surveys to discriminate vegetation types.

Despite the effects of weather conditions, such as variability in insolation within and between surveys on acquired UAV imagery in this study, evidence of statistical differences between plant communities were still found. It is hypothesized that if mitigation measures are taken to control scene illumination, such as fixing white balance and even radiometrically calibrating the sensor prior to each flight, the variance in spectral and structural measurements of plant community types will decrease and evidence of statistical differences will become even more apparent.

Processing UAV imagery requires a lot of time, computing power and trial and error. Processing the imagery by far took the most time of any task in this study. The most time-consuming part of processing the UAV imagery was producing the dense 3D point cloud. It took one or two days to produce a point cloud for one of the surveyed sites using the 'high' density setting in Agisoft. The 'Ultra high' setting was not possible to

execute because the computer used to process the images did not have enough memory. Choosing the 'high' density setting provided plenty of structural detail for the vegetation, producing over a hundred million 3D points across a 25-hectare site flown at 50 meters altitude. It is recommended to ensure the computer used to process the UAV imagery has sufficient memory for the task.

The quality of the orthomosaics produced by Agisoft was excellent. Break lines and other artifacts created by mosaicking the images were rare and the opposition surge observed in some surveys conducted in the summer was mostly mitigated since landscape features that may have occurred within a hot-spot in one image were observed from different angles in other images. The orthomosaics made it possible to view the entirety of each study site in very high resolution and allowed for the computation of spectral statistics to help discriminate the plant communities.

The overall quality of the 3D point clouds produced from SfM photogrammetric processing of the UAV imagery was very good. Errors in 3D reconstruction of vegetation and other landscape features were seldom observed. Trees and shrubs were accurately reconstructed; however, canopy heights were generally underestimated based on field measurements, which is consistent with Fraser et al. (2016) and Aasen et al. (2015). Underestimates of canopy height mostly occur because the ground is not directly visible from the aircraft since it is often blocked by foliage, consequently not allowing a 3D measurement of the ground to be taken. Canopy height measurements from UAV imagery therefore represent the difference between the top of the canopy and the point nearest the ground. This is a general limitation with current 3D reconstruction techniques using UAV imagery alone. Improved processing algorithms may help to produce better

bare-earth (ground) models from UAV imagery and achieve better estimates of true canopy height of the vegetation.

Featureless and homogeneous surfaces can cause problems in image stitching and computation of 3D information using SfM photogrammetry (Eltner et al., 2015). To mosaic images and compute 3D information, the software needs to identify features/objects to match images. This issue was apparent when processing images in the summer, particularly NIR imagery. NIR imagery had slightly lower resolution than the RGB imagery (4 cm pixels compared to 2 cm pixels at 50 meters altitude), and vegetation captured in the summer can appear very homogeneous, causing certain parts of the study sites to have poor image matching. Some options exist to alleviate these problems. Flying at a higher altitude will reduce image resolution but increase the viewshed of each image, possibly allowing for the detection of more features to match. Another option, which proved successful in this study, is to create manual tie points for the problematic images within the software, which is like georeferencing a set of images with GCPs except manual tie points are only created in the software and are determined solely by the user specifically to help match images, since it is likely that some features in the images are still recognizable by the user, even though the software was not able to create matches.

One of the greatest challenges with processing the UAV imagery was accurately georeferencing the surveys and having the surveys accurately overlay on top of each other. Initially, using 10-12 GCPs per site allowed surveys to overlay with moderate precision. In some areas, particularly between GCPs, positioning errors from one survey to another ranged from one to several feet. It is hypothesized that this was caused by landforms, such as boulders and hills, being captured from slightly different viewing

angles of the aircraft from one survey to another, giving the perception that parts of the landscape were shifting while other parts remained in the same place. Normally, orthorectifying the images using a digital elevation model is meant to mitigate this problem; however, distortions and positioning errors were still noticeable after the initial georeferencing. To mitigate this issue in this study, summer surveys were treated as the reference and additional targets were created across each site in ArcGIS, which were then incorporated for the georeferencing of the spring surveys. This allowed the surveys to overlay much better, reducing most of the positioning errors to only a few centimeters, and prevented the need to go back into the field to collect more GCPs and re-survey the sites.

The results of this study emphasize the value and effectiveness of using UAVs to discriminate and map plant communities in the coastal barrens. Although UAVs currently have some limitations, such as constraints on survey size due to battery life, inability to penetrate the canopy to obtain elevation measurements directly from the ground with standard sensors, and continued tightening of regulations of operating UAVs, their benefits for research in plant ecology are many fold: low cost, adaptability for equipping different kinds of sensors, including hyperspectral sensors, ease of access to difficult sites, and high spatial, spectral, and temporal resolution (Cruzan et al., 2016).

Satellite imagery has been successfully used to map broad categories of vegetation (Ustin and Gamon, 2010); however, they have not yet been adequate for mapping plant communities at the fine scale, particularly in the coastal barrens where landscapes are patchworks of plant communities. This is because pixel sizes from satellite imagery are usually greater than 1m, which would be insufficient to resolve the important

details of vegetation (Adam et al., 2010; Cruzan et al., 2016). Furthermore, satellites currently lack the ability to collect high-resolution 3D structural information of vegetation canopies, which was found to be very useful for discriminating the plant communities in this study. Nonetheless, satellite technology is improving very quickly and could eventually be very useful for fine scale mapping of vegetation, especially with multispectral sensors.

Manned aircraft can obtain imagery with sub-meter resolution and can also be equipped with high-powered sensors like hyperspectral and LIDAR (Light Detection and Ranging). LIDAR emits laser pulses to collect 3D data about the earth's surface. Studies have found that it is useful for assessing canopy heights of vegetation, since the laser pulses can penetrate canopies and provide ground signal returns (Baltsavias, 1999; Asner et al., 2015); however, when compared to SfM photogrammetry from a UAV, LIDAR from traditional aircraft platforms are unable to achieve the spatial resolution needed to reconstruct fine-scale geomorphological features (Kalacska et al., 2017). Furthermore, employing manned aircraft is much costlier than the costs associated with purchasing most UAVs. More recently, ground-based LIDAR have been used in various applications to create highly detailed 3D point clouds with sub-centimeter resolution, providing the ability to accurately quantify biomass of vegetation and compute biophysical parameters such as leaf area index (LAI) (Loudermilk et al., 2009). This application of LIDAR shows potential for mapping vegetation structure; however, currently costs are very high for collecting ground LIDAR and it is limited to relatively small areas (Kalacska et al., 2017).

Although it was not within the scope of this study to compare different remote sensing platforms, it may be worthwhile in future studies to examine which platform or combination of platforms yield the best results for discriminating plant communities at the fine scale.

One of the greatest controversies in the field of ecology has been the debate of whether plant communities exist as discrete, recognizable units (Clements, 1916) versus existing as a continuum of species along environmental gradients (Gleason, 1926). Although it is generally agreed upon that species are distributed individualistically, there is also growing agreement that assemblages of species as communities can be recognized as identifiable units (van der Maarel and Franklin, 2013). Porter (2013) used clustering analysis to identify three distinct dwarf heath plant communities occurring in the coastal barrens of Nova Scotia. These communities were recurring across multiple sites, had similar species abundances and compositions, and had similarly associated environmental conditions. The findings of this study add support to the modern synthesis of the two plant community paradigms: upon reviewing the field plot data, it was clear that no two field plots were exactly the same compositionally, which is in agreement with Gleason's view of species distributions; however, it was also evident that patterns existed in the field plot data, and statistical analysis of UAV imagery showed that evidence of differences between the classified plant communities existed, suggesting that plant communities in the coastal barrens of Halifax, Nova Scotia can be recognized as discrete units.



## **Implications and Future Work**

This study offers the first empirical evidence that UAVs can be used to discriminate plant communities at different classification levels in the coastal barrens. This means that, with a certain level of confidence, the distributions of plant communities can be mapped. Distribution maps of the communities at a fine scale have not yet been possible for the coastal barrens, and producing them will help to further our understanding of the spatial patterns of the plant communities, learn more about the processes that form and change them and the ecosystem as a whole, assess ecosystem health, estimate biophysical parameters such as biomass, and focus conservation efforts (Grossman et al., 1994; He et al., 2005; Tart et al., 2005; Adam et al., 2010). It is also possible to use the statistical information to build a spectral and structural library of the known plant community types to help locate communities and predict their distributions in previously unknown areas (Zomer, Trabucco, & Ustin, 2009). This can further make field sampling efforts more focused and efficient. Lastly, when assigning plant community classification based on field plot data alone was difficult, UAV imagery offered a bird's eye view of the field plots and offered spectral and 3D structural information as another line of evidence to form the classifications. The use for UAVs in plant ecology research may not be limited to only vegetation mapping, but also for assisting field work and how ecologists describe and define plant communities.

The next steps forward are to apply the knowledge from this study to produce fine scale distribution maps of plant communities in the coastal barrens. This will improve our understanding of the spatial patterns and distributions of the plant communities that inhabit the coastal barrens, in which information is currently limited. Future work should

continue to investigate other potentially useful spectral and structural indices that can be derived from processed multispectral UAV imagery to discriminate plant communities, in addition to exploring the use of image texture metrics, i.e. statistics on the spatial arrangements of colors and intensities in an image. Doing so would likely improve classification accuracies of the plant communities from UAV imagery. It would also be worthwhile comparing UAVs with other remote sensing platforms for mapping plant communities in the coastal barrens. Furthermore, identifying the most optimal spatial resolution for collecting spectral, structural, and textural statistics as well as season to discriminate plant communities based on plant phenologies would further enhance mapping efforts. Lastly, UAVs equipped with hyperspectral sensors, although relatively costly, have already been shown to discriminate vegetation at the species level (Nevalainen et al., 2017) and should be a consideration for discriminating and mapping plant communities in the coastal barrens and other ecosystems.

## Conclusion

In this study, a UAV equipped with RGB and NIR sensors was used to determine if plant communities can be discriminated from each other in the coastal barrens of Halifax, Nova Scotia. All plant community classification except for one pair could be discriminated with 95% confidence. The formation class classification yielded higher classification accuracies than the association level classification. Most confusion was found between structurally similar classifications, and merging confused groups substantially increased classification accuracy. These results show that when spectral and structural characteristics of vegetation are extracted from multispectral UAV imagery, plant communities can be discriminated and recognized as discrete units, adding support to the modern synthesis of Gleason's (1926) and Clements' (1916) views that, although species may be distributed individualistically, assemblages of species as communities can be recognized as identifiable units. Furthermore, the findings suggest that plant communities can be mapped in the coastal barrens at different classification levels using UAVs, which has not been demonstrated until now. Producing detailed distribution maps of plant communities can be directly used to focus conservation efforts and manage the protection of these ecosystems while also telling a great deal about the spatial patterns of the plant communities and the processes that govern them. Future research should begin using UAV imagery to map the distributions of plant communities in the coastal barrens and investigate ways to optimize image acquisition and processing techniques to discriminate plant communities with the greatest level of confidence.

## References

- Aasen, H., Burkart, A., Bolten, A., & Bareth, G. (2015). Generating 3D hyperspectral information with lightweight UAV snapshot cameras for vegetation monitoring: from camera calibration to quality assurance. *ISPRS Journal of Photogrammetry and Remote Sensing*, *108*, 245-259.
- Ackermann, E. R. (2011). *Sequential land cover classification*. (Doctoral dissertation, University of Pretoria).
- Adam, E., Mutanga, O., & Rugege, D. (2010). Multispectral and hyperspectral remote sensing for identification and mapping of wetland vegetation: a review. *Wetlands Ecology and Management*, *18*(3), 281-296.
- Agisoft Photoscan Professional (Version 1.3.2) [Software]. (2017). Retrieved from <http://www.agisoft.com/downloads/installer/>.
- Anderson, R. C., Fralish, J. S. & Baskin, J. M. (1999). Savannas, barrens, and rock outcrop plant communities of North America. Cambridge University Press, Cambridge, UK.
- Anderson, R. R. (1970). Spectral reflectance characteristics and automated data reduction techniques which identify wetland and water quality conditions in the Chesapeake Bay.
- ArcGIS (Version 10.3.1) [Software]. (2014). Environmental Systems Research Institute (ESRI), Redlands, California.
- Asner, G. P., Ustin, S. L., Townsend, P. A., Martin, R. E., & Chadwick, K. D. (2015). Forest biophysical and biochemical properties from hyperspectral and LiDAR remote sensing. *Land resources monitoring, modeling and mapping with remote sensing*. CRC Press, Taylor & Francis Group, 429-448.
- Baltsavias, E. P. (1999). A comparison between photogrammetry and laser scanning. *ISPRS Journal of photogrammetry and Remote Sensing*, *54*(2), 83-94.
- Buratti, B. J., Hillier, J. K., & Wang, M. (1996). The lunar opposition surge: Observations by Clementine. *Icarus*, *124*(2), 490-499.
- Burley, S. T. (2009). Forest expansion into coastal barrens in Nova Scotia, Canada.
- Burley, S. T., & Lundholm, J. T. (2010). Environmental predictors of forest expansion on open coastal barrens. *Biodiversity and Conservation*, *19*(11), 3269-3285.

- Burley, S. T., Harper, K. A., & Lundholm, J. T. (2010). Vegetation composition, structure and soil properties across coastal forest–barren ecotones. *Plant Ecology*, *211*(2), 279-296.
- Cameron, R. P., & Bondrup-Nielsen, S. (2013). Plant Communities within Atlantic Coastal Heathlands in Nova Scotia. *Northeastern Naturalist*, *20*(4).
- Canadian National Vegetation Classification (CNVC) [online] 2013. Sault Ste. Marie, ON, Canada. Accessed 2015. Accessed on October 08, 2017 from: <http://cnvc-cnvc.ca>.
- Clements, F. (1916). *Plant succession: An analysis of the development of vegetation*. Washington, DC: Carnegie Institute of Washington Publication.
- Corcoran, J., Knight, J., Pelletier, K., Rampi, L., & Wang, Y. (2015). The effects of point or polygon based training data on RandomForest classification accuracy of wetlands. *Remote Sensing*, *7*(4), 4002-4025.
- Cruzan, M. B., Weinstein, B. G., Grasty, M. R., Kohn, B. F., Hendrickson, E. C., Arredondo, T. M., & Thompson, P. G. (2016). Small unmanned aerial vehicles (micro-UAVs, drones) in plant ecology. *Applications in Plant Sciences*, *4*(9), 1600041.
- Dandois, J. P. (2014). *Remote sensing of vegetation structure using computer vision*. University of Maryland, Baltimore County.
- Dandois, J. P., & Ellis, E. C. (2013). High spatial resolution three-dimensional mapping of vegetation spectral dynamics using computer vision. *Remote Sensing of Environment*, *136*, 259-276.
- Davidson, S. J., Santos, M. J., Sloan, V. L., Watts, J. D., Phoenix, G. K., Oechel, W. C., & Zona, D. (2016). Mapping Arctic Tundra Vegetation Communities Using Field Spectroscopy and Multispectral Satellite Data in North Alaska, USA. *Remote Sensing*, *8*(12), 978.
- De Reu, J., Bourgeois, J., Bats, M., Zwertvaegher, A., Gelorini, V., De Smedt, P., ... & Van Meirvenne, M. (2013). Application of the topographic position index to heterogeneous landscapes. *Geomorphology*, *186*, 39-49.
- Ditmer, M. A., Vincent, J. B., Werden, L. K., Tanner, J. C., Laske, T. G., Iaizzo, P. A., ... & Fieberg, J. R. (2015). Bears show a physiological but limited behavioral response to unmanned aerial vehicles. *Current Biology*, *25*(17), 2278-2283.
- Demers, M. N. (1991). Classification and purpose in automated vegetation maps. *Geographical Review*, 267-280.

- Eltner, A., Kaiser, A., Castillo, C., Rock, G., Neugirg, F., & Abellan, A. (2015). Image-based surface reconstruction in geomorphometry—merits, limits and developments of a promising tool for geoscientists. *Image*, 3, 1445-1508.
- Faber-Langendoen, D., Keeler-Wolf, T., Meidinger, D., Tart, D., Hoagland, B., Josse, C., ... & Comer, P. (2014). EcoVeg: a new approach to vegetation description and classification. *Ecological Monographs*, 84(4), 533-561.
- Ferrier, S. (2002). Mapping spatial pattern in biodiversity for regional conservation planning: where to from here?. *Systematic biology*, 51(2), 331-363.
- Fisher, R. A. (1936). The use of multiple measurements in taxonomic problems. *Annals of human genetics*, 7(2), 179-188.
- Ford, A., & Roberts, A. (1998). Colour space conversions. *Westminster University, London, 1998*, 1-31.
- Franklin, J. (2010). Mapping species distributions: spatial inference and prediction. Cambridge University Press.
- Fraser, R., Olthof, I., Lantz, T. C., & Schmitt, C. (2016). UAV Photogrammetry for Mapping Vegetation in the Low-Arctic. *Arctic Science*, (ja).
- Galidaki, G., Zianis, D., Gitas, I., Radoglou, K., Karathanassi, V., Tsakiri–Strati, M., ... & Mallinis, G. (2017). Vegetation biomass estimation with remote sensing: focus on forest and other wooded land over the Mediterranean ecosystem. *International Journal of Remote Sensing*, 38(7), 1940-1966.
- Gilmore, M. S., Wilson, E. H., Barrett, N., Civco, D. L., Prisloe, S., Hurd, J. D., & Chadwick, C. (2008). Integrating multi-temporal spectral and structural information to map wetland vegetation in a lower Connecticut River tidal marsh. *Remote Sensing of Environment*, 112(11), 4048-4060.
- Gleason, H. A. (1926). The individualistic concept of the plant association. *Bulletin of the Torrey botanical club*, 7-26.
- Gonçalves, J., Henriques, R., Alves, P., Sousa-Silva, R., Monteiro, A. T., Lomba, Â., ... & Honrado, J. (2015). Evaluating an unmanned aerial vehicle-based approach for assessing habitat extent and condition in fine-scale early successional mountain mosaics. *Applied Vegetation Science*.
- Grossman, D. H., Goodin, K. L., Li, X., Faber-Langendoen, D., Anderson, M., Bourgeron, P., & Vaughn, R. (1994). Field Methods For Vegetation Mapping. NBS/NPS Vegetation Mapping Program. The Nature Conservancy, Arlington, VA, and Environmental Systems Research Institute, Redlands, CA.

Guillot, B., & Pouget, F. (2015). Uav Application in Coastal Environment, Example of the Oleron Island for Dunes and Dikes Survey. *The International Archives of Photogrammetry, Remote Sensing and Spatial Information Sciences*, 40(3), 321.

He, C., Zhang, Q., Li, Y., Li, X., & Shi, P. (2005). Zoning grassland protection area using remote sensing and cellular automata modeling—a case study in Xilingol steppe grassland in northern China. *Journal of Arid Environments*, 63(4), 814-826.

He, K. S., Bradley, B. A., Cord, A. F., Rocchini, D., Tuanmu, M. N., Schmidtlein, S., ... & Pettorelli, N. (2015). Will remote sensing shape the next generation of species distribution models?. *Remote Sensing in Ecology and Conservation*, 1(1), 4-18.

Heumann, B. W., Hackett, R. A., & Monfils, A. K. (2015). Testing the spectral diversity hypothesis using spectroscopy data in a simulated wetland community. *Ecological Informatics*, 25, 29-34.

Hoechstetter, S., Walz, U., Dang, L. H., & Thinh, N. X. (2008). Effects of topography and surface roughness in analyses of landscape structure—a proposal to modify the existing set of landscape metrics. *Landscape Online*, 3, 1-14.

Huete, A., Didan, K., Miura, T., Rodriguez, E. P., Gao, X., & Ferreira, L. G. (2002). Overview of the radiometric and biophysical performance of the MODIS vegetation indices. *Remote Sensing of Environment*, 83(1), 195-213.

Jenness, J. (2013). DEM Surface Tools. Jenness Enterprises. Available at: [http://www.jennessent.com/arcgis/surface\\_area.htm](http://www.jennessent.com/arcgis/surface_area.htm).

Kalacska, M., Chmura, G. L., Lucanus, O., Bérubé, D., & Arroyo-Mora, J. P. (2017). Structure from motion will revolutionize analyses of tidal wetland landscapes. *Remote Sensing of Environment*, 199, 14-24.

Kataoka, T., Kaneko, T., Okamoto, H., & Hata, S. (2003). Crop growth estimation system using machine vision. *Advanced Intelligent Mechatronics*, 2, 1079-1083.

Kelcey, J., & Lucieer, A. (2012). Sensor correction and radiometric calibration of a 6-band multispectral imaging sensor for UAV remote sensing. In *The 12th Congress of the International Society for Photogrammetry and Remote Sensing*, 39, 393-398.

Laliberte, A. S., & Rango, A. (2008). Incorporation of texture, intensity, hue, and saturation for rangeland monitoring with unmanned aircraft imagery. *The International Archives of the Photogrammetry, Remote Sensing, and Spatial Information Sciences*.

Loudermilk, E. L., Hiers, J. K., O'Brien, J. J., Mitchell, R. J., Singhania, A., Fernandez, J. C., ... & Slatton, K. C. (2009). Ground-based LIDAR: a novel approach to quantify fine-scale fuelbed characteristics. *International Journal of Wildland Fire*, 18(6), 676-685.

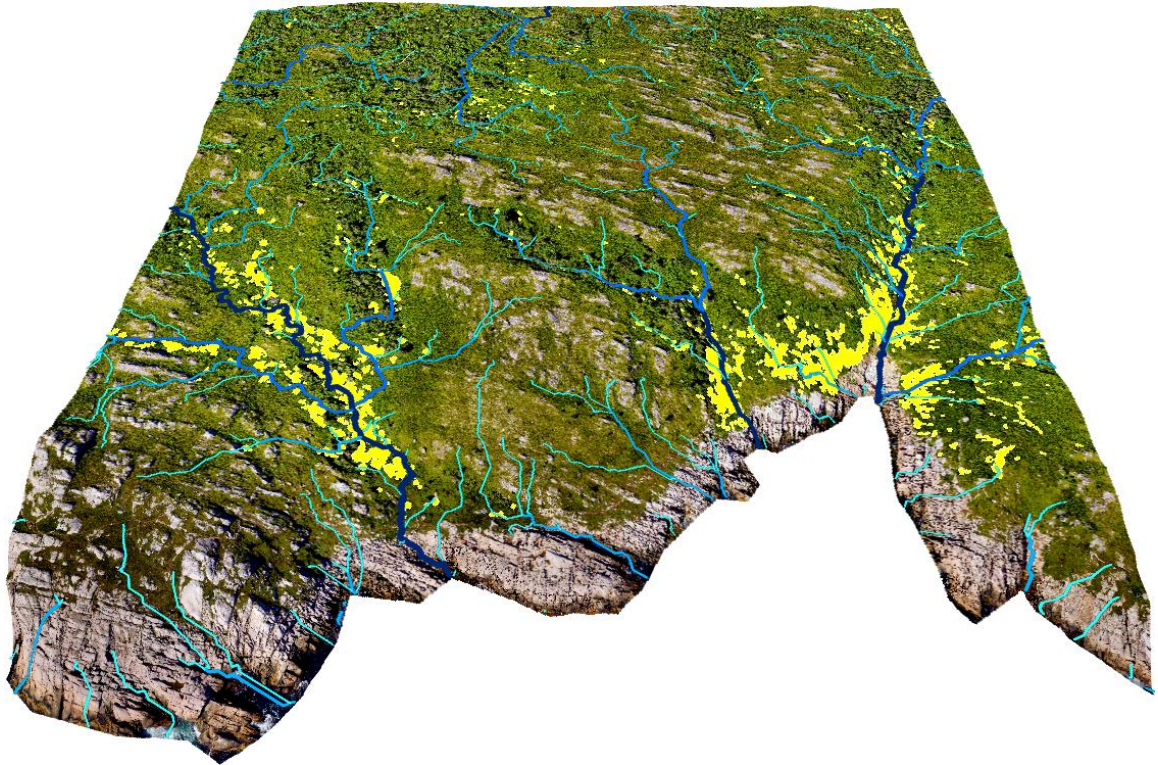
- Lyons, M., Brandis, K., Callaghan, C., McCann, J., Mills, C., Ryall, S., & Kingsford, R. (2017). Bird interactions with drones, from individuals to large colonies. *bioRxiv*, 109926.
- Mansfield, E. R., & Helms, B. P. (1982). Detecting multicollinearity. *The American Statistician*, 36(3a), 158-160.
- Mathews, A. J., & Jensen, J. L. (2013). Visualizing and quantifying vineyard canopy LAI using an unmanned aerial vehicle (UAV) collected high density structure from motion point cloud. *Remote Sensing*, 5(5), 2164-2183.
- McGarigal, K., Tagil, S., & Cushman, S. A. (2009). Surface metrics: an alternative to patch metrics for the quantification of landscape structure. *Landscape Ecology*, 24(3), 433-450.
- Micheletti, N., Chandler, J. H., & Lane, S. N. (2015). Structure from motion (SFM) photogrammetry. *Geomorphological Techniques*, Chap. 2, Sec. 2.2.
- Molinaro, A. M., Simon, R., & Pfeiffer, R. M. (2005). Prediction error estimation: a comparison of resampling methods. *Bioinformatics*, 21(15), 3301-3307.
- Monk, J., Ierodiaconou, D., Bellgrove, A., Harvey, E., & Laurenson, L. (2011). Remotely sensed hydroacoustics and observation data for predicting fish habitat suitability. *Continental Shelf Research*, 31(2), S17-S27.
- National Park Service. (2011). Vegetation Classification Guidelines: National Park Service Vegetation Inventory, Version 2.0.
- Nevalainen, O., Honkavaara, E., Tuominen, S., Viljanen, N., Hakala, T., Yu, X., ... & Tommaselli, A. M. (2017). Individual tree detection and classification with UAV-based photogrammetric point clouds and hyperspectral imaging. *Remote Sensing*, 9(3), 185.
- Oberndorfer, E. C., & Lundholm, J. T. (2009). Species richness, abundance, rarity and environmental gradients in coastal barren vegetation. *Biodiversity and Conservation*, 18(6), 1523-1553.
- Ørka, H. O., & Hauglin, M. (2016). Use of remote sensing for mapping of non-native conifer species. *INA Fagrapport*, 33.
- Porter, C. (2013). Classification of dwarf heath plant communities on the coastal barrens of Nova Scotia. Thesis. Master of Science. Saint Mary's University, Halifax, Nova Scotia.
- R Core Team, 2017. A Language and Environment for Statistical Computing. R Foundation for Statistical Computing, Vienna, Austria. <https://www.R-project.org>



- Remondino, F., Barazzetti, L., Nex, F., Scaioni, M., & Sarazzi, D. (2011). UAV photogrammetry for mapping and 3d modeling—current status and future perspectives. *International Archives of the Photogrammetry, Remote Sensing and Spatial Information Sciences*, 38(1), C22.
- Salovaara, K. J., Thessler, S., Malik, R. N., & Tuomisto, H. (2005). Classification of Amazonian primary rain forest vegetation using Landsat ETM+ satellite imagery. *Remote Sensing of Environment*, 97(1), 39-51.
- Sturdivant, E. J., Lentz, E. E., Thieler, E. R., Farris, A. S., Weber, K. M., Remsen, D. P., ... & Henderson, R. E. (2017). UAS-SfM for Coastal Research: Geomorphic Feature Extraction and Land Cover Classification from High-Resolution Elevation and Optical Imagery. *Remote Sensing*, 9(10), 1020.
- Tart, D., Williams, C. K., Brewer, C. K., DiBenedetto, J. P., & Schwind, B. (2005). Section 1: existing vegetation classification and mapping framework. Gen. Tech. Rep. WO-67. In *Existing Vegetation Classification and Mapping Technical Guide Version, 1*.
- Turner, M. G. (1989). Landscape ecology: the effect of pattern on process. *Annual review of ecology and systematics*, 20(1), 171-197.
- Ustin, S. L., & Gamon, J. A. (2010). Remote sensing of plant functional types. *New Phytologist*, 186(4), 795-816.
- van der Maarel, E., & Franklin, J. (2013). *Vegetation Ecology. Second Edition*. Wiley-Blackwell.
- Vas, E., Lescroël, A., Duriez, O., Boguszewski, G., & Grémillet, D. (2015). Approaching birds with drones: first experiments and ethical guidelines. *Biology letters*, 11(2), 20140754.
- Zellweger, F., Braunisch, V., Baltensweiler, A., & Bollmann, K. (2013). Remotely sensed forest structural complexity predicts multi species occurrence at the landscape scale. *Forest Ecology and Management*, 307, 303-312.
- Zheng, L., Zhang, J., & Wang, Q. (2009). Mean-shift-based color segmentation of images containing green vegetation. *Computers and Electronics in Agriculture*, 65(1), 93-98.
- Zomer, R. J., Trabucco, A., & Ustin, S. L. (2009). Building spectral libraries for wetlands land cover classification and hyperspectral remote sensing. *Journal of environmental management*, 90(7), 2170-2177.
- Zweig, C. L., Burgess, M. A., Percival, H. F., & Kitchens, W. M. (2015). Use of unmanned aircraft systems to delineate fine-scale wetland vegetation communities. *Wetlands*, 35(2), 303-309.

# 3

## Landscape Patterns of Plant Communities in the Coastal Barrens of Halifax, Nova Scotia



*Osmunda cinnamomea* and stream networks at Chebucto Head, Nova Scotia

## **Abstract**

The coastal barrens of Halifax, Nova Scotia are patchy mosaics of plant communities that experience harsh environmental conditions. Despite the harsh conditions, many rare and uncommon species inhabit these ecosystems, making them a high priority for conservation. Little is known of the landscape patterns of plant communities in the coastal barrens. In 2016, multispectral aerial imagery was collected from an unmanned aerial vehicle at three coastal barrens sites in Halifax, Nova Scotia: Chebucto Head, Prospect Bay, and Polly's Cove. Images were processed using structure from motion photogrammetry to create 3D models and orthomosaics of the landscapes, which were used with ground truthing field plot data to produce detailed maps of plant community patches and landscape features. Environmental factors, such as elevation, stream networks and wind exposure were also mapped to help understand the structure and spatial heterogeneity of the landscapes. Sites were dominated by shrublands and dwarf heath; however, many other types of communities co-existed, including bogs, salt marshes, and tree islands. Plant community patches varied in size, shape, abundance, and spatial distribution from one plant community type to another and in many cases from one site to another. Landscape patterns were driven by various combinations of environmental factors, including slope position, proximity to stream networks, elevation, and distance to coastline. Overall site differences could be mostly explained by the degree of topographic heterogeneity of each landscape. UAVs are an excellent option for mapping plant communities and understanding the structure of landscapes and future research should consider using UAVs for environmental monitoring.

## Introduction

Coastal barrens are mosaics of plant communities and different types of habitats that exist in harsh environmental conditions (Oberndorfer and Lundholm, 2009; Burley and Lundholm, 2010; Porter, 2013). They can be diverse and contain rare and uncommon species, making them a high priority for conservation. Near Halifax, Nova Scotia, coastal barrens are abundant and previous research has attempted to document their species and plant communities (Oberndorfer and Lundholm, 2009; Burley and Lundholm, 2010; Cameron and Bondrup-Nielsen, 2013; Porter, 2013). Currently, the distributions, spatial relationships, and spatial configurations of species and communities across coastal barrens landscapes are unknown. Understanding these aspects of landscape pattern are critical to revealing landscape function and processes that govern them, and ultimately how to manage and protect them.

Landscape ecology is the study of interacting organisms and their distributions across landscapes. A landscape is scale-dependent and often refers to a land surface of a region and its associated habitats (Turner, 1989). A popular view of landscapes is the patch-corridor-matrix model (Forman, 1995), which describes landscapes as being composed of patches, corridors, and a background matrix. Patches are relatively discrete areas with relatively homogeneous environmental conditions (McGarigal and Marks, 1995). Corridors are linear elements in a landscape that are usually isolated in a background matrix. Lastly, the matrix is the most extensive and connected element in the landscape (McGarigal and Marks, 1995). This view of landscapes as mosaics has often held true for both urban and natural landscapes. Organisms and their habitats within a landscape can occur across a wide range of spatial scales, influencing population

dynamics and the overall structure and function of the ecosystem (Johnson et al., 1992). To understand the ecological function of landscapes and how they change over time, landscape structure must be quantified, i.e. the composition and spatial configurations of its components or patches (McGarigal and Marks, 1995). Landscape structure can be quantified by computing various kinds of landscape metrics from land cover maps (McGarigal and Marks, 1995). Remote sensing is a promising tool that can help to make accurate land cover maps.

Remote sensing is the science of obtaining information from objects at a distance. A great deal can be learned from mapping remotely sensed data, including vegetation productivity, biomass, stress levels of vegetation, disturbance regimes, nutrient cycling, leaf water content, chlorophyll, and lastly the spatial patterns and distributions of organisms (Adam et al., 2010; Ustin and Gamon, 2010; Homolova et al., 2013; Asner et al., 2015; Minařík and Langhammer, 2016; Galidaki et al., 2017). Many different platforms can be used for remote sensing, including satellites, manned aircraft, and more recently unmanned aerial vehicles (UAVs). Each platform has its own limitations associated with factors such as costs, timing, geographic scale, and resolution. Satellites, such as the SPOT4-VEGETATION satellite, which has a 1 km pixel resolution, have been used to make global landcover maps (Xie et al., 2008). Most satellites have resolutions greater than 1 meter, which is insufficient to resolve important details of vegetation for mapping at the fine scale (Adam et al., 2010; Cruzan et al., 2016). Manned aircraft can be equipped with sensors and flown much closer to the earth's surface, obtaining sub-meter resolution and having the ability to also collect detailed 3D structural information from vegetation canopies and the earth's surface (Hill and Thomson, 2005;

Asner et al., 2015). Manned aircraft are expensive to operate, and the spatial resolution is often still too coarse to resolve important morphological features of vegetation to make accurate classifications (Kalacska et al., 2017), especially for the coastal barrens where plant community patches can be less than a meter wide. A more promising option for collecting high-resolution remotely sensed data are UAVs.

Commercial UAVs can capture very high-resolution aerial imagery across broad extents with pixel sizes in the low centimeters, giving landscape ecology an entirely new perspective (Gonçalves et al., 2015; Zweig et al., 2015; Sturdivant et al., 2017). They are relatively low-cost, can survey many hectares of land in a single flight, and can achieve high temporal resolution, since survey frequency mostly depends on the availability of the pilot and weather conditions. UAVs can be equipped with many different types of sensors as well, allowing them to collect hyperspectral imagery, thermal imagery, and in some cases LIDAR at very high spatial resolutions. Another advantage of UAVs is that they collect sequential overlapping imagery close to the ground, which allows 3D information to be computed for the landscape using structure from motion (SfM) photogrammetry (Micheletti et al., 2015). This can provide realistic 3D models of landscapes, providing enormous opportunities for quantitative and spatial analysis of landscape topography and 3D vegetation structure. Based on previous applications of UAVs, UAVs may be a good solution for mapping plant communities in the coastal barrens at the fine-scale for quantifying their landscape patterns.

The aim of this study is to quantify the landscape patterns of plant communities at three coastal barrens sites in Halifax, Nova Scotia. This will be achieved by the following objectives: 1) To quantify the landscape composition and spatial configuration of plant

community patches at the fine-scale (minimum area of 0.3 m<sup>2</sup> per patch) for three coastal barrens sites in Halifax, Nova Scotia: Chebucto Head, Prospect Bay, and Polly's Cove; 2) To evaluate the landscape patterns of plant community patches in relation to environmental factors; and, 3) To compare the landscape structure of Chebucto Head, Prospect Bay, and Polly's Cove.

## Methods

### Study Area and Scale

In Nova Scotia and other provinces in Atlantic Canada, coastal barrens are abundant (Porter, 2013). Many iconic coastal barrens sites exist near Halifax, Nova Scotia and three were selected for this study: Polly's Cove (Figure 3.1A), Prospect Bay (Figure 3.1B), and Chebucto Head (Figure 3.1C). The extent of each site measured 500 by 500 m in the shape of a square, which is approximately 25 ha per site. Although there are many definitions for a landscape (McGarigal and Mark, 1995), for the purposes of this study a landscape will be defined as an area of land that contains a mosaic of patches, which will be equivalent to a "site". A "patch" refers to the smallest unit or component of a landscape and will be specifically defined as a discrete, relatively homogeneous area such as a plant community or a landscape feature (e.g. a boulder). A plant community will be defined as "a relatively uniform piece of vegetation in a uniform environment, with a recognizable floristic composition and structure that is relatively distinct from the surrounding vegetation" (van der Maarel and Franklin, 2013). Finally, a "class" is a discrete category within a classification system, such as a plant community type.



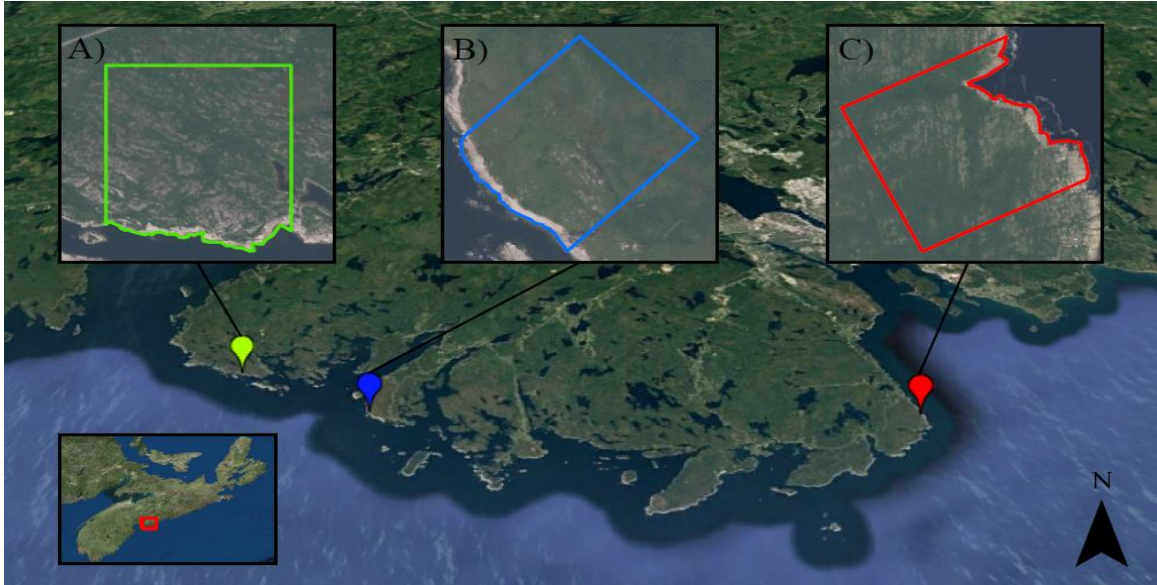


Figure 3.1. Three coastal barrens landscapes selected as study sites in the Halifax region of Nova Scotia, Canada: Polly's Cove (A), Prospect Bay (B), and Chebucto Head (C).

### Data Collection and Processing

The coastal barrens are known for their high-degree of patchiness, particularly at small scales. To capture this fine-scale patchiness for evaluating the landscape structure of each landscape, a minimum patch size of 0.3 m<sup>2</sup> was designated. Therefore, the resolution or grain of the remotely sensed data must be even finer to resolve patches in the landscape. For this study, a UAV was selected as the remote sensing platform since they can collect aerial imagery with sub-decimeter resolution, are relatively inexpensive, and can be used to map large areas in short periods of time. The UAV, a DJI Phantom 3 Professional quadcopter equipped with an RGB (Red-Green-Blue) camera and a Sentera near-infrared (NIR) sensor, was flown in May and August 2016 at the three study sites to collect high-resolution multispectral aerial imagery. Pix4DCapture (Pix4D, Lausanne, Switzerland), a flight planning mobile application, was used to make customized grid missions and autonomously pilot the unmanned aerial vehicle to collect sequential

imagery across each site. In May, the aircraft was flown at an above-ground altitude of 90 m, providing 4 cm pixel resolution for the RGB camera and 8 cm pixel resolution for the NIR sensor. In August, the aircraft was flown at 50 m above-ground altitude, providing 2 cm pixel resolution for the RGB camera and 4 cm pixel resolution for the NIR sensor. Image overlap was set to 80% and sidelap at 60% with both sensors oriented downward.

Images were processed using Agisoft Photoscan Professional (v. 1.3.2, Agisoft LLC, St Petersburg, Russia). Agisoft is one of the most common softwares currently used to process aerial imagery using SfM photogrammetry and is often used to stitch aerial images together to create high-resolution orthomosaics and compute 3D information to generate 3D point clouds and digital surface models. First, images were aligned using the *Align Photos* tool with the *Accuracy* setting set to 'High', *Generic preselection* unchecked, *Reference preselection* checked, *Key point limit* set at 40000, *Tie point limit* set at 4000, and *Adaptive camera model fitting* checked. Afterward, ground control points (GCPs) were added to accurately georeference the models. GCPs are commonly used to georeference aerial surveys and usually consist of a visible target placed in the field with known XYZ coordinates. For this study, 10 to 12 9-inch red plastic plates were evenly spread out across each site prior to aerial surveys and a real-time kinematic (RTK) was used to obtain the geographic coordinates of the center of each GCP with a horizontal accuracy of 1-2 cm and a vertical accuracy of 2-6 cm. Additional control points were added to the models from the spring, which were derived from the digital elevation models (DEM) from the summer surveys. This improved the alignment of the spring and summer surveys. After GCPs were incorporated into the models, the *Optimize Cameras* command was run to georeference the models. Next, the *Build Dense Pointcloud* tool was

run with *Quality* set to ‘High’ and *Depth filtering* as ‘Moderate’, creating a dense point cloud. Subsequently, the *Build DEM* tool was used to create an elevation model. Lastly, the *Build Orthomosaic* tool was run with *Surface* set to ‘DEM’, *Blending Mode* as ‘Mosaic’, *Enable color correction* unchecked, and *Enable hole filling* checked, which created an orthomosaic of the imagery for each survey. The final products that were exported from the software and used for further analysis were the RGB & NIR orthomosaics and the 3D point clouds. Image acquisition and processing results can be viewed in Table 2.1.

Spectral indices were derived from the RGB and NIR orthomosaics from the May and August surveys. Structural indices were derived from the 3D point cloud and subsequently digital elevation model from August. In total, 44 mapped indices were created (see Table A2.1). These indices were later used in conjunction with RGB orthomosaics to create a classified plant community map for each site.

### **Image Classification**

Plant community maps were generated from UAV imagery using an object-based image classification approach (also known as object-based image analysis or OBIA) in ArcGIS (v. 10.3.1, Environmental Research Systems Institute, Redlands, California). OBIA reduces noise and the undesired salt-and-pepper effect often produced from conventional per-pixel classification techniques, particularly from classifying high-resolution imagery, by segmenting an image into spatially and spectrally-similar objects (Blaschke, 2010). A classifier is later used to classify each segmented object rather than each pixel. For this study, the support vector machine (SVM) classifier was chosen. It has

performed well in previous studies at classifying vegetation compared to other classification techniques, can handle high-dimensional datasets, and is robust to having low sample sizes (Tzotsos and Argialas, 2008; Dronova et al., 2012; Burai et al., 2015; Pande-Chhetri et al., 2017). First, a segmented 3-band raster image, a support raster, and ground truthing data were used to generate a classified raster image for each site using the SVM classifier available in ArcGIS. Afterward, the classified images were post-processed to remove noise and fix obvious errors. Lastly, a 10-fold cross-validation was done by randomly splitting the ground truthing data 10 times into sets of 50% training and 50% testing data to assess the map accuracy. This methodology was applied individually to each site. The image classification workflow is illustrated below in Figure 3.2.

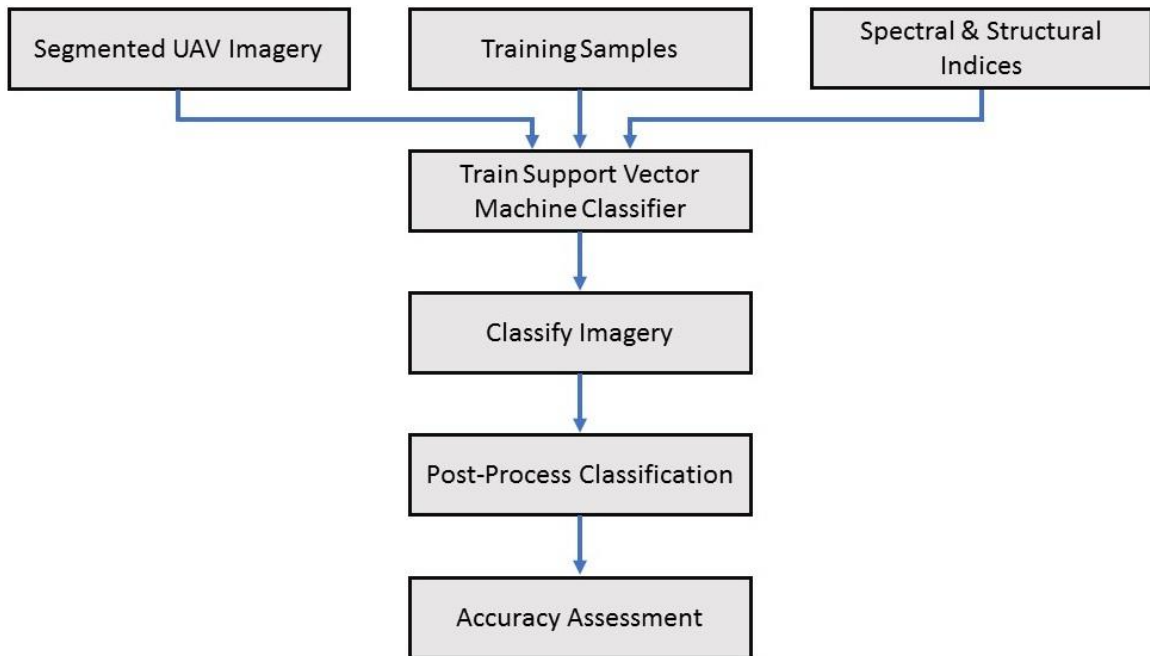


Figure 3.2. Flowchart illustrating the image classification workflow used in this study to derive plant community maps from UAV imagery.

First, UAV imagery were segmented into spectrally-similar objects using the *Segment Mean Shift* tool in ArcGIS. The tool can only operate on an image with a

maximum number of 3 bands, so either the May or the August RGB imagery were used depending on which yielded the best classification results. The amount of spatial and spectral smoothing of the image was controlled by three settings within the tool: spectral detail (0-20), spatial detail (0-20) and the minimum segment size (in pixels). From trial and error, the most optimal settings were found to be 20, 20, and 20 respectively.

To support the classification, a supporting raster was made. A support raster is optional for the *Train Support Vector Machine Classifier* tool in ArcGIS and is used to provide additional information (i.e. spectral or structural) to support the classification. The support raster was made by running principal components analysis (PCA). Principal components analysis is a multivariate technique that transforms a dataset into a new set of principal components that have reduced dimensionality, are uncorrelated, and retain the maximum amount of variation explained by the original dataset (Jolliffe, 1986). The analysis was run using the *Principal Components* tool in ArcGIS on the 44 spectral and structural indices. The first 32 bands of the output PCA raster were extracted, since the SVM classifier tool has a 32-band limit.

To train the SVM classifier, training samples in the form of polygons were required. Ground truthing data from field plots were collected at each site from June to August in 2016, with each plot measuring approximately 4 by 4 m (16 m<sup>2</sup>) except for when plant community patches were smaller or irregularly shaped. All taxa were recorded in each plot and the percent cover of the most dominant taxa were visually estimated. Each field plot was assigned an association level plant community classification, which is based on the Canadian National Vegetation Classification (CNVC, 2013). The CNVC is a standardized 8-level hierarchy in which the association

level is the finest level of plant community classification and is based primarily on floristic criteria such as dominant species. To achieve the greatest level of representation of plant community types for each site, field plot locations were determined using a combination of stratified random sampling and strategic sampling, including the interpretation of aerial imagery and identifying areas to sample while in the field (Table 2.4). The locations of each field plot were subsequently mapped in ArcGIS. Lastly, plant community patches were delineated as training polygons based on the field plot locations, UAV imagery, plot photographs, and field data sheets.

The segmented RGB orthomosaic, the support raster, and the training sample polygons were input into the *Train Support Vector Machine Classifier* tool in ArcGIS to create a classifier definition file. The *Segment Attributes* parameter within the tool allows the user to select the following attributes to compute from the input image: ‘color’, ‘mean’, ‘std’, ‘count’, ‘compactness’ and ‘rectangularity’. Classification accuracies varied using different combinations of these parameters and best results were found through trial and error for each site. For Chebucto Head, only ‘mean’ and ‘std’ were selected; for Prospect Bay all were selected; for Polly’s Cove ‘color’, ‘mean’ and ‘std’ were selected. Another optional parameter is *Max Number of Samples Per Class*; for Chebucto Head this parameter was set to the default value of 100 and for Prospect Bay and Polly’s Cove it was set to 0, meaning it would use all samples. From the tool inputs and the parameter settings, the tool creates a classifier definition file, which was subsequently input along with the segmented RGB orthomosaic and support raster into the *Classify Raster* tool to create a classified raster image.

Classified images were post-processed to remove noise, smooth out patch boundaries, and remove obvious classification errors. First, the *Majority Filter* tool was used to filter out initial noise with *number of neighbors to use* set to 8 and *replacement threshold* set to 'half'. Next, the *Boundary Clean* tool was used to smooth out the boundaries of each patch with *sorting technique* set to 'descend' and *Run expansion and shrinking twice* checked. Afterward, a minimum mapping unit of 30 cm<sup>2</sup> was set for each patch except for *Cladonia* spp using the *Region Group* tool followed by the *SetNull* tool and lastly by running the *Nibble* tool. Larger plant community types, such as tree islands, were given a minimum mapping unit of 1.6 m<sup>2</sup>. The *Region Group* tool groups connected cells of the same values into regions. Parameter settings for the *Region Group* tool included setting *Number of neighbors to use* to '4' and *Zone grouping method* to 'within'. Next, a written expression was input into the *SetNull* tool to nullify the output regions from the *Region Group* tool that did not meet the minimum size criteria mentioned above. Lastly, the *Nibble* tool was used to replace the nullified regions from the *Set Null* tool with their nearest neighboring regions/patches. Finally, each class was separately examined and compared with the original UAV imagery to identify and manually fix any obvious classification error. Manually fixing errors was only done after the accuracy assessments so as not to introduce bias.

To assess the classification accuracy of the maps, a 10-fold cross-validation was done by randomly splitting the ground truthing data 10 times into sets of 50% training data and 50% testing data. Each training set was used to create a classified map, producing 10 validation maps, while the testing sets were used to evaluate whether the validation maps correctly classified the locations of the testing data. To assess the

accuracy of the validation maps, the centroid point of each polygon was used to extract the class values from the validation maps using the *Extract Values to Points* tool in ArcGIS. Tables were later exported from ArcGIS and imported into R (v. 3.4.1; R Core Team, 2017) to compute confusion matrices, comparing actual and predicted values from the ground truth locations for each class. Overall accuracy was computed by summing the total correctly classified ground truth points divided by the total number of ground truth points. Classes that were not plant communities, such as rocks or dead trees, were excluded from the accuracy assessment. Accuracies were subsequently averaged across the 10 validation sets to arrive at a final accuracy estimate. This method for assessing map accuracy was chosen to accommodate for classes with low sample sizes. Ideally, a leave-one-out cross-validation technique would have been done, where one field plot sample is removed from the training set at a time and used to assess whether the validation map correctly predicted that location. This method would have resulted in creating hundreds of validation maps and would not be feasible due to the length of time to create a map.

Following the accuracy assessment, plant community types from the association level classification with a high number of misclassifications with other plant community types were merged together to form a broadened association level classification. The *Reclassify by Table* tool in ArcGIS was used to reclassify the classified rasters. Following this, the accuracy assessment was re-run.



## Landscape Pattern Analysis

Landscape structure was described in terms of landscape composition (global) and the spatial configuration of patch types that make up the landscape (local), such as size, shape, and aggregation. Various landscape metrics were used to quantify these aspects of landscape structure. Landscape metrics were calculated using FRAGSTATS (v. 4.0, McGarigal et al., 2012) and ArcGIS. Measures of landscape composition included: number of classes (class richness), most dominant communities, largest patch, total number of patches, patch density, and total vegetation cover (Table 3.1; McGarigal et al., 2012). Class-level metrics for the spatial configurations of patches included: patch area, patch perimeter, number of patches, perimeter-area ratio, shape index, and related circumscribing circle index (Table 3.2; McGarigal et al., 2012). In addition to these metrics, the average nearest neighbor ratio of each class, i.e. plant community type, was calculated using the *Average Nearest Neighbor* tool in ArcGIS. It is a measure of the degree of clustering or dispersion of each class across the landscape. Furthermore, a neighborhood analysis was done to determine the top three most common neighbors for each class. This was done using the *Polygon Neighbor* tool in ArcGIS, which quantifies the length of edge shared between patches and their adjacent neighbors.

Some patch metrics listed in Table 3.2 were summarized using the area-weighted mean rather than the mean. The area-weighted mean was chosen because it offers a landscape-centric perspective of the patches by weighting patches based on their area, which reflects conditions when a location on a landscape is chosen at random (McGarigal et al., 2012). In landscape ecology studies, it is often the preferred method to calculate the mean, because larger patches theoretically have more influence on landscape function.

Table 3.1. Landscape-level metrics used to describe landscape composition.

<b>Metric</b>	<b>Description</b>
Landscape Area	Area (hectares) of the landscape or study area.
Number of Classes	Number of plant community classification (also known as class richness).
Most Dominant Communities	Top three most dominant plant communities based on percentage of landscape occupied. Expressed as the total area of a class divided by the total area of the site, multiplied by 100.
Largest Patch	Largest plant community patch in the landscape (hectares).
Total Number of Patches	The total number of plant community patches in the landscape.
Patch Density	Density of plant community patches in the landscape. Expressed as the number of plant community patches per hectare of land.
Total Vegetation Cover	The total vegetation cover of the landscape (%). Expressed as the total area of all plant communities divided by the total area of the site, multiplied by 100.

Table 3.2. Class-level metrics used to describe the spatial configurations of plant community patches within a landscape.

<b>Metric</b>	<b>Description</b>
Class Area	Total area of a class (hectares).
Number of Patches	The number of patches in a class.
Patch Area	The area-weighted mean area (square meters) of patches in a class.
Patch Perimeter	The area-weighted mean perimeter (meters) of patches in a class.
Perimeter-Area Ratio	The area-weighted mean of the perimeter-area ratio (meters) of patches in a class. Expressed as the perimeter divided by the area. Commonly used as a measure of shape complexity.
Shape Index	The area-weighted mean of the shape index of patches in a class. Expressed as the perimeter divided by the square root of the patch area and adjusted by a constant for a square standard. It is a measure of shape complexity. Values range from 0 to infinity, where a value 1 indicates the shape of a square and increasing values indicate increasing shape complexity.
Related Circumscribing Circle Index	The area-weighted mean of the related circumscribing circle index of patches in a class. Values range from 0 to 1, where a value of 0 indicates a circle and values approaching 1 indicate elongated linear patches.
Average Nearest Neighbor Ratio	A measure of the degree of clustering or dispersion of a class across a landscape. It is the ratio of the average distance of each feature's centroid and its nearest neighbor's centroid of the same class, divided by the expected distance from the feature to its nearest neighbor of the same class in a hypothetical random distribution. Calculated using the <i>Average Nearest Neighbor</i> tool in ArcGIS. If the value of the index is less than 1, the pattern is clustered; if the value is greater than 1, the pattern is dispersed; if the value is 0, the pattern is random.
Most Common Neighbors	Top three most common neighbors of a class. Calculated using the <i>Polygon Neighbor</i> tool in ArcGIS. The tool quantifies the length of edge shared between patches and their adjacent neighbors for each class.

### **Environmental Factors**

Eight environmental factors were chosen to further describe the landscape structure of each site and to help interpret the landscape patterns of plant communities. These included: elevation above sea-level, distance from coastline, wind exposure, hydrology (stream order), incoming solar radiation, slope position classification, local

surface ruggedness, and global surface ruggedness (Table 3.3). Each environmental factor took the form of a 2 m raster of the landscape. Seven of the environmental factors were derived from the DEM produced from SfM photogrammetry of the UAV imagery; distance from coastline was computed separately without a DEM. Statistics were computed by first running the *Region Group* tool in ArcGIS on the classified plant community raster, followed by inputting the regions and environmental rasters into the *Zonal Statistics as Table* tool. Doing so obtained statistics for each region/patch for each environmental factor. Statistics were later exported from ArcGIS as tables and imported into R for further analysis. Quantitative variables were analyzed by computing 95% confidence intervals about the area-weighted means for each class. Categorical variables (i.e. hydrology and slope position classification) were analyzed by computing area-weighted counts for each class.

Table 3.3. Environmental factors computed for plant community patches.

Environmental Factor	Description
Elevation Above Sea-level	The area-weighted mean elevation above sea level (meters) of patches in a class. Measured from the 2 m bare ground DEM.
Distance from Coastline	The area-weighted mean distance (meters) of patches in a class from the coastline. Calculated using the <i>Euclidean Distance</i> tool in ArcGIS.
Wind Exposure	The area-weighted mean value of wind exposure for patches in a class. Wind exposure was modeled using a combination of wind direction data, in the form of a wind rose, and hillshades from a 2 m DEM. Values were scaled to range from 0 to 100.
Hydrology (Stream Order)	Stream networks were derived from a 2 m DEM using the <i>Hydrology</i> toolset in ArcGIS. Statistics for patches were calculated by first obtaining the maximum stream order value within a 10 m search radius of each patch followed by computing area-weighted counts of all patches for each class in R. Stream order values are expressed as integers and typically range from 0 to 10, although maximum values could be lower depending on the number of intersecting streams. Stream order increases when streams of the same order intersect.
Incoming Solar Radiation	The area-weighted mean incoming solar radiation (Watt hours/m <sup>2</sup> ) of one year (2016) for patches in a class. Calculated using the <i>Incoming Solar Radiation</i> tool in ArcGIS. Values were scaled to range from 0 to 100.
Slope Position	Majority slope position classification for each patch followed by computing area-weighted counts of all patches for each class in R. Calculated using <i>Slope Position Classification</i> tool from the Topography Tools ArcGIS toolbox (Dilts, 2015). Possible slope positions include: valley, toe slope, flat, midslope, upper slope, and ridge.
Surface Ruggedness	The area-weighted mean local and global surface ruggedness for a patch. Measures of topographic heterogeneity at two scales. Calculated using the <i>Roughness</i> tool from the Geomorphometry and Gradient Metrics toolbox for ArcGIS (Evans et al., 2014). Values were scaled to range from 0 to 100.

Elevation gradients are known to affect the distributions and structure of plant communities (Choler et al., 2001; Lomolino, 2001). Elevation above sea-level can potentially influence the amounts of wind exposure, salt spray, precipitation, and other environmental factors received by plant communities. Elevation above sea-level was

directly derived from the digital elevation model produced from the SfM photogrammetric processing of the UAV imagery (Figure A2.1). The DEM was derived from the 3D point cloud produced from SfM photogrammetry of the UAV imagery and had a 2 m resolution with values representing the minimum elevation of the 3D point cloud to simulate a ground elevation model rather than a canopy model. This 2 m bare ground elevation model was used for deriving all environmental factors that required the use of a DEM in this study.

The distance of a plant community patch from the coastline can potentially influence the amount of salt spray, wind exposure, and possibly other environmental factors received by the patch (Burley and Lundholm, 2009). Furthermore, disturbance regimes may be higher near the coastline since all three sites have popular hiking trails near the coastline, which may further affect distribution patterns of the plant communities. A 2 m raster of distance from the coastline was made by selecting the boundary line of the site that runs along the coast and executing the *Euclidean Distance* tool in ArcGIS, with the *cell size* parameter set to 2 m (Figure A2.2).

Wind exposure is likely one of the most important driving forces that influence the ecology of the coastal barrens (Burley and Lundholm, 2010; Porter, 2013). Exposure to wind can uproot plants, cause physical damage by tearing, stripping, and abrasion, and can erode topsoil which can further limit the establishment of plants (Cleugh et al., 1998; De Langre, 2008). It can also influence other environmental factors, such as precipitation patterns and salt spray (Baker et al., 2001). Creating a model simulating wind exposure across a landscape is therefore crucial for examining the landscape patterns of plant communities in the coastal barrens. For this study, wind exposure was modeled for each

landscape using a combination of wind direction data and a digital elevation model (Figure A2.3; Mikita et al., 2010). A wind rose representing three years of wind direction data for Chebucto Head was obtained from the Duncan's Cove weather station ([https://www.windfinder.com/windstatistics/duncans-cove\\_halifax](https://www.windfinder.com/windstatistics/duncans-cove_halifax)); a wind rose representing four years of wind direction data for Polly's Cove and Prospect Bay was obtained from the East Dover weather station ([https://www.windfinder.com/windstatistics/east\\_dover\\_nova\\_scotia](https://www.windfinder.com/windstatistics/east_dover_nova_scotia)). First, the *Hillshade* tool in ArcGIS was used. A hillshade is a hypothetical illumination of an elevation model from a hypothetical light source, where each pixel in the raster receives an illumination value from 0 to 255. The position of the illumination source is determined by setting the horizontal angle or azimuth (0° to 360°) and the vertical angle from the horizontal plane (0 to 90°). To mimic wind exposure across an elevation model, a vertical angle of illumination of 5° was recommended from previous literature (Boose et al., 1994; Mikita et al., 2010). Sixteen hillshade models with vertical angles of illumination of 5° were created from a 2 m elevation model. Each hillshade model had the horizontal angle of illumination set to one of sixteen cardinal directions (e.g. N, NNE, NE, etc.). All sixteen hillshades were each weighted by their percent contribution to their corresponding cardinal direction in the windrose model. Lastly, all sixteen weighted hillshades were added together using *Raster Calculator* in ArcGIS to form a final model of wind exposure. Values were later scaled to range from 0 to 100.

An additional consideration for the wind exposure model of Polly's Cove was a large barrier island sitting in front of the site (Figure 3.3). It is possible that the barrier island provides sheltering from wind and possibly other environmental factors such as

salt spray to parts of the site. To consider these potential effects of the barrier island, an additional set of aerial images were collected in August 2016 from the UAV and were subsequently processed using SfM photogrammetry to derive an elevation model for the island. This additional elevation model was combined with the original elevation model for Polly's Cove. The combined elevation model was only incorporated into the wind exposure model and the incoming solar radiation model but was not used for the other environmental factors since it was not expected to have influenced them.

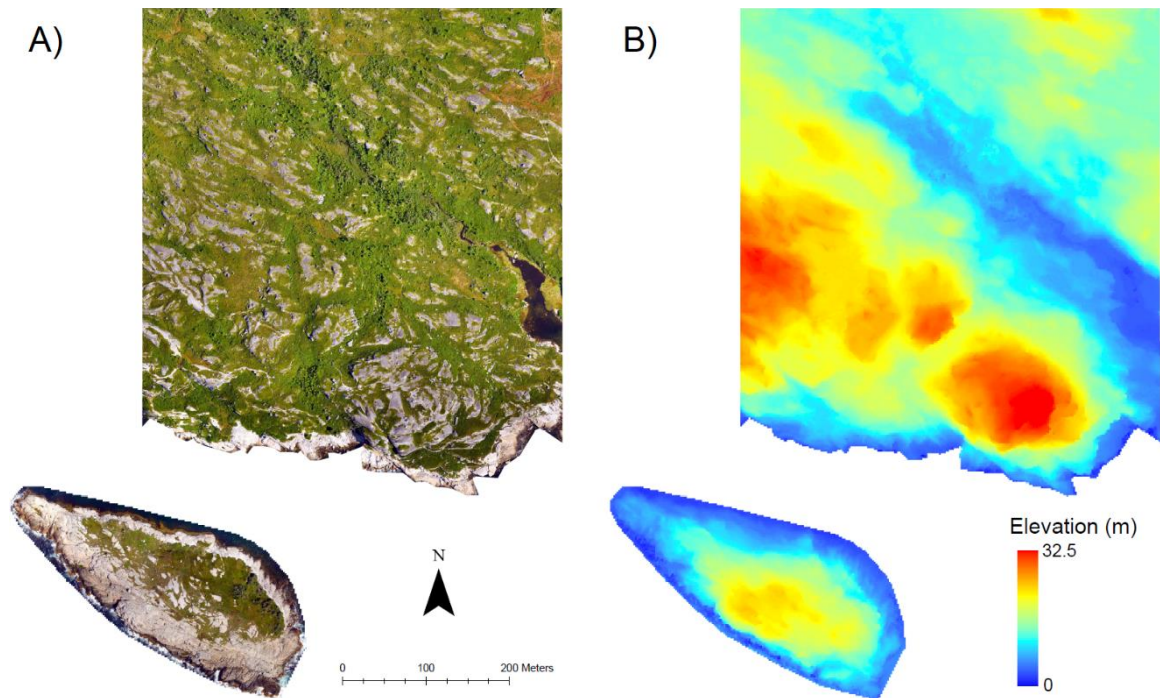


Figure 3.3. A) color imagery of the Polly's Cove study site and the barrier island near the site. B) A digital elevation model of the Polly's Cove study site and the barrier island near the site. It was hypothesized that the barrier island may shelter parts of the site and consequently influence the landscape patterns of the plant communities.

The flow of water across a surface can influence where different plant communities can grow (Silvertown et al., 1999; Zinko et al., 2005). For example, streams or rivers flowing through a landscape would likely be inhabited by riparian and wetland vegetation. Conversely, areas on exposed ridges would have lower flow accumulation,



dryer soil conditions and would be inhabited by more drought tolerant plants. To simulate the flow of water across each site, stream networks were derived from 2 m digital elevation models using the *Hydrology* toolset in ArcGIS (Figure A2.4). The following methods used to derive stream networks are like the methods used by Murphy et al. (2008). First, a 2 m elevation model derived from the UAV imagery was input into the *Fill* tool in ArcGIS. This fills the depressions or sinks of a DEM to remove imperfections. Next, the fill raster was used in the *Flow Direction* tool to create a flow direction raster. A flow direction raster indicates the direction that water is flowing across the surface. The flow direction raster is then used in the *Flow Accumulation* tool to create a flow accumulation raster. The flow accumulation raster represents for each cell the number of adjacent cells that flow into that cell. Areas with high flow accumulation may indicate stream channels. Afterward, the flow accumulation raster was input into the *Con* (conditional) tool with *Input true raster or constant value* set as the flow direction raster and *Input false raster or constant value* also set as the flow direction raster. Doing so created a stream network raster. Lastly, the output stream network raster was used in the *Stream Order* tool to assign a stream order value to each stream using the Strahler method (Strahler, 1952). According to the Strahler method, stream order is a hierarchical classification in which stream order increases when two streams of the same order intersect to create a larger stream. Streams with larger stream orders are more substantial and have greater water flow than streams with lesser stream order values.

Plants can respond differently to shaded environments compared to being in direct sunlight (Buckland-Nicks et al., 2016). This is because the amount of sunlight received on the earth's surface can influence many biotic and abiotic conditions, such as growth

potential for plants (sunlight is a key component for photosynthesis), surface temperature, evapotranspiration rate, evaporation rate of water from the soil, and so on. Modeling the amount of sunlight received across a landscape could therefore be an important factor influencing the landscape patterns of plant communities. To model incoming solar radiation, the *Area Solar Radiation* tool in ArcGIS was used. The 2 m DEM for each site was input into the tool along with the following parameter settings: *Latitude* set as the latitude of the input DEM; *Sky size / Resolution* set as the default value 200; *Time configuration* set to the calendar year of 2016 with *Start day* as 1 and *End day* as 366; *Day interval* set to 7; *Hour interval* set as the default value 0.5. The result is a raster representing the maximum possible incoming solar radiation in watt hours per m<sup>2</sup> for the land surface for the entirety of 2016 (Figure A2.5). Values were later scaled to range from 0 to 100.

Topographic slope position (e.g. valley, ridge, or flat), can influence soil conditions, moisture regimes, wind exposure, and other environmental conditions, all of which can affect the distributions and composition of plant communities (Zawawi, 2015). Slope position was calculated across a 2 m DEM using the *Slope Position Classification* tool from the Topography Tools toolbox for ArcGIS (Dilts, 2015). First, the *Topographic Position Index* tool from the same toolbox was run to create a topographic position index (TPI) raster with a certain focal search distance. For the slope position classification, a search distance of 30 m was chosen. The TPI raster was subsequently input into the *Slope Position Classification* tool along with the 2 m DEM to create a slope position raster with cells classified as either a valley, toe slope, flat, midslope, upper slope, or ridge (Figure A2.6).

Topographic heterogeneity at different scales can influence the distributions and composition of plant communities across landscapes due to its influence on other environmental factors such as wind exposure and edaphic conditions, like slope position (Vivian-Smith, 1997; Sebastia, 2004; Burley and Lundholm, 2010). For this study, surface ruggedness (topographic heterogeneity) was measured at two distinct scales: a 3x3 neighborhood from a 2 m DEM (local) and a 51x51 neighborhood from a 2 m DEM (global). Surface ruggedness was computed from the 2 m DEM using the *Roughness* tool from the Geomorphometry and Gradient Metrics toolbox for ArcGIS (Evans et al., 2014). For local surface ruggedness, the following parameters were used: the 2 m DEM as the *Select DEM* and a rectangular 3x3 cell window for *Analysis Window*. For global surface ruggedness, the following parameters were used: the 2 m DEM as the *Select DEM* and a rectangular 51x51 cell window for *Analysis Window*. Executing the tool created 2 surface ruggedness rasters representing topographic heterogeneity at two scales: local (Figure A2.7) and global (A2.8). Values of surface ruggedness were later scaled to range from 0 to 100.

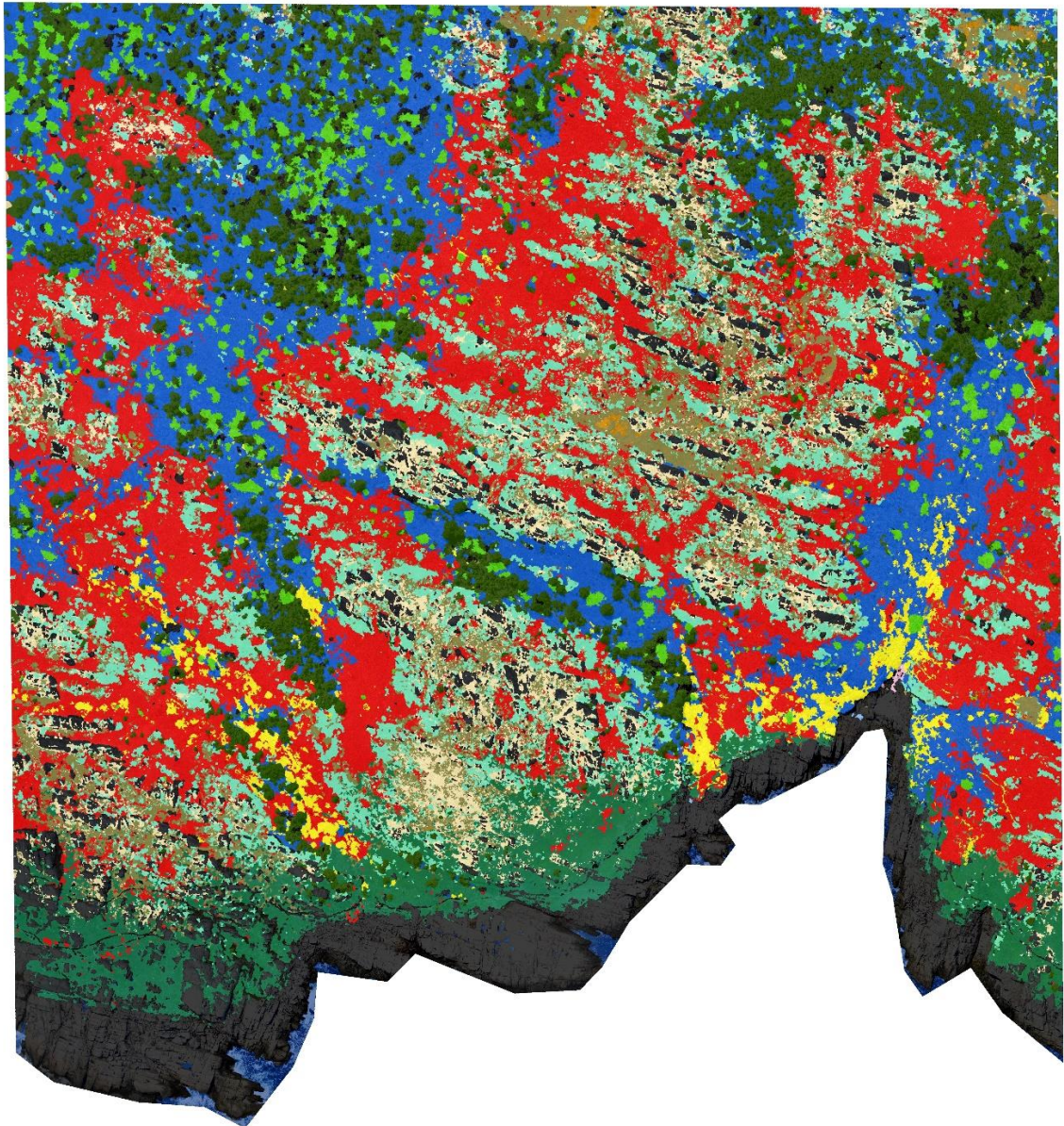
## Results

### Chebucto Head













Classification of high-resolution UAV imagery at Chebucto Head yielded a highly detailed map of plant community patches at the broadened association level classification and landscape features (Figure 3.4). The overall classification accuracy of plant communities was 87% (Table 3.4). Generally, misclassifications arose between structurally similar communities such as *Gaylussacia baccata* shrubland and Mixed tall shrubs (see confusion matrix in Table A2.2). Plant communities with low field plot samples (< 4) also tended to have more misclassifications.

Table 3.4. Classification accuracies of mapped plant communities from the broadened association level classification at Chebucto Head.

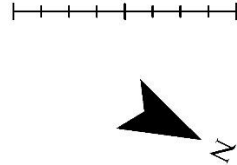
Plant Community	Accuracy (%)
Broadleaf tree island	55
<i>Calamagrostis canadensis</i> coastal vegetation	80
<i>Calystegia sepium</i> coastal lithomorphic	100
<i>Cladonia spp.</i>	100
Coniferous tree island	93
<i>Empetrum nigrum</i> - <i>Juniperus communis</i> dwarf heath	90
<i>Gaylussacia baccata</i> shrubland	86
<i>Gaylussacia</i> shrub bog	87
<i>Juniperus communis</i> - <i>Corema conradii</i> lithomorphic	87
Mixed tall shrubs	55
Open bog	97
<i>Osmunda cinnamomea</i> seep	85
<b>Overall</b>	<b>87</b>



**Classification**

- |  |   |
|--|---|
|  Broadleaf tree island  |  <i>Gaylussacia baccata</i> shrubland                            |
|  <i>Calamagrostis canadensis</i> coastal vegetation             |  <i>Gaylussacia</i> shrub bog                                    |
|  <i>Calystegia sepium</i> coastal lithomorphic                  |  <i>Juniperus communis</i> - <i>Corema conradii</i> lithomorphic |
|  <i>Cladonia</i> spp.   |  Mixed tall shrubs   |
|  Coniferous tree island   |  Open bog  |
|  <i>Empetrum nigrum</i> - <i>Juniperus communis</i> dwarf heath |  <i>Osmunda cinamomea</i> seep                                   |

0 50 100 Meters



**Other**



- |  |
|--|
|  Rocks / Bare Ground / Dead Trees |
|  Water                            |

Figure 3.4. Mapped plant communities from the broadened association level classification at Chebucto Head, Nova Scotia.

The study area at Chebucto Head measured 22.9 ha, consisted of 12 plant community types and contained 33,198 plant community patches - a patch density of 1,450 per hectare. The total vegetation cover of the landscape was 85.7%, the remainder being mostly exposed rocks and cliff faces (Figure 3.5C). Generally, the landscape was dominated by shrublands (39.2%), dwarf heath (16.9%), and tree islands (14.4%) (Figure 3.5A). The most dominant plant communities were *Gaylussacia baccata* shrubland (22.9%), Mixed tall shrubs (15.2%), and Coniferous tree island (11.6%) respectively. The landscape topography was heterogeneous, consisting of midslopes (30.4%), flats (18.5%), and ridges (15.1%), as well as several long and deep valleys (Figure 3.5D). Lastly, a map of stream networks showed that three major streams flow across the site and drain into the ocean (Figure 3.5B).

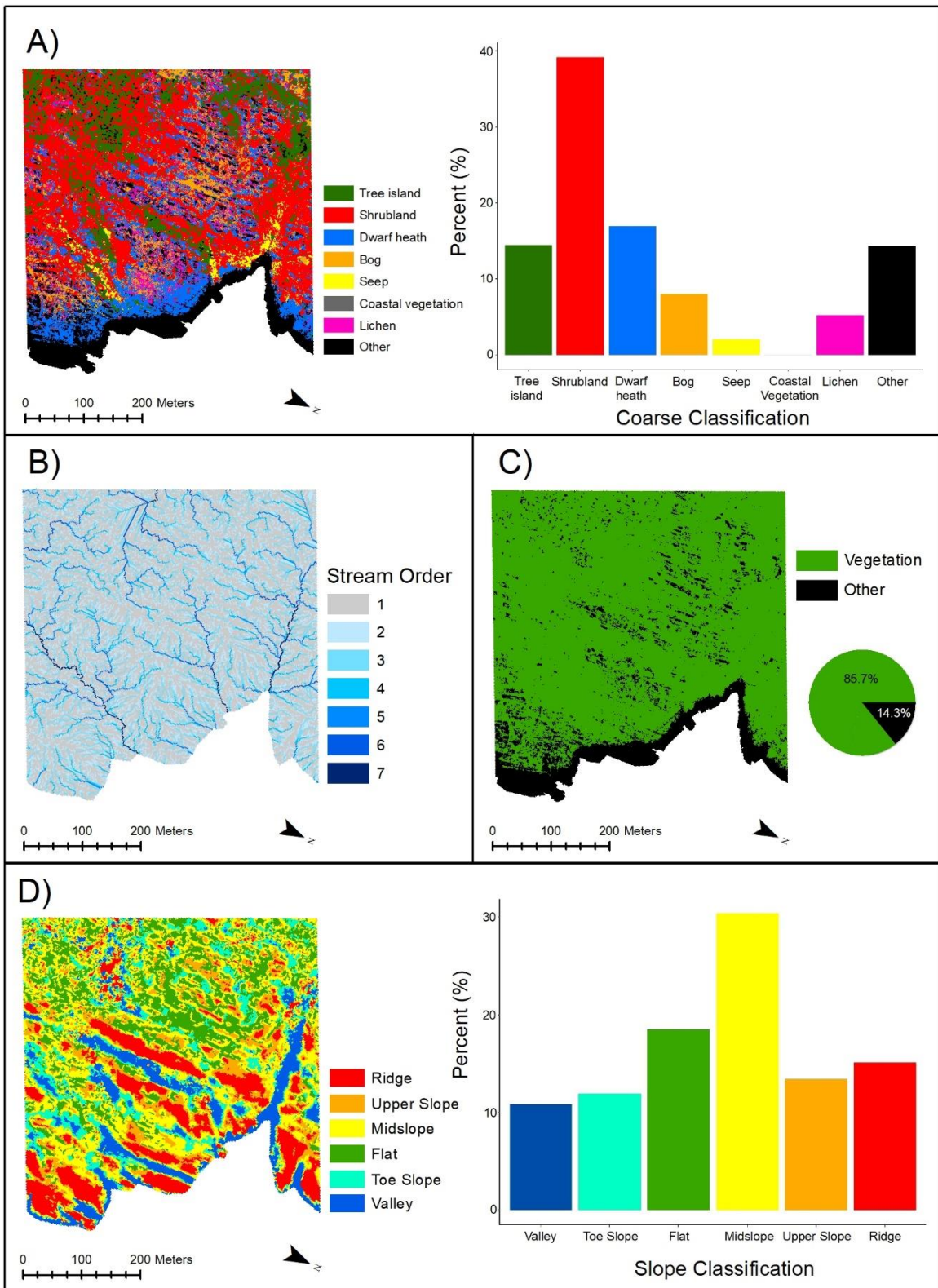


Figure 3.5. Landscape composition of Chebucto Head: A) Coarse classification of plant communities; B) Stream networks; C) Vegetation cover; and D) Slope classification.

Total class areas ranged from 13 m<sup>2</sup> (*Calystegia sepium* coastal lithomorphic) to 5.48 ha (*Gaylussacia baccata* shrubland) (Table 3.5). The number of patches also ranged greatly from 2 (*Calamagrostis canadensis* coastal vegetation) to 17,040 (*Cladonia spp.*), although most classes ranged from 500 to 5,000 patches. Area-weighted mean patch areas were relatively small for coastal vegetation, Open bogs, and *Cladonia spp.* Interestingly, Broadleaf tree islands had small patch areas, suggesting most patches consisted of one to several trees. As expected, *Juniperus communis* - *Corema conradii* lithomorphic also showed small patch areas, since the community is abundant near exposed rock faces. Larger patch areas were recorded for shrublands, tall shrubs, *Empetrum nigrum* - *Juniperus communis* dwarf heath, and Coniferous tree islands.

Based on the shape index, classes with the greatest shape complexity were *Gaylussacia baccata* shrubland, *Empetrum nigrum* - *Juniperus communis* dwarf heath, and Mixed tall shrubs (Table 3.5). Classes with lowest shape complexity were *Calystegia sepium* coastal lithomorphic, Open bog, and Broadleaf tree island. Related circumscribing circle index (area-weighted) ranged from 0.57 to 0.78, indicating that most patches were more elongated and rectangular rather than circular. Lastly, average nearest neighbor ratios for all classes were below 1, signifying that all communities had some degree of clustering at the landscape scale.

A neighborhood analysis of plant communities at Chebucto Head revealed that tree islands were most often neighbored by Mixed tall shrubs and vice versa (Table 3.6). *Gaylussacia baccata* shrublands were often adjacent to *Gaylussacia* shrub bog, *Juniperus communis* - *Corema conradii* lithomorphic, and Mixed tall shrubs. *Gaylussacia* shrub bog, *Juniperus communis* - *Corema conradii* lithomorphic, and *Cladonia spp.* were all



strongly associated with each other. Open bogs were often found next to *Gaylussacia* shrub bogs, *Cladonia spp.*, and Coniferous tree islands. Interestingly, *Osmunda cinnamomea* seep was often adjacent to *Gaylussacia baccata* shrublands and Mixed tall shrubs, which was observed while in the field. Both *Calamagrostis canadensis* coastal vegetation and *Calystegia sepium* coastal lithomorphs were associated with *Osmunda cinnamomea* seeps. Lastly, *Empetrum nigrum* - *Juniperus communis* dwarf heath was often adjacent to *Juniperus communis* - *Corema conradii* lithomorphs, *Gaylussacia* shrub bog, and *Cladonia spp.*

Table 3.5. Summary of the spatial configurations of plant community patches at Chebucto Head. \*AW = Area-weighted.

Classification	Class Area (ha)	Number of Patches	Patch Area (m <sup>2</sup> )		Patch Perimeter (m)		Perimeter-Area Ratio		Shape Index		Related Circumscribing Circle Index		Average Nearest Neighbor Ratio
			AW* Mean	SD	AW Mean	SD	AW Mean	SD	AW Mean	SD	AW Mean	SD	
Broadleaf tree island	0.64	586	30.67	14.72	56.45	24.57	2.32	14.48	2.46	0.54	0.57	0.14	0.79
<i>Calamagrostis canadensis</i> coastal vegetation	< 0.01	2	31.44	22.09	75.49	49.26	2.54	1.89	3.35	0.86	0.78	0.16	0.05
<i>Calystegia sepium</i> coastal lithomorph	< 0.01	5	4.19	2.24	12.82	4.47	3.65	2.59	1.60	0.12	0.58	0.07	0.6
<i>Cladonia spp.</i>	1.20	17040	56.38	6.25	166.79	18.47	5.81	12.76	4.13	0.49	0.67	0.14	0.63
Coniferous tree island	2.64	798	1118	189.59	1197	202.31	1.44	13.35	7.05	1.10	0.68	0.16	0.92
<i>Empetrum nigrum</i> - <i>Juniperus communis</i> dwarf heath	1.26	928	2870	196.89	3772	258.61	1.85	11.69	15.56	1.11	0.78	0.14	0.48
<i>Gaylussacia baccata</i> shrubland	5.48	1985	6628	426.82	8313	536.33	1.60	14.32	22.16	1.57	0.77	0.15	0.71
<i>Gaylussacia</i> shrub bog	1.80	5152	161.58	23.51	413.79	60.94	4.43	10.70	6.25	0.99	0.71	0.14	0.81
<i>Juniperus communis</i> - <i>Corema conradii</i> lithomorph	2.61	4527	60.87	17.82	124.64	35.90	2.94	12.33	3.64	0.75	0.67	0.14	0.89
Mixed tall shrubs	3.49	1121	2454	274.60	2812	315.20	1.69	15.15	12.52	1.51	0.76	0.16	0.76
Open bog	0.03	74	24.32	8.61	50.53	17.43	3.33	15.08	2.64	0.57	0.66	0.16	0.3
<i>Osmunda cinnamomea</i> seep	0.47	980	112.76	22.69	178.13	35.84	2.98	6.30	3.96	0.65	0.69	0.13	0.55

Table 3.6. The top three most common neighbors of each plant community type at Chebucto Head.

Plant Community	Top Neighboring Communities	Shared Edge Length (m)
Broadleaf tree island	Mixed tall shrubs	8668
	Coniferous tree island	4031
	<i>Gaylussacia baccata</i> shrubland	1483
<i>Calamagrostis canadensis</i> coastal vegetation	<i>Osmunda cinnamomea</i> seep	14.0
	Mixed tall shrubs	12.4
	<i>Gaylussacia</i> shrub bog	2.6
<i>Calystegia sepium</i> coastal lithomorphic	<i>Osmunda cinnamomea</i> seep	2.8
	<i>Gaylussacia baccata</i> shrubland	1.1
	<i>Empetrum nigrum</i> - <i>Juniperus communis</i> dwarf heath	0.6
<i>Cladonia</i> spp.	<i>Gaylussacia</i> shrub bog	22103
	<i>Juniperus communis</i> - <i>Corema conradii</i> lithomorphic	14586
	<i>Gaylussacia baccata</i> shrubland	12297
Coniferous tree island	Mixed tall shrubs	18201
	<i>Juniperus communis</i> - <i>Corema conradii</i> lithomorphic	5221
	<i>Gaylussacia baccata</i> shrubland	4034
<i>Empetrum nigrum</i> - <i>Juniperus communis</i> dwarf heath	<i>Juniperus communis</i> - <i>Corema conradii</i> lithomorphic	4937
	<i>Gaylussacia</i> shrub bog	3507
	<i>Cladonia</i> spp.	3258
<i>Gaylussacia baccata</i> shrubland	<i>Gaylussacia</i> shrub bog	22358
	<i>Juniperus communis</i> - <i>Corema conradii</i> lithomorphic	18392
	Mixed tall shrubs	16700
<i>Gaylussacia</i> shrub bog	<i>Juniperus communis</i> - <i>Corema conradii</i> lithomorphic	24681
	<i>Gaylussacia baccata</i> shrubland	22358
	<i>Cladonia</i> spp.	22103
<i>Juniperus communis</i> - <i>Corema conradii</i> lithomorphic	<i>Gaylussacia</i> shrub bog	24681
	<i>Gaylussacia baccata</i> shrubland	18392
	<i>Cladonia</i> spp.	14586
Mixed tall shrubs	Coniferous tree island	18201
	<i>Gaylussacia baccata</i> shrubland	16700
	Broadleaf tree island	8668
Open bog	<i>Gaylussacia</i> shrub bog	758.5
	<i>Cladonia</i> spp.	38.5
	Coniferous tree island	25.9
<i>Osmunda cinnamomea</i> seep	<i>Gaylussacia baccata</i> shrubland	6092
	Mixed tall shrubs	5726
	<i>Gaylussacia</i> shrub bog	647.3

Environmental conditions differed greatly for plant communities at Chebucto Head (Table 3.7; see Figures A2.1-A2.8 for mapped environmental factors; see Figures A2.9-16 for confidence intervals and bar plots). Most plant communities occurred at elevations greater than 20 m; however, several plant communities mostly occurred at lower elevations, which included *Empetrum nigrum* - *Juniperus communis* dwarf heath, *Osmunda cinnamomea* seep, and coastal vegetation. Tree islands, Mixed tall shrubs and Open bogs were usually situated greater than 200 m from the coastline; *Gaylussacia baccata* shrubland, *Gaylussacia shrub* bog, *Cladonia spp.*, and *Juniperus communis* - *Corema conradii* lithomorphic ranged between 150 to 200 m from the coast; *Osmunda cinnamomea* seep was on average about 100 m from the coastline, and *Empetrum nigrum* - *Juniperus communis* dwarf heath and Coastal vegetation normally were within 50 m of the coastline.

Coastal vegetation recorded highest values of wind exposure, although both community types had lower sample sizes and consequently had greater error (Table 3.7). Other communities with relatively high wind exposure values included tree islands, Mixed tall shrubs and *Empetrum nigrum* - *Juniperus communis* dwarf heath. Conversely, communities with lower wind exposure values were Open bogs, *Gaylussacia shrub* bog, and *Cladonia spp.* Plant communities with highest stream order values (6 or above) were *Osmunda cinnamomea* seep, *Calamagrostis canadensis* coastal vegetation, and Open bog; the community with the lowest stream order (drier) value was *Cladonia spp.* (3); all other communities had stream orders of 4 or 5. Incoming solar radiation did not vary much between communities, although Coastal vegetation had relatively lower solar

radiation values compared to other communities, likely because the communities occurred in a sheltered valley.

Most communities at Chebucto Head occurred on midslopes, including tree islands, shrublands, and dwarf heath (Table 3.7). Interestingly, *Gaylussacia shrub* bog occurred on flats and Open bogs occurred on toe slopes. *Cladonia spp.* was often associated with ridges. Coastal vegetation and *Osmunda cinnamomea* seep occurred in valleys. Local surface ruggedness was generally low for most communities; local ruggedness was elevated for coastal vegetation likely because they occurred along a rocky shoreline; communities with lowest values were Open bog, *Gaylussacia shrub* bog, *Gaylussacia baccata* shrubland, and *Cladonia spp.* Lastly, global surface ruggedness was elevated for Coastal vegetation, *Empetrum nigrum* - *Juniperus communis* dwarf heath, and *Osmunda cinnamomea* seep; intermediate values were observed for shrublands, *Cladonia spp.*, and *Juniperus communis* - *Corema conradii* lithomorphic; lower global ruggedness values were observed from Open bogs, tree islands, and *Gaylussacia shrub* bog.

Table 3.7. Environmental factors for plant communities at Chebucto Head. \*AW = Area-weighted; C.I = Area-weighted 95% confidence interval.

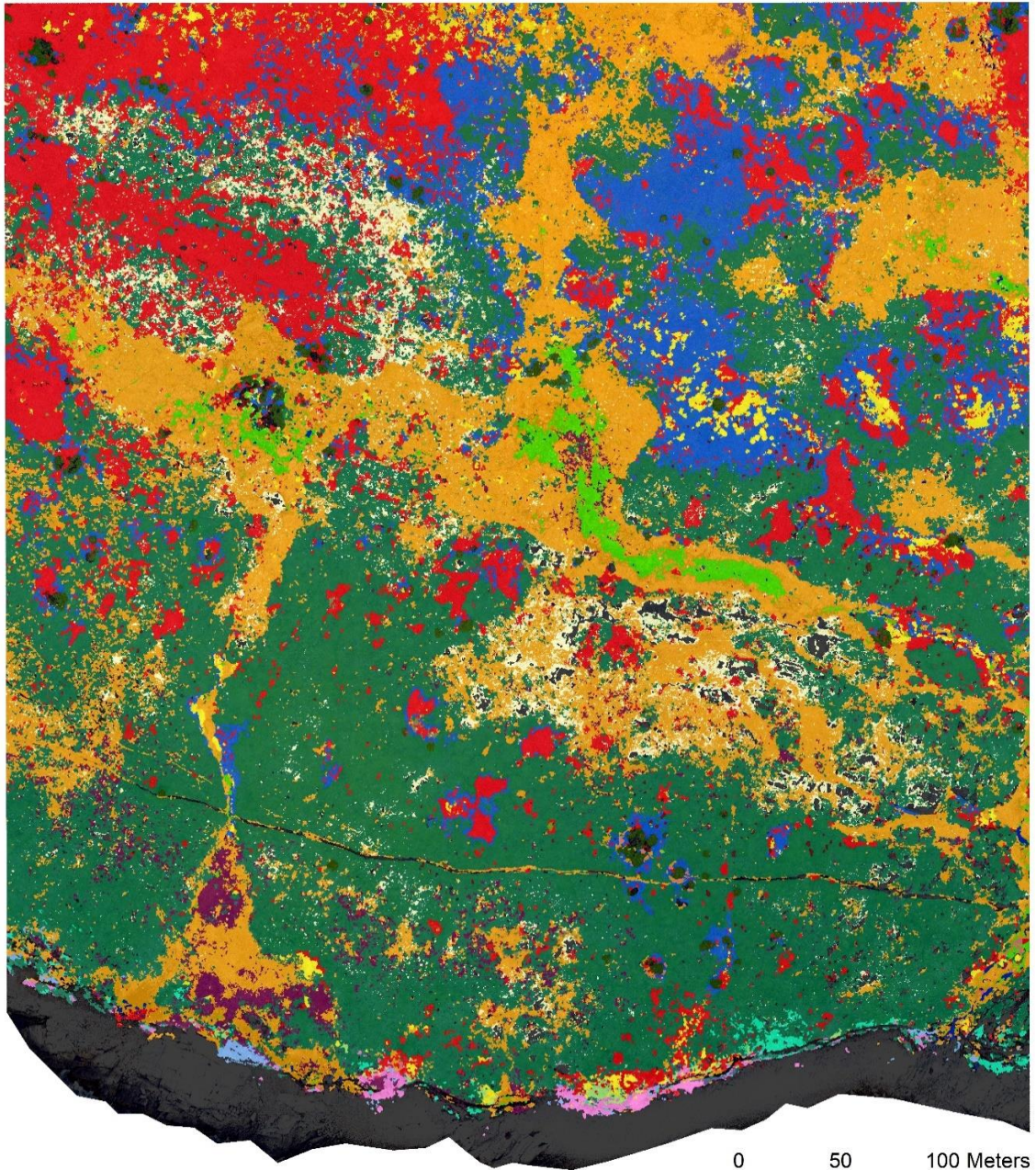
Plant Community	Elevation Above Sea-level (m)	Distance from Coastline (m)	Wind Exposure	Hydrology (Stream Order)	Incoming Solar Radiation	Slope Position	Local Surface Ruggedness	Global Surface Ruggedness
	AW Mean $\pm$ 95% C.I.*	AW Mean $\pm$ 95% C.I.	AW Mean $\pm$ 95% C.I.	Most Frequent (AW)	AW Mean $\pm$ 95% C.I.	Most Frequent (AW)	AW Mean $\pm$ 95% C.I.	AW Mean $\pm$ 95% C.I.
Broadleaf tree island	27.81 $\pm$ 0.27	296.1 $\pm$ 7.82	14.63 $\pm$ 0.56	4	83.71 $\pm$ 0.48	Midslope	1.78 $\pm$ 0.11	5.31 $\pm$ 0.59
<i>Calamagrostis canadensis</i> coastal vegetation	6.05 $\pm$ 1.91	24.85 $\pm$ 17.42	24.01 $\pm$ 6.54	7	67.14 $\pm$ 56.43	Valley	4.27 $\pm$ 4.65	38.31 $\pm$ 18.3
<i>Calystegia sepium</i> coastal lithomorphic	4.27 $\pm$ 1.09	9.11 $\pm$ 4.36	21.28 $\pm$ 27.87	5	73.79 $\pm$ 12.49	Valley	3.1 $\pm$ 4.59	45.36 $\pm$ 5.28
<i>Cladonia</i> spp.	27.1 $\pm$ 0.08	182.36 $\pm$ 1.19	7.3 $\pm$ 0.06	3	85.83 $\pm$ 0.05	Ridge	0.41 $\pm$ 0.007	8.43 $\pm$ 0.11
Coniferous tree island	27.64 $\pm$ 0.31	279.91 $\pm$ 6.17	12.29 $\pm$ 0.33	5	84.07 $\pm$ 0.27	Midslope	1.21 $\pm$ 0.07	4.04 $\pm$ 0.4
<i>Empetrum nigrum</i> - <i>Juniperus communis</i> dwarf heath	14.64 $\pm$ 0.34	46.84 $\pm$ 1.11	10.32 $\pm$ 0.39	4	81.44 $\pm$ 0.29	Midslope	1.23 $\pm$ 0.07	34.48 $\pm$ 0.83
<i>Gaylussacia baccata</i> shrubland	25.45 $\pm$ 0.21	200.73 $\pm$ 3.14	8.27 $\pm$ 0.11	4	87.37 $\pm$ 0.11	Midslope	0.34 $\pm$ 0.01	8.83 $\pm$ 0.38
<i>Gaylussacia</i> shrub bog	27.18 $\pm$ 0.14	187.53 $\pm$ 2.06	6.5 $\pm$ 0.08	4	86.78 $\pm$ 0.07	Flat	0.22 $\pm$ 0.008	6.82 $\pm$ 0.19
<i>Juniperus communis</i> - <i>Corema conradii</i> lithomorphic	26.58 $\pm$ 0.16	188.78 $\pm$ 2.28	8.74 $\pm$ 0.13	4	86.26 $\pm$ 0.1	Midslope	0.51 $\pm$ 0.02	8.64 $\pm$ 0.25
Mixed tall shrubs	25.98 $\pm$ 0.24	253.37 $\pm$ 6.21	11.34 $\pm$ 0.26	4	84.66 $\pm$ 0.26	Midslope	0.88 $\pm$ 0.04	8.87 $\pm$ 0.57
Open bog	29.91 $\pm$ 0.4	279.57 $\pm$ 16.81	5.93 $\pm$ 0.2	6	87.77 $\pm$ 0.17	Toe Slope	0.04 $\pm$ 0.008	0.86 $\pm$ 0.45
<i>Osmunda cinnamomea</i> seep	15.62 $\pm$ 0.29	99.06 $\pm$ 4.12	10.33 $\pm$ 0.45	7	81.96 $\pm$ 0.45	Valley	1.03 $\pm$ 0.07	22.85 $\pm$ 1.03

## Prospect Bay

Classification of high-resolution UAV imagery at Prospect Bay yielded a highly detailed map of plant communities and landscape features at the fine-scale (Figure 3.6). The overall classification accuracy of plant communities was 85% (Table 3.8). Generally, misclassifications arose between structurally similar communities, such as between different types of bogs and shrublands (see confusion matrix in Table A2.3). Classifications with low field plot samples (< 4) also tended to have more misclassifications.

Table 3.8. Classification accuracies of mapped plant communities from the broadened association level classification at Prospect Bay.

<b>Plant Community</b>	<b>Accuracy (%)</b>
<i>Alnus viridis</i> shrubland	70
<i>Betula papyrifera</i> tree island	90
<i>Cladonia spp.</i>	100
Coniferous tree island	100
<i>Empetrum nigrum</i> - <i>Juniperus communis</i> dwarf heath	92
<i>Eriophorum russeolum</i> bog	100
<i>Festuca rubra</i> - <i>Solidago sempervirens</i> - <i>Trifolium repens</i> disturbed coastal vegetation	100
<i>Gaylussacia baccata</i> shrubland	79
<i>Gaylussacia</i> shrub bog	57
Grass/Sedge/Open bog	85
<i>Juncus balticus</i> brackish marsh	67
<i>Juniperus horizontalis</i> dwarf heath	50
<i>Lonicera villosa</i> shrubland	100
<i>Maianthemum trifolium</i> bog	100
Mixed tall shrubs	70
<i>Morella pensylvanica</i> shrubland	70
<i>Osmunda cinnamomea</i> seep	78
<i>Spartina pectinata</i> brackish marsh	73
<i>Toxicodendron radicans</i> coastal vegetation	80
<b>Overall</b>	<b>85</b>



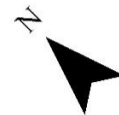
**Classification**

- Alnus viridis* shrubland
- Betula papyrifera* tree island
- Cladonia* spp.
- Coniferous tree island
- Empetrum nigrum* - *Juniperus communis* dwarf heath
- Eriophorum russeolum* bog

- Festuca rubra* - *Solidago sempervirens* - *Trifolium repens* disturbed coastal vegetation
- Gaylussacia baccata* shrubland
- Gaylussacia* shrub bog
- Grass/Sedge/Open bog
- Juncus balticus* brackish marsh
- Juniperus horizontalis* dwarf heath

- Lonicera villosa* shrubland
- Maianthemum trifolium* bog
- Mixed tall shrubs
- Morella pensylvanica* shrubland
- Osmunda cinamomea* seep
- Spartina pectinata* brackish marsh
- Toxicodendron radicans* coastal vegetation

0 50 100 Meters



**Other**

- Rocks / Bare Ground / Dead Trees
- Water

Figure 3.6. Mapped plant communities from the broadened association level classification at Prospect Bay, Nova Scotia.



The study area at Prospect Bay measured 28 ha, consisted of 19 plant community types and contained 63,312 plant community patches - a patch density of 2,263 per hectare. The total vegetation cover of the landscape was 92.3%, the remainder being mostly exposed rocks and cliff faces (Figure 3.7C). Generally, the landscape was dominated by dwarf heath (38%), shrublands (22.9%), and bogs (22.5%) (Figure 3.7A). The most dominant plant communities were *Empetrum nigrum* - *Juniperus communis* dwarf heath (37.7%), Grass/Sedge/Open bog (20.6%), and *Gaylussacia baccata* shrubland (14%) respectively. The landscape topography was mostly homogeneous, largely consisting of gentle slopes or flats (57.2%) (Figure 3.7D). Most topographic heterogeneity was observed along the rocks and cliff faces that follow the coastline. Lastly, a map of stream networks showed that two major streams extend across the site and drain into the ocean (Figure 3.7B).

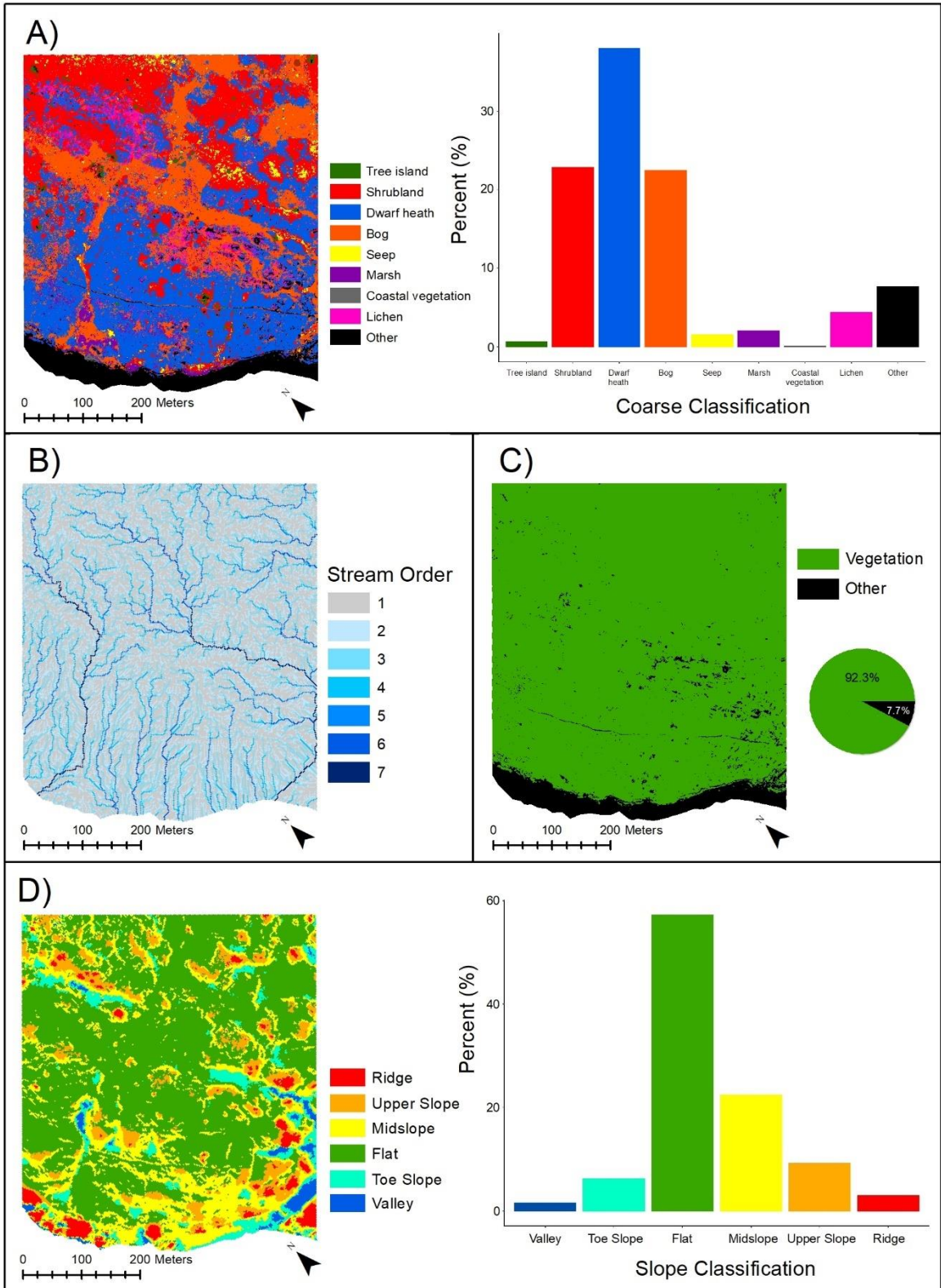


Figure 3.7. Landscape composition of Prospect Bay: A) Coarse classification of plant communities; B) Stream networks; C) Vegetation cover; and D) Slope classification.

Total class areas ranged from 23 m<sup>2</sup> (*Betula papyrifera* tree island) to 10.56 ha (*Empetrum nigrum* - *Juniperus communis* dwarf heath) (Table 3.9). The number of patches ranged from 3 (*Toxicodendron radicans* coastal vegetation) to 36,523 (*Cladonia* spp.), although most classes ranged between 100 and 6,000 patches. Area-weighted mean patch areas were small for most shrublands (< 35 m<sup>2</sup>) except for *Gaylussacia baccata* shrubland and Mixed tall shrubs which had large average patch areas. Tree islands also had small patch areas, as well as *Gaylussacia* shrub bog, *Cladonia* spp., *Osmunda cinnamomea* seep, and *Eriophorum russeolum* bog. Plant communities with the largest patch areas were *Empetrum nigrum* - *Juniperus communis* dwarf heath and Grass/Sedge/Open bog.

Perimeter-area ratios (area-weighted) of patches were generally smaller for classes with larger patch areas and larger for patches with smaller areas (Table 3.9). The only exception was Coniferous tree island, which had an area-weighted mean patch size of 37.60 m<sup>2</sup> and a perimeter-area ratio of only 2.02, suggesting patches had lower shape complexity. This was supported by a shape index score of 2.47 and a related circumscribing circle index of 0.48, indicating the patch shapes are regular and more circular rather than elongated and rectangular. Other classes with low shape index scores were *Alnus viridis* shrubland, *Lonicera villosa* shrubland, *Gaylussacia* shrub bog, and *Betula papyrifera* tree island. Classes with greater shape complexity included *Empetrum nigrum* - *Juniperus communis* dwarf heath, Grass/Sedge/Open bog, Mixed tall shrubs, and *Gaylussacia baccata* shrubland. Related circumscribing circle index (area-weighted) ranged from 0.48 (Coniferous tree island) to 0.82 (*Toxicodendron radicans* coastal

vegetation). Lastly, average nearest neighbor ratios showed that plant communities exhibited clustering at the landscape scale.

A neighborhood analysis of plant communities at Prospect Bay showed that Tree islands were most often adjacent to Mixed tall shrubs and *Gaylussacia baccata* shrubland (Table 3.10). *Gaylussacia baccata* shrubland and Mixed tall shrubs were the most common neighbors of each other. Other shrublands were frequently neighbored by either *Empetrum nigrum* - *Juniperus communis* dwarf heath or *Gaylussacia baccata* shrubland. *Empetrum nigrum* - *Juniperus communis* dwarf heath was most often associated with Grass/Sedge/Open bog, *Cladonia* spp., and Mixed tall shrubs. *Juniperus horizontalis* dwarf heath was largely adjacent to *Empetrum nigrum* - *Juniperus communis* dwarf heath. Smaller bogs were commonly neighbored by Grass/Sedge/Open bog and *Empetrum nigrum* - *Juniperus communis* dwarf heath while the larger bog, Grass/Sedge/Open bog, was mostly associated with *Empetrum nigrum* - *Juniperus communis* dwarf heath and *Cladonia* spp. *Gaylussacia* shrub bog was often next to *Gaylussacia baccata* shrubland, *Cladonia* spp., and Grass/Sedge/Open bog. *Osmunda cinnamomea* seep was frequently neighbored by *Gaylussacia baccata* shrubland and Mixed tall shrubs. Coastal vegetation was often adjacent to marshes and *Empetrum nigrum* - *Juniperus communis* dwarf heath. Marshes were often next to *Empetrum nigrum* - *Juniperus communis* dwarf heath. Lastly, *Cladonia* spp. was associated with Grass/Sedge/Open bog, *Empetrum nigrum* - *Juniperus communis* dwarf heath, and *Gaylussacia baccata* shrubland.

Table 3.9. Summary of the spatial configurations of plant community patches at Prospect Bay. \*AW = Area-weighted.

Plant Community	Class Area (ha)	Number of Patches	Patch Area (m)		Patch Perimeter (m)		Perimeter-Area Ratio		Shape Index		Related Circumscribing Circle Index		Average Nearest Neighbor Ratio
			AW* Mean	SD	AW Mean	SD	AW Mean	SD	AW Mean	SD	AW Mean	SD	
<i>Alnus viridis</i> shrubland	0.09	715	2.58	1.29	11.01	4.30	5.63	11.80	1.79	0.41	0.53	0.14	0.65
<i>Betula papyrifera</i> tree island	< 0.01	5	6.53	3.27	26.57	13.13	4.53	35.22	2.70	0.97	0.59	0.05	0.60
<i>Cladonia</i> spp.	1.22	36523	36.15	3.45	112.45	10.85	7.63	19.77	3.73	0.40	0.65	0.13	0.67
Coniferous tree island	0.20	142	36.70	17.92	60.85	27.17	2.02	21.90	2.47	0.63	0.48	0.14	0.59
<i>Empetrum nigrum</i> - <i>Juniperus communis</i> dwarf heath	10.56	4884	43096	962.02	43463	970.98	1.55	29.40	45.50	1.38	0.71	0.18	0.79
<i>Eriophorum russeolum</i> bog	0.03	192	20.34	5.47	65.71	16.81	6.00	18.74	3.47	0.69	0.66	0.13	0.16
<i>Festuca rubra</i> - <i>Solidago sempervirens</i> - <i>Trifolium repens</i> disturbed coastal vegetation	0.03	97	69.91	15.24	108.96	23.06	3.24	27.15	3.20	0.55	0.68	0.19	0.14
<i>Gaylussacia baccata</i> shrubland	3.91	4519	3644	176.80	4795	233.16	2.46	25.00	15.27	1.09	0.70	0.16	0.80
<i>Gaylussacia</i> shrub bog	0.19	1386	4.11	1.95	22.01	9.46	6.70	16.62	2.59	0.63	0.63	0.13	0.51
Grass/Sedge/Open bog	5.76	5888	10405	317.78	14860	468.95	2.43	27.24	31.03	1.38	0.78	0.18	0.81
<i>Juncus balticus</i> brackish marsh	0.50	2553	149.01	17.00	343.78	39.27	5.47	20.37	5.52	0.79	0.68	0.14	0.50
<i>Juniperus horizontalis</i> dwarf heath	0.06	207	40.60	10.76	79.99	20.12	3.98	15.25	3.09	0.59	0.66	0.14	0.21
<i>Lonicera villosa</i> shrubland	0.02	106	5.42	2.55	20.20	8.30	5.20	18.22	2.19	0.51	0.60	0.15	0.27
<i>Maianthemum trifolium</i> bog	0.32	462	337.26	48.01	506.46	74.28	2.58	24.66	6.59	0.99	0.75	0.17	0.36
Mixed tall shrubs	2.34	1689	1650	150.12	3151	291.31	3.08	34.27	16.65	2.05	0.73	0.20	0.57
<i>Morella pensylvanica</i> shrubland	0.04	140	34.05	9.07	120.64	31.32	4.92	23.02	4.37	0.87	0.67	0.15	0.15
<i>Osmunda cinnamomea</i> seep	0.46	1750	32.93	8.88	87.92	23.41	4.73	21.79	3.66	0.85	0.63	0.15	0.53
<i>Spartina pectinata</i> brackish marsh	0.07	109	157.02	31.83	273.63	54.47	2.64	18.43	5.02	0.82	0.74	0.14	0.18
<i>Toxicodendron radicans</i> coastal vegetation	< 0.01	3	19.70	12.01	65.73	37.41	3.53	1.48	3.63	1.00	0.82	0.14	0.31

Table 3.10. The top three most common neighbors of each plant community type at Prospect Bay.

Plant Community	Top Neighboring Communities	Shared Edge Length (m)
<i>Alnus viridis</i> shrubland	<i>Gaylussacia baccata</i> shrubland	1809
	<i>Empetrum nigrum</i> - <i>Juniperus communis</i> dwarf heath	1634
	Mixed tall shrubs	661.1
<i>Betula papyrifera</i> tree island	<i>Gaylussacia baccata</i> shrubland	73.8
	Mixed tall shrubs	12.5
	Coniferous tree island	10.8
<i>Cladonia</i> spp.	Grass/Sedge/Open bog	34567
	<i>Empetrum nigrum</i> - <i>Juniperus communis</i> dwarf heath	31578
	<i>Gaylussacia baccata</i> shrubland	14284
Coniferous tree island	Mixed tall shrubs	1342
	<i>Empetrum nigrum</i> - <i>Juniperus communis</i> dwarf heath	757.8
	<i>Gaylussacia baccata</i> shrubland	703.7
<i>Empetrum nigrum</i> - <i>Juniperus communis</i> dwarf heath	Grass/Sedge/Open bog	60070
	<i>Cladonia</i> spp.	31578
	Mixed tall shrubs	24277
<i>Eriophorum russeolum</i> bog	Grass/Sedge/Open bog	1772
	<i>Empetrum nigrum</i> - <i>Juniperus communis</i> dwarf heath	23.9
	<i>Maianthemum trifolium</i> bog	10.3
<i>Festuca rubra</i> - <i>Solidago sempervirens</i> - <i>Trifolium repens</i> disturbed coastal vegetation	<i>Juncus balticus</i> brackish marsh	194.1
	<i>Empetrum nigrum</i> - <i>Juniperus communis</i> dwarf heath	176.1
	Grass/Sedge/Open bog	174.9
<i>Gaylussacia baccata</i> shrubland	Mixed tall shrubs	31419
	<i>Empetrum nigrum</i> - <i>Juniperus communis</i> dwarf heath	17385
	<i>Cladonia</i> spp.	14284
<i>Gaylussacia</i> shrub bog	<i>Gaylussacia baccata</i> shrubland	3845
	<i>Cladonia</i> spp.	3192
	Grass/Sedge/Open bog	2570
Grass/Sedge/Open bog	<i>Empetrum nigrum</i> - <i>Juniperus communis</i> dwarf heath	60070
	<i>Cladonia</i> spp.	34567
	<i>Gaylussacia baccata</i> shrubland	10723
<i>Juncus balticus</i> brackish marsh	<i>Empetrum nigrum</i> - <i>Juniperus communis</i> dwarf heath	14704
	Grass/Sedge/Open bog	9832
	<i>Cladonia</i> spp.	646.2

(continued) Table 3.10. The top three most common neighbors of each plant community type at Prospect Bay.

Plant Community	Top Neighboring Communities	Shared Edge Length (m)
<i>Juniperus horizontalis</i> dwarf heath	<i>Empetrum nigrum</i> - <i>Juniperus communis</i> dwarf heath	1661
	<i>Spartina pectinata</i> brackish marsh	153.4
	<i>Juncus balticus</i> brackish marsh	134.5
<i>Lonicera villosa</i> shrubland	<i>Empetrum nigrum</i> - <i>Juniperus communis</i> dwarf heath	338.7
	Grass/Sedge/Open bog	184.2
	Mixed tall shrubs	116.7
<i>Maianthemum trifolium</i> bog	Grass/Sedge/Open bog	6173
	<i>Empetrum nigrum</i> - <i>Juniperus communis</i> dwarf heath	627.1
	<i>Juncus balticus</i> brackish marsh	529.2
Mixed tall shrubs	<i>Gaylussacia baccata</i> shrubland	31419
	<i>Empetrum nigrum</i> - <i>Juniperus communis</i> dwarf heath	24277
	<i>Osmunda cinnamomea</i> seep	4972
<i>Morella pensylvanica</i> shrubland	<i>Empetrum nigrum</i> - <i>Juniperus communis</i> dwarf heath	525.2
	<i>Gaylussacia baccata</i> shrubland	495.6
	<i>Osmunda cinnamomea</i> seep	283.2
<i>Osmunda cinnamomea</i> seep	<i>Gaylussacia baccata</i> shrubland	11642
	Mixed tall shrubs	4972
	Grass/Sedge/Open bog	2922
<i>Spartina pectinata</i> brackish marsh	<i>Empetrum nigrum</i> - <i>Juniperus communis</i> dwarf heath	314.4
	<i>Morella pensylvanica</i> shrubland	249.0
	<i>Juncus balticus</i> brackish marsh	191.3
<i>Toxicodendron radicans</i> coastal vegetation	<i>Spartina pectinata</i> brackish marsh	50.7
	<i>Empetrum nigrum</i> - <i>Juniperus communis</i> dwarf heath	8.1
	<i>Osmunda cinnamomea</i> seep	8.0

Environmental factors for plant communities at Prospect Bay indicated many interesting relationships (Table 3.11; see Figures A2.1-A2.8 for mapped environmental factors; see Figures A2.17-24 for confidence intervals and bar plots). In general, plant communities belonged to one of two altitudinal groupings: those occurring at elevations less than 15 m above sea-level and those occurring at elevations greater than 15 m.

Lower-altitude plant communities included Coastal vegetation, marshes, *Juniperus horizontalis* dwarf heath, and two smaller, i.e. shorter shrublands, (*Morella pensylvanica* shrubland & *Lonicera villosa* shrubland). Higher altitude communities included bogs, tree islands, larger shrublands (*Gaylussacia baccata* shrubland & Mixed tall shrubs), *Alnus viridis* shrubland, *Osmunda cinnamomea* seep, *Cladonia* spp., and *Empetrum nigrum* - *Juniperus communis* dwarf heath. Distance from the coastline was highly correlated with elevation above sea-level ( $r^2 = 0.83$ ), and plant communities similarly fell into two groups: lower altitude communities within 150 meters of the coastline and higher altitude communities that were further than 150 meters from the coastline.

Wind exposure was highest for plant communities nearest the coastline, which included *Toxicodendron radicans* coastal vegetation, *Spartina pectinata* brackish marsh, *Juniperus horizontalis* dwarf heath, and *Morella pensylvanica* shrubland (Table 3.11). Communities with lowest wind exposure values were *Eriophorum russeolum* bog, *Maianthemum trifolium* bog, *Gaylussacia shrub* bog, and Grass/Sedge/Open bog. Analysis of stream networks showed that *Maianthemum trifolium* bog occurred in very wet areas (stream order of 7). The next highest stream order was 5, which was recorded from the other bogs, *Betula papyrifera* tree island, and *Juncus balticus* brackish marsh. All other communities had stream orders of either 3 or 4. Incoming solar radiation had little variability between communities with values mostly ranging from 88 to 90, although communities nearest the coastline appeared to experience higher amounts of solar radiation, including *Toxicodendron radicans* coastal vegetation and *Spartina pectinata* brackish marsh. A closer look at the slope positions of the two communities and the solar radiation map (Figure A2.5B) suggests that both communities are angled on



upper slopes and midslopes and are facing south relative to the general slope in that area, which is likely the optimal position for receiving the most amount of sunlight from both the east and west.

Most plant communities at Prospect Bay occurred on flat or gentle sloping areas (Table 3.11). Several exceptions included *Juniperus horizontalis* dwarf heath, which occurred on ridges, *Toxicodendron radicans* coastal vegetation and *Morella pensylvanica* shrubland, which occurred on upper slopes, and Coniferous tree island, *Lonicera villosa* shrubland, and *Spartina pectinata* brackish marsh, all of which occurred on midslopes. The strong association of plant communities with flat areas at Prospect Bay was probably due to much of the site consisting of flats and gentle slopes (57.2%; Figure 3.7D). Local surface ruggedness was generally very low for all communities. Values were larger for plant communities nearest the coastline, such as *Toxicodendron radicans* coastal vegetation, *Spartina pectinata* brackish marsh, and *Juniperus horizontalis* dwarf heath. Local ruggedness values were particularly low for bogs. Similarly, global surface ruggedness was high for plant communities near the coastline and low for bogs.

Table 3.11. Environmental factors for plant communities at Prospect Bay. \*AW = Area-weighted; C.I = Area-weighted 95% confidence interval.

Plant Community	Elevation Above Sea-level (m)	Distance from Coastline (m)	Wind Exposure	Hydrology (Stream Order)	Incoming Solar Radiation	Slope Position	Local Surface Ruggedness	Global Surface Ruggedness
	AW Mean ± 95 % C.I.*	AW Mean ± 95 % C.I.	AW Mean ± 95 % C.I.	Most Frequent (AW)	AW Mean ± 95 % C.I.	Most Frequent (AW)	AW Mean ± 95 % C.I.	AW Mean ± 95 % C.I.
<i>Alnus viridis</i> shrubland	20.55 ± 0.26	273.65 ± 6.6	4.58 ± 0.35	3	89.29 ± 0.17	Flat	0.03 ± 0.003	9.34 ± 0.78
<i>Betula papyrifera</i> tree island	20.26 ± 2.66	334.62 ± 214.85	2.84 ± 1.12	5	89.02 ± 0.4	Flat	0.02 ± 0.02	8.46 ± 9.69
<i>Cladonia spp.</i>	21.41 ± 0.03	301.98 ± 1.01	2.79 ± 0.03	4	89.45 ± 0.01	Flat	0.01 ± 0.0003	7.87 ± 0.08
Coniferous tree island	21.49 ± 0.59	322.19 ± 20.53	7.18 ± 0.93	4	88.88 ± 0.36	Midslope	0.07 ± 0.01	8.24 ± 1.61
<i>Empetrum nigrum</i> - <i>Juniperus communis</i> dwarf heath	17.26 ± 0.11	212.2 ± 3.72	4.18 ± 0.06	4	89.93 ± 0.03	Flat	0.02 ± 0.0006	18.06 ± 0.32
<i>Eriophorum russeolum</i> bog	22.15 ± 0.04	513.37 ± 3.42	1.52 ± 0.02	5	88.47 ± 0.07	Flat	0.001 ± 0.0001	0.86 ± 0.05
<i>Festuca rubra</i> - <i>Solidago sempervirens</i> - <i>Trifolium repens</i> disturbed coastal vegetation	7.11 ± 0.28	35.91 ± 1.45	3.58 ± 0.83	4	89.87 ± 0.42	Flat	0.02 ± 0.007	49.33 ± 3.67
<i>Gaylussacia baccata</i> shrubland	23.06 ± 0.12	371.94 ± 3.23	3.71 ± 0.07	4	89.42 ± 0.04	Flat	0.02 ± 0.0006	9.3 ± 0.34
<i>Gaylussacia</i> shrub bog	22.58 ± 0.16	371.88 ± 4.23	2.01 ± 0.05	4	89.42 ± 0.06	Flat	0.01 ± 0.0005	6.95 ± 0.28
Grass/Sedge/Open bog	18.95 ± 0.1	298.24 ± 3.06	2.07 ± 0.03	5	89.18 ± 0.02	Flat	0.007 ± 0.0003	6.98 ± 0.27
<i>Juncus balticus</i> brackish marsh	12.37 ± 0.15	118.42 ± 2.54	2.96 ± 0.08	5	89.57 ± 0.04	Flat	0.01 ± 0.0006	18.94 ± 0.5
<i>Juniperus horizontalis</i> dwarf heath	8.03 ± 0.14	34.2 ± 1.12	12.33 ± 1.05	3	89.97 ± 0.58	Ridge	0.09 ± 0.01	69.68 ± 2.92
<i>Lonicera villosa</i> shrubland	11.24 ± 0.95	87.24 ± 7.2	6.09 ± 1.09	4	90.2 ± 0.54	Midslope	0.04 ± 0.008	31.23 ± 3.62
<i>Maianthemum trifolium</i> bog	19.63 ± 0.26	305.83 ± 5.89	1.77 ± 0.06	7	88.94 ± 0.04	Flat	0.003 ± 0.0007	3.01 ± 0.48
Mixed tall shrubs	22.25 ± 0.12	397.91 ± 4.65	2.74 ± 0.08	3	89.08 ± 0.06	Flat	0.02 ± 0.0009	4.48 ± 0.26
<i>Morella pensylvanica</i> shrubland	6.79 ± 0.13	33.96 ± 1.14	10.68 ± 1.03	3	91.07 ± 0.46	Upper Slope	0.07 ± 0.009	62.98 ± 3.1
<i>Osmunda cinnamomea</i> seep	20.68 ± 0.22	355.4 ± 5.73	3.1 ± 0.12	4	88.88 ± 0.09	Flat	0.02 ± 0.001	8.7 ± 0.66
<i>Spartina pectinata</i> brackish marsh	5.6 ± 0.16	27.75 ± 0.87	17.98 ± 1.69	4	92.33 ± 0.44	Midslope	0.16 ± 0.02	63.95 ± 3.26
<i>Toxicodendron radicans</i> coastal vegetation	6.02 ± 0.37	24.07 ± 5.51	26.66 ± 11.39	4	95.45 ± 8.61	Upper Slope	0.25 ± 0.11	83.98 ± 18.29

## Polly's Cove

Classification of high-resolution UAV imagery at Polly's Cove yielded a highly detailed map of plant communities and landscape features (Figure 3.8). The overall classification accuracy of plant communities was 78% (Table 3.12). Most misclassifications arose between structurally similar communities, the majority resulting between *Gaylussacia baccata* shrubland, Mixed tall shrubs, Broadleaf tree island, and *Rubus allegheniensis* - *Morella pensylvanica* coastal vegetation (see confusion matrix in Table A2.4). Plant communities with low field plot samples (< 4) also tended to have more misclassifications.

Table 3.12. Classification accuracies of mapped plant communities from the broadened association level classification at Polly's Cove.

Plant Community	Accuracy (%)
Broadleaf tree island	53
<i>Calamagrostis canadensis</i> coastal vegetation	40
<i>Carex nigra</i> - <i>Festuca rubra</i> coastal vegetation	100
<i>Carex nigra</i> bog	100
<i>Carex vesicaria</i> bog	100
<i>Cladonia</i> spp.	100
Coniferous tree island	90
<i>Empetrum nigrum</i> - <i>Juniperus communis</i> dwarf heath	55
<i>Gaylussacia baccata</i> shrubland	81
<i>Gaylussacia</i> shrub bog	56
<i>Ilex glabra</i> shrubland	90
<i>Juncus balticus</i> brackish marsh	60
<i>Juniperus communis</i> - <i>Corema conradii</i> lithomorphic	85
<i>Juniperus horizontalis</i> dwarf heath	60
Mixed tall shrubs	17
<i>Osmunda cinnamomea</i> seep	98
<i>Rubus allegheniensis</i> - <i>Morella pensylvanica</i> coastal vegetation	15
<i>Spartina patens</i> salt marsh	100
<i>Thalictrum pubescens</i> coastal vegetation	100
<i>Trichophorum caespitosum</i> bog	55
<b>Overall</b>	<b>78</b>

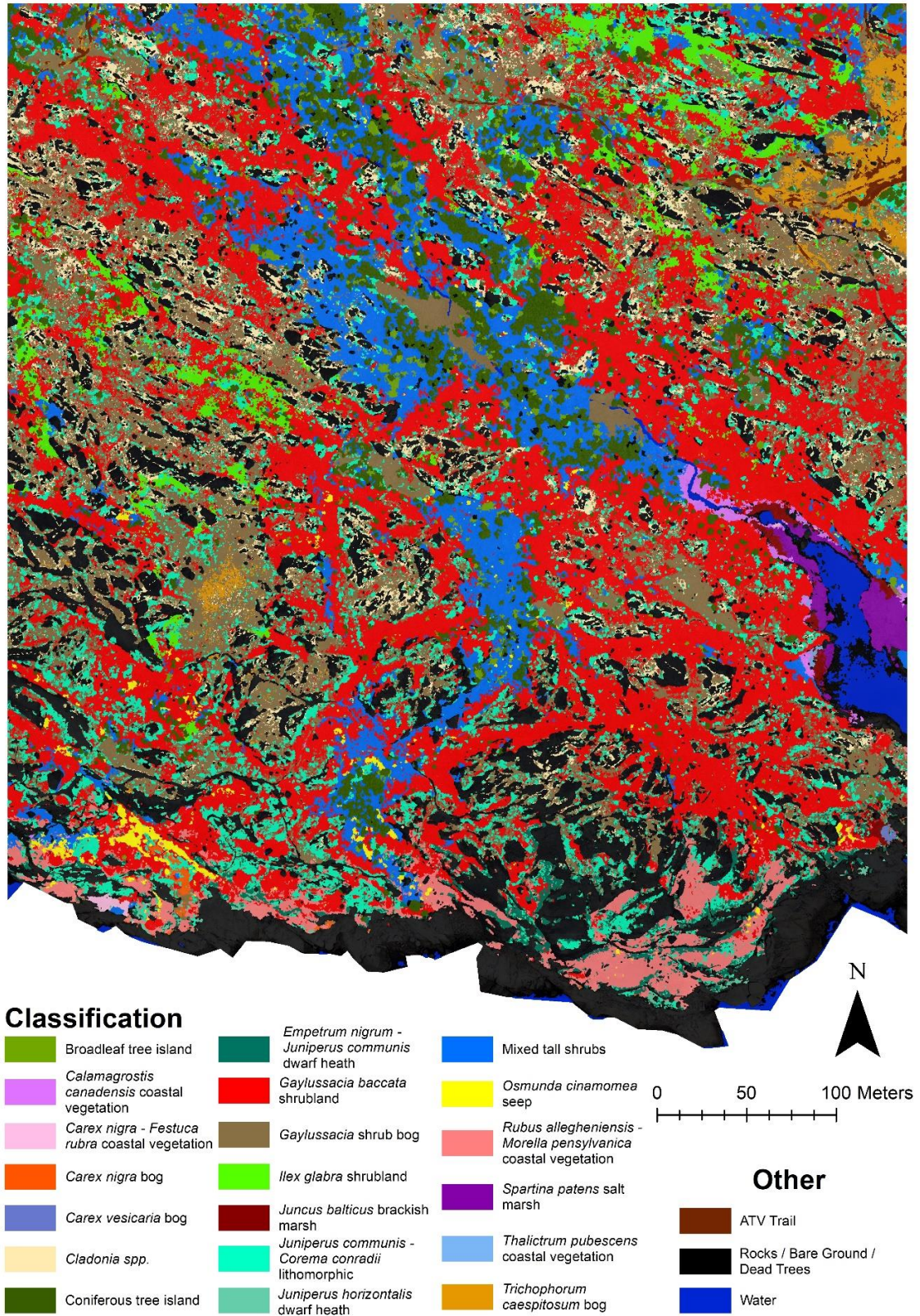


Figure 3.8. Mapped plant communities from the broadened association level classification at Polly's Cove, Nova Scotia.

The study area at Polly's Cove measured 27.4 ha, consisted of 20 plant community types and contained 53,595 plant community patches - a patch density of 1,957 per hectare. The total vegetation cover of the landscape was 79.3%, the remainder being mostly exposed rocks, cliff faces, and a body of salt water from the ocean occupying the southeast corner of the site (Figure 3.9C). Generally, the landscape was dominated by shrublands (38.1%), bogs (17.7%), and dwarf heath (9.2%) (Figure 3.9A). The most dominant plant communities were *Gaylussacia baccata* shrubland (27.9%), *Gaylussacia* shrub bog (16.5%), and *Juniperus communis* - *Corema conradii* lithomorphic (8.1%) respectively. The landscape topography was heterogeneous, largely consisting of midslopes (24.2%), ridges (18%), and valleys (16.6). (Figure 3.9D). Toe slopes, flats, and upper slopes were also prevalent, however, indicating a very high degree of topographic heterogeneity across the landscape. Lastly, a map of stream networks showed that one major stream extended diagonally across the site towards the inlet of salt water to the southeast and two other lesser streams flowed north to south, draining into the ocean (Figure 3.9B).

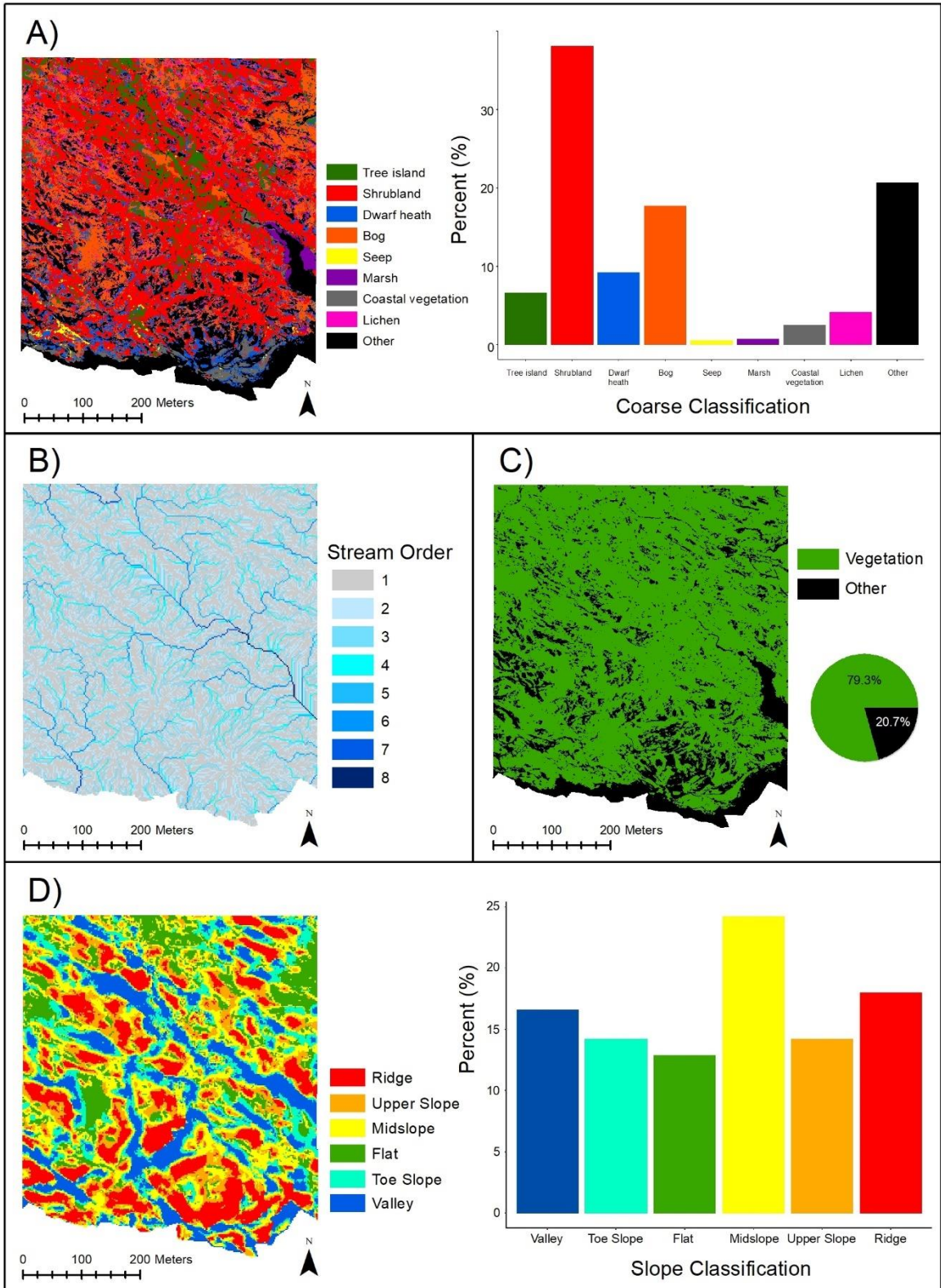


Figure 3.9. Landscape composition of Polly's Cove: A) Coarse classification of plant communities; B) Stream networks; C) Vegetation cover; and D) Slope classification.

Total class areas ranged from 43 m<sup>2</sup> (*Thalictrum pubescens* coastal vegetation) to 7.64 ha (*Gaylussacia baccata* shrubland) (Table 3.13). The number of patches ranged from 6 (*Thalictrum pubescens* coastal vegetation) to 23,299 (*Cladonia spp.*), although most classes consisted between 100 and 8,000 patches. Area-weighted mean patch areas were small for *Juniperus horizontalis* dwarf heath, *Cladonia spp.*, Broadleaf tree island, *Juniperus communis* - *Corema conradii* lithomorphic, and *Empetrum nigrum* - *Juniperus communis* dwarf heath. Classes with larger patch areas included *Gaylussacia baccata* shrubland and Mixed tall shrubs.

Plant communities with low shape complexities based on the shape index (area-weighted) included *Juniperus horizontalis* dwarf heath, Broadleaf tree island, *Juniperus communis* - *Corema conradii* lithomorphic, *Empetrum nigrum* - *Juniperus communis* dwarf heath, and *Cladonia spp.* (Table 3.13). Plant communities with larger shape complexities included *Gaylussacia baccata* shrubland, *Gaylussacia* shrub bog, *Trichophorum caespitosum* bog, and Mixed tall shrubs. Related circumscribing circle index (area-weighted) ranged from 0.52 (*Carex vesicaria* bog) to 0.77 (Mixed tall shrubs & *Trichophorum caespitosum* bog). Average nearest neighbor ratios indicated that plant communities were clustered at the landscape scale.

Tree islands were often neighbored by Mixed tall shrubs and *Gaylussacia baccata* shrubland (Table 3.14). Shrublands were often associated with *Gaylussacia* shrub bog, *Juniperus communis* - *Corema conradii* lithomorphic, as well as other types of shrublands. *Empetrum nigrum* - *Juniperus communis* dwarf heath was mostly associated with *Juniperus communis* - *Corema conradii* lithomorphic and *Rubus allegheniensis* - *Morella pensylvanica* coastal vegetation. *Juniperus horizontalis* dwarf heath was also

associated with *Juniperus communis* - *Corema conradii* lithomorphic and *Rubus allegheniensis* - *Morella pensylvanica* coastal vegetation, as well as *Empetrum nigrum* - *Juniperus communis* dwarf heath. *Juniperus communis* - *Corema conradii* lithomorphic was frequently adjacent to *Gaylussacia* shrub bog, *Gaylussacia baccata* shrubland, and *Cladonia spp.* All bogs were associated with *Gaylussacia* shrub bog and *Juniperus communis* - *Corema conradii* lithomorphic. *Gaylussacia* shrub bog was often neighbored by *Gaylussacia baccata* shrubland, *Cladonia spp.*, and *Juniperus communis* - *Corema conradii* lithomorphic. *Osmunda cinnamomea* seep was associated with *Gaylussacia baccata* shrubland. Both *Spartina patens* salt marsh and *Juncus balticus* brackish marsh were associated with each other as well as with *Calamagrostis canadensis* coastal vegetation. All Coastal vegetation types were associated with either Mixed tall shrubs, *Gaylussacia baccata* shrubland, or both. *Carex nigra* - *Festuca rubra* coastal vegetation and *Thalictrum pubescens* coastal vegetation were also strongly associated with *Calamagrostis canadensis* coastal vegetation. *Calamagrostis canadensis* coastal vegetation also had an association with *Juncus balticus* brackish marsh. *Rubus allegheniensis* - *Morella pensylvanica* coastal vegetation was often neighbored by *Gaylussacia baccata* shrubland, *Empetrum nigrum* - *Juniperus communis* dwarf heath, and *Juniperus communis* - *Corema conradii* lithomorphic. Lastly, *Cladonia spp.* was frequently neighbored by *Gaylussacia* shrub bog, *Gaylussacia baccata* shrubland, and *Juniperus communis* - *Corema conradii* lithomorphic.



Table 3.13. Summary of the spatial configurations of plant community patches at Polly's Cove. \*AW = Area-weighted.

Plant Community	Class Area (ha)	Number of Patches	Patch Area (m)		Patch Perimeter (m)		Perimeter-Area Ratio		Shape Index		Related Circumscribing Circle Index		Average Nearest Neighbor Ratio
			AW* Mean	SD	AW Mean	SD	AW Mean	SD	AW Mean	SD	AW Mean	SD	
Broadleaf tree island	0.24	398	13.85	6.87	34.10	13.60	3.31	12.66	2.34	0.50	0.61	0.15	0.70
<i>Calamagrostis canadensis</i> coastal vegetation	0.07	63	64.48	24.76	92.46	33.38	2.24	2.58	3.04	0.72	0.75	0.12	0.22
<i>Carex nigra</i> - <i>Festuca rubra</i> coastal vegetation	0.01	9	119.66	43.58	128.69	45.02	1.36	2.39	2.93	0.56	0.72	0.12	0.16
<i>Carex nigra</i> bog	0.02	34	57.05	18.40	103.39	31.85	2.65	2.25	3.38	0.67	0.64	0.10	0.16
<i>Carex vesicaria</i> bog	0.01	7	48.98	19.35	83.90	31.78	2.10	32.57	3.00	0.60	0.52	0.25	0.05
<i>Cladonia</i> spp.	1.12	23299	10.77	2.21	37.91	7.68	6.84	10.47	2.66	0.42	0.66	0.14	0.62
Coniferous tree island	1.56	1311	130.73	37.41	146.97	40.91	1.83	7.98	2.94	0.55	0.58	0.14	0.88
<i>Empetrum nigrum</i> - <i>Juniperus communis</i> dwarf heath	0.28	1023	20.14	6.88	49.93	15.96	3.99	5.87	2.64	0.52	0.67	0.13	0.39
<i>Gaylussacia baccata</i> shrubland	7.64	3780	6255	352.45	7068	400.33	1.73	11.79	18.98	1.34	0.76	0.14	0.80
<i>Gaylussacia</i> shrub bog	4.53	7746	629.26	59.95	1460	141.65	3.59	11.50	11.38	1.27	0.76	0.15	0.88
<i>Ilex glabra</i> shrubland	0.65	967	157.60	31.61	276.92	55.92	2.86	10.31	5.04	0.90	0.72	0.14	0.38
<i>Juncus balticus</i> brackish marsh	0.06	47	88.38	32.02	129.86	46.30	1.91	2.57	3.46	0.80	0.75	0.14	0.12
<i>Juniperus communis</i> - <i>Corema conradii</i> lithomorphhic	2.21	7472	19.54	6.96	48.04	16.03	3.81	9.17	2.56	0.51	0.63	0.14	0.97
<i>Juniperus horizontalis</i> dwarf heath	0.03	149	5.92	2.73	18.99	7.39	4.60	10.27	1.99	0.38	0.63	0.13	0.27
Mixed tall shrubs	2.14	982	1130	154.31	1511	207.73	1.98	13.31	9.72	1.37	0.77	0.15	0.68
<i>Osmunda cinnamomea</i> seep	0.14	370	83.52	17.45	123.54	25.14	3.04	5.12	3.09	0.47	0.68	0.12	0.45
<i>Rubus allegheniensis</i> - <i>Morella pennsylvanica</i> coastal vegetation	0.58	718	340.06	51.50	384.79	58.78	2.27	7.66	4.93	0.75	0.73	0.13	0.35
<i>Spartina patens</i> salt marsh	0.14	20	512.83	177.41	262.25	101.08	0.82	20.11	3.19	0.94	0.69	0.20	0.10
<i>Thalictrum pubescens</i> coastal vegetation	< 0.01	6	23.70	11.93	72.37	34.08	3.53	36.20	3.64	0.96	0.74	0.27	0.03
<i>Trichophorum caespitosum</i> bog	0.28	385	713.91	71.13	1111	112.93	2.64	9.95	9.91	1.10	0.77	0.14	0.24

Table 3.14. The top three most common neighbors of each plant community type at Polly's Cove.

Plant Community	Top Neighboring Communities	Shared Edge Length (m)
Broadleaf tree island	Mixed tall shrubs	3711
	Coniferous tree island	1893
	<i>Gaylussacia baccata</i> shrubland	1737
<i>Calamagrostis canadensis</i> coastal vegetation	<i>Gaylussacia baccata</i> shrubland	487.5
	<i>Juncus balticus</i> brackish marsh	176.4
	Mixed tall shrubs	143.4
<i>Carex nigra</i> - <i>Festuca rubra</i> coastal vegetation	Mixed tall shrubs	25.5
	<i>Calamagrostis canadensis</i> coastal vegetation	21.9
	<i>Gaylussacia baccata</i> shrubland	21.2
<i>Carex nigra</i> bog	<i>Juniperus communis</i> - <i>Corema conradii</i> lithomorphic	213.5
	<i>Gaylussacia</i> shrub bog	123.7
	<i>Rubus allegheniensis</i> - <i>Morella pensylvanica</i> coastal vegetation	100.2
<i>Carex vesicaria</i> bog	<i>Gaylussacia</i> shrub bog	33.5
	<i>Juncus balticus</i> brackish marsh	29.2
	<i>Juniperus communis</i> - <i>Corema conradii</i> lithomorphic	21.4
<i>Cladonia</i> spp.	<i>Gaylussacia</i> shrub bog	39483
	<i>Gaylussacia baccata</i> shrubland	7919
	<i>Juniperus communis</i> - <i>Corema conradii</i> lithomorphic	6334
Coniferous tree island	Mixed tall shrubs	10498
	<i>Gaylussacia baccata</i> shrubland	6582
	<i>Juniperus communis</i> - <i>Corema conradii</i> lithomorphic	3257
<i>Empetrum nigrum</i> - <i>Juniperus communis</i> dwarf heath	<i>Juniperus communis</i> - <i>Corema conradii</i> lithomorphic	3878
	<i>Rubus allegheniensis</i> - <i>Morella pensylvanica</i> coastal vegetation	2438
	<i>Gaylussacia baccata</i> shrubland	875.8
<i>Gaylussacia baccata</i> shrubland	<i>Gaylussacia</i> shrub bog	49204
	<i>Juniperus communis</i> - <i>Corema conradii</i> lithomorphic	19224
	Mixed tall shrubs	14012
<i>Gaylussacia</i> shrub bog	<i>Gaylussacia baccata</i> shrubland	49204
	<i>Cladonia</i> spp.	39483
	<i>Juniperus communis</i> - <i>Corema conradii</i> lithomorphic	34192
<i>Ilex glabra</i> shrubland	<i>Gaylussacia baccata</i> shrubland	8665
	<i>Gaylussacia</i> shrub bog	2791
	<i>Juniperus communis</i> - <i>Corema conradii</i> lithomorphic	2154
<i>Juncus balticus</i> brackish marsh	<i>Spartina patens</i> salt marsh	279.6
	<i>Calamagrostis canadensis</i> coastal vegetation	176.4
	<i>Gaylussacia</i> shrub bog	133.3

(continued) Table 3.14. The top three most common neighbors of each plant community type at Polly's Cove.

Plant Community	Top Neighboring Communities	Shared Edge Length (m)
<i>Juniperus communis</i> - <i>Corema conradii</i> lithomorphic	<i>Gaylussacia</i> shrub bog	34192
	<i>Gaylussacia baccata</i> shrubland	19224
	<i>Cladonia</i> spp.	6334
<i>Juniperus horizontalis</i> dwarf heath	<i>Empetrum nigrum</i> - <i>Juniperus communis</i> dwarf heath	342.1
	<i>Juniperus communis</i> - <i>Corema conradii</i> lithomorphic	218.9
	<i>Rubus allegheniensis</i> - <i>Morella pensylvanica</i> coastal vegetation	171.3
Mixed tall shrubs	<i>Gaylussacia baccata</i> shrubland	14012
	Coniferous tree island	10498
	<i>Gaylussacia</i> shrub bog	3742
<i>Osmunda cinnamomea</i> seep	<i>Gaylussacia baccata</i> shrubland	2137
	Mixed tall shrubs	1016
	<i>Rubus allegheniensis</i> - <i>Morella pensylvanica</i> coastal vegetation	557.6
<i>Rubus allegheniensis</i> - <i>Morella pensylvanica</i> coastal vegetation	<i>Gaylussacia baccata</i> shrubland	3773
	<i>Empetrum nigrum</i> - <i>Juniperus communis</i> dwarf heath	2438
	<i>Juniperus communis</i> - <i>Corema conradii</i> lithomorphic	1947
<i>Spartina patens</i> salt marsh	<i>Juncus balticus</i> brackish marsh	279.6
	<i>Calamagrostis canadensis</i> coastal vegetation	113.6
	<i>Gaylussacia baccata</i> shrubland	11.6
<i>Thalictrum pubescens</i> coastal vegetation	<i>Calamagrostis canadensis</i> coastal vegetation	65.7
	<i>Juncus balticus</i> brackish marsh	42.8
	<i>Gaylussacia baccata</i> shrubland	19.6
<i>Trichophorum caespitosum</i> bog	<i>Gaylussacia</i> shrub bog	5016
	<i>Juniperus communis</i> - <i>Corema conradii</i> lithomorphic	341.5
	<i>Cladonia</i> spp.	177.6

Many associations were observed when plant communities at Polly's Cove were related to environmental factors (Table 3.15; see Figures A2.1-A2.8 for mapped environmental factors; see Figures A2.25-32 for confidence intervals and bar plots). Mean elevations for plant communities ranged from just below a meter to 16 meters. Plant communities at higher elevations included *Empetrum nigrum* - *Juniperus communis* dwarf heath, *Juniperus communis* - *Corema conradii* lithomorphic, *Gaylussacia shrub* bog, *Cladonia* spp., and *Ilex glabra* shrubland. Plant communities at lower elevations

included *Spartina patens* salt marsh, *Thalictrum pubescens* coastal vegetation, *Juncus balticus* brackish marsh, *Calamagrostis canadensis* coastal vegetation, *Carex nigra* - *Festuca rubra* coastal vegetation, and *Carex vesicaria* bog. Tree islands, shrublands, *Cladonia spp.*, *Trichophorum caespitosum* bog, and *Gaylussacia shrub* bog were situated further from the coastline (> 250 m). Other communities, including *Juniperus communis* - *Corema conradii* lithomorphic, *Calamagrostis canadensis* coastal vegetation, *Thalictrum pubescens* coastal vegetation, marshes, and *Osmunda cinnamomea* seep, occurred at more intermediate distances from the coastline (between 100 to 250 m). Plant communities found nearest the coastline (< 100 m) included *Carex nigra* - *Festuca rubra* coastal vegetation, *Juniperus horizontalis* dwarf heath, *Carex nigra* bog, *Rubus allegheniensis* - *Morella pensylvanica* coastal vegetation, and *Carex vesicaria* bog. It should be noted that although distance from coastline values for marshes and some of the coastal vegetation were recorded at intermediate ranges (between 100 to 250 meters), the plant communities in the south-eastern portion of the site were actually near a salt water inlet (see plant community map in Figure 3.8). For this study, the inlet was not included as part of the coastline.

Wind exposure was highest for *Rubus allegheniensis* - *Morella pensylvanica* coastal vegetation, *Empetrum nigrum* - *Juniperus communis* dwarf heath, and *Juniperus horizontalis* dwarf heath (Table 3.15). Communities with low wind exposure values included bogs, marshes, and other Coastal vegetation. Analysis of stream networks at Polly's Cove showed a high variability in moisture regimes for different communities. Plant communities in the wettest areas were *Calamagrostis canadensis* coastal vegetation, *Carex nigra* bog, *Osmunda cinnamomea* seep, Coniferous tree island, and

*Trichophorum caespitosum* bog. Plant communities in dryer areas included *Cladonia spp.*, *Empetrum nigrum* - *Juniperus communis* dwarf heath, and *Juniperus communis* - *Corema conradii* lithomorph. All other communities had intermediate moisture regimes. A large amount of variability was observed in incoming solar radiation as well. Communities with low solar radiation values included tree islands, *Gaylussacia baccata* shrubland, Mixed tall shrubs, and *Cladonia spp.* Higher values of solar radiation were recorded from *Juniperus horizontalis* dwarf heath, *Rubus allegheniensis* - *Morella pensylvanica* coastal vegetation, *Carex nigra* - *Festuca rubra* coastal vegetation, and *Empetrum nigrum* - *Juniperus communis* dwarf heath.

Slope position classifications varied for plant communities (Table 3.15). Ridges were the most common slope position for *Cladonia spp.*, *Empetrum nigrum* - *Juniperus communis* dwarf heath, *Juniperus communis* - *Corema conradii* lithomorph, *Juniperus horizontalis* dwarf heath, and *Rubus allegheniensis* - *Morella pensylvanica* coastal vegetation. Midslopes often associated with tree islands, and *Gaylussacia baccata* shrubland. Flat areas were occupied by *Trichophorum caespitosum* bog, *Gaylussacia shrub* bog, and *Carex vesicaria* bog. Toe slopes were common to two of the Coastal vegetation types: *Carex nigra* - *Festuca rubra* coastal vegetation and *Thalictrum pubescens* coastal vegetation. Valleys were often occupied by marshes, *Osmunda cinnamomea* seep, *Carex nigra* bog, *Calamagrostis canadensis* coastal vegetation, *Ilex glabra* shrubland, and Mixed tall shrubs. Local surface ruggedness was high for *Rubus allegheniensis* - *Morella pensylvanica* coastal vegetation, *Empetrum nigrum* - *Juniperus communis* dwarf heath, and *Juniperus horizontalis* dwarf heath. Conversely, local ruggedness was noticeably low for *Trichophorum caespitosum* bog, *Carex vesicaria*

bog, *Spartina patens* salt marsh, and *Juncus balticus* brackish marsh. Similarly, global surface ruggedness was highest for *Rubus allegheniensis* - *Morella pensylvanica* coastal vegetation, *Empetrum nigrum* - *Juniperus communis* dwarf heath, and *Juniperus horizontalis* dwarf heath. Global surface ruggedness was particularly low for *Ilex glabra* shrubland and *Trichophorum caespitosum* bog.

Table 3.15. Environmental factors for plant communities at Polly’s Cove. \*AW = Area-weighted; C.I = Area-weighted 95% confidence interval.

Plant Community	Elevation Above Sea-level (m)	Distance from Coastline (m)	Wind Exposure	Hydrology (Stream Order)	Incoming Solar Radiation	Slope Position	Local Surface Ruggedness	Global Surface Ruggedness
	AW Mean ± 95% C.I.*	AW Mean ± 95% C.I.	AW Mean ± 95% C.I.	Most Frequent (AW)	AW Mean ± 95% C.I.	Most Frequent (AW)	AW Mean ± 95% C.I.	AW Mean ± 95% C.I.
Broadleaf tree island	9.84 ± 0.34	360.88 ± 9.57	15.08 ± 1	4	76.57 ± 0.89	Midslope	1.17 ± 0.12	6.61 ± 0.53
<i>Calamagrostis canadensis</i> coastal vegetation	1.54 ± 0.34	212.64 ± 10.1	5.74 ± 0.92	8	81.6 ± 1.24	Valley	0.4 ± 0.07	7.77 ± 1.53
<i>Carex nigra</i> - <i>Festuca rubra</i> coastal vegetation	2.16 ± 1.02	25.5 ± 72.82	6.95 ± 2.5	5	87.05 ± 2.85	Toe Slope	0.26 ± 0.07	24.46 ± 5.27
<i>Carex nigra</i> bog	6.25 ± 0.5	34.47 ± 3.95	4.33 ± 1.88	7	85.33 ± 0.97	Valley	0.27 ± 0.25	26.21 ± 2.33
<i>Carex vesicaria</i> bog	2.62 ± 0.23	41.88 ± 7.2	1.36 ± 0.66	5	83.63 ± 1.9	Flat	0.06 ± 0.06	5.7 ± 0.61
<i>Cladonia</i> spp.	14.82 ± 0.05	328.97 ± 1.18	7.47 ± 0.08	3	80.89 ± 0.08	Ridge	0.42 ± 0.007	5.35 ± 0.05
Coniferous tree island	9.47 ± 0.2	345.49 ± 5.33	8.98 ± 0.35	6	80.36 ± 0.33	Midslope	0.63 ± 0.03	5.19 ± 0.25
<i>Empetrum nigrum</i> - <i>Juniperus communis</i> dwarf heath	16.08 ± 0.39	45.23 ± 1.36	24.71 ± 0.88	3	87.04 ± 0.48	Ridge	2.71 ± 0.19	46.72 ± 1.32
<i>Gaylussacia baccata</i> shrubland	12.72 ± 0.12	259.96 ± 3.64	10.17 ± 0.14	4	80.47 ± 0.16	Midslope	0.61 ± 0.01	9.81 ± 0.22
<i>Gaylussacia</i> shrub bog	14.96 ± 0.11	282.66 ± 2.42	5.08 ± 0.1	5	82.1 ± 0.1	Flat	0.26 ± 0.008	6.3 ± 0.13
<i>Ilex glabra</i> shrubland	14.56 ± 0.18	377.25 ± 5.12	8.2 ± 0.3	4	85.16 ± 0.28	Valley	0.37 ± 0.01	3.85 ± 0.1
<i>Juncus balticus</i> brackish marsh	1.37 ± 0.17	158.73 ± 17.42	2.93 ± 0.84	5	82.97 ± 0.65	Valley	0.14 ± 0.04	10.86 ± 1.69
<i>Juniperus communis</i> - <i>Corema conradii</i> lithomorphic	15.22 ± 0.12	222.23 ± 2.85	10.96 ± 0.21	3	83.49 ± 0.16	Ridge	0.73 ± 0.02	12.18 ± 0.27
<i>Juniperus horizontalis</i> dwarf heath	9.72 ± 1	25.58 ± 3.3	23.58 ± 2.37	4	90.32 ± 0.93	Ridge	2.51 ± 0.67	36.98 ± 2.84
Mixed tall shrubs	9.76 ± 0.23	317.66 ± 7.08	11.53 ± 0.4	4	78.88 ± 0.36	Valley	0.83 ± 0.03	8.73 ± 0.41
<i>Osmunda cinnamomea</i> seep	10.96 ± 0.42	106.92 ± 9.23	8.08 ± 0.61	7	81.98 ± 0.57	Valley	0.62 ± 0.09	19.42 ± 1.21
<i>Rubus allegheniensis</i> - <i>Morella pennsylvanica</i> coastal vegetation	12.7 ± 0.39	35.26 ± 1.2	24.98 ± 0.97	4	88.73 ± 0.44	Ridge	2.9 ± 0.29	50.87 ± 1.4
<i>Spartina patens</i> salt marsh	0.9 ± 0.02	169.87 ± 9.24	2.73 ± 0.78	4	82.24 ± 1.07	Valley	0.13 ± 0.09	15.16 ± 2.68
<i>Thalictrum pubescens</i> coastal vegetation	1.35 ± 0.1	148.05 ± 19.03	4.16 ± 7.73	5	82.86 ± 6.95	Toe Slope	0.34 ± 0.72	7.02 ± 0.41
<i>Trichophorum caespitosum</i> bog	12.3 ± 0.33	382.67 ± 8.51	1.82 ± 0.12	6	83.92 ± 0.12	Flat	0.04 ± 0.01	1.18 ± 0.09

## Discussion

For the first time, landscape patterns of plant community patches in the coastal barrens near Halifax, Nova Scotia were quantified at the fine-scale. Mapping plant community patches using high-resolution multispectral UAV imagery provided many insights into the overall structure of coastal barrens landscapes and the spatial patterns and relationships of the plant communities that occupy them. All three sites exhibited complex spatial patterns of plant communities, a wide spectrum of environmental gradients and topographic heterogeneity, and a high degree of patchiness. Furthermore, plant community patches varied greatly in size, shape, abundance, and spatial distribution from one plant community type to another and in many cases from one site to another. It is without a doubt that these complex landscape patterns are linked to various combinations of environmental factors; however, which combinations of environmental factors and for which communities remains to be determined.

Coastal barrens landscapes in Halifax, Nova Scotia were dominated by shrublands and dwarf heath; however, their spatial patterns were not always consistent among sites. Interestingly, the most dominant plant community across the three sites was *Gaylussacia baccata* shrubland, occupying on average 21.6% of the three landscapes. Some studies have suggested that *Gaylussacia baccata* is the dominant shrub in the coastal barrens of eastern North America (Strang, 1972; Matlack et al., 1993; Harper, 1995; Dunwiddie et al., 1996); however, no study has been able to confirm this until now by using distributional maps. Dominance, however, was site-specific, and although *Gaylussacia baccata* shrubland was overall the most dominant community across the three landscapes,



*Empetrum nigrum* - *Juniperus communis* dwarf heath was most dominant at Prospect Bay.

*Gaylussacia baccata* shrubland tended to have very large patch areas with irregular shapes, occurring mostly on midslopes. Similar to Porter (2013), *Gaylussacia baccata* shrubland was often found in higher elevations further from the coastline. However, two types of dwarf heath were most abundant across the three sites but had inconsistent spatial patterns among sites: *Empetrum nigrum* - *Juniperus communis* dwarf heath and *Juniperus communis* - *Corema conradii* lithomorphic. At Prospect Bay, *Empetrum nigrum* - *Juniperus communis* dwarf heath was the most abundant of all communities, occupying 38% of the landscape. The community had large patch areas with irregular shapes and mostly occurred on flats and midslopes closer to the coastline but also extending further inland. Interestingly, since the topography of Prospect Bay was homogeneous with few rock outcrops, *Juniperus communis* - *Corema conradii* lithomorphic was non-existent at the site. Conversely, at Chebucto Head and Polly's Cove, *Juniperus communis* - *Corema conradii* lithomorphic was the dominant dwarf heath, mostly occupying exposed rock faces and ridges with small to medium patch sizes and simpler patch shapes. *Empetrum nigrum* - *Juniperus communis* dwarf heath was found within 150 m of the coastline for the two sites; however, its abundance was much lower at Polly's Cove (0.28 ha) when compared to Chebucto Head (1.26 ha). This may be partly caused by the large barrier island (Figure 3.3) at Polly's Cove providing shelter from wind and salt spray for parts of the site nearest the water, which could have created more favorable conditions for other communities such as *Rubus allegheniensis* - *Morella pennsylvanica* coastal vegetation and bogs. This would support the hypothesis of Cameron

and Bondrup-Nielsen (2013) that taller shrub communities rather than dwarf heath would exist near the coastline if it weren't for the high winds and salt spray.

Tree islands were common at Chebucto Head and Polly's Cove but were seldom at Prospect Bay. Coniferous tree island patches were mostly large with simple shapes while Broadleaf tree islands also had simple shapes but had much smaller patch areas and were often intermixed with Coniferous tree islands and Mixed tall shrubs. Mixed tall shrubs were more prevalent across the three sites and had large irregular patch areas. Analysis of stream networks indicated that both tree islands and tall shrubs mostly occurred in moderately wet areas and further inland, which is consistent with Burley and Lundholm (2010). Although tree islands were recorded as occurring on midslopes from the slope position model, they actually occurred in valleys and on flats. The misclassification of slope position resulted from the limitation of computing ground elevation models from UAV imagery; 3D information can only be computed from what the UAV can 'see', so only vegetation canopies, not the ground beneath vegetation canopies, were reconstructed. This can be mostly alleviated by generalizing the elevation model to a coarser resolution, for example 2 m, and assigning the minimum elevation value within each cell. This technique of computing a ground DEM will still be limited for larger stands of trees when there is no visible ground nearby. This issue was not as apparent for Mixed tall shrubs, where they were found mostly on midslopes at Chebucto Head, flats at Prospect Bay, and valleys at Polly's Cove. Interestingly, a strong relationship was found between tree islands and tall shrubs, where tall shrubs often surrounded tree islands (Burley et al., 2010). It is possible that this was due to succession, where tree islands colonized valleys and gradually succeeded the original tall shrub

communities. Another explanation could be due to topographic gradients: tree islands may be more suited to sheltered valleys and the transition from valleys to midslopes provided more suitable habitat for tall shrubs rather than tree islands.

Various types of bogs were present at all three sites although they were most abundant at Prospect Bay and Polly's Cove. Patch areas, numbers, and shapes varied according to the type of bog, but most had small to medium sized patch areas with simple shapes. The main exception was at Prospect Bay, where Grass/Sedge/Open bogs were the second most dominant plant community type, occupied 20.6% of the landscape, and had irregular patch shapes. What was most interesting was that the majority of bogs seemed to depend on two main environmental factors occurring at two different scales: slope position classification (local) and the spatial distribution of stream networks across the landscape (global), which would depend on the shape of the landscape as a whole. Bogs mostly occurred on flat areas that had one or more higher order streams either flowing directly into it or was flowing nearby. This dependency of bogs on flat areas and stream networks would explain the large prevalence of bogs at Prospect Bay, since the site was mostly composed of flat areas or gentle slopes and had two main streams that undulated across the site, tracing the distribution of the bogs.

In addition to slope position and location of stream networks, bogs also occurred in areas of low wind exposure, low local and global topographic ruggedness, and mostly at higher altitudes and distances further from the coastline. One exception was at Polly's Cove, where two bogs were found occurring near the coastline. Their unusual occurrence near the coastline was likely caused by the sheltering of wind and salt spray from the large barrier island to the south-west of the site (Figure 3.3).

Spatial patterns of marshes and seeps varied from one site to another. *Osmunda cinnamomea* seep was the only kind of seep detected and was present at all sites. Spatial patterns were very similar at Chebucto Head and Polly's Cove, where *Osmunda cinnamomea* seep inhabited valleys with highest stream orders, mostly occurred within 150 meters of the coastline and in intermediate elevations. Conversely, at Prospect Bay *Osmunda cinnamomea* seep was recorded in higher elevations, further from the coastline (> 300 meters), in flat areas and with medium stream orders. Patches were small to medium-sized and had low shape complexity. Interestingly, across all three sites *Osmunda cinnamomea* seep was most often adjacent to *Gaylussacia baccata* shrubland and Mixed tall shrubs.

Marshes were only observed at Prospect Bay and Polly's Cove. Spatial patterns of marshes at the two sites were quite different. At Prospect Bay, *Juncus balticus* brackish marsh was observed in an alluvial fan in the south-western portion of the site accompanied by Grass/Sedge/Open bogs, whereas at Polly's Cove, *Juncus balticus* brackish marsh accompanied *Spartina patens* salt marsh in a salt water inundation zone in the south-eastern portion of the site and in much lower elevations (< 2 m). These findings are consistent with Porter et al. (2015), who found that *Spartina patens* salt marsh often was competitively dominant in the lower areas of salt water inundation zones with higher salt concentration and *Juncus balticus* brackish marsh occupied slightly higher elevations. The other marsh at Prospect Bay was *Spartina pectinata* brackish marsh, which occurred in low elevations closer to the coastline and on midslopes. All types of marshes generally had small to medium-sized patch areas with low to intermediate shape complexities. It is hypothesized that marshes were not observed at Chebucto Head because of the

topography of the site. Based on observations from Prospect Bay and Polly's Cove and previous studies on salt marshes (Porter et al., 2015; van Proosdij et al., 2006), marshes are more suited to low elevations, particularly for salt water marshes requiring tidal inundation, and simple flat terrain. Since much of Chebucto Head's coastline is rugged cliffs with few flat areas near the coastline, there is no suitable habitat for marshes at the site.

Coastal vegetation was a class used to capture all other communities occurring along the coastline, mostly being herbaceous. Each site had unique coastal vegetation types, although *Calamagrostis canadensis* coastal vegetation was present at both Chebucto Head and Polly's Cove. Coastal vegetation mostly inhabited areas of low elevation closest to the coastline and experienced medium to high amounts of wind exposure and surface ruggedness (local and global). Patch numbers were mostly low and sizes of patches were small to medium-sized with low to medium shape complexity.

Perhaps one of the most unexpected results of this study was the sheer abundance of *Cladonia* spp. at all three sites. Lichens can be very sensitive to disturbance and many species of lichens are listed as either uncommon or rare, making them a high priority for conservation efforts (Christensen and Johnsen, 2001; Porter, 2013). The presence of lichen in the coastal barrens in Nova Scotia has been previously noted (Oberndorfer and Lundholm, 2009; Cameron and Bondrup-Nielsen, 2013; Porter, 2013); however, no study to date has been able to quantify its abundance across a landscape due to the coarseness of previous remote sensing techniques. The amount of lichen occupying each site was very similar: Chebucto Head had 1.2 ha of *Cladonia* spp.; Prospect Bay had 1.22 ha; and Polly's Cove had 1.12 ha. Patches were numerous across each landscape (> 15,000) and

tended to be small to medium-sized with low to intermediate shape complexity. At Chebucto Head and Polly's Cove, lichen was most abundant on ridges and rock exposures with low moisture availability. At Prospect Bay, however, rock exposures were infrequent, and lichen instead inhabited flat, gentle sloping areas that were moderately wet. Interestingly, this same habitat type occurred on the eastern part of Chebucto Head, 50-100 m from the coastline, where an unexpectedly dense population of *Cladonia spp.* was observed. This suggests that there are at least two environmental scenarios for which *Cladonia spp.* are likely to occur in dense populations on a landscape: on dry rock-exposed ridges or on moderately wet flats or gentle slopes. This is supported by Oberndorfer and Lundholm (2009), who found that various species of *Cladonia* occupy different niches and habitats in the coastal barrens. Having knowledge of the locations and environmental requirements of rare or uncommon species across a landscape could help to better focus conservation efforts for protecting sensitive species like lichen.

Patch perimeters were highly correlated with patch areas ( $r^2 = 0.99$ ). Perimeter-area ratios (area-weighted) of patches were generally smaller for classes with larger patch areas compared to classes with smaller patch areas. Although perimeter-area ratio and shape index are both measures of shape complexity, results from the two metrics were not consistent for classes with larger patch areas. For example, *Gaylussacia baccata* shrubland had an area-weighted perimeter-area ratio of 1.60, the second lowest score, but had an area-weighted shape index of 22.16, the highest shape index recording for any class at Chebucto Head. This is consistent with Patton (1975), who proposed the shape index as an alternative to the conventional perimeter-area ratio as a measure of shape complexity, since perimeter-area ratio fails to account for differences in patch sizes.

Instead, shape index evaluates the complexity of a patch by comparing it to a circle or square standard.

In this study, environmental factors, including elevation and wind exposure, were mapped across each site to help understand the structure and spatial heterogeneity of the landscapes. Chebucto Head and Polly's Cove had similarly high degrees of topographic heterogeneity and as a result had similar landscape patterns for the dominant vegetation types. Topographic variability of Prospect Bay was much different, having a much more homogeneous and uniform landscape. Not surprisingly, plant communities and their spatial patterns were quite different. Based on these findings, using 3D models from the SfM photogrammetric processing of UAV imagery and GIS techniques to model environmental factors gave many useful insights into the dynamic nature of coastal barrens and helped to explain the complex spatial patterns of the plant communities. Further research should continue to fine-tune the current methods used to derive environmental conditions for landscapes, such as wind exposure models, and develop new techniques for modeling other environmental conditions that may be useful for characterizing a landscape's environment and understanding its landscape patterns.

Historically, humans have caused a wide range of disturbances to coastal barrens, in some cases maintaining them by preventing re-forestation, such as accidental or purposeful fires, grazing from livestock, clear-cutting for timber, and creation of hiking trails (Heikens and Robertson, 1994; Mitchell et al., 2000; Motzkin and Foster, 2002; Kerbirou et al., 2008; von Oheimb et al., 2008). These activities have been found to impact biodiversity, species richness, and threaten rare species. Anthropogenic disturbances were clearly visible at all sites using high-resolution UAV imagery. At

Chebucto Head, numerous hiking trails extended along the coastal cliffs and dwarf heath and several paths were noticed further inland that traced through shrublands and several tree islands. At Prospect Bay, two main hiking trails dissected the site horizontally, one along the coastline and the other 100-150 m from the coastline. Polly's Cove was perhaps the most disturbed, with numerous hiking trails tracing the coastline as well as multiple ATV Trails carving out bogs at the back of the site (see mapped ATV trails in Figure 3.8). To gain a better understanding of the extent and impacts of disturbances on coastal environments and how they impact the landscape patterns of vegetation, the use of multispectral imagery and the Normalized Differentiation of Vegetation Index (NDVI) is a strong possibility. For example, Minařík and Langhammer (2016) used multispectral UAV imagery to assess disturbance dynamics in a forest and found that NDVI was one of the best indices for identifying individual trees that were healthy, dead, and infested with bark beetles. It is unfortunate that coastal ecosystems like the coastal barrens are subject to such amounts of disturbance, which highlights the importance of developing better monitoring tools and management practices to protect them.

Harper et al. (2005) discuss the importance of edge to interior relationships and how the amount of edge of a habitat patch can influence habitat fragmentation, habitat loss, changes in biodiversity and species richness, and community structure. Although it was not within the scope of this study to quantify edge-interior relationships of plant community patches in relation to habitat fragmentation and biodiversity, several metrics were quantified for patches in this study that relate to edge-interior relationships, including perimeter-area ratio, shape index, and the amount of edge shared with other plant communities. Natural edges of fine scale plant community patches were detectable



from UAV imagery which made it possible to quantify edge-interior relationships.

Given the important implications of edge-interior relationships for habitats and ecosystem biodiversity, future research should consider the use of UAVs as a tool to detect natural edges of plant communities and to quantify edge-interior relationships at different spatial scales.

Classifying landscapes with UAV imagery can be highly accurate and can offer an unprecedented level of detail about the structure and composition of a landscape (Cunliffe et al., 2016; Fraser et al., 2016). Furthermore, maps provide a way to qualitatively and quantitatively analyze spatial patterns and relationships of vegetation and other features across landscapes, offering many different avenues for research in landscape ecology and other scientific fields. Although final overall classification accuracies of plant community patches from UAV imagery were very good for all three sites, many challenges were encountered, and it was a lengthy process to optimize the image classification methodology. The Support Vector Machines classifier in ArcGIS proved to be excellent for classifying UAV imagery compared to other methods tested, such as Supervised Maximum Likelihood. The classifier was quite robust for low sample sizes, although most issues encountered with misclassifications were related to classes with not enough samples. A minimum of 4 field plot samples is ideal for each class, although realistically this isn't always possible. Consider the example of *Toxicodendron radicans* coastal vegetation (poison ivy) at Prospect Bay: only two patches were identified in the entire landscape, therefore it would be impossible to have any more than two field plot samples unless samples were pseudoreplicates (i.e. multiple samples from

the same patch). As with many tools, trial and error was needed to find out the best settings and parameters for the image classifier.

The most challenging communities to classify were those with low field plot samples and those that were either structurally and/or spectrally similar to other communities. *Rubus allegheniensis* - *Morella pensylvanica* coastal vegetation at Polly's Cove was one of the more difficult communities to classify because it only had a few samples and it was similar in appearance to several other communities, such as *Gaylussacia baccata* shrubland. Mixed tall shrubs were also challenging to classify at Chebucto Head and Polly's Cove because of a similar appearance to *Gaylussacia baccata* shrubland. To reduce misclassifications between these two communities at the two sites, a decision tree approach was used after the initial image classification procedure; the two shrublands were temporarily joined as one group and subsequently re-split based on a cutoff value using a structural index, such as Topographic Position Index (TPI), since Mixed tall shrubs have greater structural variability and are generally taller than *Gaylussacia baccata* shrubland. The cutoff value was selected by calculating 95% confidence intervals of the mean values of the structural index for each community and the value that best split the two groups as chosen. Doing so improved classification accuracies of the shrublands at both sites, although Mixed tall shrubs still classified poorly at Polly's Cove due to low sample sizes. Using this post-classification technique may be helpful when the initial classification yields poor results for one or more classes and there is a known index or parameter that can later be used to separate them.

From observation, many misclassifications should have been preventable. For example, sometimes Coniferous tree islands were misclassified as dwarf heath due to

their similar spectral appearance; however, their differences in structure should have prevented those misclassifications. Furthermore, most communities could be easily discriminated by visually inspecting the RGB imagery alone, suggesting that the SVM classifier wasn't always making the best decisions given the information provided. Although results were overall still very good using the SVM classifier, future research should continue to explore, improve, and develop better machine learning algorithms for classifying UAV imagery.

In this study, detailed 3D models of landscapes were made by processing UAV imagery in Agisoft software using SfM photogrammetry. The purpose of generating high-resolution 3D models was 2-fold: 1) to assist image classification by digitally reconstructing vegetation canopies and deriving structural indices of plant communities, and 2) to model environmental factors such as elevation and wind exposure to understand the landscape patterns of plant communities. Using Agisoft to create 3D landscape models provided realistic representations of the landscapes with very few computational errors. Many structural differences were found between plant communities using the 3D landscape models, and environmental factors derived from the elevation models were able to explain many important landscape patterns and relationships of the plant communities across the landscapes. One challenge with using UAV imagery to derive 3D models is the creation of bare earth/bare ground models. Objects or surfaces can only be digitally reconstructed if they are in direct view of the aircraft, so the ground beneath vegetation canopies is often not measured and incorporated into the 3D models. This poses limitations for estimating canopy height of vegetation and computing bare ground models for deriving environmental indices such as stream networks and slope position

classifications (Dandois, 2014; Aasen et al., 2015; Cunliffe et al., 2016; Fraser et al., 2016). One option is to generalize the elevation model to a coarser resolution and assign the minimum elevation value observed for each cell. Future research should investigate techniques to optimize the derivation of bare ground models from UAV imagery when bare ground is not visible and further improve the computation of 3D models from UAV imagery using SfM photogrammetry.

### **Implications and Future Work**

To the author's knowledge, this is the first study to reveal the landscape structure of coastal barrens using detailed maps of plant communities, landscape features, and environmental factors. Novel techniques in remote sensing and image processing were used to derive high-resolution 3D models and orthomosaics of coastal barrens landscapes, shedding a new light on their true complexity and patchiness. The findings of this study show that landscape patterns of plant communities in the coastal barrens are very complex but are linked to various combinations of environmental factors, particularly slope position, proximity to stream networks, elevation, and the distance from the coastline. Furthermore, creating highly detailed maps of plant community patches and quantifying their spatial patterns and distributional statistics, such as total area occupied, can help to better inform conservation managers about what measures are needed to protect these ecosystems and where to allocate resources in future efforts. Maps not only serve as communication tools for scientific researchers but can also help to better inform the public and showcase the brilliant diversity and complexity of these ecosystems. Future work should continue to expand on spectral and structural indices to use for

discriminating plant communities, explore other environmental factors for characterizing coastal environments and how they relate to the landscape patterns of plant communities, and investigate new ways to quantify and interpret the spatial patterns of vegetation from plant community maps. Optimizing and standardizing image acquisition techniques, camera settings, and image processing techniques for UAV imagery will help to improve classification accuracies of plant community maps, conduct temporal analyses, and will make maps more comparable. Lastly, more work is still needed to document the different species and plant communities occurring in these coastal environments and assign classifications using standardized classification systems, such as the Canadian National Vegetation Classification (CNVC).

## Conclusion

In this study, the landscape structure of three coastal barrens sites in the Halifax region was revealed through maps of plant community patches, landscape features, and environmental factors. Coastal barrens were dominated by shrublands and dwarf heath; however, many other types of communities co-existed, including bogs, salt marshes, and tree islands. Sites displayed a wide spectrum of environmental gradients and topographic heterogeneity, providing many different habitat types and niches, resulting in complex spatial patterns of vegetation and a high degree of patchiness. Plant community patches varied in size, shape, abundance, and spatial distribution from one plant community type to another and in many cases from one site to another. One of the most unexpected results of this study was the predominance of *Cladonia spp.* lichen; lichen occupied 4-5% of each landscape and dense populations were found on dry, rock-exposed ridges and on mildly wet slopes and flats. This is a significant finding because many species of lichen are uncommon or rare, highlighting the conservation value of coastal barrens and the need to protect them. 3D models from the SfM photogrammetric processing of UAV imagery were essential for computing structural indices for image classification and for deriving environmental factors such as stream networks and wind exposure models. Lastly, mapping plant community patches at the fine-scale with high accuracy would not have been possible without the use of aerial imagery with sub-decimeter resolutions. Maps offer tremendous potential for quantifying spatial patterns and relationships of species and communities across landscapes, can inform conservation managers, and can be used as communication tools to inform and engage the public. Future research should

continue to explore the use of UAVs for mapping species and communities across coastal  
barrens landscapes and quantify their landscape patterns.

## References

- Aasen, H., Burkart, A., Bolten, A., & Bareth, G. (2015). Generating 3D hyperspectral information with lightweight UAV snapshot cameras for vegetation monitoring: from camera calibration to quality assurance. *ISPRS Journal of Photogrammetry and Remote Sensing*, *108*, 245-259.
- Adam, E., Mutanga, O., & Rugege, D. (2010). Multispectral and hyperspectral remote sensing for identification and mapping of wetland vegetation: a review. *Wetlands Ecology and Management*, *18*(3), 281-296.
- ArcGIS (Version 10.3.1) [Software]. (2014). Environmental Systems Research Institute (ESRI), Redlands, California.
- Asner, G. P., Ustin, S. L., Townsend, P. A., Martin, R. E., & Chadwick, K. D. (2015). Forest biophysical and biochemical properties from hyperspectral and LiDAR remote sensing. *Land resources monitoring, modeling and mapping with remote sensing*. CRC Press, Taylor & Francis Group, 429-448.
- Baker, R. D., Lynn, B. H., Boone, A., Tao, W. K., & Simpson, J. (2001). The influence of soil moisture, coastline curvature, and land-breeze circulations on sea-breeze-initiated precipitation. *Journal of Hydrometeorology*, *2*(2), 193-211.
- Blaschke, T. (2010). Object based image analysis for remote sensing. *ISPRS journal of photogrammetry and remote sensing*, *65*(1), 2-16.
- Boose, E. R., Foster, D. R., & Fluet, M. (1994). Hurricane impacts to tropical and temperate forest landscapes. *Ecological Monographs*, *64*(4), 369-400.
- Buckland-Nicks, M., Heim, A., & Lundholm, J. (2016). Spatial environmental heterogeneity affects plant growth and thermal performance on a green roof. *Science of the Total Environment*, *553*, 20-31.
- Burai, P., Deák, B., Valkó, O., & Tomor, T. (2015). Classification of herbaceous vegetation using airborne hyperspectral imagery. *Remote Sensing*, *7*(2), 2046-2066.
- Burley, S. T., & Lundholm, J. T. (2010). Environmental predictors of forest expansion on open coastal barrens. *Biodiversity and conservation*, *19*(11), 3269-3285.
- Burley, S. T., Harper, K. A., & Lundholm, J. T. (2010). Vegetation composition, structure and soil properties across coastal forest–barren ecotones. *Plant ecology*, *211*(2), 279-296.
- Cameron, R. P., & Bondrup-Nielsen, S. (2013). Plant Communities within Atlantic Coastal Heathlands in Nova Scotia. *Northeastern Naturalist*, *20*(4).



Canadian National Vegetation Classification (CNVC) [online] 2013. Sault Ste. Marie, ON, Canada. Accessed 2015. Accessed on October 08, 2017 from: <http://cnvc-cnvc.ca>.

Choler, P., Michalet, R., & Callaway, R. M. (2001). Facilitation and competition on gradients in alpine plant communities. *Ecology*, 82(12), 3295-3308.

Christensen, S. N., & Johnsen, I. (2001). The lichen-rich coastal heath vegetation on the isle of Anholt, Denmark—conservation and management. *Journal of Coastal Conservation*, 7(1), 13-22.

Cleugh, H. A., Miller, J. M., & Böhm, M. (1998). Direct mechanical effects of wind on crops. *Agroforestry Systems*, 41(1), 85-112.

Cruzan, M. B., Weinstein, B. G., Grasty, M. R., Kohn, B. F., Hendrickson, E. C., Arredondo, T. M., & Thompson, P. G. (2016). Small unmanned aerial vehicles (micro-UAVs, drones) in plant ecology. *Applications in Plant Sciences*, 4(9), 1600041.

Cunliffe, A. M., Brazier, R. E., & Anderson, K. (2016). Ultra-fine grain landscape-scale quantification of dryland vegetation structure with drone-acquired structure-from-motion photogrammetry. *Remote Sensing of Environment*, 183, 129-143.

Dandois, J. P. (2014). *Remote sensing of vegetation structure using computer vision*. University of Maryland, Baltimore County.

De Langre, E. (2008). Effects of wind on plants. *Annu. Rev. Fluid Mech.*, 40, 141-168.

Dilts, T.E. (2015). Topography Tools for ArcGIS 10.1. University of Nevada Reno. Available at: <http://www.arcgis.com/home/item.html?id=b13b3b40fa3c43d4a23a1a09c5fe96b9>

Dronova, I., Gong, P., Clinton, N. E., Wang, L., Fu, W., Qi, S., & Liu, Y. (2012). Landscape analysis of wetland plant functional types: The effects of image segmentation scale, vegetation classes and classification methods. *Remote Sensing of Environment*, 127, 357-369.

Dunwiddie, P. W., Zaremba, R. E., & Harper, K. A. (1996). A classification of coastal heathlands and sandplain grasslands in Massachusetts. *Rhodora*, 117-145.

Evans, J.S., Oakleaf, J., Cushman, S.A., & Theobald, D. (2014). An ArcGIS Toolbox for Surface Gradient and Geomorphometric Modeling, version 2.0-0. Available at: <http://evansmurphy.wixsite.com/evansspatial/arcgis-gradient-metrics-toolbox>.

Fraser, R., Olthof, I., Lantz, T. C., & Schmitt, C. (2016). UAV Photogrammetry for Mapping Vegetation in the Low-Arctic. *Arctic Science*, (ja).

- Forman, R. T. (1995). Some general principles of landscape and regional ecology. *Landscape ecology*, 10(3), 133-142.
- Galidaki, G., Zianis, D., Gitas, I., Radoglou, K., Karathanassi, V., Tsakiri–Strati, M., ... & Mallinis, G. (2017). Vegetation biomass estimation with remote sensing: focus on forest and other wooded land over the Mediterranean ecosystem. *International Journal of Remote Sensing*, 38(7), 1940-1966.
- Gonçalves, J., Henriques, R., Alves, P., Sousa-Silva, R., Monteiro, A. T., Lomba, Â., ... & Honrado, J. (2015). Evaluating an unmanned aerial vehicle-based approach for assessing habitat extent and condition in fine-scale early successional mountain mosaics. *Applied Vegetation Science*.
- Harper, K. A. (1995). Effect of expanding clones of *Gaylussacia baccata* (black huckleberry) on species composition in sandplain grassland on Nantucket Island, Massachusetts. *Bulletin of the Torrey Botanical Club*, 124-133.
- Harper, K. A., Macdonald, S. E., Burton, P. J., Chen, J., Brosofske, K. D., Saunders, S. C., ... & Esseen, P. A. (2005). Edge influence on forest structure and composition in fragmented landscapes. *Conservation Biology*, 19(3), 768-782.
- Heikens, A. L., & Robertson, P. A. (1994). Barrens of the Midwest: a review of the literature. *Castanea*, 184-194.
- Hill, R. A., & Thomson, A. G. (2005). Mapping woodland species composition and structure using airborne spectral and LiDAR data. *International Journal of Remote Sensing*, 26(17), 3763-3779.
- Homolova, L., Malenovsky, Z., Clevers, J. G., Garcia-Santos, G., & Schaepman, M. E. (2013). Review of optical-based remote sensing for plant trait mapping. *Ecological Complexity*, 15, 1-16.
- Johnson, A. R., Wiens, J. A., Milne, B. T., & Crist, T. O. (1992). Animal movements and population dynamics in heterogeneous landscapes. *Landscape ecology*, 7(1), 63-75.
- Jolliffe, I. T. (1986). Principal Component Analysis and Factor Analysis. In *Principal component analysis* (pp. 115-128). Springer New York.
- Kalacska, M., Chmura, G. L., Lucanus, O., Bérubé, D., & Arroyo-Mora, J. P. (2017). Structure from motion will revolutionize analyses of tidal wetland landscapes. *Remote Sensing of Environment*, 199, 14-24.
- Kerbiriou, C., Leviol, I., Jiguet, F., & Julliard, R. (2008). The impact of human frequentation on coastal vegetation in a biosphere reserve. *Journal of Environmental Management*, 88(4), 715-728.

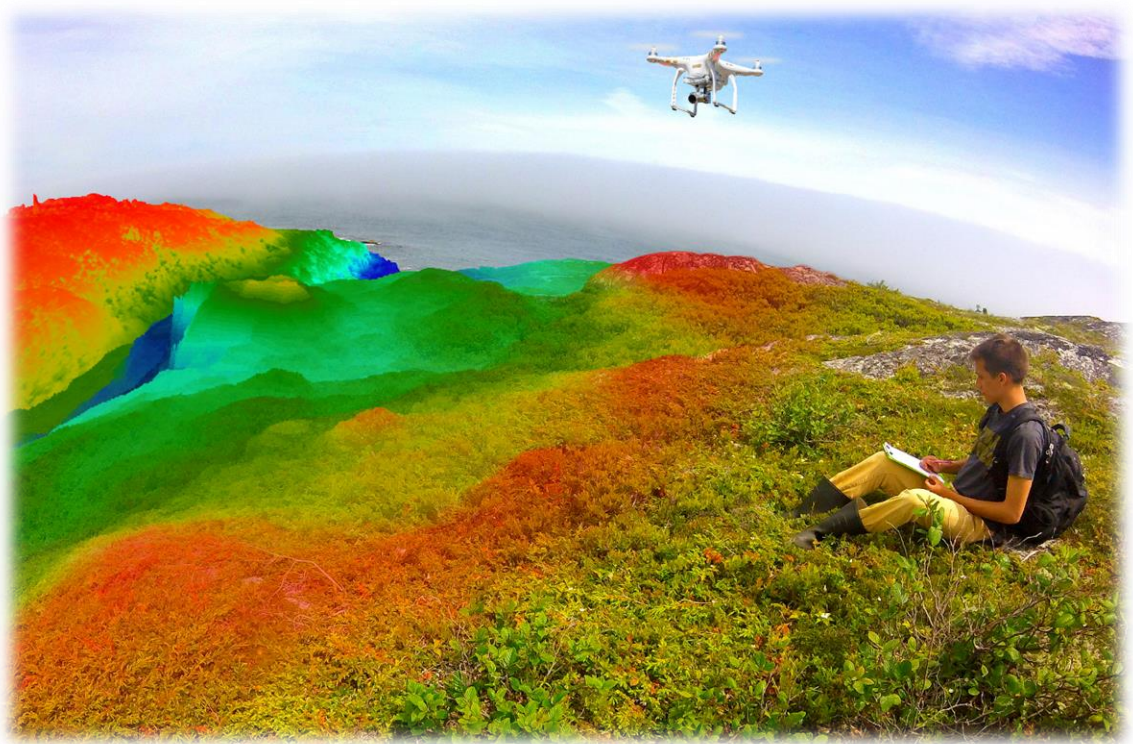
- Lomolino, M. (2001). Elevation gradients of species-density: historical and prospective views. *Global Ecology and Biogeography*, 10(1), 3-13.
- Matlack, G. R., Gibson, D. J., & Good, R. E. (1993). Regeneration of the shrub *Gaylussacia baccata* and associated species after low-intensity fire in an Atlantic coastal plain forest. *American Journal of Botany*, 119-126.
- McGarigal, K., & Marks, B. J. (1995). Spatial pattern analysis program for quantifying landscape structure. *Gen. Tech. Rep. PNW-GTR-351. US Department of Agriculture, Forest Service, Pacific Northwest Research Station.*
- McGarigal, K., SA Cushman, & E Ene. (2012). FRAGSTATS v4: Spatial Pattern Analysis Program for Categorical and Continuous Maps. Computer software program produced by the authors at the University of Massachusetts, Amherst. Available at the following web site: <http://www.umass.edu/landeco/research/fragstats/fragstats.html>
- Micheletti, N., Chandler, J. H., & Lane, S. N. (2015). Structure from motion (SFM) photogrammetry. *Geomorphological Techniques*, Chap. 2, Sec. 2.2.
- Mikita, T., & Klimánek, M. (2010). Topographic exposure and its practical applications. *Journal of Landscape Ecology*, 3(1), 42-51.
- Minařík, R., & Langhammer, J. (2016). Use of a Multispectral UAV photogrammetry for detection and tracking of forest disturbance dynamics. *International Archives of the Photogrammetry, Remote Sensing & Spatial Information Sciences*, 41.
- Mitchell, R. J., Auld, M. H., Le Duc, M. G., & Robert, M. H. (2000). Ecosystem stability and resilience: a review of their relevance for the conservation management of lowland heaths. *Perspectives in Plant Ecology, Evolution and Systematics*, 3(2), 142-160.
- Motzkin, G., & Foster, D. R. (2002). Grasslands, heathlands and shrublands in coastal New England: historical interpretations and approaches to conservation. *Journal of Biogeography*, 29(10-11), 1569-1590.
- Murphy, P. N., Ogilvie, J., Meng, F. R., & Arp, P. (2008). Stream network modelling using lidar and photogrammetric digital elevation models: a comparison and field verification. *Hydrological Processes*, 22(12), 1747-1754.
- Oberndorfer, E. C., & Lundholm, J. T. (2009). Species richness, abundance, rarity and environmental gradients in coastal barren vegetation. *Biodiversity and Conservation*, 18(6), 1523-1553.
- Pande-Chhetri, R., Abd-Elrahman, A., Liu, T., Morton, J., & Wilhelm, V. L. (2017). Object-based classification of wetland vegetation using very high-resolution unmanned air system imagery. *European Journal of Remote Sensing*, 50(1), 564-576.

- Patton, D. R. (1975). A diversity index for quantifying habitat "edge". *Wildlife Society Bulletin (1973-2006)*, 3(4), 171-173.
- Porter, C. (2013). Classification of dwarf heath plant communities on the coastal barrens of Nova Scotia. Thesis. Master of Science. Saint Mary's University, Halifax, Nova Scotia.
- Porter, C., Lundholm, J., Bowron, T., Lemieux, B., van Proosdij, D., Neatt, N., & Graham, J. (2015). Classification and environmental correlates of tidal wetland vegetation in Nova Scotia, Canada. *Botany*, 93(12), 825-841.
- R Core Team, 2017. A Language and Environment for Statistical Computing. R Foundation for Statistical Computing, Vienna, Austria. <https://www.R-project.org>
- Sebastiá, M. T. (2004). Role of topography and soils in grassland structuring at the landscape and community scales. *Basic and Applied Ecology*, 5(4), 331-346.
- Silvertown, J., Dodd, M. E., Gowing, D. J., & Mountford, J. O. (1999). Hydrologically defined niches reveal a basis for species richness in plant communities. *Nature*, 400(6739), 61.
- Strahler, A. N. (1952). Hypsometric (area-altitude) analysis of erosional topography. *Geological Society of America Bulletin*, 63(11), 1117-1142.
- Strang, R. M. (1972). Ecology and land use of the barrens of western Nova Scotia. *Canadian Journal of Forest Research*, 2(3), 276-290.
- Sturdivant, E. J., Lentz, E. E., Thieler, E. R., Farris, A. S., Weber, K. M., Remsen, D. P., ... & Henderson, R. E. (2017). UAS-SfM for Coastal Research: Geomorphic Feature Extraction and Land Cover Classification from High-Resolution Elevation and Optical Imagery. *Remote Sensing*, 9(10), 1020.
- Turner, M. G. (1989). Landscape ecology: the effect of pattern on process. *Annual review of ecology and systematics*, 20(1), 171-197.
- Ustin, S. L., & Gamon, J. A. (2010). Remote sensing of plant functional types. *New Phytologist*, 186(4), 795-816.
- van der Maarel, E., & Franklin, J. (2013). *Vegetation Ecology*. Second Edition. Wiley-Blackwell.
- van Proosdij, D., Davidson-Arnott, R. G., & Ollerhead, J. (2006). Controls on spatial patterns of sediment deposition across a macro-tidal salt marsh surface over single tidal cycles. *Estuarine, Coastal and Shelf Science*, 69(1-2), 64-86.

- Vivian-Smith, G. (1997). Microtopographic heterogeneity and floristic diversity in experimental wetland communities. *Journal of Ecology*, 71-82.
- von Oheimb, G., Härdtle, W., Naumann, P. S., Westphal, C., Assmann, T., & Meyer, H. (2008). Long-term effects of historical heathland farming on soil properties of forest ecosystems. *Forest Ecology and Management*, 255(5), 1984-1993.
- Xie, Y., Sha, Z., & Yu, M. (2008). Remote sensing imagery in vegetation mapping: a review. *Journal of plant ecology*, 1(1), 9-23.
- Zawawi, A. B. A. (2015). Terrain Analysis and Site Evaluation: Integrating a Geospatial Approach for Subtropical Forest Management Planning (Doctoral dissertation).
- Zinko, U., Seibert, J., Dynesius, M., & Nilsson, C. (2005). Plant species numbers predicted by a topography-based groundwater flow index. *Ecosystems*, 8(4), 430-441.
- Zweig, C. L., Burgess, M. A., Percival, H. F., & Kitchens, W. M. (2015). Use of unmanned aircraft systems to delineate fine-scale wetland vegetation communities. *Wetlands*, 35(2), 303-309.

# 4

## Synthesis



*The coastal barrens of Chebucto Head, Nova Scotia viewed from a UAV*

The coastal barrens of Halifax, Nova Scotia are patchy mosaics of plant communities that experience harsh environmental conditions. Despite their harsh conditions, coastal barrens are diverse ecosystems and are inhabited by rare and uncommon species, making them a high priority for conservation (Oberndorfer and Lundholm, 2009; Burley and Lundholm, 2010; Porter, 2013). Currently, maps have never been made of the plant communities in the coastal barrens of Halifax, Nova Scotia, and thus there is little knowledge of their distributions, spatial patterns and relationships, and spatial configurations across the landscapes. The purpose of this study was to evaluate the use of an unmanned aerial vehicle (UAV) to discriminate plant communities, map their distributions, and to quantify the landscape structure of coastal barrens in the Halifax region of Nova Scotia.

In 2016, a UAV was used to collect high-resolution multispectral imagery at three coastal barrens sites in the Halifax region of Nova Scotia: Chebucto Head, Prospect Bay, and Polly's Cove. Ground truthing field plot data were also collected in 2016 to document the locations of plant communities at all three sites. Plant communities were classified at three classification levels based on the Canadian National Vegetation Classification (CNVC, 2013): the association level, which is based primarily on floristic criteria; the broadened association level, which was formed by merging confused classes from the association level; and the formation class, which is based primarily on physiognomy. Images were processed using structure from motion (SfM) photogrammetry to create 3D models and orthomosaics of the landscapes, from which spectral and structural indices were derived and evaluated for discriminating the plant communities using linear discriminant analysis (LDA). All plant communities from the

three classification levels were discriminated with 95% confidence except for one pair in the association level classification – two very similar shrub bogs. Overall classification accuracy for the association level classification was lower (63%) than the formation class classification (92%); however, merging confused groups to form the broadened association level classification improved the accuracy to 83%. It was found that most confusion arose between plant communities that were structurally similar. These results show that plant communities in the coastal barrens can be discriminated at different classification levels using UAV imagery.

In the second part of this study, UAV imagery from 2016 was classified using the support vector machines (SVM) classifier in ArcGIS to produce detailed maps of plant community patches from the broadened association level classification based on the CNVC as well as landscape features. Environmental factors were also mapped to further describe landscape structure and to understand the landscape patterns of plant communities. Sites were dominated by shrublands and dwarf heath; however, other communities co-existed as well, including bogs, salt marshes, and tree islands. Interestingly, the most abundant community across all sites was *Gaylussacia baccata* shrubland, which is consistent with several other studies on coastal barrens (Strang, 1972; Matlack et al., 1993; Harper, 1995; Dunwiddie et al., 1996). Site-specifically, however, Prospect Bay was dominated by *Empetrum nigrum* - *Juniperus communis* dwarf heath. Each site showed complex spatial patterns of plant communities, a wide spectrum of environmental gradients and topographic heterogeneity, and a high degree of patchiness. Plant community patches varied in size, shape, abundance, and spatial distribution for different types of plant communities. Landscape patterns of most plant communities were



related to various combinations of environmental factors, including slope position, proximity to stream networks, elevation, and distance to coastline. Furthermore, the degree of topographic heterogeneity of the site could explain the landscape patterns of the dominant plant communities. For example, Chebucto Head and Polly's Cove had similarly high levels of topographic heterogeneity and was composed of many valleys, midslopes, flats, and ridges. As a result, most inland vegetation were shrublands with dwarf heath and lichen inhabiting rock-exposed areas and dwarf heath and other coastal vegetation occupying areas nearest the coastline. Conversely, Prospect Bay had very flat at homogeneous terrain, providing habitat for bogs and dwarf heath.

The findings of this study show that plant communities in the coastal barrens can be discriminated at different classification levels using high-resolution multispectral imagery collected from a UAV. Classifying UAV imagery with ground truthing data from field plots can yield highly accurate and detailed maps of plant community patches across landscapes, offering tremendous potential for quantifying landscape patterns, spatial interrelationships, and revealing the underlying structure of landscapes.

Applications for using UAVs as a mapping and monitoring tool for these ecosystems are limitless: mapping disturbance regimes, stress, and health of vegetation and ecosystems; evaluating impacts of climate change; informing conservation managers about how to design protected areas and where to allocate resources; communicate, inform, and engage the public using maps; quantifying interior-edge relationships for assessing habitat fragmentation and impacts on ecosystem biodiversity; quantifying spatial distributions, relationships, and configurations of vegetation and their patches; mapping biophysical parameters, such as biomass, chlorophyll content in leaves, nutrient cycles, leaf water

content, and vegetation productivity; and lastly, conducting preliminary surveys of landscapes to evaluate types of habitats and to target field sampling efforts. These applications of UAVs are not limited to the coastal barrens and can be applied to nearly any terrestrial ecosystem.

Aircraft altitude, seasonality, weather conditions, and camera settings are all important considerations for classifying UAV imagery to develop landcover maps. Flight altitude of the aircraft determines the ground resolution/pixel size of the imagery. For this study, 50 m altitude offered plenty of spectral and structural detail of plant communities and landscape features and only required 1 additional flight to encompass the same study area as compared to the 90 m altitude surveys. Surveying the sites in both the spring and summer offered contrasting views of plant communities and their changes in phenology. Some communities were best discriminated during the spring, such as *Cladonia spp.*, and others during the summer, such as coastal herbaceous vegetation. It is therefore highly recommended to consider seasonal changes in vegetation for mapping plant communities across landscapes. Weather conditions, such as wind, time of day, time of year, cloud cover and illumination, and temperature, can affect the acquisition and quality of aerial imagery collected from the UAV. For coastal environments with high winds, it is recommended to survey earlier in the day. For illumination, cloudy skies are preferable because the landscape is more evenly lit and surface reflectance of sunlight for water and plant leaves is much lower. In cases where cloudy skies are infrequent, it is alternatively best to survey in full sun with no clouds. Lastly, most problems with illumination can be mitigated by controlling the settings of the UAV sensor(s). Setting the white balance and exposure settings to a constant value will help keep illumination and colors constant in

images. Another option is to collect only raw images; however, this requires much more storage space and potentially a lot of image editing. For this study, white balance was fixed for summer surveys but was set to automatic for the spring; consequently, colors of vegetation were not as consistent for spring surveys, particularly at Prospect Bay, which may have resulted in lower classification accuracies for some communities.

One of the greatest debates in ecology is whether plant communities exist as discrete patches (Clements, 1916) or as a continuum of species along environmental gradients (Gleason, 1926). The modern synthesis of these two views assumes that plant species are distributed individualistically but can form associations or communities that are in discrete and recognizable units (van der Maarel and Franklin, 2013; Porter, 2013). The findings of this study add support to the modern synthesis of the plant community: when field data were reviewed, it was clear that no two plant communities that were sampled had identical compositions, which agrees with Gleason's view of species distributions. What was also apparent, however, was that there were trends in the field plot data and it was clear that discrete, recurring associations existed. This was further supported when spectral and structural indices from UAV imagery were used to successfully discriminate 99% of plant community comparisons with 95% confidence, indicating that there are inherent differences between plant community types. Furthermore, for the first time classified UAV imagery showed plant communities distributed across each coastal barrens landscape as discrete patches with various shapes, sizes, and abundances, which can be verified by comparing the classified maps to the original RGB imagery. Classified maps of plant community patches were highly accurate at predicting the plant community classification from ground truthing field plot data,

adding insurmountable evidence that plant communities in the coastal barrens can be observed as discrete, recognizable units.

### **Implications and Future Work**

For the first time, empirical evidence has shown that multispectral imagery collected from UAVs can discriminate plant communities in the coastal barrens at different classification levels. It is also for the first time that detailed maps of plant community patches were made for coastal barrens in Nova Scotia. Furthermore, no other study to the author's knowledge has revealed the structure of coastal barrens landscapes at the level of detail of this study. This was all made possible by using novel techniques for acquiring images with UAVs, such as using mobile applications to autonomously control the UAV to collect sequential overlapping images and using SfM photogrammetry to create high-resolution orthomosaics and compute 3D landscape models. Applications of UAVs and their use for mapping and monitoring ecosystems like the coastal barrens are limitless. Future research should continue to explore, develop, and improve methods for acquiring and processing UAV imagery. Researchers should also explore new spectral and structural indices to help map vegetation types and improve methods for deriving environmental factors from 3D surfaces, such as wind exposure. Lastly, mapping coastal barrens landscapes and documenting their species and communities will improve our understanding of their landscape structure, function, and dynamics – all of which can better inform land managers, conservation managers, and policy makers.

## References

- Burley, S. T., Harper, K. A., & Lundholm, J. T. (2010). Vegetation composition, structure and soil properties across coastal forest–barren ecotones. *Plant Ecology*, 211(2), 279-296.
- Canadian National Vegetation Classification (CNVC) [online] 2013. Sault Ste. Marie, ON, Canada. Accessed 2015. Accessed on October 08, 2017 from: <http://cnvc-cnvc.ca>.
- Clements, F. (1916). *Plant succession: An analysis of the development of vegetation*. Washington, DC: Carnegie Institute of Washington Publication.
- Dunwiddie, P. W., Zaremba, R. E., & Harper, K. A. (1996). A classification of coastal heathlands and sandplain grasslands in Massachusetts. *Rhodora*, 117-145.
- Gleason, H. A. (1926). The individualistic concept of the plant association. *Bulletin of the Torrey botanical club*, 7-26.
- Harper, K. A. (1995). Effect of expanding clones of *Gaylussacia baccata* (black huckleberry) on species composition in sandplain grassland on Nantucket Island, Massachusetts. *Bulletin of the Torrey Botanical Club*, 124-133.
- Matlack, G. R., Gibson, D. J., & Good, R. E. (1993). Regeneration of the shrub *Gaylussacia baccata* and associated species after low-intensity fire in an Atlantic coastal plain forest. *American Journal of Botany*, 119-126.
- Oberndorfer, E. C., & Lundholm, J. T. (2009). Species richness, abundance, rarity and environmental gradients in coastal barren vegetation. *Biodiversity and Conservation*, 18(6), 1523-1553.
- Porter, C. (2013). Classification of dwarf heath plant communities on the coastal barrens of Nova Scotia. Thesis. Master of Science. Saint Mary's University, Halifax, Nova Scotia.
- Strang, R. M. (1972). Ecology and land use of the barrens of western Nova Scotia. *Canadian Journal of Forest Research*, 2(3), 276-290.
- van der Maarel, E., & Franklin, J. (2013). *Vegetation Ecology. Second Edition*. Wiley-Blackwell.

# Appendix I

## Tables

Table A1.1. Specifications of the unmanned aerial vehicle used in this study.

<b>Aircraft</b>	
Model	DJI Phantom 3 Professional
Aircraft Type	Quadcopter
Weight	1.280 kg
Max Speed	16 m/s or 58 km/h
Max Flight Time	~23 minutes
Operating Temperature	0° to 40°C
Satellite Positioning System	GPS/GLONASS
<b>Sensor 1: RGB Gimbal Camera</b>	
Sensor	1/2.3" CMOS
Effective Pixels	12.4
Lens	FOV 94° 20 mm (35 mm format equivalent) f/2.8 focus at ∞
ISO Range	100-3200 (video); 100-1600 (photo)
Image Size	4000x3000
Still photography modes	Single shot; Burst Shooting (3/5/7 frames); Auto Exposure Bracketing (AEB) (3/5 bracketed frames); Time-lapse
Video Recording Modes	UHD: 4096x2160p 24/25. 3840x2160p 24/25/30; FHD: 1920x1080p 24/25/30/48/50/60; HD: 1280x720p 24/25/30/48/50/60
Max Video Bitrate	60 Mbps
Photo	JPEG, DNG (RAW)
Video	MP4, MOV (MPEG-4 AVC/H.264)
Supported SD Cards	Micro SD
Ground Sampling Distance	~4 cm (90 m altitude); ~2 cm (50 m altitude)
<b>Sensor 2: Sentra NIR Sensor</b>	
Sensor	1.2MP CMOS
Lens Focal Length	4.14 mm
Image Format	JPEG, TIFF
Supported SD Cards	Micro SD
Ground Sampling Distance	~8 cm (90 m altitude); ~4 cm (50 m altitude)

Table A1.2. Flight times and conditions for UAV surveys from May to August in 2016.

<b>Site</b>	<b>Date</b>	<b>Altitude Above Ground</b>	<b>Start Time</b>	<b>End Time</b>	<b>Weather</b>
<b>Chebucto Head</b>	May 25, 2016	90 m	2:05 pm	2:34pm	Partly sunny
	August 8, 2016	50 m	9:46 am	11:01am	Sunny
<b>Prospect Bay</b>	May 27, 2016	90 m	10:11 am	10:34am	Cloudy
	August 9, 2016	50 m	9:34 am	11:06am	Sunny
<b>Peggy's Cove</b>	May 29, 2016	90 m	9:47 am	10:09am	Partly sunny
	August 5, 2016	50 m	9:31 am	10:46am	Sunny



Table A1.3. Full list of indices extracted from UAV imagery and the 3D point cloud.

<b>Index</b>	<b>Description</b>
<b>R Mean May</b>	Mean of Red channel within a training polygon in May
<b>R SD May</b>	Standard deviation of Red channel within a training polygon in May
<b>R Mean August</b>	Mean of Red channel within a training polygon in August
<b>R SD August</b>	Standard deviation of Red channel within a training polygon in August
<b>Change in R Mean</b>	Change in mean of Red channel within a training polygon from May to August
<b>G Mean May</b>	Mean of Green channel within a training polygon in May
<b>G SD May</b>	Standard deviation of Green channel within a training polygon in May
<b>G Mean August</b>	Mean of Green channel within a training polygon in August
<b>G SD August</b>	Standard deviation of Green channel within a training polygon in August
<b>Change in G Mean</b>	Change in mean of Green channel within a training polygon from May to August
<b>B Mean May</b>	Mean of Blue channel within a training polygon in May
<b>B SD May</b>	Standard deviation of Blue channel within a training polygon in May
<b>B Mean August</b>	Mean of Blue channel within a training polygon in August
<b>B SD August</b>	Standard deviation of Blue channel within a training polygon in August
<b>Change in B Mean</b>	Change in mean of Blue channel within a training polygon from May to August
<b>R/B Mean May</b>	Mean of Red channel divided by Blue channel within a training polygon in May
<b>R/B SD May</b>	Standard deviation of Red channel divided by Blue channel within a training polygon in May
<b>R/B Mean August</b>	Mean of Red channel divided by Blue channel within a training polygon in August
<b>R/B SD August</b>	Standard deviation of Red channel divided by Blue channel within a training polygon in August
<b>Change in R/B Mean</b>	Change in mean of Red channel divided by Blue channel within a training polygon from May to August
<b>R/G Mean May</b>	Mean of Red channel divided by Green channel within a training polygon in May
<b>R/G SD May</b>	Standard deviation of Red channel divided by Green channel within a training polygon in May
<b>R/G Mean August</b>	Mean of Red channel divided by Green channel within a training polygon in August
<b>R/G SD August</b>	Standard deviation of Red channel divided by Green channel within a training polygon in August

(continued) Table A1.3. Full list of indices extracted from UAV imagery and the 3D point cloud.

<b>Index</b>	<b>Description</b>
<b>Change in R/G Mean</b>	Change in mean of Red channel divided by Green channel within a training polygon from May to August
<b>G/B Mean May</b>	Mean of Green channel divided by Blue channel within a training polygon in May
<b>G/B SD May</b>	Standard deviation of Green channel divided by Blue channel within a training polygon in May
<b>G/B Mean August</b>	Mean of Green channel divided by Blue channel within a training polygon in August
<b>G/B SD August</b>	Standard deviation of Green channel divided by Blue channel within a training polygon in August
<b>Change in G/B Mean</b>	Change in mean of Green channel divided by Blue channel within a training polygon from May to August
<b>NIR Mean May</b>	Mean of Near-Infrared within a training polygon in May
<b>NIR SD May</b>	Standard deviation of Near-Infrared within a training polygon in May
<b>NIR Mean August</b>	Mean of Near-Infrared within a training polygon in August
<b>NIR SD August</b>	Standard deviation of Near-Infrared within a training polygon in August
<b>Change in NIR Mean</b>	Change in mean of Near-Infrared within a training polygon from May to August
<b>NDVI Mean May</b>	Mean of NDVI within a training polygon in May. $NDVI = \frac{NIR-R}{NIR+R}$
<b>NDVI SD May</b>	Standard deviation of NDVI within a training polygon in May. $NDVI = \frac{NIR-R}{NIR+R}$
<b>NDVI Mean August</b>	Mean of NDVI within a training polygon in August. $NDVI = \frac{NIR-R}{NIR+R}$
<b>NDVI SD August</b>	Standard deviation of NDVI within a training polygon in August. $NDVI = \frac{NIR-R}{NIR+R}$
<b>Change in NDVI Mean</b>	Change in mean of NDVI within a training polygon from May to August. $NDVI = \frac{NIR-R}{NIR+R}$
<b>CIVE Mean May</b>	Mean of Color Index of Vegetation (CIVE) within a training polygon in May. $CIVE = 0.441 * R - 0.881 * G + 0.385 * B + 18.78745$
<b>CIVE SD May</b>	Standard deviation of Color Index of Vegetation (CIVE) within a training polygon in May. $CIVE = 0.441 * R - 0.881 * G + 0.385 * B + 18.78745$

(continued) Table A1.3. Full list of indices extracted from UAV imagery and the 3D point cloud.

<b>Index</b>	<b>Description</b>
<b>CIVE Mean August</b>	Mean of Color Index of Vegetation (CIVE) within a training polygon in August. $CIVE = 0.441 * R - 0.881 * G + 0.385 * B + 18.78745$
<b>CIVE SD August</b>	Standard deviation of Color Index of Vegetation (CIVE) within a training polygon in August. $CIVE = 0.441 * R - 0.881 * G + 0.385 * B + 18.78745$
<b>Change in CIVE Mean</b>	Change in mean of Color Index of Vegetation (CIVE) within a training polygon from May to August. $CIVE = 0.441 * R - 0.881 * G + 0.385 * B + 18.78745$
<b>Hue Mean May</b>	Mean of Hue in degrees (0-360°) within a training polygon in May. $Hue = \cos^{-1} \frac{(0.5*(R-G)+(R-B))}{(((R-G)^2+(R-B)(G-B))^{0.5})}$
<b>Hue SD May</b>	Standard deviation of Hue in degrees (0-360°) within a training polygon in May. $Hue = \cos^{-1} \frac{(0.5*(R-G)+(R-B))}{(((R-G)^2+(R-B)(G-B))^{0.5})}$
<b>Hue Mean August</b>	Mean of Hue in degrees (0-360°) within a training polygon in August. $Hue = \cos^{-1} \frac{(0.5*(R-G)+(R-B))}{(((R-G)^2+(R-B)(G-B))^{0.5})}$
<b>Hue SD August</b>	Standard deviation of Hue in degrees (0-360°) within a training polygon in August. $Hue = \cos^{-1} \frac{(0.5*(R-G)+(R-B))}{(((R-G)^2+(R-B)(G-B))^{0.5})}$
<b>Change in Hue Mean</b>	Change in mean of Hue in degrees (0-360°) within a training polygon from May to August. $Hue = \cos^{-1} \frac{(0.5*(R-G)+(R-B))}{(((R-G)^2+(R-B)(G-B))^{0.5})}$
<b>Saturation Mean May</b>	Mean of Saturation within a training polygon in May. $Saturation = 1 - \left( \frac{R + G + B}{3} \right) * a$
<b>Saturation SD May</b>	Standard deviation of Saturation within a training polygon in May. $Saturation = 1 - \left( \frac{R + G + B}{3} \right) * a$
<b>Saturation Mean August</b>	Mean of Saturation within a training polygon in August. $Saturation = 1 - \left( \frac{R + G + B}{3} \right) * a$
<b>Saturation SD August</b>	Standard deviation of Saturation within a training polygon in August. $Saturation = 1 - \left( \frac{R + G + B}{3} \right) * a$
<b>Change in Saturation Mean</b>	Change in mean of Saturation within a training polygon from May to August. $Saturation = 1 - \left( \frac{R + G + B}{3} \right) * a$

(continued) Table A1.3. Full list of indices extracted from UAV imagery and the 3D point cloud.

<b>Index</b>	<b>Description</b>
<b>Intensity Mean May</b>	Mean of Intensity within a training polygon in May. Intensity = $\frac{R + G + B}{3}$
<b>Intensity SD May</b>	Standard deviation of Intensity within a training polygon in May. Intensity = $\frac{R + G + B}{3}$
<b>Intensity Mean August</b>	Mean of Intensity within a training polygon in August. Intensity = $\frac{R + G + B}{3}$
<b>Intensity SD August</b>	Standard deviation of Intensity within a training polygon in August. Intensity = $\frac{R + G + B}{3}$
<b>Change in Intensity Mean</b>	Change in mean of Intensity within a training polygon from May to August. Intensity = $\frac{R + G + B}{3}$
<b>Vegetation Height Mean</b>	Mean of vegetation height calculated within a training polygon in August. Vegetation height was calculated by subtracting the minimum from the maximum elevation value within a 50-cm search radius of each pixel using the 10-cm elevation model
<b>Vegetation Height Max</b>	Maximum vegetation height calculated within a training polygon in August. Vegetation height was calculated by subtracting the minimum from the maximum elevation value within a 50-cm search radius of each pixel using the 10-cm elevation model
<b>Vegetation Height SD</b>	Standard deviation of vegetation height calculated within a training polygon in August. Vegetation height was calculated by subtracting the minimum from the maximum elevation value within a 50-cm search radius of each pixel using the 10-cm elevation model
<b>TPI Mean 5</b>	Mean of Topographic Position Index (TPI) within a training polygon in August. TPI was calculated from the 10-cm elevation model using a 5x5 pixel search window. TPI = $z_o - \bar{z}$ Where $z_o$ = elevation of central point, $\bar{z}$ = mean elevation of neighborhood
<b>TPI SD 5</b>	Standard deviation of Topographic Position Index (TPI) within a training polygon in August. TPI was calculated from the 10-cm elevation model using a 5x5 pixel search window. TPI = $z_o - \bar{z}$ Where $z_o$ = elevation of central point, $\bar{z}$ = mean elevation of neighborhood

(continued) Table A1.3. Full list of indices extracted from UAV imagery and the 3D point cloud.

<b>Index</b>	<b>Description</b>
<b>TPI Mean 11</b>	<p>Mean of Topographic Position Index (TPI) within a training polygon in August. TPI was calculated from the 10-cm elevation model using a 11x11 pixel search window.</p> $TPI = z_o - \bar{z}$ <p>Where <math>z_o</math> = elevation of central point, <math>\bar{z}</math> = mean elevation of neighborhood</p>
<b>TPI SD 11</b>	<p>Standard deviation of Topographic Position Index (TPI) within a training polygon in August. TPI was calculated from the 10-cm elevation model using a 11x11 pixel search window.</p> $TPI = z_o - \bar{z}$ <p>Where <math>z_o</math> = elevation of central point, <math>\bar{z}</math> = mean elevation of neighborhood</p>
<b>TPI Mean 33</b>	<p>Mean of Topographic Position Index (TPI) within a training polygon in August. TPI was calculated from the 10-cm elevation model using a 33x33 pixel search window.</p> $TPI = z_o - \bar{z}$ <p>Where <math>z_o</math> = elevation of central point, <math>\bar{z}</math> = mean elevation of neighborhood</p>
<b>TPI SD 33</b>	<p>Standard deviation of Topographic Position Index (TPI) within a training polygon in August. TPI was calculated from the 10-cm elevation model using a 33x33 pixel search window.</p> $TPI = z_o - \bar{z}$ <p>Where <math>z_o</math> = elevation of central point, <math>\bar{z}</math> = mean elevation of neighborhood</p>
<b>TPI Mean 111</b>	<p>Mean of Topographic Position Index (TPI) within a training polygon in August. TPI was calculated from the 10-cm elevation model using a 111x111 pixel search window.</p> $TPI = z_o - \bar{z}$ <p>Where <math>z_o</math> = elevation of central point, <math>\bar{z}</math> = mean elevation of neighborhood</p>
<b>TPI SD 111</b>	<p>Standard deviation of Topographic Position Index (TPI) within a training polygon in August. TPI was calculated from the 10-cm elevation model using a 111x111 pixel search window.</p> $TPI = z_o - \bar{z}$ <p>Where <math>z_o</math> = elevation of central point, <math>\bar{z}</math> = mean elevation of neighborhood</p>

(continued) Table A1.3. Full list of indices extracted from UAV imagery and the 3D point cloud.

<b>Index</b>	<b>Description</b>
<b>DEV Mean 5</b>	<p>Mean of Deviation of Mean Elevation (DEV) within a training polygon in August. DEV was calculated from the 10-cm elevation model using a 5x5 pixel search window.</p> $DEV = \frac{z_o - \bar{z}}{SD}$ <p>Where <math>z_o</math> = elevation of central point, <math>\bar{z}</math> = mean elevation of neighborhood, and SD = standard deviation of elevation values in the neighborhood</p>
<b>DEV SD 5</b>	<p>Standard deviation of Deviation of Mean Elevation (DEV) within a training polygon in August. DEV was calculated from the 10-cm elevation model using a 5x5 pixel search window.</p> $DEV = \frac{z_o - \bar{z}}{SD}$ <p>Where <math>z_o</math> = elevation of central point, <math>\bar{z}</math> = mean elevation of neighborhood, and SD = standard deviation of elevation values in the neighborhood</p>
<b>DEV Mean 11</b>	<p>Mean of Deviation of Mean Elevation (DEV) within a training polygon in August. DEV was calculated from the 10-cm elevation model using a 11x11 pixel search window.</p> $DEV = \frac{z_o - \bar{z}}{SD}$ <p>Where <math>z_o</math> = elevation of central point, <math>\bar{z}</math> = mean elevation of neighborhood, and SD = standard deviation of elevation values in the neighborhood</p>
<b>DEV SD 11</b>	<p>Standard deviation of Deviation of Mean Elevation (DEV) within a training polygon in August. DEV was calculated from the 10-cm elevation model using a 11x11 pixel search window.</p> $DEV = \frac{z_o - \bar{z}}{SD}$ <p>Where <math>z_o</math> = elevation of central point, <math>\bar{z}</math> = mean elevation of neighborhood, and SD = standard deviation of elevation values in the neighborhood</p>
<b>DEV Mean 33</b>	<p>Mean of Deviation of Mean Elevation (DEV) within a training polygon in August. DEV was calculated from the 10-cm elevation model using a 33x33 pixel search window.</p> $DEV = \frac{z_o - \bar{z}}{SD}$ <p>Where <math>z_o</math> = elevation of central point, <math>\bar{z}</math> = mean elevation of neighborhood, and SD = standard deviation of elevation values in the neighborhood</p>

(continued) Table A1.3. Full list of indices extracted from UAV imagery and the 3D point cloud.

<b>Index</b>	<b>Description</b>
<b>DEV SD 33</b>	<p>Standard deviation of Deviation of Mean Elevation (DEV) within a training polygon in August. DEV was calculated from the 10-cm elevation model using a 33x33 pixel search window.</p> $DEV = \frac{z_o - \bar{z}}{SD}$ <p>Where <math>z_o</math> = elevation of central point, <math>\bar{z}</math> = mean elevation of neighborhood, and SD = standard deviation of elevation values in the neighborhood</p>
<b>DEV Mean 111</b>	<p>Mean of Deviation of Mean Elevation (DEV) within a training polygon in August. DEV was calculated from the 10-cm elevation model using a 111x111 pixel search window.</p> $DEV = \frac{z_o - \bar{z}}{SD}$ <p>Where <math>z_o</math> = elevation of central point, <math>\bar{z}</math> = mean elevation of neighborhood, and SD = standard deviation of elevation values in the neighborhood</p>
<b>DEV SD 111</b>	<p>Standard deviation of Deviation of Mean Elevation (DEV) within a training polygon in August. DEV was calculated from the 10-cm elevation model using a 111x111 pixel search window.</p> $DEV = \frac{z_o - \bar{z}}{SD}$ <p>Where <math>z_o</math> = elevation of central point, <math>\bar{z}</math> = mean elevation of neighborhood, and SD = standard deviation of elevation values in the neighborhood</p>
<b>Curvature Mean</b>	<p>Mean of Curvature Index (concavity/convexity) within a training polygon in August. Curvature Index was calculated from the 10-cm elevation model using the Curvature tool with the <i>Profile</i> setting within the DEM Surface Tools toolbox in ArcGIS. (<a href="http://www.jennessent.com/arcgis/surface_area.htm">http://www.jennessent.com/arcgis/surface_area.htm</a>)</p>
<b>Curvature SD</b>	<p>Standard deviation of Curvature Index (concavity/convexity) within a training polygon in August. Curvature Index was calculated from the 10-cm elevation model using the Curvature tool with the <i>Profile</i> setting within the DEM Surface Tools toolbox in ArcGIS. (<a href="http://www.jennessent.com/arcgis/surface_area.htm">http://www.jennessent.com/arcgis/surface_area.htm</a>)</p>
<b>Slope Mean</b>	<p>Mean of Slope in degrees (0-90°) within a training polygon in August. Slope was calculated from the 10-cm elevation model using the Slope (Spatial Analyst) tool in ArcGIS.</p>
<b>Slope SD</b>	<p>Standard deviation of Slope in degrees (0-90°) within a training polygon in August. Slope was calculated from the 10-cm elevation model using the Slope (Spatial Analyst) tool in ArcGIS.</p>

(continued) Table A1.3. Full list of indices extracted from UAV imagery and the 3D point cloud.

<b>Index</b>	<b>Description</b>
<b>3D Surface Area Ratio</b>	3D Surface Area – Planimetric Area ratio within a training polygon in August. $\frac{\text{3D Surface Area of triangulated point cloud}}{\text{2D Planar Surface Area}}$
<b>Point Cloud Density</b>	Density of 3D point cloud (per m <sup>2</sup> ) within a training polygon in August



Table A1.4. Final list of indices after redundant and multicollinear indices were identified and removed using variance inflation factor (VIF) analysis.

<b>Index</b>	<b>Description</b>
<b>R Mean May</b>	Mean of Red channel within a training polygon in May
<b>R SD May</b>	Standard deviation of Red channel within a training polygon in May
<b>Change in R Mean</b>	Change in mean of Red channel within a training polygon from May to August
<b>R/B Mean May</b>	Mean of Red channel divided by Blue channel within a training polygon in May
<b>R/B Mean August</b>	Mean of Red channel divided by Blue channel within a training polygon in August
<b>R/G Mean May</b>	Mean of Red channel divided by Green channel within a training polygon in May
<b>R/G SD May</b>	Standard deviation of Red channel divided by Green channel within a training polygon in May
<b>R/G SD August</b>	Standard deviation of Red channel divided by Green channel within a training polygon in August
<b>G/B SD May</b>	Standard deviation of Green channel divided by Blue channel within a training polygon in May
<b>NIR Mean May</b>	Mean of Near-Infrared within a training polygon in May
<b>NIR SD May</b>	Standard deviation of Near-Infrared within a training polygon in May
<b>NIR Mean August</b>	Mean of Near-Infrared within a training polygon in August
<b>NDVI Mean May</b>	Mean of NDVI within a training polygon in May. $NDVI = \frac{NIR-R}{NIR+R}$
<b>NDVI SD May</b>	Standard deviation of NDVI within a training polygon in May. $NDVI = \frac{NIR-R}{NIR+R}$
<b>NDVI Mean August</b>	Mean of NDVI within a training polygon in August. $NDVI = \frac{NIR-R}{NIR+R}$
<b>NDVI SD August</b>	Standard deviation of NDVI within a training polygon in August. $NDVI = \frac{NIR-R}{NIR+R}$
<b>CIVE Mean August</b>	Mean of Color Index of Vegetation (CIVE) within a training polygon in August. $CIVE = 0.441 * R - 0.881 * G + 0.385 * B + 18.78745$
<b>CIVE SD August</b>	Standard deviation of Color Index of Vegetation (CIVE) within a training polygon in August. $CIVE = 0.441 * R - 0.881 * G + 0.385 * B + 18.78745$
<b>Hue Mean May</b>	Mean of Hue in degrees (0-360°) within a training polygon in May. $Hue = \cos^{-1} \frac{(0.5 * (R-G) + (R-B))}{((R-G)^2 + (R-B)(G-B))^{0.5}}$

(continued) Table A1.4. Final list of indices after redundant and multicollinear indices were identified and removed using variance inflation factor (VIF) analysis.

<b>Index</b>	<b>Description</b>
<b>Hue SD May</b>	Standard deviation of Hue in degrees (0-360°) within a training polygon in May. $\text{Hue} = \cos^{-1} \frac{(0.5*(R-G)+(R-B))}{(((R-G)^2+(R-B)(G-B))^{0.5})}$
<b>Hue SD August</b>	Standard deviation of Hue in degrees (0-360°) within a training polygon in August. $\text{Hue} = \cos^{-1} \frac{(0.5*(R-G)+(R-B))}{(((R-G)^2+(R-B)(G-B))^{0.5})}$
<b>Saturation SD May</b>	Standard deviation of Saturation within a training polygon in May. $\text{Saturation} = 1 - \left( \frac{R+G+B}{3} \right) * a$
<b>Saturation SD August</b>	Standard deviation of Saturation within a training polygon in August. $\text{Saturation} = 1 - \left( \frac{R+G+B}{3} \right) * a$
<b>Vegetation Height SD</b>	Standard deviation of vegetation height calculated within a training polygon in August. Vegetation height was calculated by subtracting the minimum from the maximum elevation value within a 50-cm search radius of each pixel using the 10-cm elevation model
<b>TPI Mean 5</b>	Mean of Topographic Position Index (TPI) within a training polygon in August. TPI was calculated from the 10-cm elevation model using a 5x5 pixel search window. $\text{TPI} = z_o - \bar{z}$ <p>Where <math>z_o</math> = elevation of central point, <math>\bar{z}</math> = mean elevation of neighborhood</p>
<b>TPI Mean 111</b>	Mean of Topographic Position Index (TPI) within a training polygon in August. TPI was calculated from the 10-cm elevation model using a 111x111 pixel search window. $\text{TPI} = z_o - \bar{z}$ <p>Where <math>z_o</math> = elevation of central point, <math>\bar{z}</math> = mean elevation of neighborhood</p>
<b>DEV Mean 5</b>	Mean of Deviation of Mean Elevation (DEV) within a training polygon in August. DEV was calculated from the 10-cm elevation model using a 5x5 pixel search window. $\text{DEV} = \frac{z_o - \bar{z}}{\text{SD}}$ <p>Where <math>z_o</math> = elevation of central point, <math>\bar{z}</math> = mean elevation of neighborhood, and SD = standard deviation of elevation values in the neighborhood</p>

(continued) Table A1.4. Final list of indices after redundant and multicollinear indices were identified and removed using variance inflation factor (VIF) analysis.

<b>Index</b>	<b>Description</b>
<b>DEV SD 5</b>	<p>Standard deviation of Deviation of Mean Elevation (DEV) within a training polygon in August. DEV was calculated from the 10-cm elevation model using a 5x5 pixel search window.</p> $DEV = \frac{z_o - \bar{z}}{SD}$ <p>Where <math>z_o</math> = elevation of central point, <math>\bar{z}</math> = mean elevation of neighborhood, and SD = standard deviation of elevation values in the neighborhood</p>
<b>DEV Mean 33</b>	<p>Mean of Deviation of Mean Elevation (DEV) within a training polygon in August. DEV was calculated from the 10-cm elevation model using a 33x33 pixel search window.</p> $DEV = \frac{z_o - \bar{z}}{SD}$ <p>Where <math>z_o</math> = elevation of central point, <math>\bar{z}</math> = mean elevation of neighborhood, and SD = standard deviation of elevation values in the neighborhood</p>
<b>DEV SD 33</b>	<p>Standard deviation of Deviation of Mean Elevation (DEV) within a training polygon in August. DEV was calculated from the 10-cm elevation model using a 33x33 pixel search window.</p> $DEV = \frac{z_o - \bar{z}}{SD}$ <p>Where <math>z_o</math> = elevation of central point, <math>\bar{z}</math> = mean elevation of neighborhood, and SD = standard deviation of elevation values in the neighborhood</p>
<b>DEV Mean 111</b>	<p>Mean of Deviation of Mean Elevation (DEV) within a training polygon in August. DEV was calculated from the 10-cm elevation model using a 111x111 pixel search window.</p> $DEV = \frac{z_o - \bar{z}}{SD}$ <p>Where <math>z_o</math> = elevation of central point, <math>\bar{z}</math> = mean elevation of neighborhood, and SD = standard deviation of elevation values in the neighborhood</p>
<b>DEV SD 111</b>	<p>Standard deviation of Deviation of Mean Elevation (DEV) within a training polygon in August. DEV was calculated from the 10-cm elevation model using a 111x111 pixel search window.</p> $DEV = \frac{z_o - \bar{z}}{SD}$ <p>Where <math>z_o</math> = elevation of central point, <math>\bar{z}</math> = mean elevation of neighborhood, and SD = standard deviation of elevation values in the neighborhood</p>
<b>Curvature Mean</b>	<p>Mean of Curvature Index (concavity/convexity) within a training polygon in August. Curvature Index was calculated from the 10-cm elevation model using the Curvature tool with the <i>Profile</i> setting within the DEM Surface Tools toolbox in ArcGIS. (<a href="http://www.jennessent.com/arcgis/surface_area.htm">http://www.jennessent.com/arcgis/surface_area.htm</a>)</p>

(continued) Table A1.4. Final list of indices after redundant and multicollinear indices were identified and removed using variance inflation factor (VIF) analysis.

<b>Index</b>	<b>Description</b>
<b>Slope SD</b>	Standard deviation of Slope in degrees (0-90°) within a training polygon in August. Slope was calculated from the 10-cm elevation model using the Slope (Spatial Analyst) tool in ArcGIS.
<b>3D Surface Area Ratio</b>	3D Surface Area – Planimetric Area ratio within a training polygon in August. $\frac{\text{3D Surface Area of triangulated point cloud}}{\text{2D Planar Surface Area}}$
<b>Point Cloud Density</b>	Density of 3D point cloud (per m <sup>2</sup> ) within a training polygon in August

Table A1.5. List of plant species identified and their frequencies from field plot sampling.

Plant Species Name	Common Name	Frequency (# plots)
<i>Abies balsamea</i>	Balsam fir	9
<i>Acer rubrum</i>	Red maple	22
<i>Achillea millefolium</i>	Common yarrow	4
<i>Agrostis capillaris</i>	Colonial bent grass	3
<i>Alnus viridis</i>	Green alder	124
<i>Amelanchier spp</i>	Serviceberry	51
<i>Ammophila breviligulata</i>	American beach grass	1
<i>Andromeda polifolia</i>	Bog rosemary	2
<i>Aralia nudicaulis</i>	Wild sarsaparilla	62
<i>Arctostaphylos uva-ursi</i>	Common bearberry	37
<i>Arethusa bulbosa</i>	Dragon orchid	19
<i>Betula papyrifera</i>	Paper birch	19
<i>Calamagrostis canadensis</i>	Bluejoint reed grass	10
<i>Calamagrostis pickeringii</i>	Pickering's reed grass	44
<i>Calopogon tuberosus</i>	Tuberous grass pink	24
<i>Calystegia sepium</i>	Hedge false bindweed	2
<i>Campanula rotundifolia</i>	Common harebell	4
<i>Carex bullata</i>	Button sedge	2
<i>Carex exilis</i>	Coastal sedge	12
<i>Carex folliculata</i>	Northern long sedge	3
<i>Carex nigra</i>	Smooth black sedge	64
<i>Carex pauciflora</i>	Few-flowered sedge	3
<i>Carex stricta</i>	Tussock sedge	2
<i>Carex trisperma</i>	Three-seeded sedge	18
<i>Carex vesicaria</i>	Inflated sedge	1
<i>Chamaedaphne calyculata</i>	Leatherleaf	18
<i>Cladonia spp</i>	Cladonia lichen	115
<i>Clintonia borealis</i>	Yellow bluebead lily	7
<i>Corema conradii</i>	Broom crowberry	78
<i>Cornus canadensis</i>	Bunchberry	132
<i>Danthonia spicata</i>	Poverty oat grass	9
<i>Deschampsia flexuosa</i>	Wavy hair grass	31
<i>Dicranum spp</i>	Dicranum Moss	3
<i>Drosera intermedia</i>	Spoon-leaved sundew	7
<i>Drosera rotundifolia</i>	Round-leaved sundew	55
<i>Eleocharis spp</i>	Eleocharis	1
<i>Empetrum eamesii</i>	Red crowberry	11
<i>Empetrum nigrum</i>	Black crowberry	131

(continued) Table A1.5. List of plant species identified and their frequencies from field plot sampling.

<b>Plant Species Name</b>	<b>Common Name</b>	<b>Frequency (# plots)</b>
<i>Eriophorum vaginatum</i>	Tussock cottongrass	23
<i>Eriophorum virginicum</i>	Tawny cottongrass	11
<i>Festuca rubra</i>	Red fescue	20
<i>Fragaria virginiana</i>	Wild strawberry	5
<i>Gaultheria procumbens</i>	Eastern teaberry	104
<i>Gaylussacia baccata</i>	Black huckleberry	182
<i>Gaylussacia bigeloviana</i>	Dwarf huckleberry	71
<i>Glaux maritima</i>	Sea milkwort	5
<i>Hudsonia ericoides</i>	Pinebarren golden heather	3
<i>Ilex glabra</i>	Inkberry	15
<i>Ilex mucronata</i>	Mountain holly	94
<i>Ilex verticillata</i>	Common winterberry	18
<i>Iris spp</i>	Iris	21
<i>Juncus balticus</i>	Baltic rush	12
<i>Juncus gerardii</i>	Black-grass rush	3
<i>Juniperus communis</i>	Common juniper	185
<i>Juniperus horizontalis</i>	Creeping juniper	24
<i>Kalmia angustifolia</i>	Sheep laurel	188
<i>Kalmia polifolia</i>	Pale bog laurel	35
<i>Larix laricina</i>	Tamarack	19
<i>Lathyrus japonicus</i>	Beach pea	5
<i>Ledum groenlandicum</i>	Common labrador tea	95
<i>Ligusticum scoticum</i>	Scotch lovage	2
<i>Limonium carolinianum</i>	Sea lavender	1
<i>Linnaea borealis</i>	Twinflower	1
<i>Liverwort spp</i>	Liverwort	1
<i>Lonicera villosa</i>	Mountain fly honeysuckle	10
<i>Luzula multiflora</i>	Common woodrush	1
<i>Lycopodium spp</i>	Club moss	8
<i>Maianthemum canadense</i>	Wild lily-of-the-valley	76
<i>Maianthemum stellatum</i>	Starry false solomon's seal	1
<i>Maianthemum trifolium</i>	Three-leaved false soloman's seal	52
<i>Melampyrum lineare</i>	Narrowleaf cow wheat	12
<i>Morella pensylvanica</i>	Northern bayberry	126
<i>Myrica gale</i>	Sweet gale	39
<i>Oclemena acuminata</i>	Whorled wood aster	34

(continued) Table A1.5. List of plant species identified and their frequencies from field plot sampling.

<b>Plant Species Name</b>	<b>Common Name</b>	<b>Frequency (# plots)</b>
<i>Osmunda cinnamomea</i>	Cinnamon fern	62
<i>Panicum spp</i>	Panicum	3
<i>Photinia melanocarpa</i>	Black chokeberry	113
<i>Picea glauca</i>	White spruce	5
<i>Picea mariana</i>	Black spruce	48
<i>Pinus banksiana</i>	Jack pine	3
<i>Pinus strobus</i>	Eastern white pine	6
<i>Plantago maritima</i>	Seaside plantain	9
<i>Potentilla anserina</i>	Silverweed cinquefoil	3
<i>Prenanthes trifoliolata</i>	Lion's paw	39
<i>Prunus pensylvanica</i>	Pin cherry	12
<i>Pteridium aquilinum</i>	Bracken fern	118
<i>Rhododendron canadense</i>	Rhodora	102
<i>Rhynchospora alba</i>	White beakrush	10
<i>Ribes spp</i>	Gooseberry	2
<i>Rosa virginiana</i>	Virginia rose	14
<i>Rubus allegheniensis</i>	Alleghaney blackberry	38
<i>Rubus chamaemorus</i>	Bake apple	8
<i>Sagina nodosa</i>	Knotted pearlwort	1
<i>Sarracenia purpurea</i>	Northern pitcher plant	66
<i>Scutellaria galericulata</i>	Marsh skullcap	1
<i>Sibbaldiopsis tridentata</i>	Three-toothed cinquefoil	42
<i>Sisyrinchium montanum</i>	Mountain blue-eyed-grass	2
<i>Solidago bicolor</i>	White goldenrod	23
<i>Solidago puberula</i>	Downy goldenrod	31
<i>Solidago rugosa</i>	Rough-stemmed goldenrod	5
<i>Solidago sempervirens</i>	Seaside goldenrod	17
<i>Solidago uliginosa</i>	Northern bog goldenrod	42
<i>Sorbus aucuparia</i>	European mountain ash	2
<i>Spartina pectinata</i>	Prairie cord grass	3
<i>Sphagnum spp</i>	Sphagnum moss	94
<i>Spiraea alba</i>	White meadowsweet	9
<i>Symphyotrichum novi-belgii</i>	New York aster	17
<i>Thalictrum pubescens</i>	Tall meadow-rue	3
<i>Toxicodendron radicans</i>	Poison ivy	2
<i>Triadenum fraseri</i>	Fraser's marsh St John's-wort	1
<i>Trichophorum caespitosum</i>	Tufted clubrush	63

(continued) Table A1.5. List of plant species identified and their frequencies from field plot sampling.

<b>Plant Species Name</b>	<b>Common Name</b>	<b>Frequency (# plots)</b>
<i>Trifolium repens</i>	White clover	1
<i>Triglochin maritima</i>	Seaside arrowgrass	1
<i>Vaccinium angustifolium</i>	Late lowbush blueberry	140
<i>Vaccinium macrocarpon</i>	Large cranberry	50
<i>Vaccinium oxycoccos</i>	Small cranberry	31
<i>Vaccinium vitis-idaea</i>	Mountain cranberry	22
<i>Viburnum nudum</i>	Northern wild raisin	109



Table A1.6. Full list of classes from the association level plant community classification across all three sites from field plot sampling.

Association Level Classification	Frequency (# plots)
<i>Empetrum nigrum</i> - <i>Ammophila brevigulata</i> dwarf heath	1
<i>Empetrum nigrum</i> - <i>Juniperus communis</i> dwarf heath	40
<i>Empetrum nigrum</i> dwarf heath	14
<i>Juniperus communis</i> - <i>Corema conradii</i> dwarf heath	2
<i>Juniperus communis</i> dwarf heath	18
<i>Juniperus horizontalis</i> dwarf heath	8
<i>Alnus viridis</i> shrubland	3
<i>Gaylussacia baccata</i> shrubland	79
<i>Gaylussacia bigeloviana</i> shrubland	7
<i>Ilex glabra</i> shrubland	8
<i>Lonicera villosa</i> shrubland	1
<i>Morella pensylvanica</i> shrubland	4
Mixed tall shrubs	22
<i>Spiraea alba</i> shrubland	2
<i>Abies balsamea</i> tree island	5
<i>Acer rubrum</i> tree island	7
<i>Betula papyrifera</i> tree island	9
<i>Larix laricina</i> tree island	8
<i>Picea glauca</i> tree island	5
<i>Picea mariana</i> tree island	26
<i>Pinus strobus</i> tree island	2
<i>Carex exilis</i> - <i>Gaylussacia bigeloviana</i> bog	6
<i>Carex nigra</i> - <i>Carex bullata</i> bog	1
<i>Carex nigra</i> bog	13
<i>Carex vesicaria</i> bog	1
<i>Eriophorum russeolum</i> bog	1
<i>Gaylussacia baccata</i> shrub bog	4
<i>Gaylussacia bigeloviana</i> shrub bog	9
<i>Gaylussacia</i> shrub bog	7
<i>Iris</i> spp. - <i>Carex nigra</i> bog	1
<i>Maianthemum trifolium</i> bog	3
<i>Morella pensylvanica</i> shrub bog	1
Open bog	13
<i>Trichophorum caespitosum</i> bog	11
<i>Festuca rubra</i> brackish marsh	1
<i>Juncus balticus</i> brackish marsh	7
<i>Spartina patens</i> salt marsh	4

(continued) Table A1.6. Full list of association level plant community classification across all three sites from field plot sampling.

Association Level Classification	Frequency (# plots)
<i>Spartina pectinata</i> brackish marsh	3
Liverwort spp. seep	1
<i>Osmunda cinnamomea</i> seep	13
<i>Calystegia sepium</i> coastal lithomorphic	1
<i>Corema conradii</i> lithomorphic	5
<i>Empetrum eamesii</i> lithomorphic	1
<i>Festuca rubra</i> coastal lithomorphic	2
<i>Hudsonia ericoides</i> lithomorphic	1
<i>Juniperus communis</i> - <i>Corema conradii</i> lithomorphic	25
<i>Lathyrus japonicus</i> coastal lithomorphic	2
<i>Plantago maritima</i> coastal lithomorphic	1
<i>Solidago sempervirens</i> coastal lithomorphic	2
<i>Trichophorum caespitosum</i> coastal lithomorphic	1
<i>Cladonia</i> spp.	39
<i>Calamagrostis canadensis</i> coastal vegetation	3
<i>Carex nigra</i> - <i>Festuca rubra</i> coastal vegetation	1
<i>Carex nigra</i> coastal vegetation	1
<i>Festuca rubra</i> - <i>Solidago sempervirens</i> - <i>Trifolium repens</i> disturbed coastal vegetation	1
<i>Juncus balticus</i> - <i>Rosa virginiana</i> coastal vegetation	1
<i>Photinia melanocarpa</i> coastal vegetation	1
<i>Rubus allegheniensis</i> - <i>Morella pensylvanica</i> coastal vegetation	4
<i>Thalictrum pubescens</i> coastal vegetation	1
<i>Toxicodendron radicans</i> coastal vegetation	1

Table A1.7. Plant community groupings for the association level classification, broadened association level classification, and formation class classification.

Association Level Classification	Broadened Association Level Classification	Formation Class Classification
<i>Gaylussacia baccata</i> shrubland	<i>Gaylussacia</i> shrubland	Shrubland
<i>Gaylussacia bigeloviana</i> shrubland		
Mixed tall shrubs	Mixed tall shrubs	
<i>Alnus viridis</i> shrubland	<i>Alnus viridis</i> shrubland	
<i>Ilex glabra</i> shrubland	<i>Ilex glabra</i> shrubland	
<i>Morella pensylvanica</i> shrubland	<i>Rubus allegheniensis</i> - <i>Morella pensylvanica</i> coastal vegetation	
<i>Rubus allegheniensis</i> - <i>Morella pensylvanica</i> coastal vegetation		
<i>Acer rubrum</i> tree island	Broadleaf Tree Island	Tree island
<i>Betula papyrifera</i> tree island		
<i>Abies balsamea</i> tree island	Coniferous Tree Island	
<i>Larix laricina</i> tree island		
<i>Picea glauca</i> tree island		
<i>Picea mariana</i> tree island		
<i>Corema conradii</i> lithomorphie	<i>Empetrum nigrum</i> - <i>Juniperus communis</i> dwarf heath	Dwarf heath
<i>Empetrum nigrum</i> - <i>Juniperus communis</i> dwarf heath		
<i>Empetrum nigrum</i> dwarf heath		
<i>Juniperus communis</i> - <i>Corema conradii</i> lithomorphie		
<i>Juniperus communis</i> dwarf heath		
<i>Juniperus horizontalis</i> dwarf heath		
<i>Cladonia</i> spp.	<i>Cladonia</i> spp.	Lichen
<i>Gaylussacia baccata</i> shrub bog	<i>Gaylussacia</i> shrub bog	Bog
<i>Gaylussacia bigeloviana</i> shrub bog		
<i>Gaylussacia</i> shrub bog		
<i>Carex exilis</i> - <i>Gaylussacia bigeloviana</i> bog		

(continued) Table A1.7. Plant community groupings for the association level classification, broadened association level classification, and formation class classification.

Association Level Classification	Broadened Association Level Classification	Formation Class Classification
<i>Carex nigra</i> bog	Grass/Sedge/Open Bog	Bog
<i>Juncus balticus</i> brackish marsh		
Open bog		
<i>Trichophorum caespitosum</i> bog		
<i>Maianthemum trifolium</i> bog	<i>Maianthemum trifolium</i> bog	Bog
<i>Osmunda cinnamomea</i> seep	<i>Osmunda cinnamomea</i> seep	Seep
<i>Spartina pectinata</i> brackish marsh	<i>Spartina pectinata</i> brackish marsh	Brackish marsh
<i>Spartina patens</i> salt marsh	<i>Spartina patens</i> salt marsh	Salt marsh
<i>Calamagrostis canadensis</i> coastal vegetation	<i>Calamagrostis canadensis</i> coastal vegetation	Other

Table A1.8. Full list of indices sorted by their “score” of importance in relation to their contribution to the linear discriminant analysis (LDA) model for each plant community classification. The score was determined by summing the weighted contributions of each index for each discriminatory axis from the LDA model.

Association Level Classification		Broadened Association Level Classification		Formation Class Classification	
Index	Score	Index	Score	Index	Score
R mean May	0.98	R mean May	1.10	R mean May	1.24
Slope SD	0.68	Slope SD	0.75	Slope SD	0.88
Saturation SD May	0.53	R G mean May	0.51	R G mean May	0.55
CIVE SD August	0.50	Saturation SD May	0.47	change R mean	0.40
change R mean	0.50	change R mean	0.45	CIVE mean August	0.37
R G mean May	0.50	TPI mean 5	0.44	CIVE SD August	0.37
Hue SD August	0.42	CIVE mean August	0.39	TPI mean 5	0.36
CIVE mean August	0.39	NIR mean May	0.35	R B mean May	0.29
TPI mean 5	0.37	R B mean May	0.33	TPI mean 111	0.28
R B mean May	0.35	CIVE SD August	0.32	NIR mean May	0.28
R G SD August	0.34	Hue SD August	0.29	R G SD August	0.28
R B mean August	0.32	R G SD August	0.28	R G SD May	0.25
NIR mean May	0.31	R G SD May	0.26	Saturation SD May	0.21
R G SD May	0.26	R B mean August	0.23	Point Density	0.20
DEV mean 111	0.25	Curvature mean	0.22	Saturation SD August	0.19
Point Density	0.24	NDVI mean May	0.22	DEV mean 5	0.19
Veg SD 50cm	0.24	DEV mean 111	0.21	DEV mean 33	0.19
DEV mean 33	0.23	DEV mean 33	0.20	DEV mean 111	0.19
NDVI mean May	0.20	Point Density	0.19	Veg SD 50cm	0.18
Curvature mean	0.20	TPI mean 111	0.18	R SD May	0.16
Hue SD May	0.19	DEV mean 5	0.15	NIR mean August	0.16
DEV mean 5	0.18	NIR mean August	0.15	Curvature mean	0.16
TPI mean 111	0.18	Hue SD May	0.15	Hue SD May	0.15

(continued) Table A1.8. Full list of indices sorted by their “score” of importance in relation to their contribution to the linear discriminant analysis (LDA) model for each plant community classification. The score was determined by summing the weighted contributions of each index for each discriminatory axis from the LDA model.

Association Level Classification		Broadened Association Level Classification		Formation Class Classification	
Index	Score	Index	Score	Index	Score
Saturation SD August	0.16	R SD May	0.14	Hue SD August	0.15
R SD May	0.15	DEV SD 33	0.14	R B mean August	0.14
NDVI SD August	0.15	NIR SD May	0.14	NDVI mean August	0.14
NIR SD May	0.15	Veg SD 50cm	0.13	DEV SD 33	0.14
NIR mean August	0.15	NDVI mean August	0.13	NDVI mean May	0.13
DEV SD 111	0.14	Saturation SD August	0.12	NIR SD May	0.12
G B SD May	0.14	G B SD May	0.12	DEV SD 111	0.10
NDVI mean August	0.13	Surface Area	0.11	G B SD May	0.10
DEV SD 33	0.13	NDVI SD August	0.11	Surface Area	0.09
DEV SD 5	0.11	DEV SD 111	0.10	NDVI SD May	0.09
Surface Area	0.09	DEV SD 5	0.10	NDVI SD August	0.07
NDVI SD May	0.08	NDVI SD May	0.08	Hue mean May	0.04
Hue mean May	0.06	Hue mean May	0.04	DEV SD 5	0.03

Table A1.9. Classification accuracies of the linear discriminant analysis (LDA) model for the association level plant community classification.

Association Level Classification	Accuracy (%)	Majority of Misclassifications
<i>Ilex glabra</i> shrubland	100	None
<i>Maianthemum trifolium</i> bog	100	None
<i>Spartina patens</i> salt marsh	100	None
<i>Cladonia</i> spp.	97	<i>Juniperus communis</i> - <i>Corema conradii</i> lithomorphic
<i>Picea mariana</i> tree island	85	<i>Betula papyrifera</i> tree island
<i>Gaylussacia baccata</i> shrubland	80	<i>Gaylussacia bigeloviana</i> shrubland
<i>Osmunda cinnamomea</i> seep	77	Mixed tall shrubs
<i>Alnus viridis</i> shrubland	67	<i>Larix laricina</i> tree island
<i>Spartina pectinata</i> brackish marsh	67	<i>Morella pensylvanica</i> shrubland
<i>Empetrum nigrum</i> - <i>Juniperus communis</i> dwarf heath	65	<i>Empetrum nigrum</i> dwarf heath
<i>Trichophorum caespitosum</i> bog	64	<i>Carex nigra</i> bog
<i>Juniperus horizontalis</i> dwarf heath	63	<i>Empetrum nigrum</i> - <i>Juniperus communis</i> dwarf heath
Open bog	62	<i>Trichophorum caespitosum</i> bog
Mixed tall shrubs	59	<i>Gaylussacia baccata</i> shrubland
<i>Juniperus communis</i> - <i>Corema conradii</i> lithomorphic	56	<i>Juniperus communis</i> dwarf heath
<i>Carex exilis</i> - <i>Gaylussacia bigeloviana</i> bog	50	<i>Gaylussacia bigeloviana</i> shrub bog
<i>Gaylussacia baccata</i> shrub bog	50	<i>Gaylussacia bigeloviana</i> shrub bog
<i>Juniperus communis</i> dwarf heath	50	<i>Juniperus communis</i> - <i>Corema conradii</i> lithomorphic
<i>Carex nigra</i> bog	46	<i>Trichophorum caespitosum</i> bog
<i>Betula papyrifera</i> tree island	44	<i>Larix laricina</i> tree island
<i>Gaylussacia bigeloviana</i> shrub bog	44	<i>Carex exilis</i> - <i>Gaylussacia bigeloviana</i> bog
<i>Acer rubrum</i> tree island	43	<i>Gaylussacia baccata</i> shrubland
<i>Abies balsamea</i> tree island	40	<i>Picea mariana</i> tree island
<i>Larix laricina</i> tree island	38	<i>Picea mariana</i> tree island

(continued) Table A1.9. Classification accuracies of the linear discriminant analysis (LDA) model for the association level plant community classification.

<b>Association Level Classification</b>	<b>Accuracy (%)</b>	<b>Majority of Misclassifications</b>
<i>Calamagrostis canadensis</i> coastal vegetation	33	<i>Osmunda cinnamomea</i> seep
<i>Empetrum nigrum</i> dwarf heath	29	<i>Empetrum nigrum</i> - <i>Juniperus communis</i> dwarf heath
<i>Gaylussacia bigeloviana</i> shrubland	29	<i>Gaylussacia baccata</i> shrubland
<i>Juncus balticus</i> brackish marsh	29	<i>Carex nigra</i> bog
<i>Morella pensylvanica</i> shrubland	25	<i>Gaylussacia baccata</i> shrubland
<i>Rubus allegheniensis</i> - <i>Morella pensylvanica</i> coastal vegetation	25	<i>Morella pensylvanica</i> shrubland
<i>Gaylussacia shrub</i> bog	14	<i>Gaylussacia bigeloviana</i> shrub bog
<i>Corema conradii</i> lithomorphic	0	<i>Empetrum nigrum</i> - <i>Juniperus communis</i> dwarf heath
<i>Picea glauca</i> tree island	0	<i>Picea mariana</i> tree island



Table A1.10. Classification accuracies of the linear discriminant analysis (LDA) model for the broadened association level plant community classification.

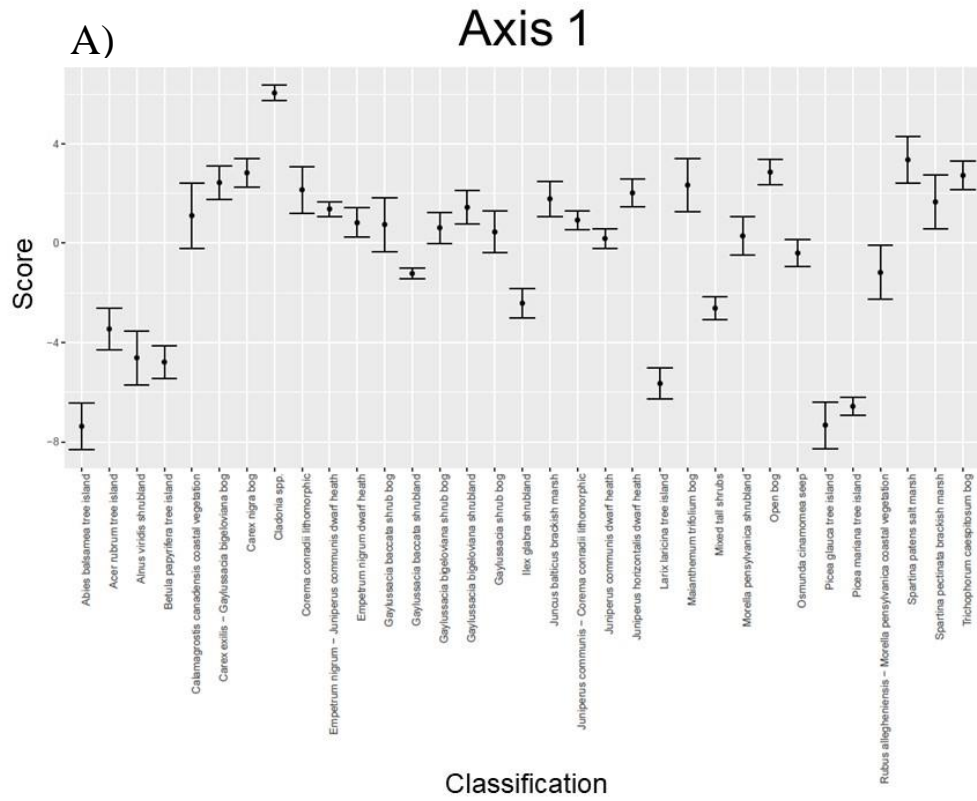
<b>Broadened Association Level Classification</b>	<b>Accuracy (%)</b>	<b>Majority of Misclassifications</b>
<i>Ilex glabra</i> shrubland	100	None
<i>Maianthemum trifolium</i> bog	100	None
<i>Spartina patens</i> salt marsh	100	None
<i>Cladonia</i> spp.	97	<i>Empetrum nigrum</i> - <i>Juniperus communis</i> dwarf heath
<i>Empetrum nigrum</i> - <i>Juniperus communis</i> dwarf heath	96	<i>Gaylussacia</i> shrub bog
Coniferous tree island	84	Broadleaf tree island
<i>Gaylussacia</i> shrubland	84	<i>Gaylussacia</i> shrub bog
<i>Osmunda cinnamomea</i> seep	77	<i>Spartina pectinata</i> brackish marsh
Grass/Sedge/Open bog	73	<i>Gaylussacia</i> shrub bog
<i>Gaylussacia</i> shrub bog	69	Grass/Sedge/Open bog
Broadleaf tree island	69	<i>Gaylussacia</i> shrubland
<i>Alnus viridis</i> shrubland	67	Coniferous tree island
<i>Spartina pectinata</i> brackish marsh	67	<i>Gaylussacia</i> shrub bog
Mixed tall shrubs	59	<i>Gaylussacia</i> shrubland
<i>Rubus allegheniensis</i> - <i>Morella pensylvanica</i> coastal vegetation	38	<i>Gaylussacia</i> shrubland
<i>Calamagrostis canadensis</i> coastal vegetation	33	<i>Osmunda cinnamomea</i> seep

Table A1.11. Classification accuracies of the linear discriminant analysis (LDA) model for the formation class plant community classification.

<b>Formation Class Classification</b>	<b>Accuracy (%)</b>	<b>Majority of Misclassifications</b>
Salt Marsh	100	None
Lichen	97	Dwarf heath
Dwarf heath	96	Lichen
Shrubland	91	Dwarf heath
Bog	90	Shrubland
Tree island	88	Shrubland
Seep	77	Shrubland
Brackish Marsh	67	Bog
Other	33	Dwarf heath

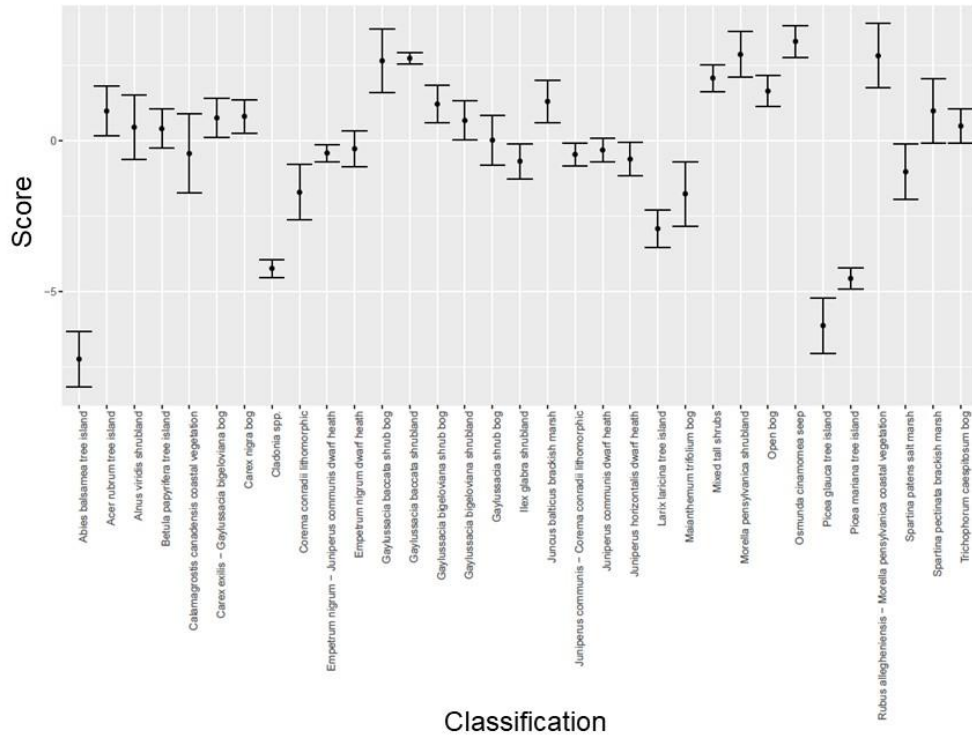
# Figures

Figure A1.1. 95% confidence intervals for the mean linear discriminant analysis (LDA) scores of plant communities from the association level classification for each discriminatory axis.



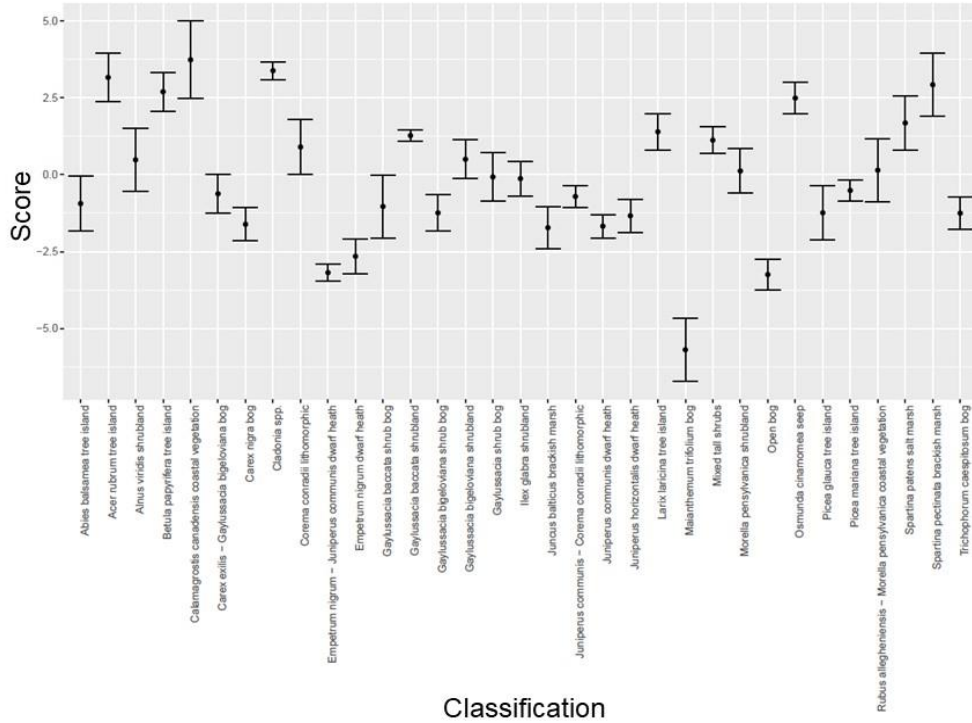
B)

Axis 2



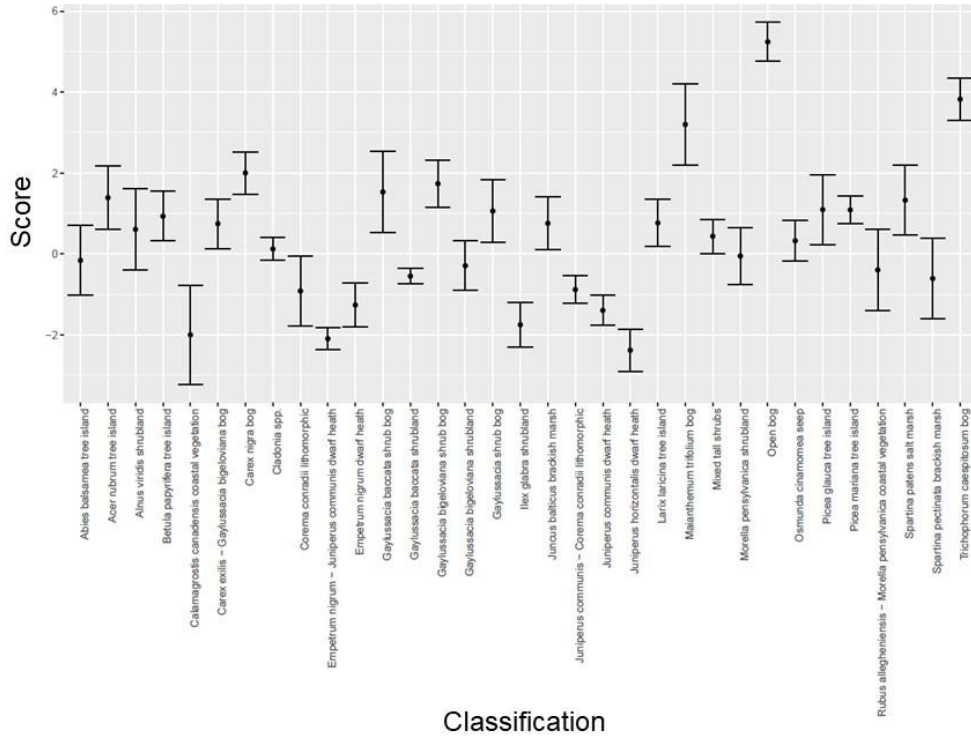
C)

Axis 3



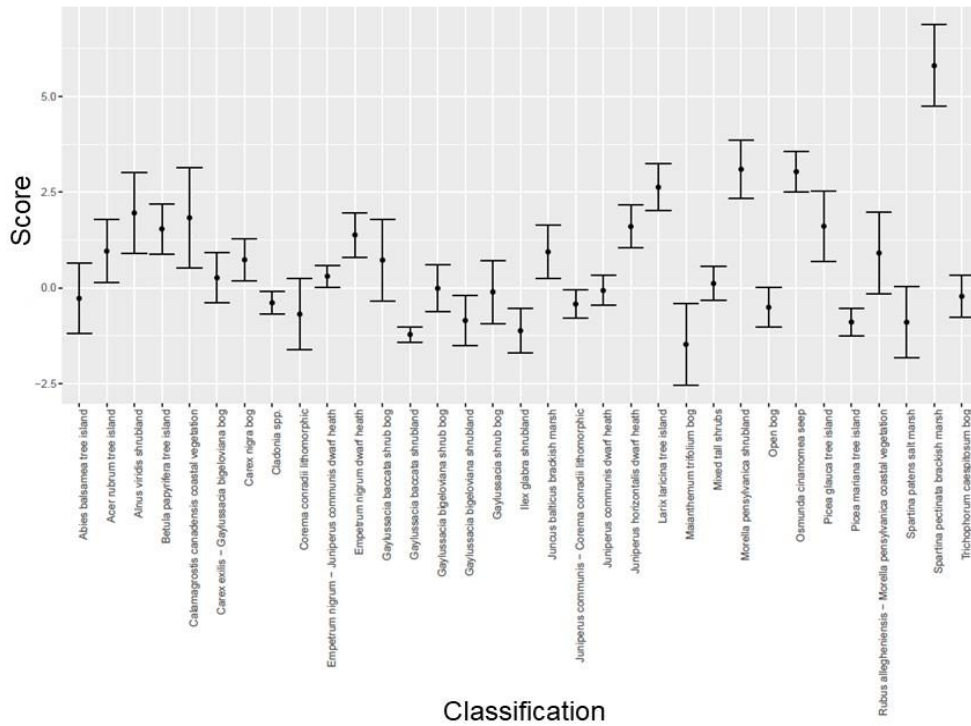
D)

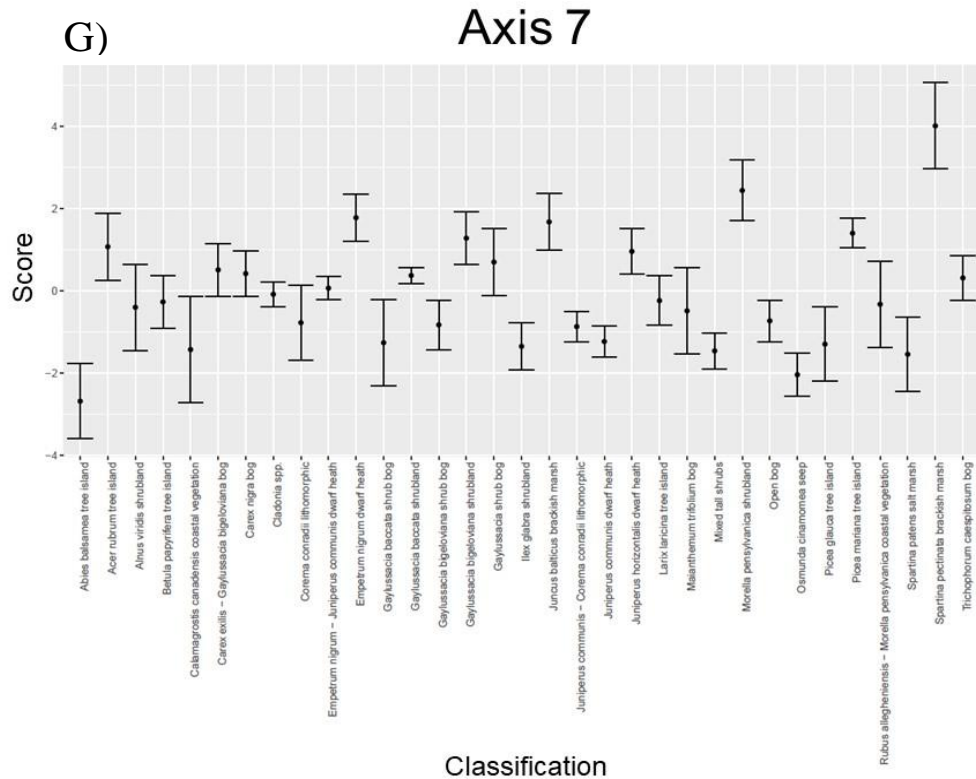
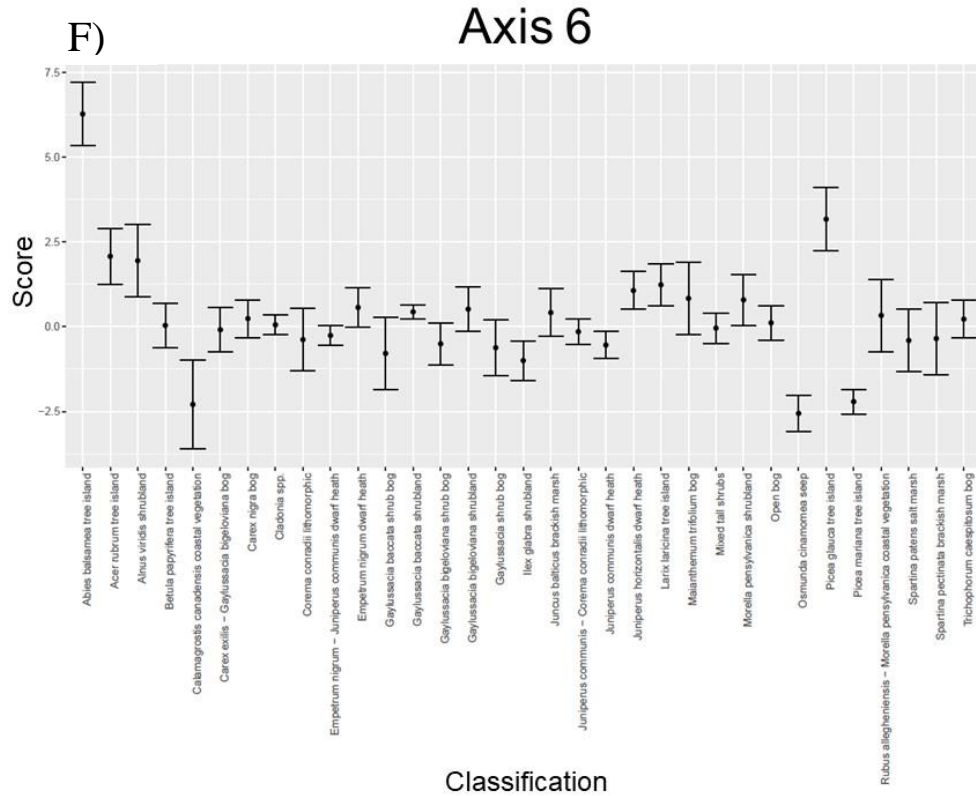
### Axis 4

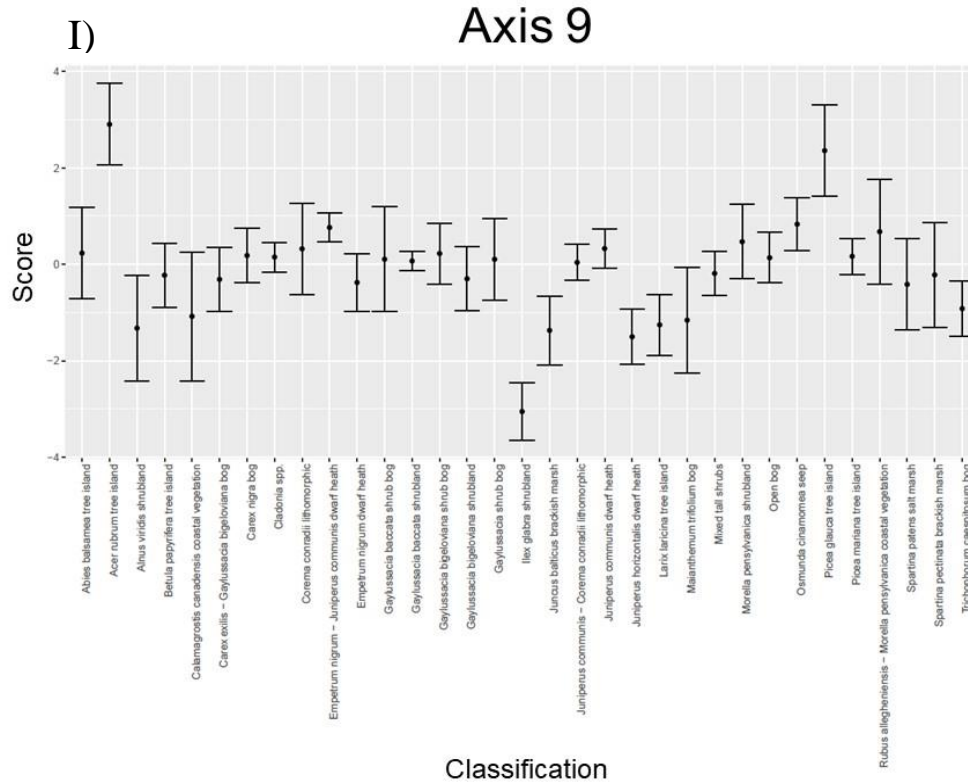
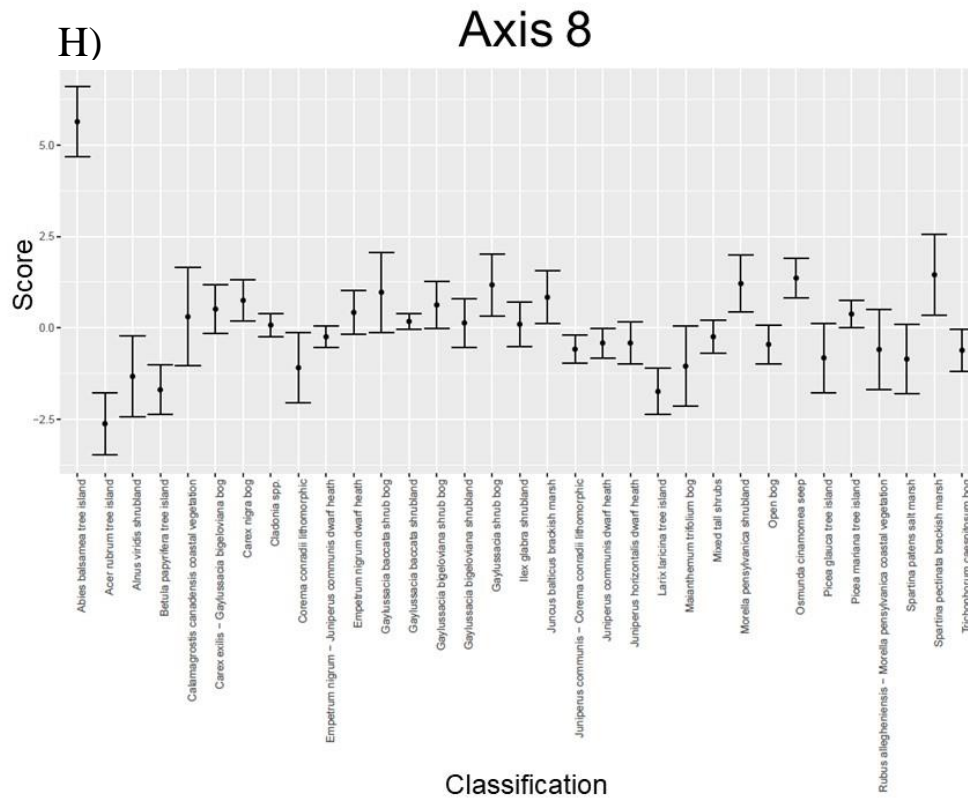


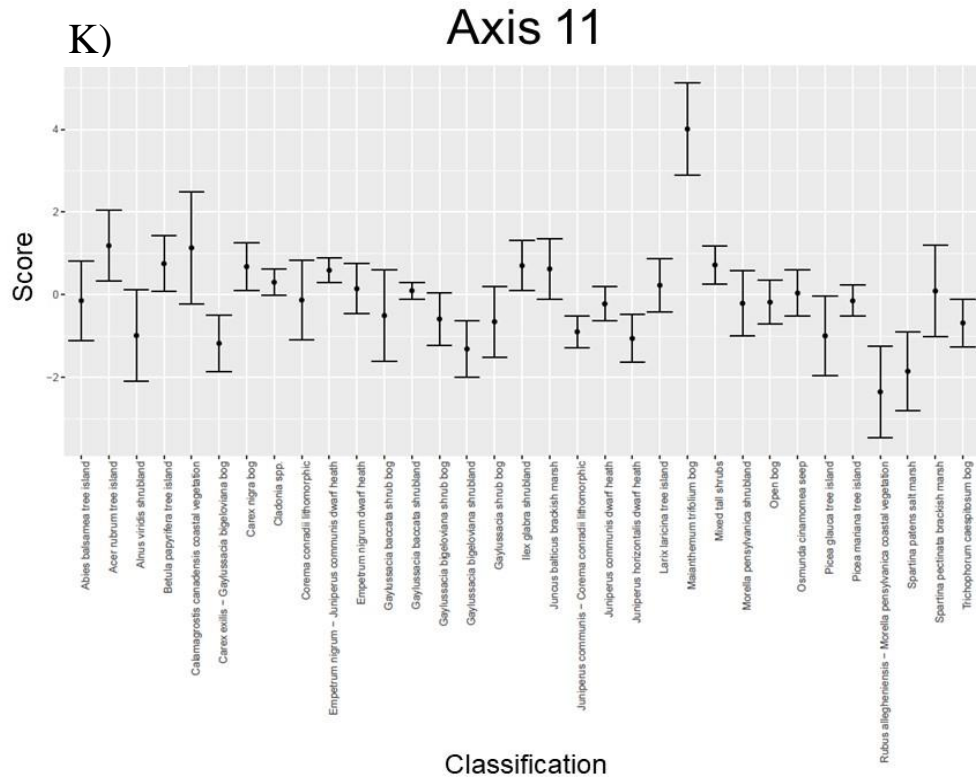
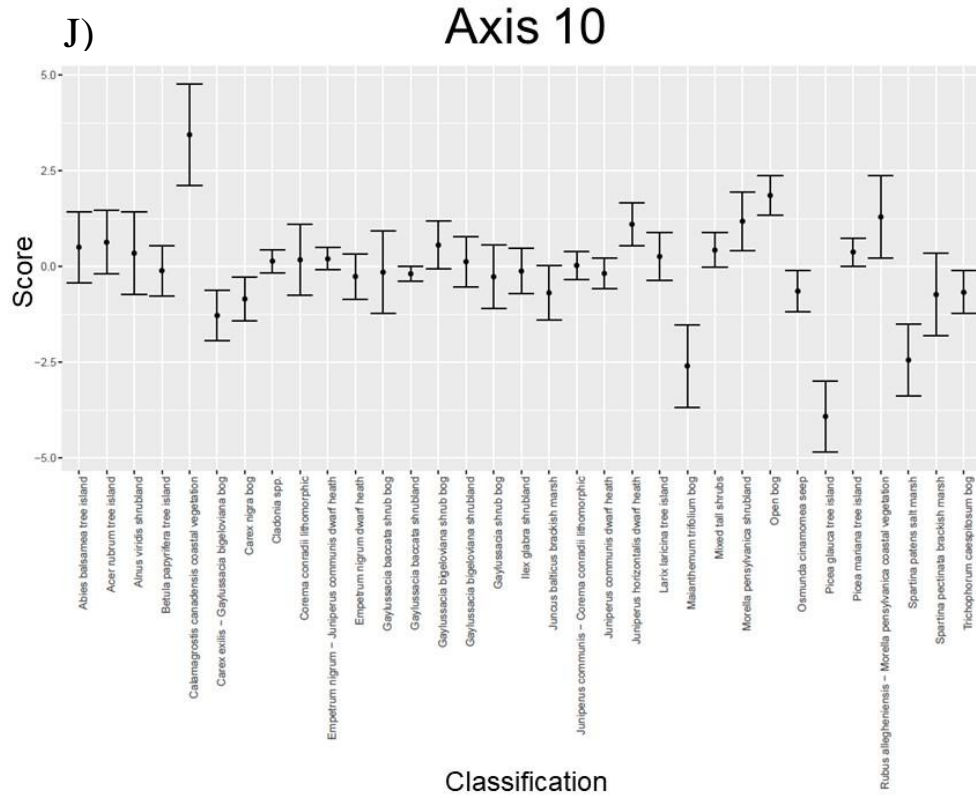
E)

### Axis 5





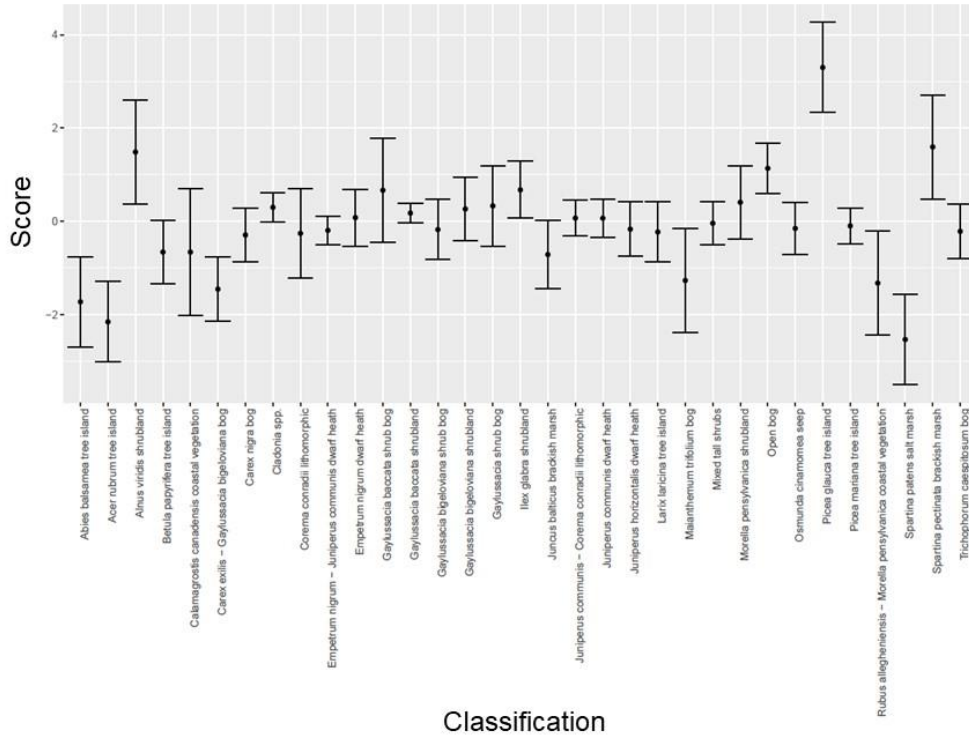






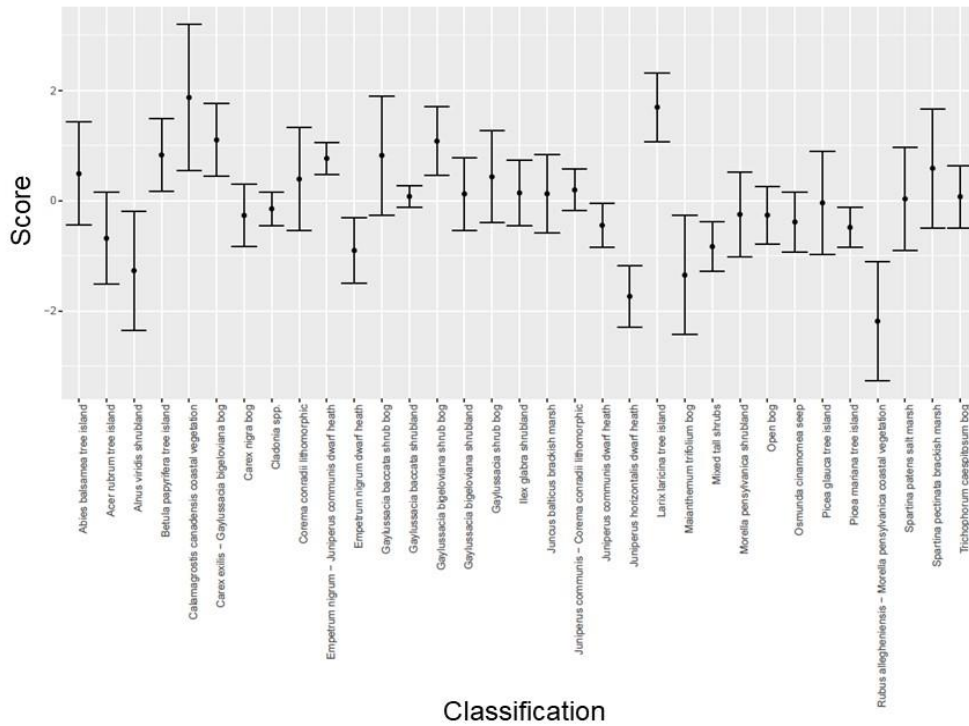
L)

## Axis 12



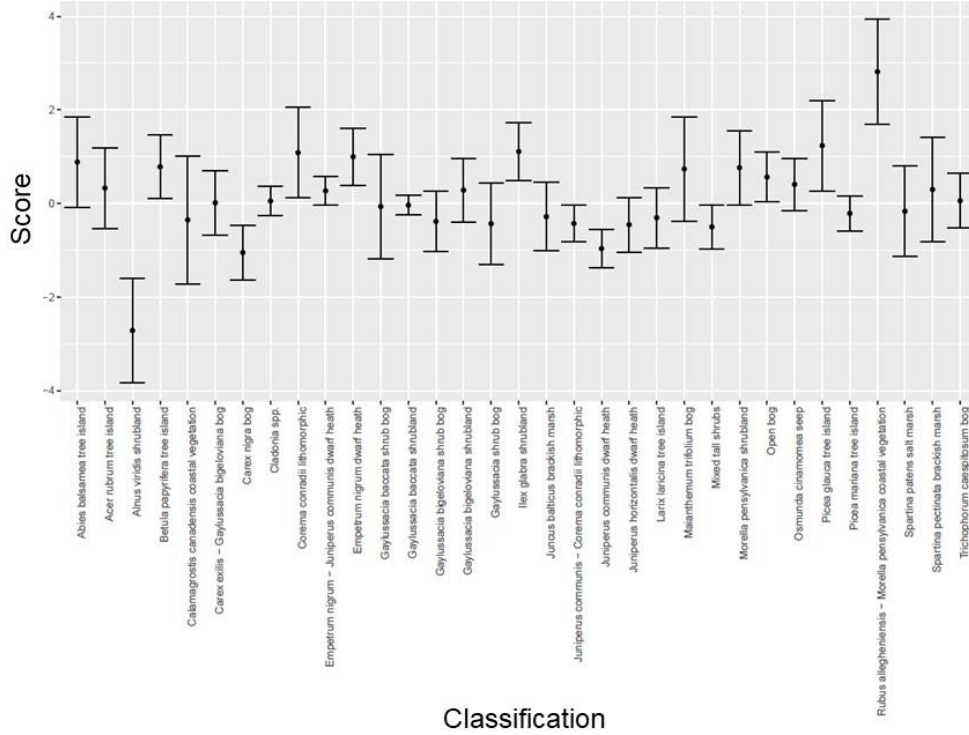
M)

## Axis 13



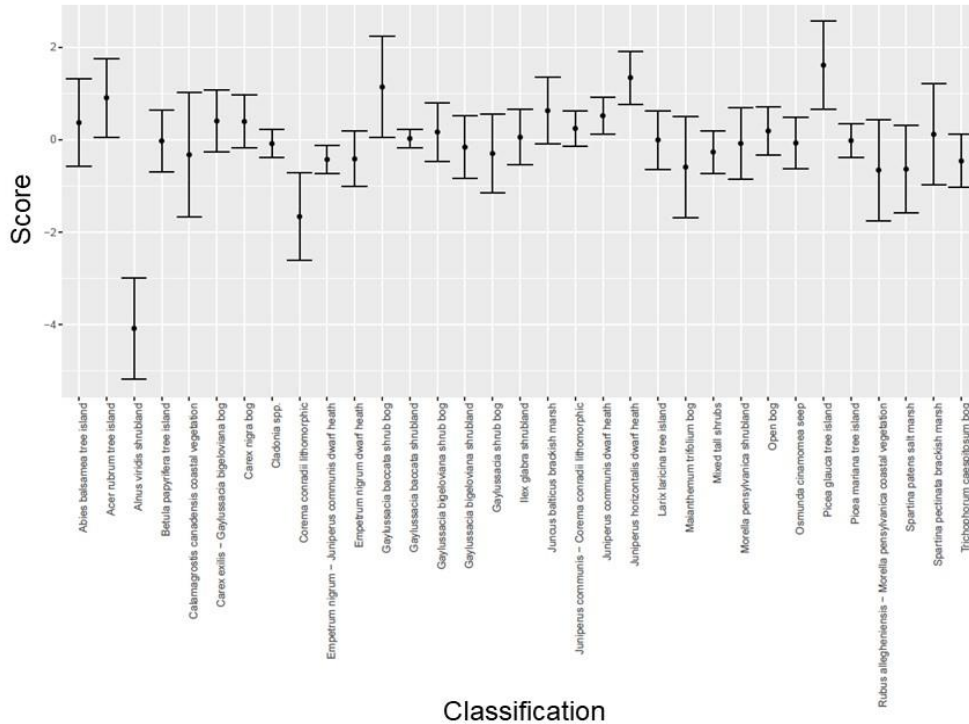
N)

Axis 14



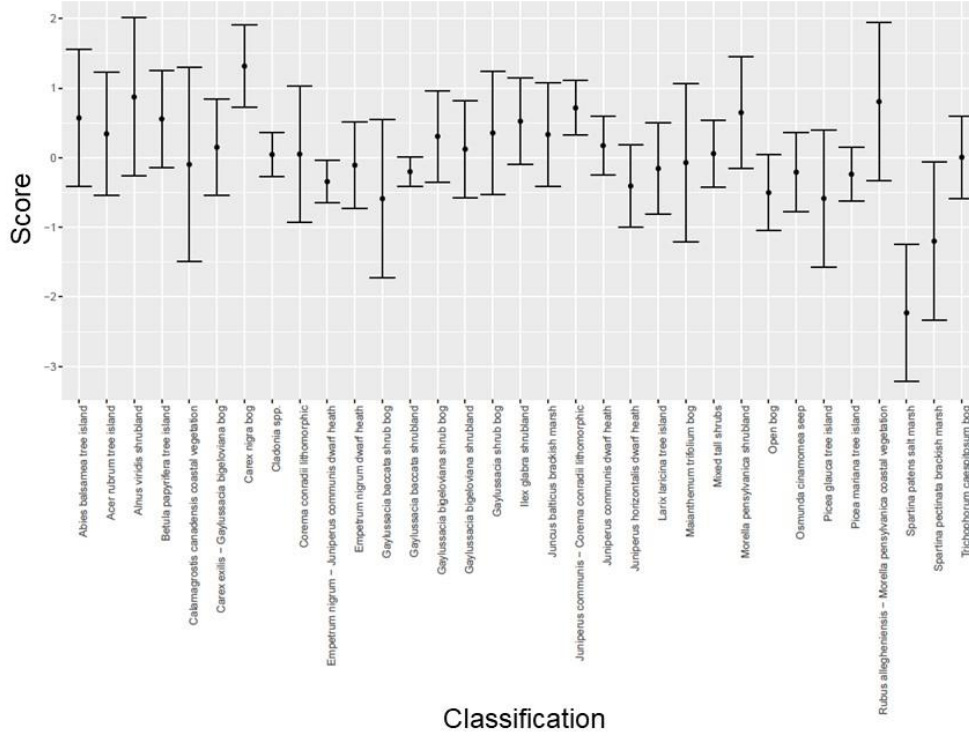
O)

Axis 15



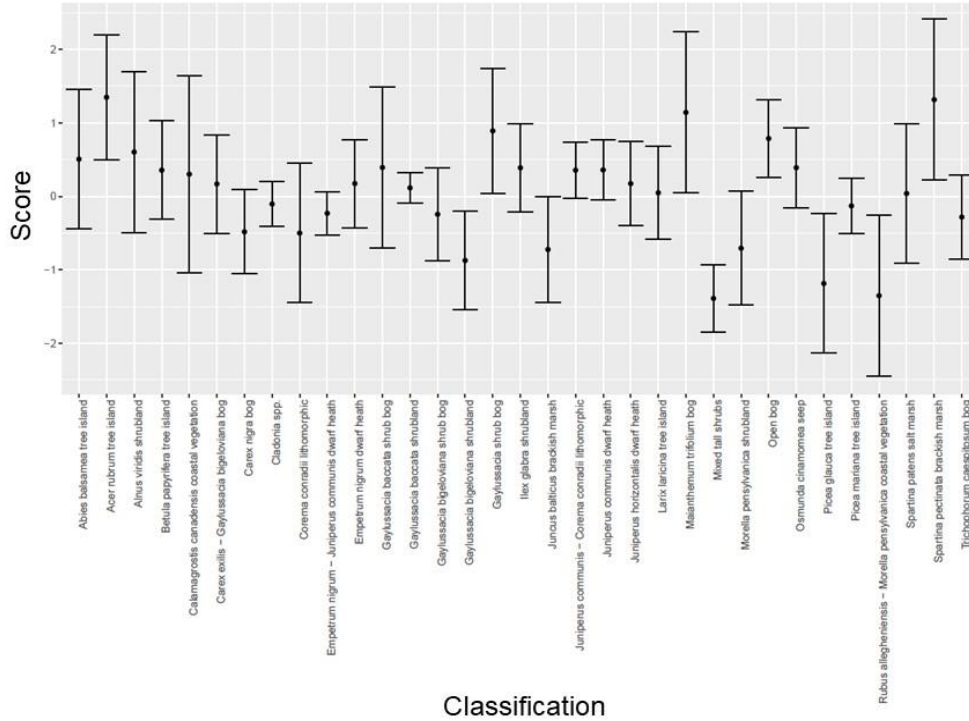
P)

## Axis 16

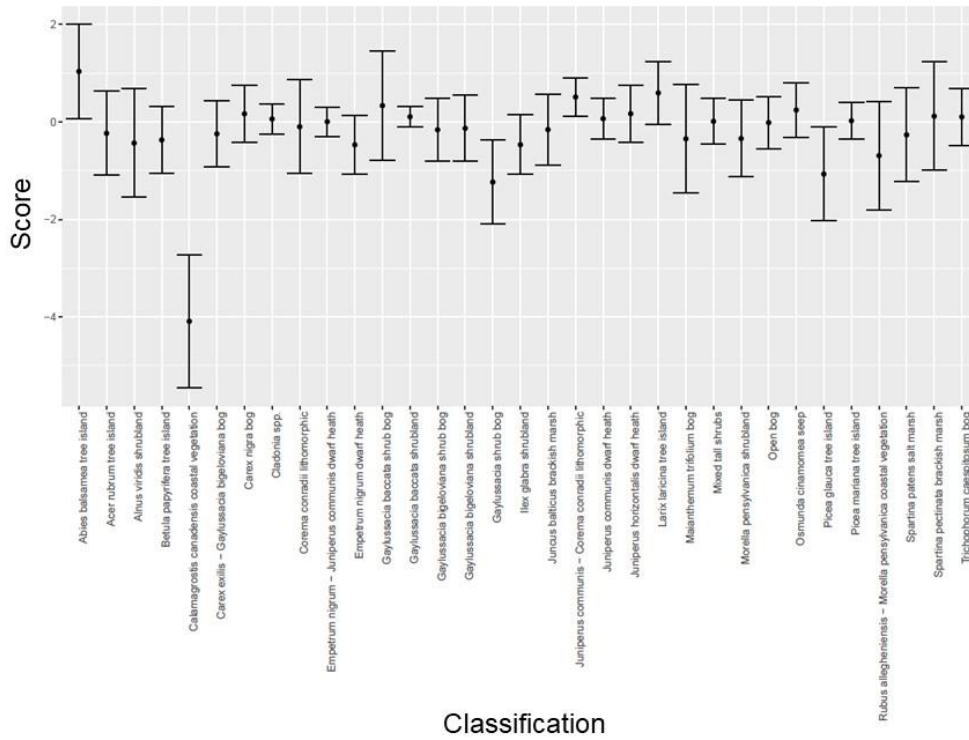


Q)

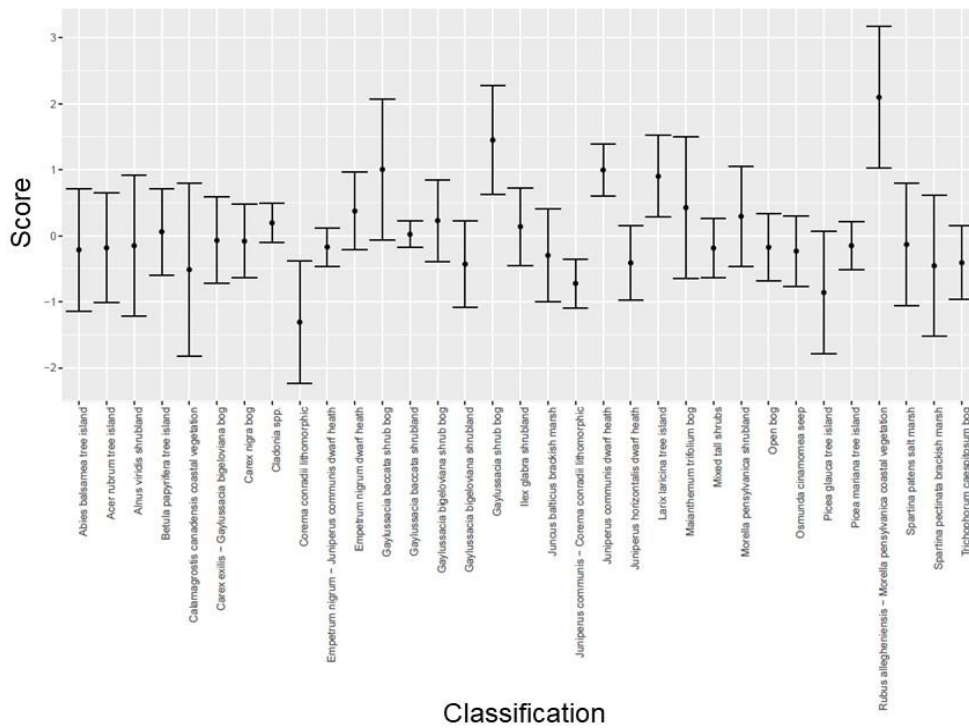
## Axis 17



## R) Axis 18

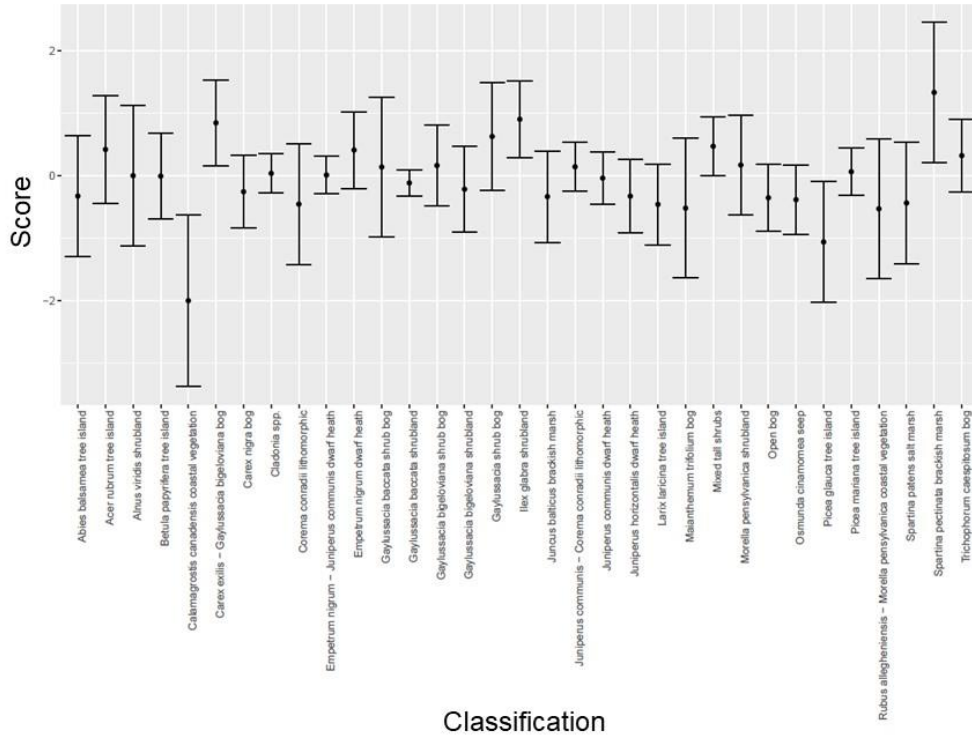


## S) Axis 19



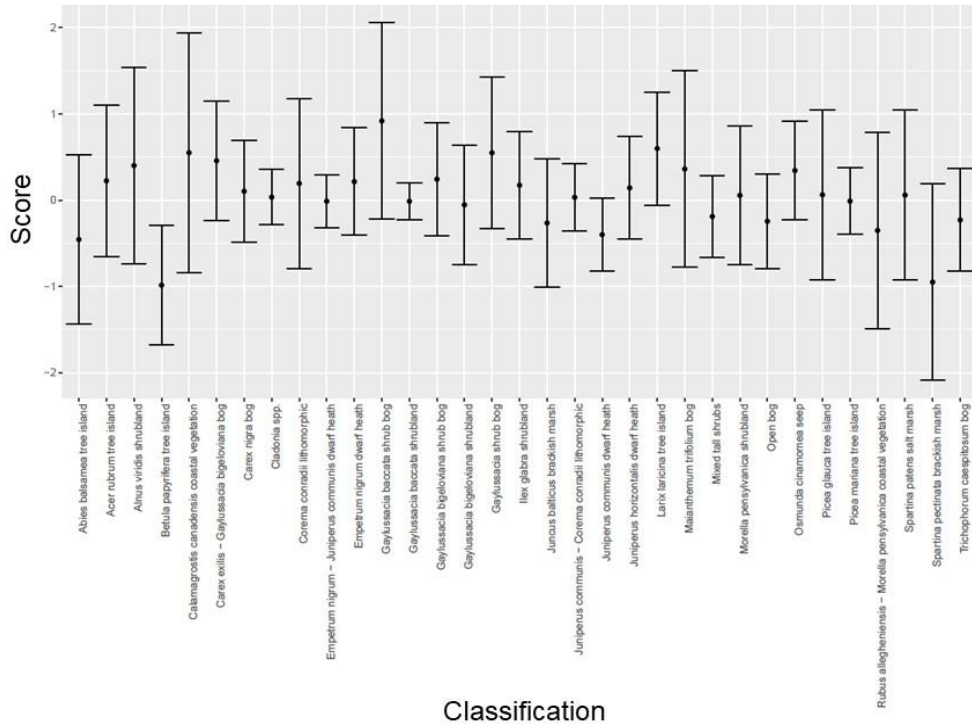
T)

## Axis 20



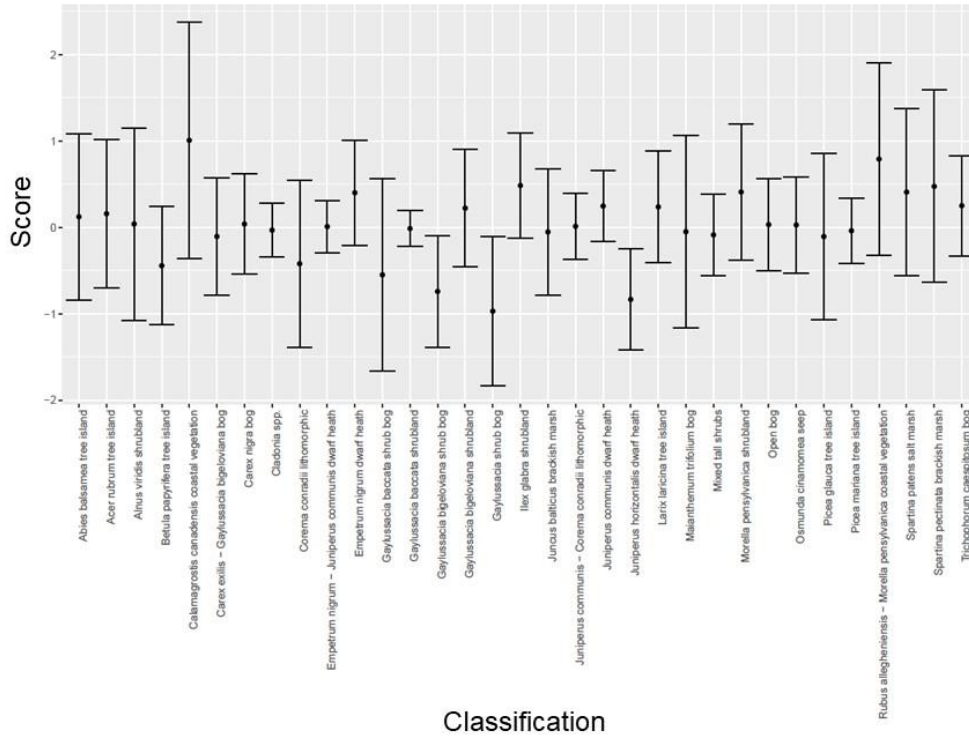
U)

## Axis 21



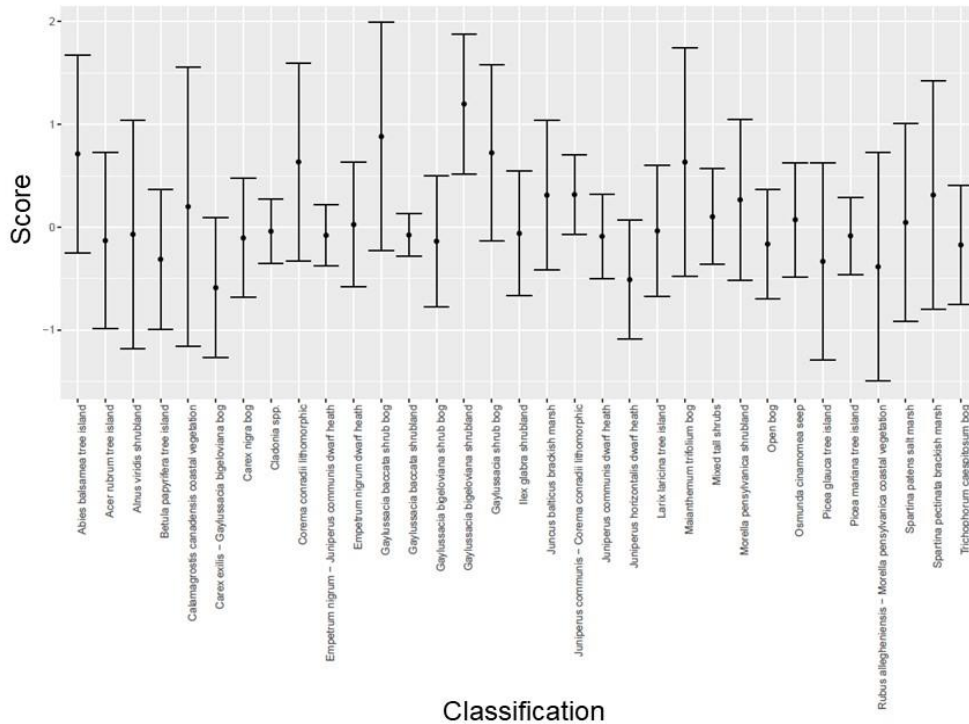
V)

## Axis 22



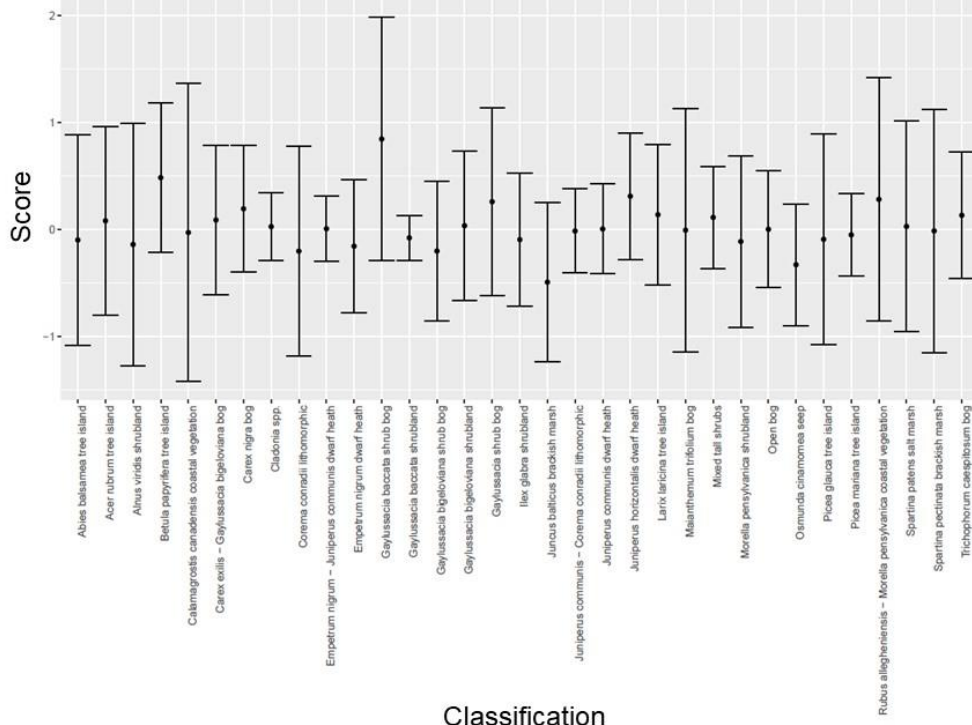
W)

## Axis 23



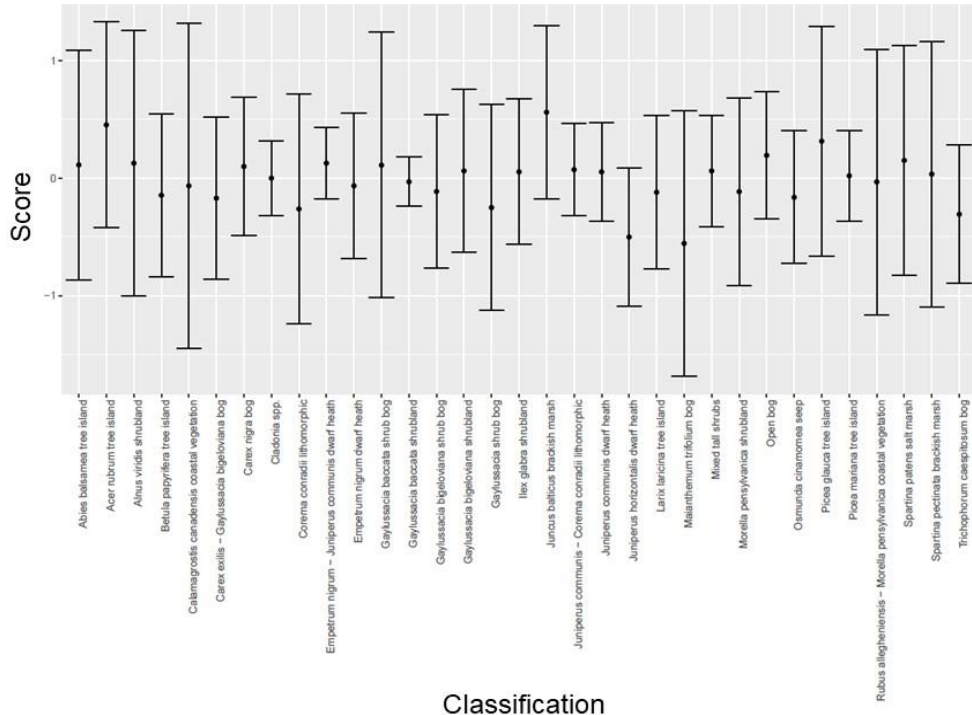
X)

## Axis 24



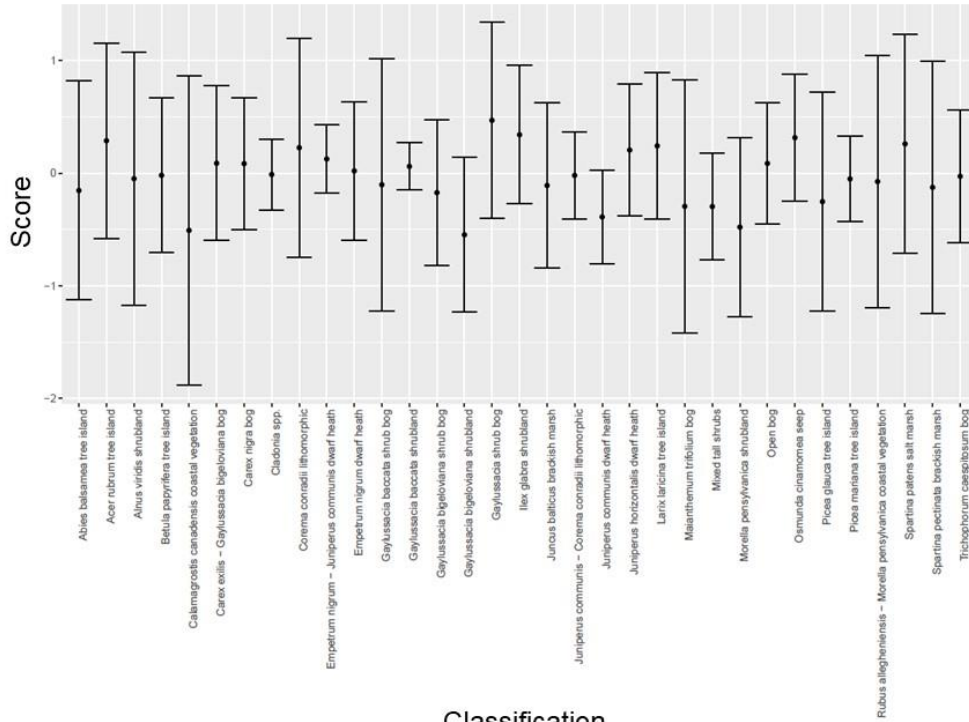
Y)

## Axis 25



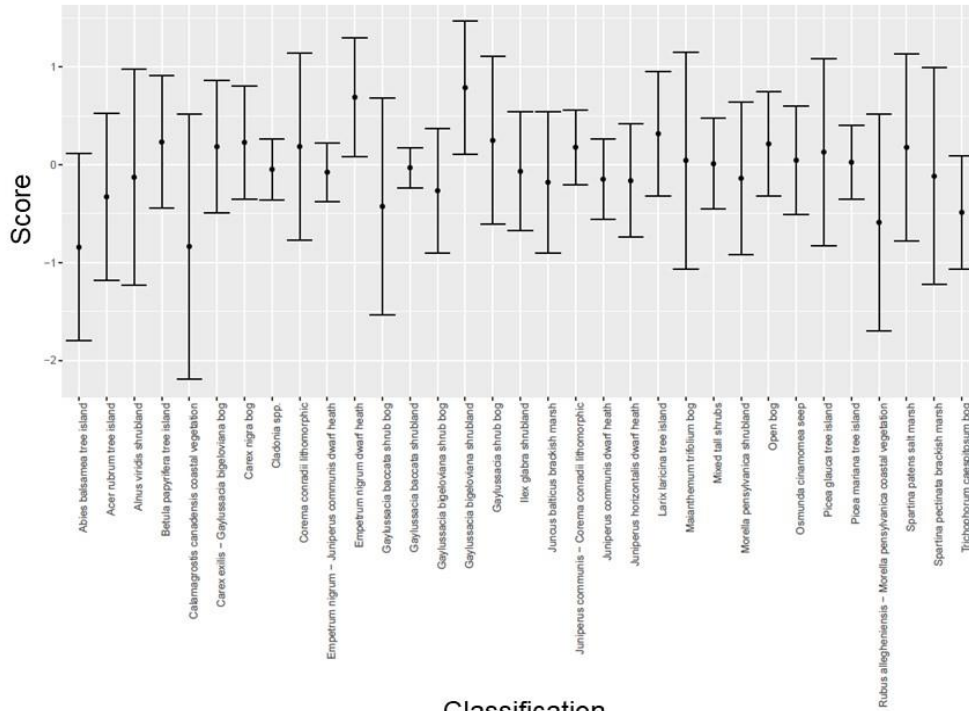
Z)

## Axis 26



AA)

## Axis 27





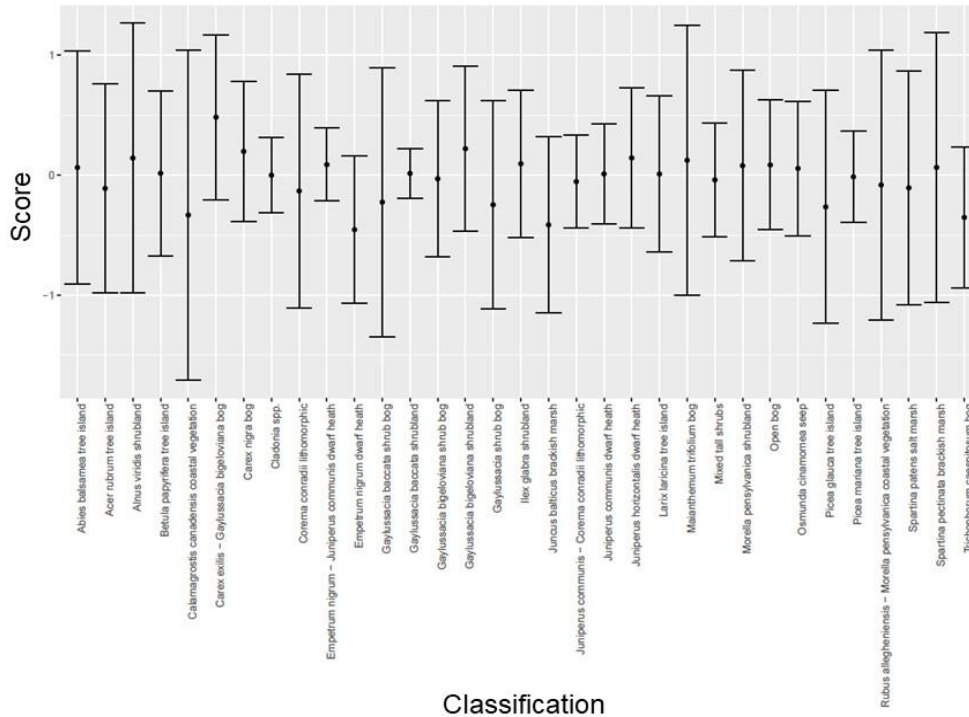
AB)

## Axis 28



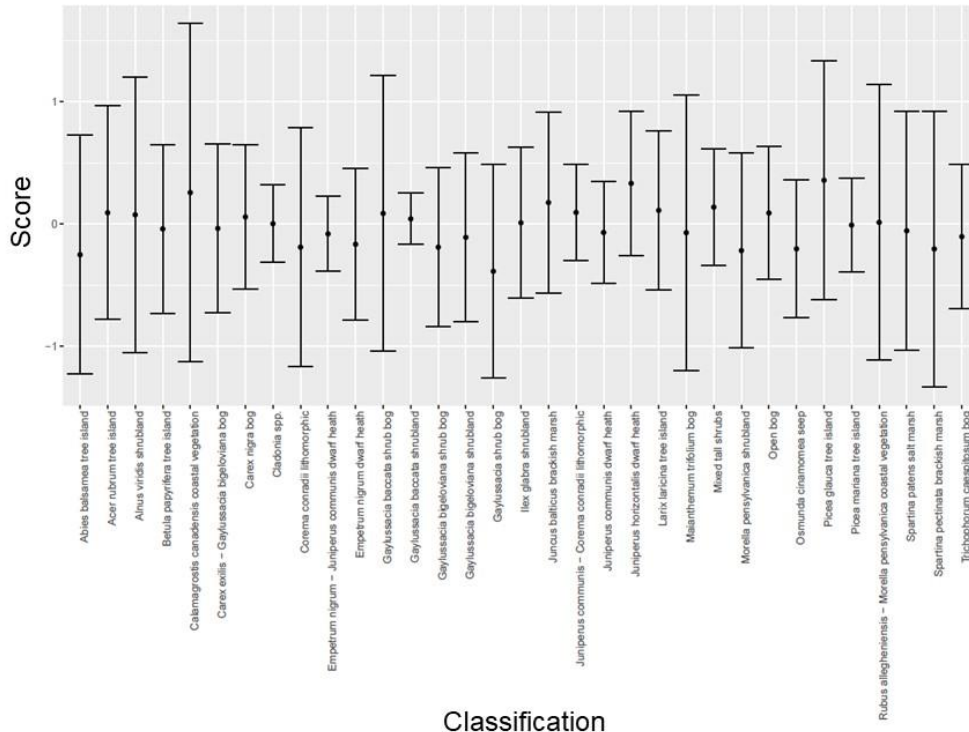
AC)

## Axis 29



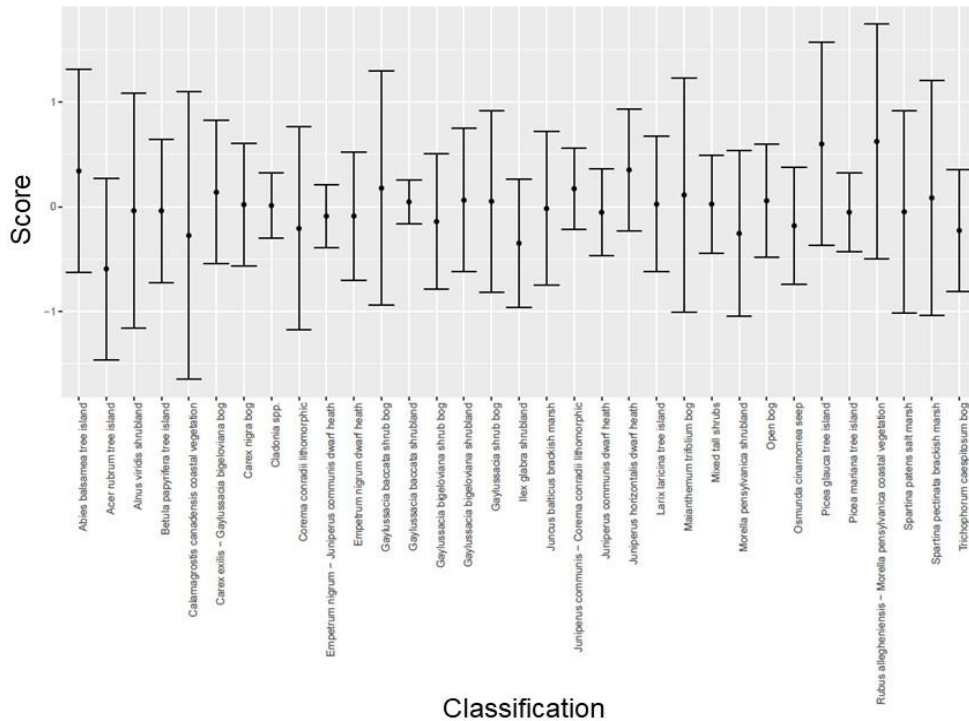
AD)

Axis 30



AE)

Axis 31



AF)

Axis 32

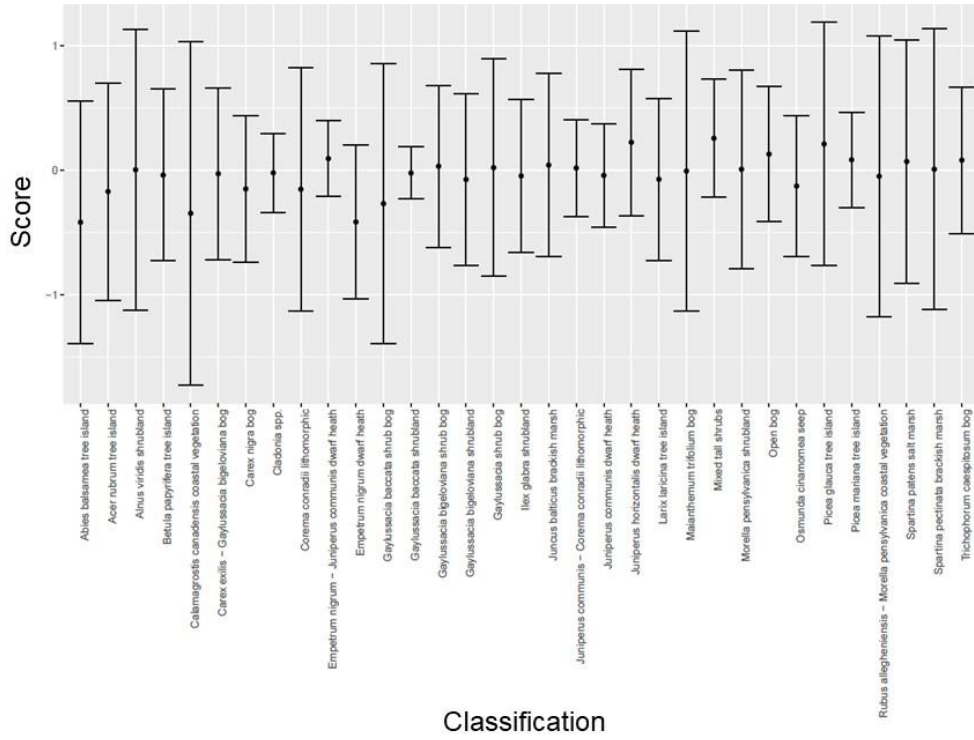
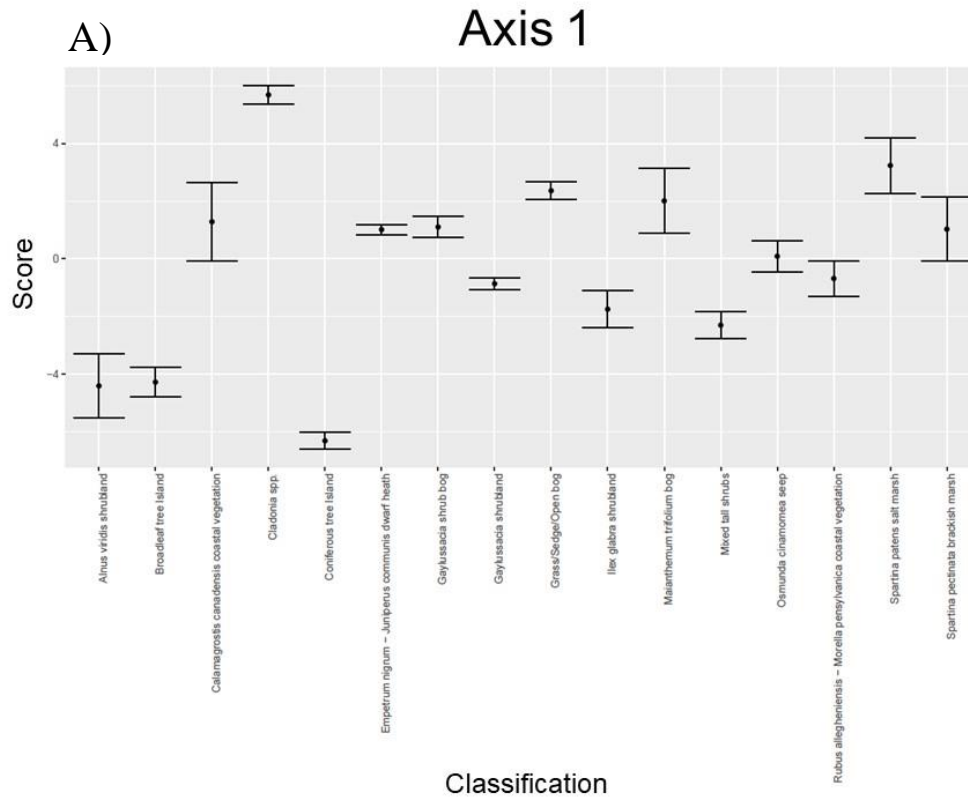
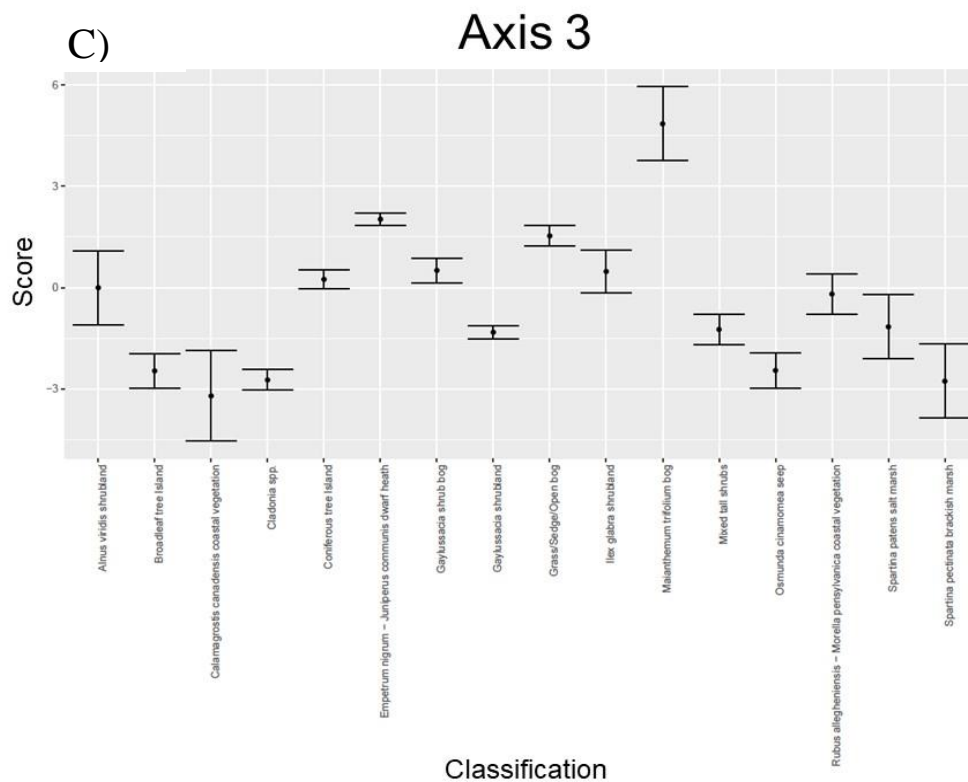
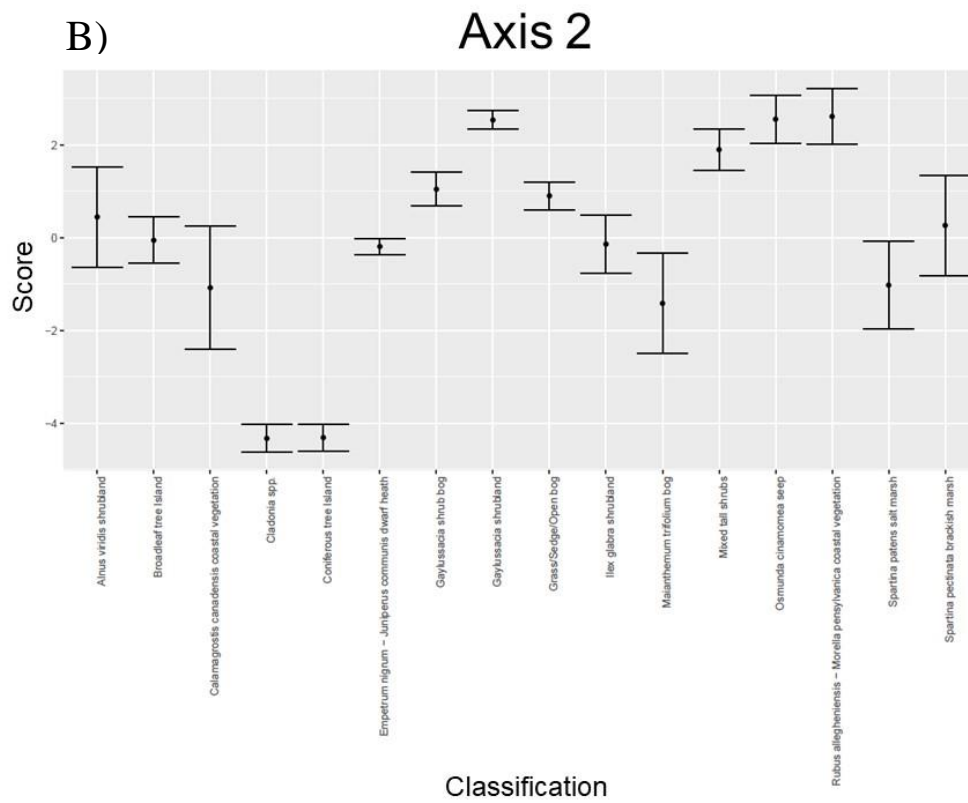
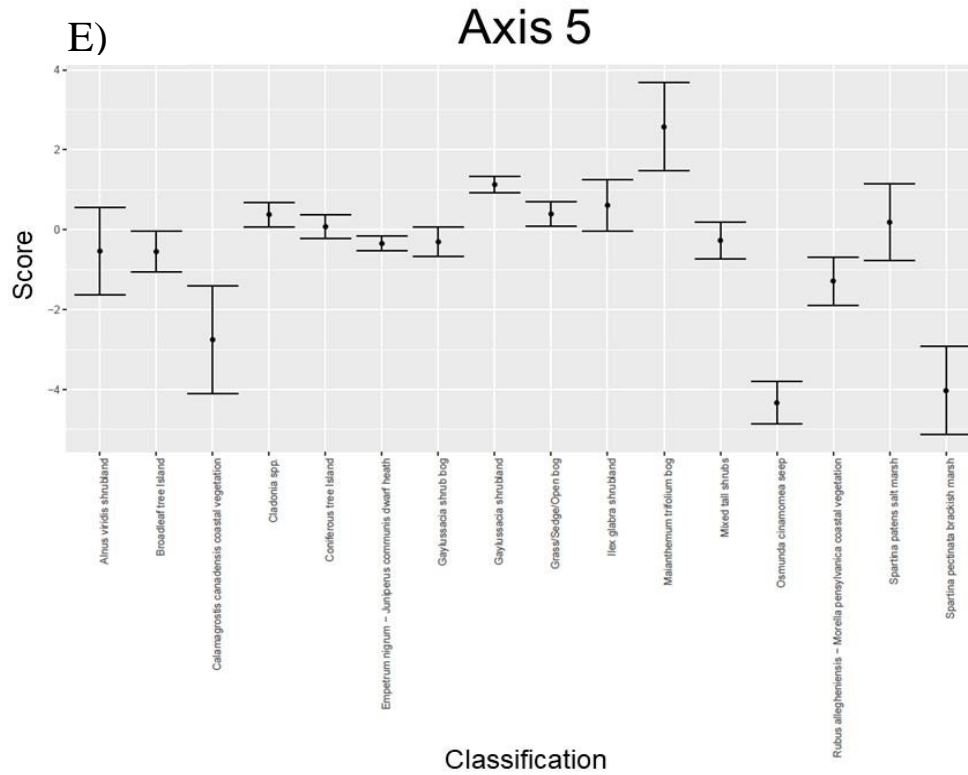
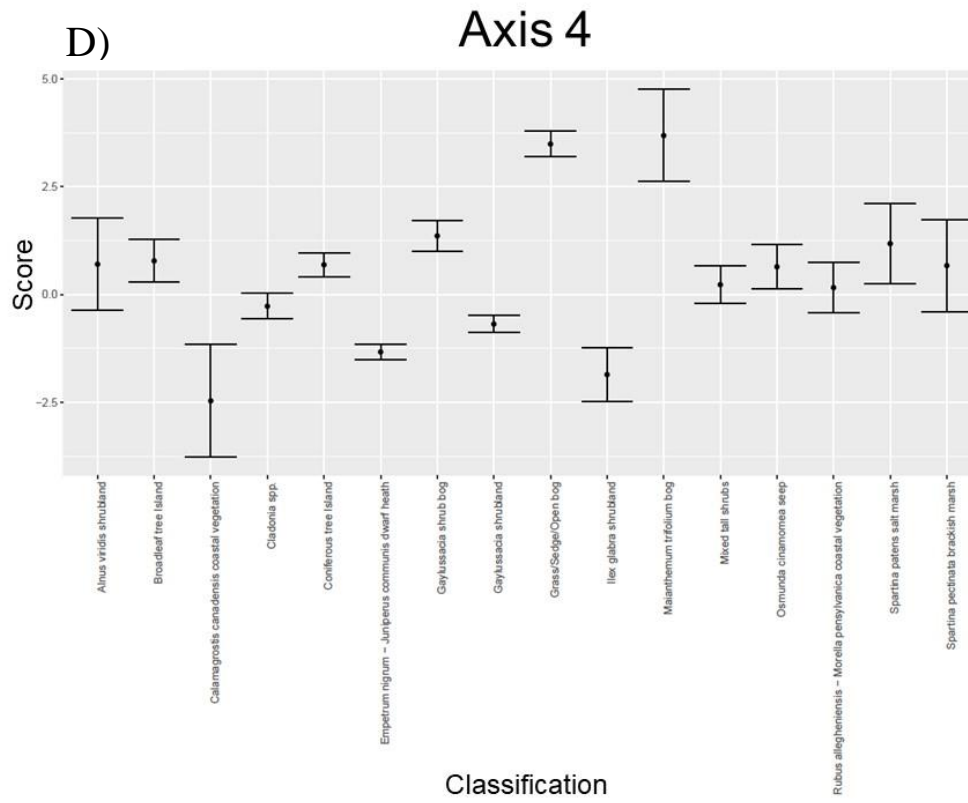


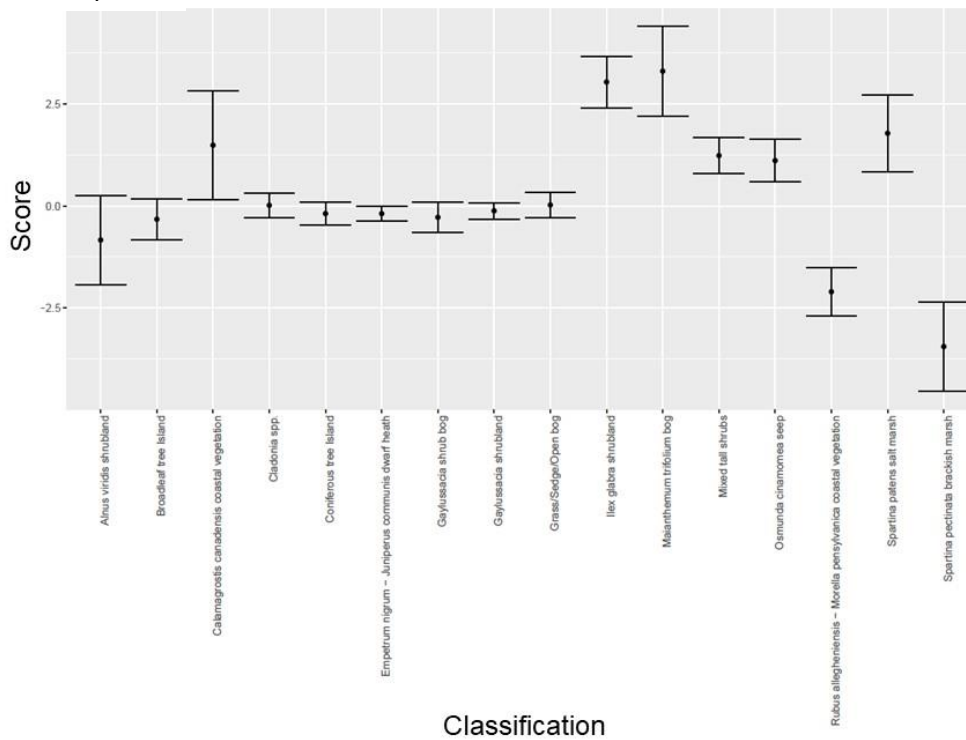
Figure A1.2. 95% confidence intervals for the mean linear discriminant analysis (LDA) scores of plant communities from the broadened association level classification for each discriminatory axis.



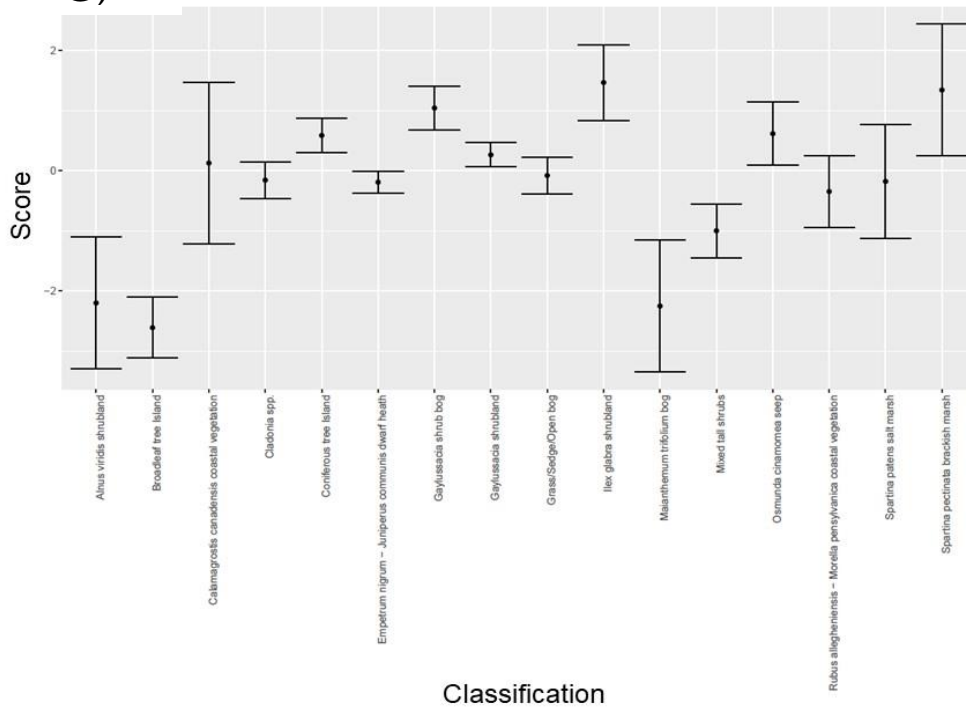


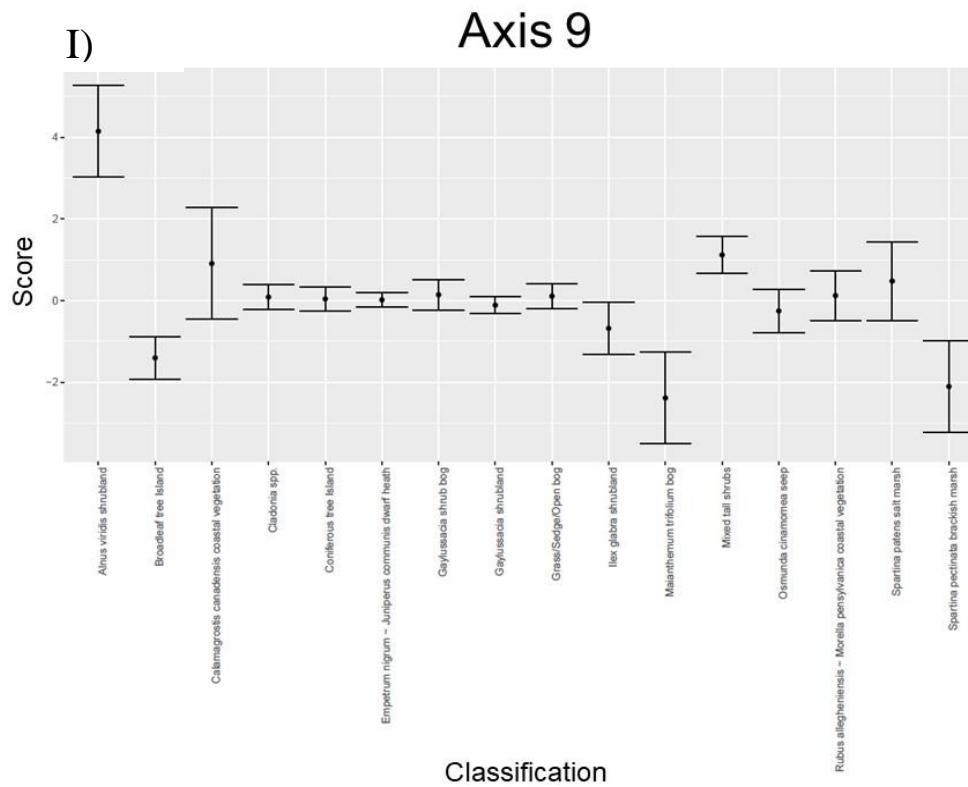
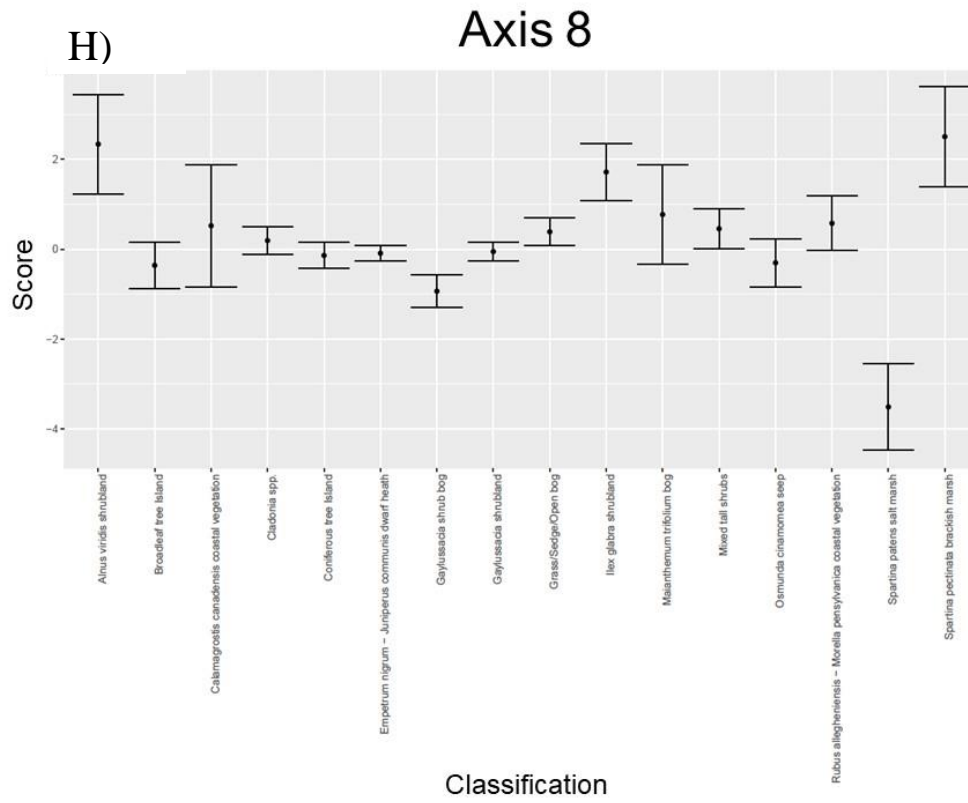


### F) Axis 6

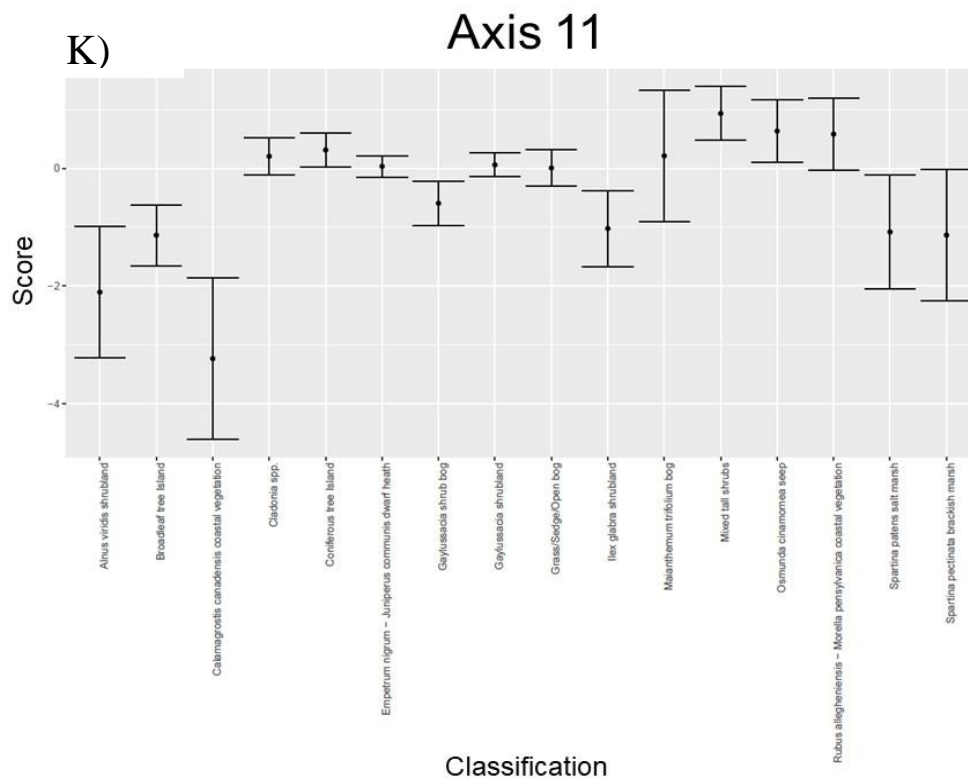
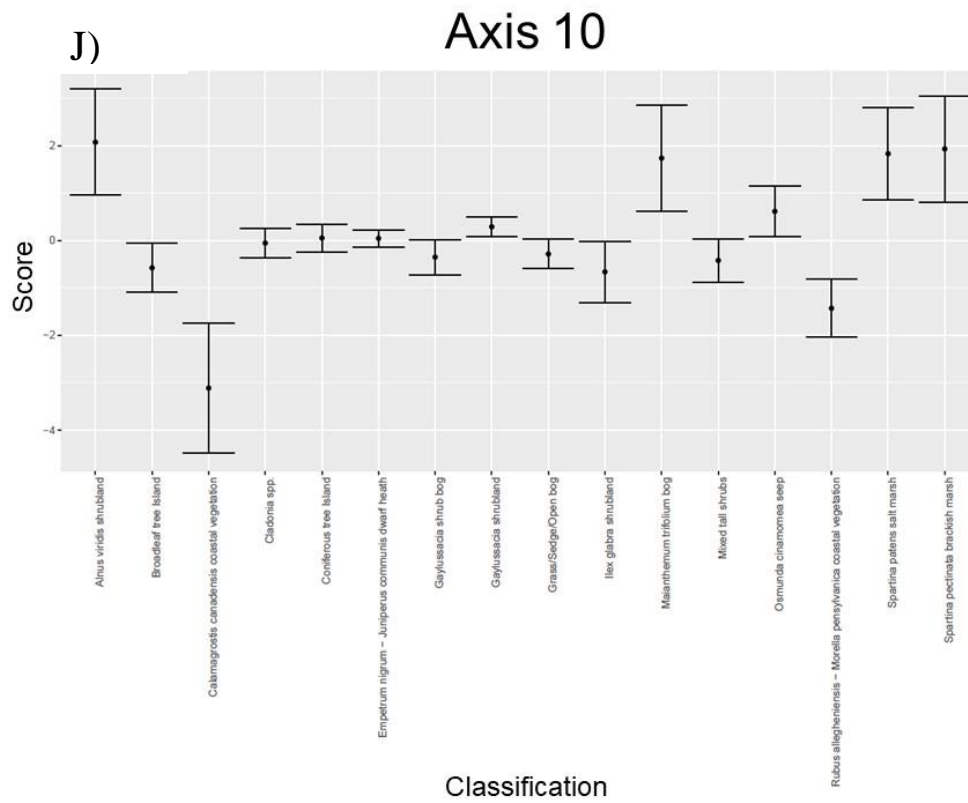


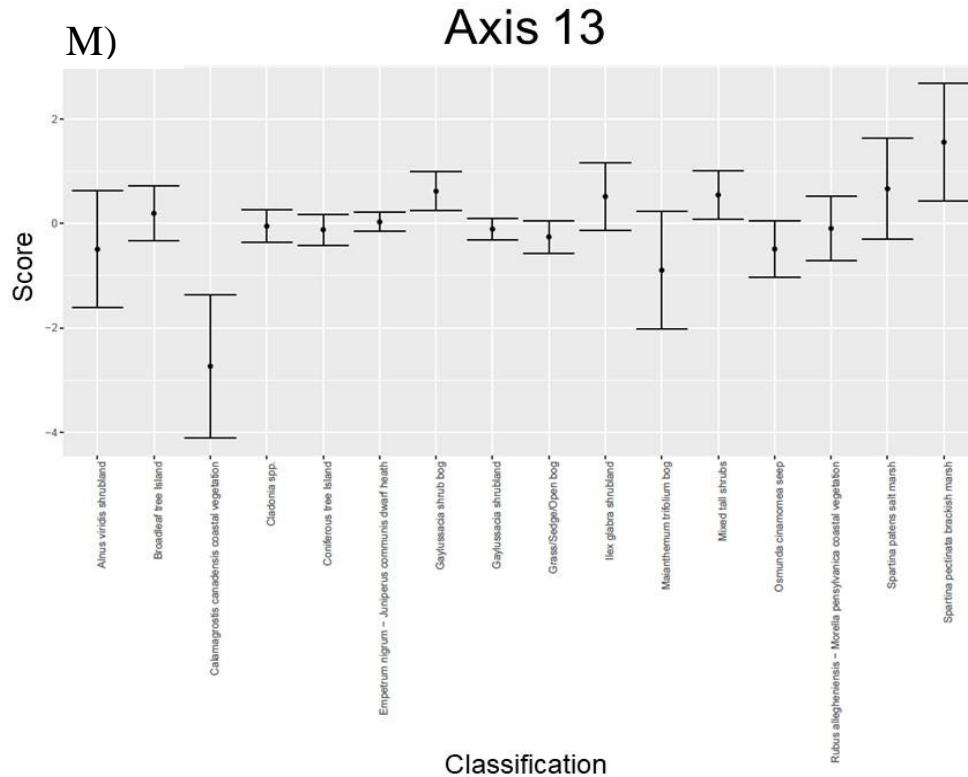
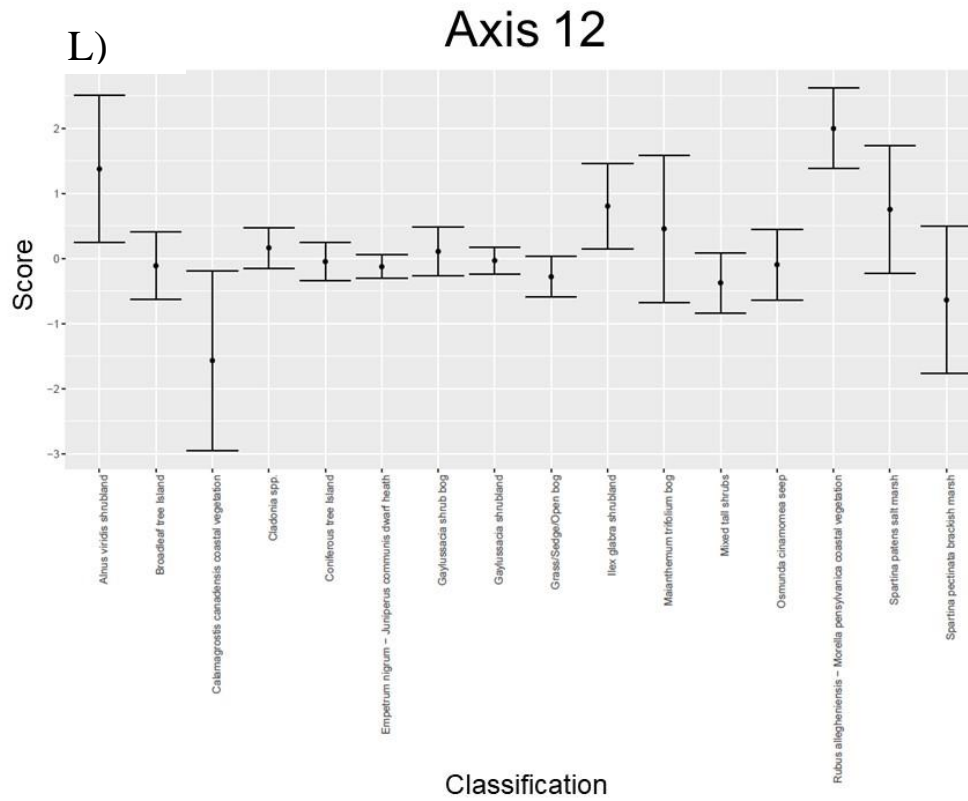
### G) Axis 7











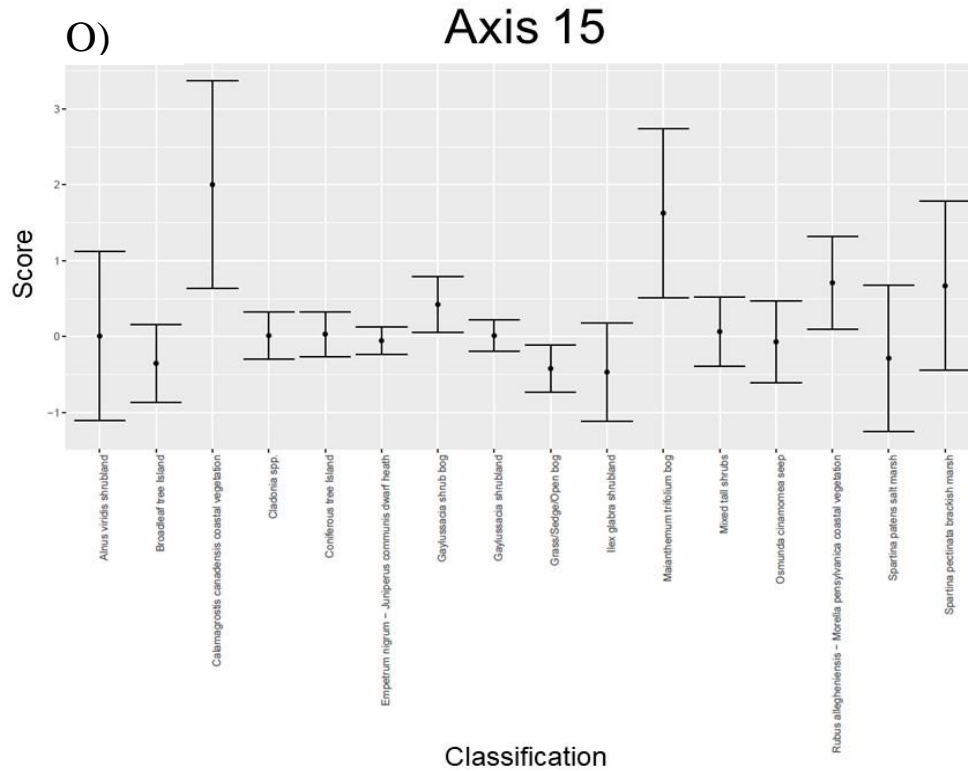
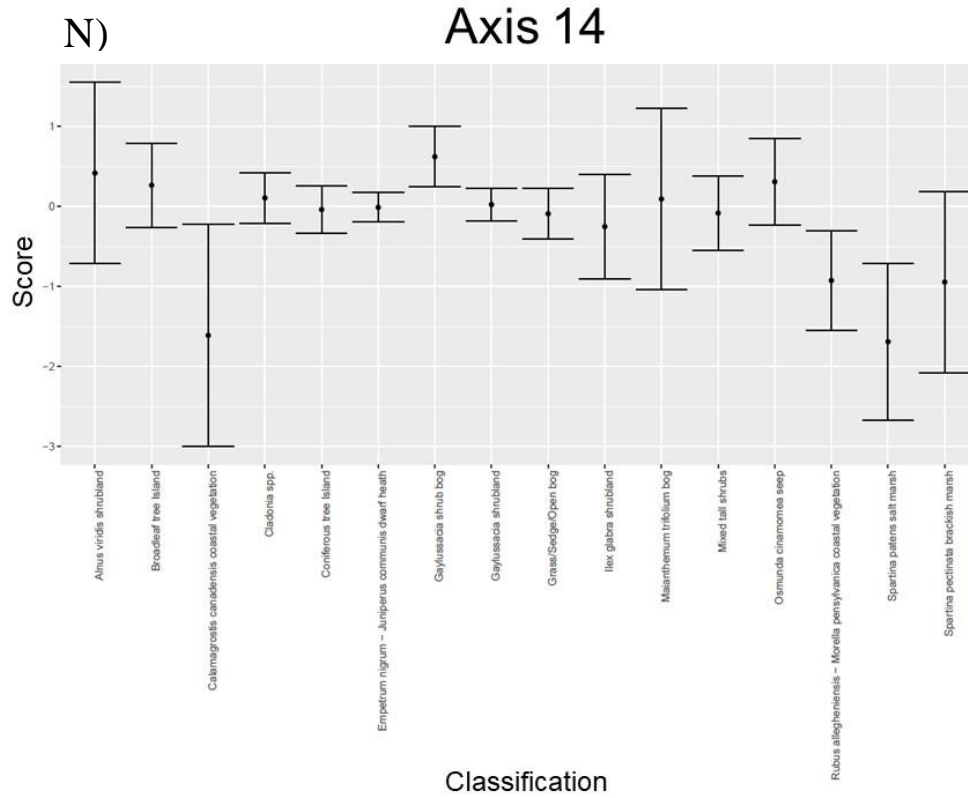
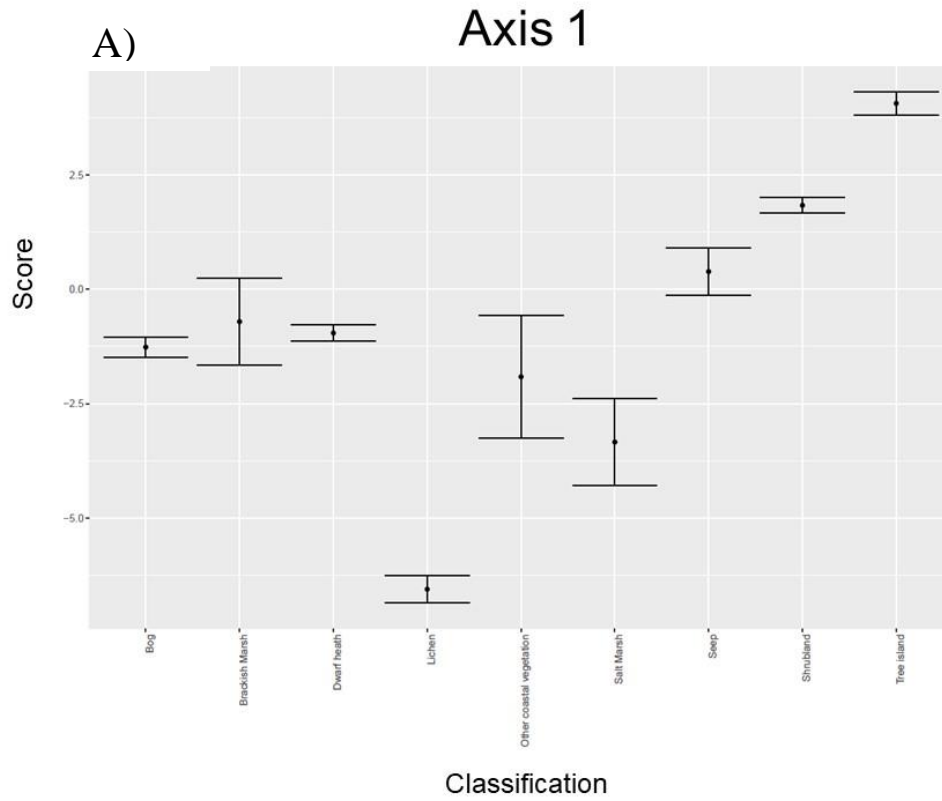
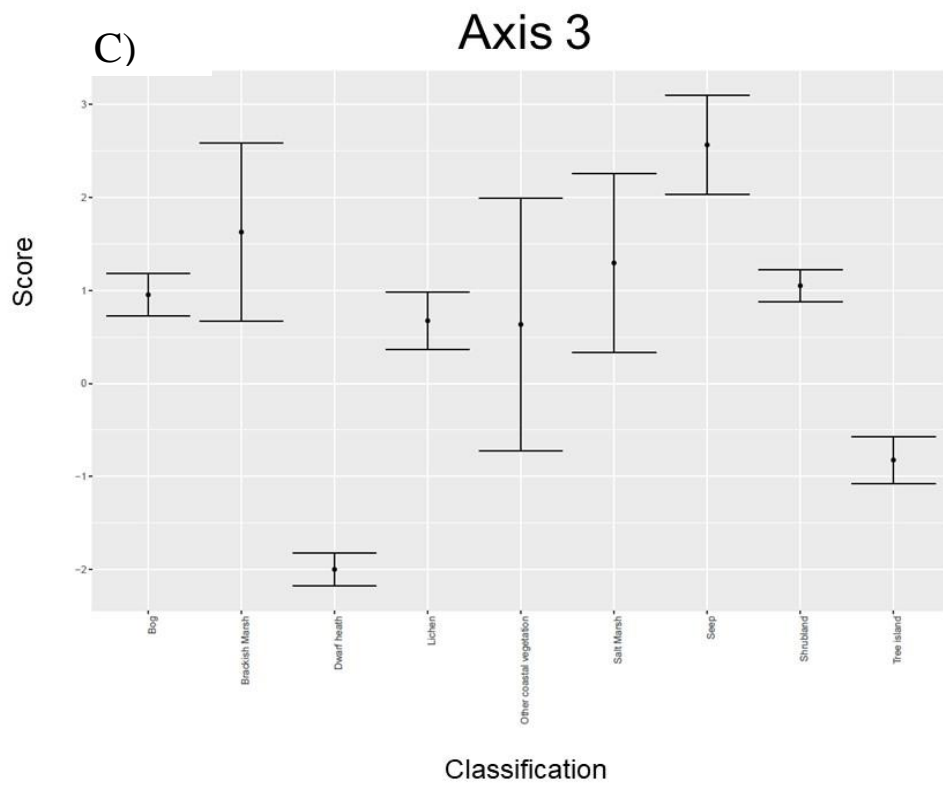
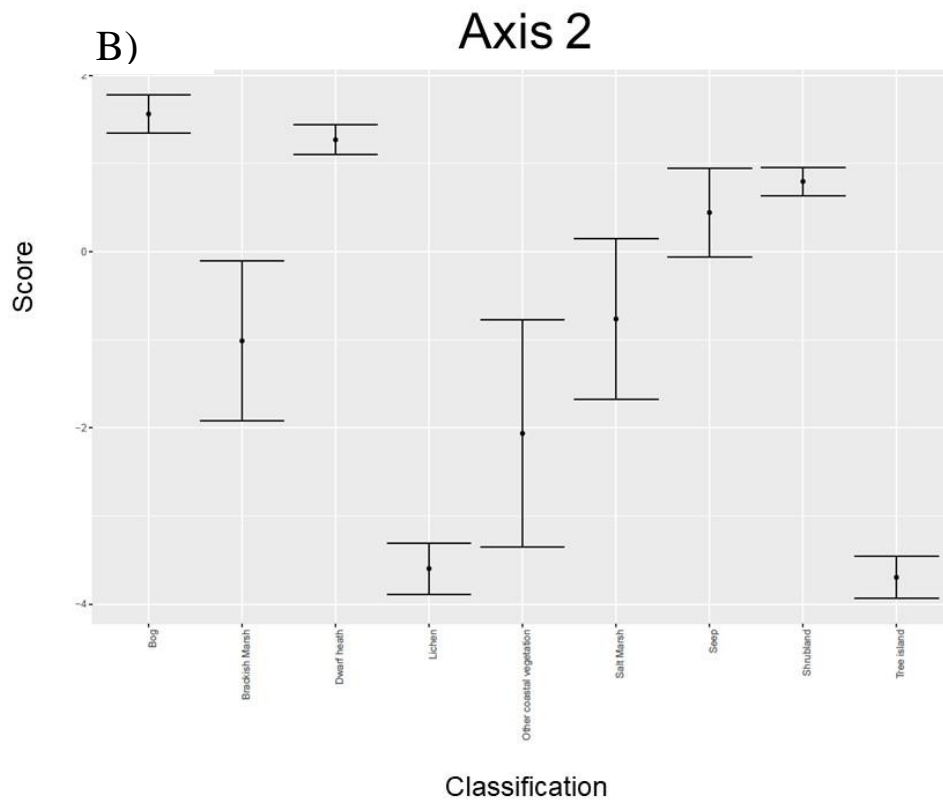
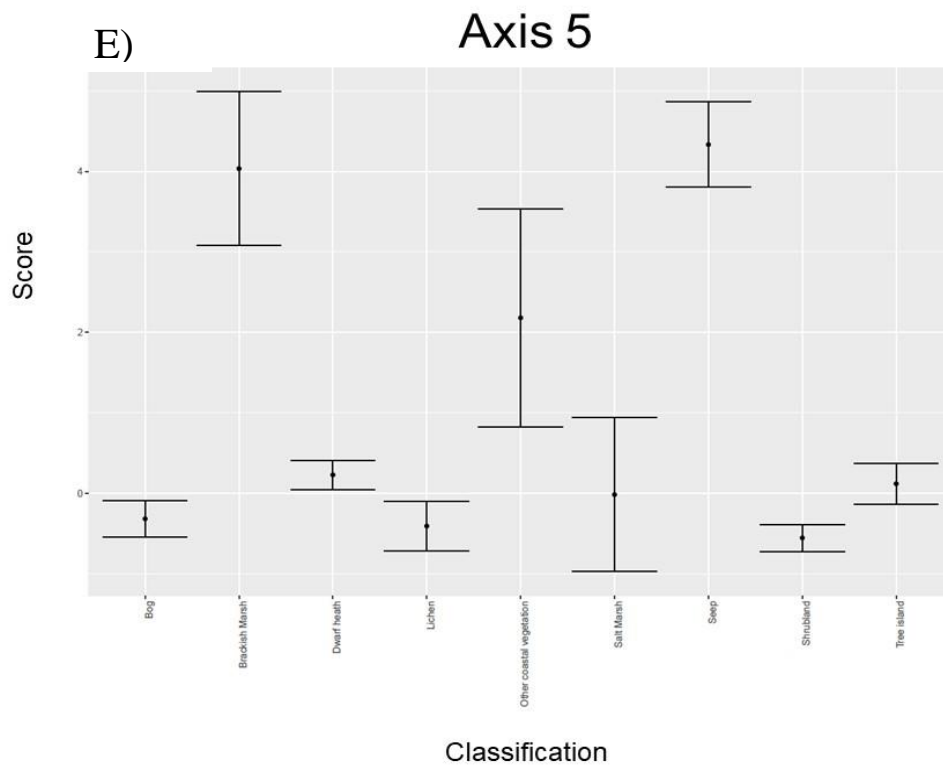
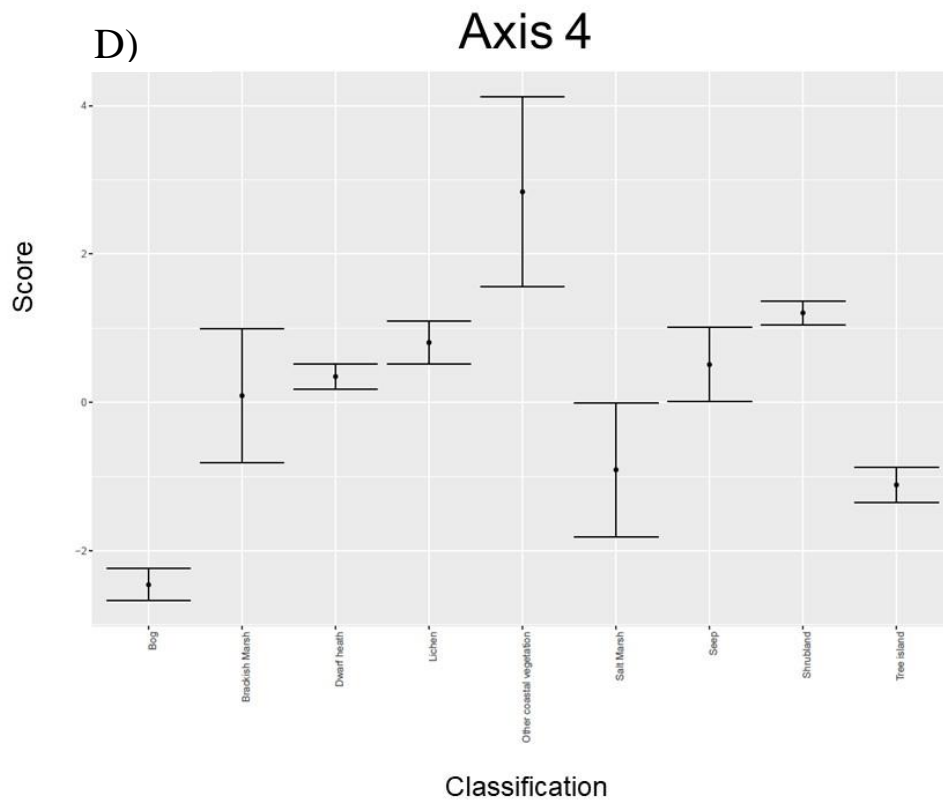


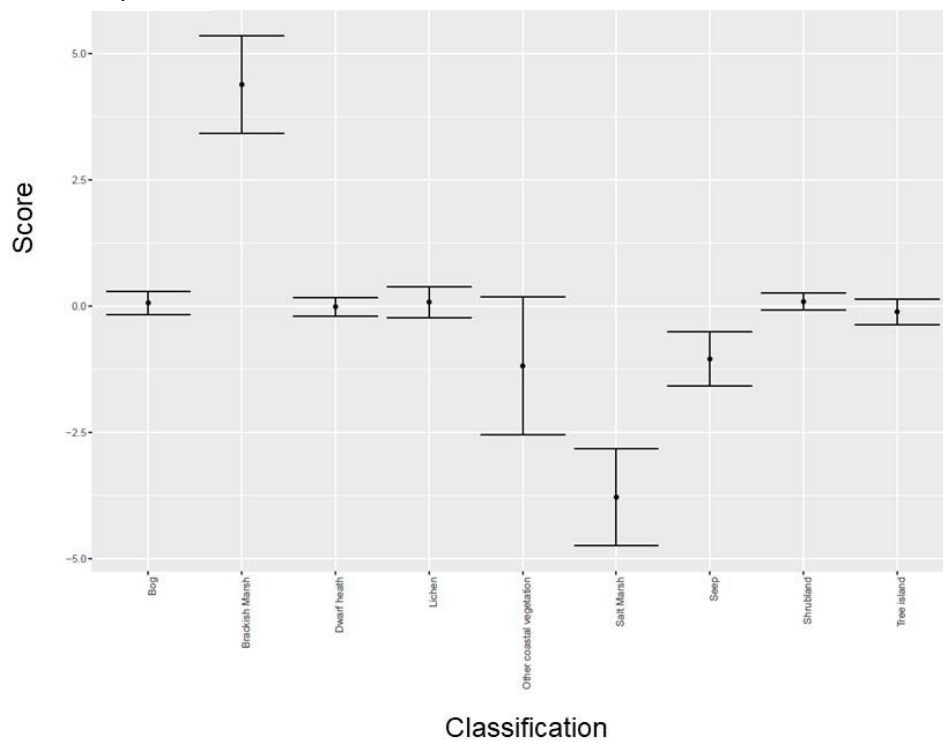
Figure A1.3. 95% confidence intervals for the mean linear discriminant analysis (LDA) scores of plant communities from the formation class classification for each discriminatory axis.



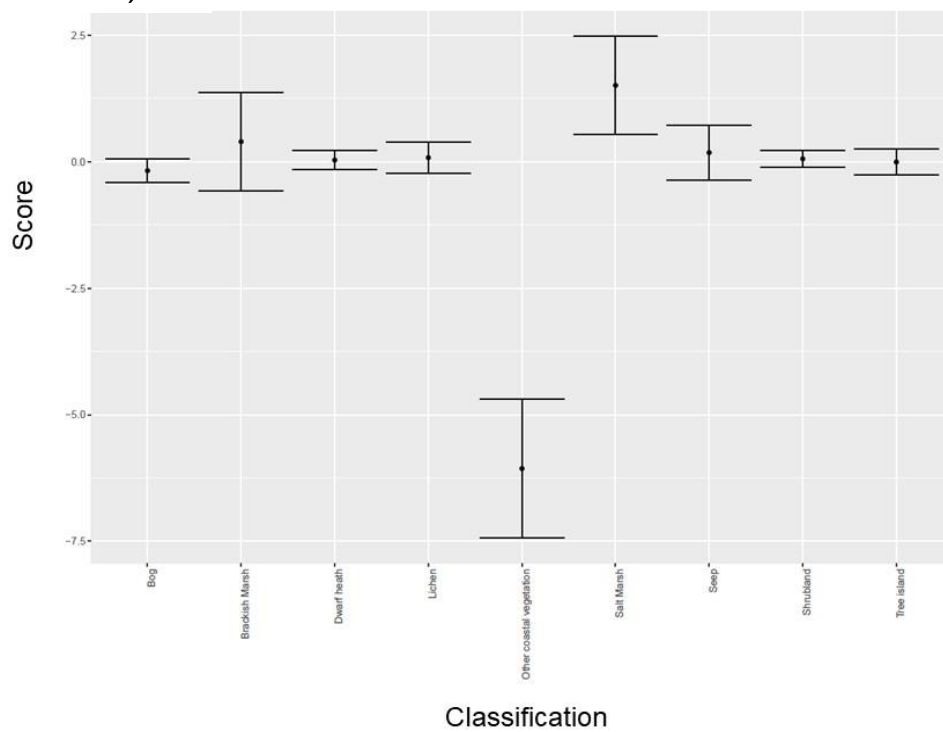




F) Axis 6

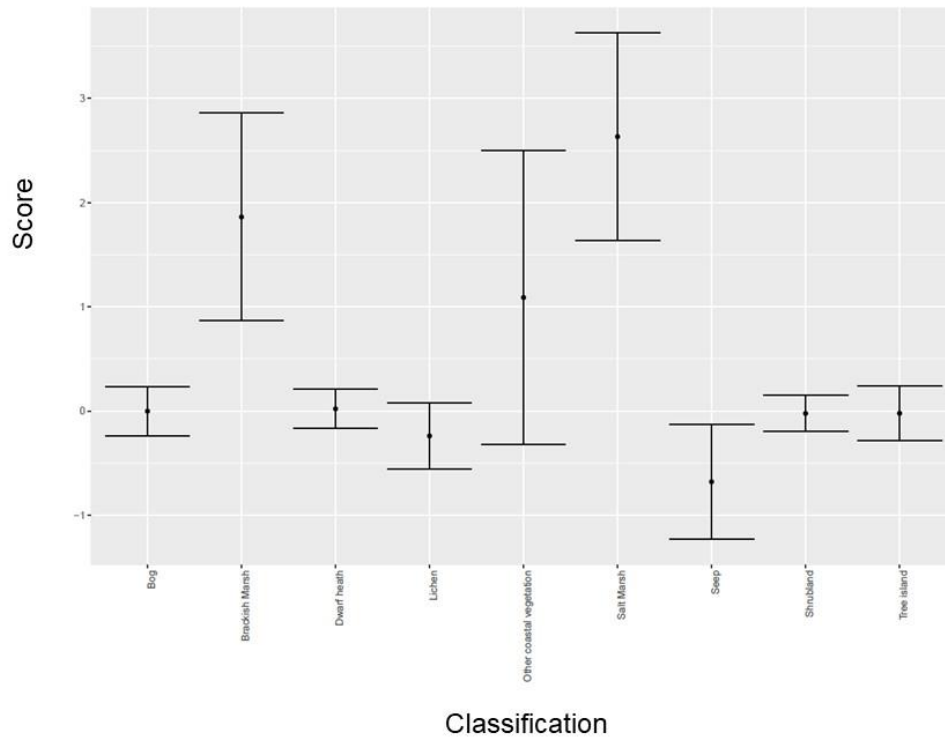


G) Axis 7



H)

Axis 8





# **Appendix II**

## Tables

Table A2.1. List of spectral and structural indices derived from UAV imagery and the 3D point cloud to classify plant communities.

Index	Description
<b>R May</b>	Red channel in May
<b>G May</b>	Green channel in May
<b>B May</b>	Blue channel in May
<b>R/B May</b>	Red channel divided by Blue channel in May
<b>R/G May</b>	Red channel divided by Green channel in May
<b>G/B May</b>	Green channel divided by Blue channel in May
<b>NIR May</b>	Near-Infrared in May
<b>NDVI May</b>	NDVI in May. $NDVI = \frac{NIR-R}{NIR+R}$
<b>CIVE May</b>	Color Index of Vegetation (CIVE) in May. $CIVE = 0.441 * R - 0.881 * G + 0.385 * B + 18.78745$
<b>Hue May</b>	Hue in degrees (0-360°) in May. $Hue = \cos^{-1} \frac{(0.5*(R-G)+(R-B))}{(((R-G)^2+(R-B)(G-B))^{0.5})}$
<b>Saturation May</b>	Saturation in May. $Saturation = 1 - \left(\frac{R+G+B}{3}\right) * a$
<b>R August</b>	Red channel in August
<b>G August</b>	Green channel in August
<b>B August</b>	Blue channel in August
<b>R/B August</b>	Red channel divided by Blue channel in August
<b>R/G August</b>	Red channel divided by Green channel in August
<b>G/B August</b>	Green channel divided by Blue channel in August
<b>NIR August</b>	Near-Infrared in August
<b>NDVI August</b>	NDVI in August. $NDVI = \frac{NIR-R}{NIR+R}$
<b>CIVE August</b>	Color Index of Vegetation (CIVE) in August. $CIVE = 0.441 * R - 0.881 * G + 0.385 * B + 18.78745$
<b>Hue August</b>	Hue in degrees (0-360°) in August. $Hue = \cos^{-1} \frac{(0.5*(R-G)+(R-B))}{(((R-G)^2+(R-B)(G-B))^{0.5})}$
<b>Saturation August</b>	Saturation in August. $Saturation = 1 - \left(\frac{R+G+B}{3}\right) * a$
<b>Change R</b>	Change in Red channel from May to August
<b>Change G</b>	Change in Green channel from May to August
<b>Change B</b>	Change in Blue channel from May to August
<b>Change R/B</b>	Change in Red channel divided by Blue channel from May to August
<b>Change R/G</b>	Change in Red channel divided by Green channel from May to August
<b>Change G/B</b>	Change in Green channel divided by Blue channel from May to August
<b>Change NIR</b>	Change in Near-Infrared from May to August

(continued) Table A2.1. List of spectral and structural indices derived from UAV imagery and the 3D point cloud to classify plant communities.

<b>Index</b>	<b>Description</b>
<b>Change NDVI</b>	Change in NDVI from May to August. $NDVI = \frac{NIR-R}{NIR+R}$
<b>Change CIVE</b>	Change in Color Index of Vegetation (CIVE) from May to August. $CIVE = 0.441 * R - 0.881 * G + 0.385 * B + 18.78745$
<b>Change Hue</b>	Change in Hue in degrees (0-360°) from May to August. $Hue = \cos^{-1} \frac{(0.5*(R-G)+(R-B))}{(((R-G)^2+(R-B)(G-B))^{0.5})}$
<b>Change Saturation</b>	Change in Saturation from May to August. Saturation = $1 - \left(\frac{R+G+B}{3}\right) * a$
<b>Vegetation Height</b>	Vegetation height in August. Vegetation height was calculated by subtracting the minimum from the maximum elevation value within a 50-cm search radius of each pixel using the 10-cm elevation model
<b>TPI 5</b>	Topographic Position Index (TPI) in August. TPI was calculated from the 10-cm elevation model using a 5x5 pixel search window. $TPI = z_o - \bar{z}$ Where $z_o$ = elevation of central point, $\bar{z}$ = mean elevation of neighborhood
<b>TPI 11</b>	Topographic Position Index (TPI) in August. TPI was calculated from the 10-cm elevation model using an 11x11 pixel search window. $TPI = z_o - \bar{z}$ Where $z_o$ = elevation of central point, $\bar{z}$ = mean elevation of neighborhood
<b>TPI 33</b>	Topographic Position Index (TPI) in August. TPI was calculated from the 10-cm elevation model using a 33x33 pixel search window. $TPI = z_o - \bar{z}$ Where $z_o$ = elevation of central point, $\bar{z}$ = mean elevation of neighborhood
<b>TPI 111</b>	Topographic Position Index (TPI) in August. TPI was calculated from the 10-cm elevation model using a 111x111 pixel search window. $TPI = z_o - \bar{z}$ Where $z_o$ = elevation of central point, $\bar{z}$ = mean elevation of neighborhood

(continued) Table A2.1. List of spectral and structural indices derived from UAV imagery and the 3D point cloud to classify plant communities.

<b>Index</b>	<b>Description</b>
<b>DEV 5</b>	Deviation of Mean Elevation (DEV) in August. DEV was calculated from the 10-cm elevation model using a 5x5 pixel search window. $DEV = \frac{z_o - \bar{z}}{SD}$ Where $z_o$ = elevation of central point, $\bar{z}$ = mean elevation of neighborhood, and SD = standard deviation of elevation values in the neighborhood
<b>DEV 11</b>	Deviation of Mean Elevation (DEV) in August. DEV was calculated from the 10-cm elevation model using an 11x11 pixel search window. $DEV = \frac{z_o - \bar{z}}{SD}$ Where $z_o$ = elevation of central point, $\bar{z}$ = mean elevation of neighborhood, and SD = standard deviation of elevation values in the neighborhood
<b>DEV 33</b>	Deviation of Mean Elevation (DEV) in August. DEV was calculated from the 10-cm elevation model using a 33x33 pixel search window. $DEV = \frac{z_o - \bar{z}}{SD}$ Where $z_o$ = elevation of central point, $\bar{z}$ = mean elevation of neighborhood, and SD = standard deviation of elevation values in the neighborhood
<b>DEV 111</b>	Deviation of Mean Elevation (DEV) in August. DEV was calculated from the 10-cm elevation model using a 111x111 pixel search window. $DEV = \frac{z_o - \bar{z}}{SD}$ Where $z_o$ = elevation of central point, $\bar{z}$ = mean elevation of neighborhood, and SD = standard deviation of elevation values in the neighborhood
<b>Curvature</b>	Curvature Index (concavity/convexity) in August. Curvature Index was calculated from the 10-cm elevation model using the Curvature tool with the <i>Profile</i> setting within the DEM Surface Tools toolbox in ArcGIS. ( <a href="http://www.jennessent.com/arcgis/surface_area.htm">http://www.jennessent.com/arcgis/surface_area.htm</a> )
<b>Slope</b>	Slope in degrees (0-90°) in August. Slope was calculated from the 10-cm elevation model using the Slope (Spatial Analyst) tool in ArcGIS.

Table A2.2. Confusion matrix of plant communities from the broadened association level classification at Chebucto Head.

	Broadleaf tree island	<i>Calamagrostis canadensis</i> coastal vegetation	<i>Calystegia sepium</i> coastal lithomorphic	<i>Cladonia</i> spp.	Coniferous tree island	<i>Empetrum nigrum</i> - <i>Juniperus communis</i> dwarf heath	<i>Gaylussacia baccata</i> shrubland	<i>Gaylussacia</i> shrub bog	<i>Juniperus communis</i> - <i>Corema conradii</i> lithomorphic	Mixed tall shrubs	Open bog	<i>Osmunda cinnamomea</i> seep
Broadleaf tree island	22	0	0	0	1	0	3	0	0	14	0	0
<i>Calamagrostis canadensis</i> coastal vegetation	0	8	0	2	0	0	0	0	0	0	0	0
<i>Calystegia sepium</i> coastal lithomorphic	0	0	10	0	0	0	0	0	0	0	0	0
<i>Cladonia</i> spp.	0	0	0	90	0	0	0	0	0	0	0	0
Coniferous tree island	1	0	0	2	93	0	1	0	3	0	0	0
<i>Empetrum nigrum</i> - <i>Juniperus communis</i> dwarf heath	0	0	0	0	0	89	0	2	8	0	0	0
<i>Gaylussacia baccata</i> shrubland	3	0	0	0	0	0	138	4	0	15	0	0
<i>Gaylussacia</i> shrub bog	0	0	0	0	0	4	3	52	0	0	1	0
<i>Juniperus communis</i> - <i>Corema conradii</i> lithomorphic	0	0	0	2	0	6	4	6	122	0	0	0
Mixed tall shrubs	7	0	0	0	0	0	11	0	0	22	0	0
Open bog	0	0	0	0	0	0	0	1	0	0	29	0
<i>Osmunda cinnamomea</i> seep	1	0	0	0	0	0	3	0	0	2	0	34

Table A2.3. Confusion matrix of plant communities from the broadened association level classification at Prospect Bay.

	<i>Alnus viridis</i> shrubland	<i>Betula papyrifera</i> tree island	<i>Cladonia</i> spp.	Coniferous tree island	<i>Empetrum nigrum</i> - <i>Juniperus communis</i> dwarf heath	<i>Eriophorum russeolum</i> bog	<i>Festuca rubra</i> - <i>Solidago sempervirens</i> - <i>Trifolium repens</i> disturbed coastal vegetation	<i>Gaylussacia baccata</i> shrubland	<i>Gaylussacia</i> shrub bog	Grass/Sedge/Open bog	<i>Juncus balticus</i> brackish marsh	<i>Juniperus horizontalis</i> dwarf heath	<i>Lonicera villosa</i> shrubland	<i>Maianthemum trifolium</i> bog	Mixed tall shrubs	<i>Morella pensylvanica</i> shrubland	<i>Osmunda cinnamomea</i> seep	<i>Spartina pectinata</i> brackish marsh	<i>Toxicodendron radicans</i> coastal vegetation
<i>Alnus viridis</i> shrubland	14	0	0	0	1	0	0	4	0	0	0	0	0	0	0	0	1	0	0
<i>Betula papyrifera</i> tree island	0	9	0	0	0	0	0	0	0	0	0	0	0	0	1	0	0	0	0
<i>Cladonia</i> spp.	0	0	58	0	0	0	0	0	0	0	0	0	0	0	0	0	0	0	0
Coniferous tree island	0	0	0	50	0	0	0	0	0	0	0	0	0	0	0	0	0	0	0
<i>Empetrum nigrum</i> - <i>Juniperus communis</i> dwarf heath	0	0	0	0	277	0	0	0	0	12	4	1	0	0	3	3	0	0	0
<i>Eriophorum russeolum</i> bog	0	0	0	0	0	10	0	0	0	0	0	0	0	0	0	0	0	0	0
<i>Festuca rubra</i> - <i>Solidago sempervirens</i> - <i>Trifolium repens</i> disturbed coastal vegetation	0	0	0	0	0	0	20	0	0	0	0	0	0	0	0	0	0	0	0
<i>Gaylussacia baccata</i> shrubland	4	0	0	0	0	0	0	63	1	0	0	0	0	0	4	0	8	0	0
<i>Gaylussacia</i> shrub bog	0	0	0	0	0	0	0	5	17	8	0	0	0	0	0	0	0	0	0
Grass/Sedge/Open bog	0	0	0	0	3	12	0	0	0	127	2	0	1	5	0	0	0	0	0
<i>Juncus balticus</i> brackish marsh	0	0	0	0	1	0	0	0	0	9	20	0	0	0	0	0	0	0	0
<i>Juniperus horizontalis</i> dwarf heath	0	0	1	0	9	0	0	0	0	0	0	10	0	0	0	0	0	0	0
<i>Lonicera villosa</i> shrubland	0	0	0	0	0	0	0	0	0	0	0	0	10	0	0	0	0	0	0
<i>Maianthemum trifolium</i> bog	0	0	0	0	0	0	0	0	0	0	0	0	0	20	0	0	0	0	0
Mixed tall shrubs	0	0	0	0	3	0	0	5	1	0	0	0	0	0	21	0	0	0	0
<i>Morella pensylvanica</i> shrubland	0	0	0	0	2	0	0	0	0	0	0	0	0	0	0	7	1	0	0
<i>Osmunda cinnamomea</i> seep	1	0	0	0	0	0	0	7	0	0	0	0	0	0	3	2	47	0	0
<i>Spartina pectinata</i> brackish marsh	0	0	0	0	0	0	0	0	0	0	5	0	0	0	0	0	0	22	3
<i>Toxicodendron radicans</i> coastal vegetation	0	0	0	0	0	0	0	0	0	0	0	0	0	0	0	0	0	2	8

Table A2.4. Confusion matrix of plant communities from the broadened association level classification at Polly's Cove.

	Broadleaf tree island	<i>Calamagrostis canadensis</i> coastal vegetation	<i>Carex nigra</i> - <i>Festuca rubra</i> coastal vegetation	<i>Carex nigra</i> bog	<i>Carex vesicaria</i> bog	<i>Cladonia</i> spp.	Coniferous tree island	<i>Empetrum nigrum</i> - <i>Juniperus communis</i> dwarf heath	<i>Gaylussacia baccata</i> shrubland	<i>Gaylussacia</i> shrub bog	<i>Ilex glabra</i> shrubland	<i>Juncus balticus</i> brackish marsh	<i>Juniperus communis</i> - <i>Corema conradii</i> lithomorphic	<i>Juniperus horizontalis</i> dwarf heath	Mixed tall shrubs	<i>Osmunda cinnamomea</i> seep	<i>Rubus allegheniensis</i> - <i>Morella pensylvanica</i> coastal vegetation	<i>Spartina patens</i> salt marsh	<i>Thalictrum pubescens</i> coastal vegetation	<i>Trichophorum caespitosum</i> bog
Broadleaf tree island	16	0	0	0	0	0	0	0	9	0	0	0	0	0	5	0	0	0	0	0
<i>Calamagrostis canadensis</i> coastal vegetation	0	4	0	3	0	0	0	0	1	2	0	0	0	0	0	0	0	0	0	0
<i>Carex nigra</i> - <i>Festuca rubra</i> coastal vegetation	0	0	10	0	0	0	0	0	0	0	0	0	0	0	0	0	0	0	0	0
<i>Carex nigra</i> bog	0	0	0	10	0	0	0	0	0	0	0	0	0	0	0	0	0	0	0	0
<i>Carex vesicaria</i> bog	0	0	0	0	10	0	0	0	0	0	0	0	0	0	0	0	0	0	0	0
<i>Cladonia</i> spp.	0	0	0	0	0	100	0	0	0	0	0	0	0	0	0	0	0	0	0	0
Coniferous tree island	1	0	0	0	0	0	98	0	3	0	1	0	3	0	3	0	0	0	0	0
<i>Empetrum nigrum</i> - <i>Juniperus communis</i> dwarf heath	0	0	0	0	0	0	0	11	0	0	1	0	8	0	0	0	0	0	0	0
<i>Gaylussacia baccata</i> shrubland	0	0	0	0	0	0	0	0	114	6	4	0	2	0	11	0	3	0	0	0
<i>Gaylussacia</i> shrub bog	0	0	0	0	0	0	0	0	11	39	0	0	3	0	0	0	0	7	0	10
<i>Ilex glabra</i> shrubland	0	0	0	0	0	0	0	0	6	0	54	0	0	0	0	0	0	0	0	0
<i>Juncus balticus</i> brackish marsh	0	0	0	0	0	0	0	0	0	1	0	6	2	0	0	0	1	0	0	0
<i>Juniperus communis</i> - <i>Corema conradii</i> lithomorphic	0	0	0	0	0	0	1	7	0	9	2	0	111	0	0	0	0	0	0	0
<i>Juniperus horizontalis</i> dwarf heath	0	0	0	0	0	0	0	6	0	0	0	0	2	12	0	0	0	0	0	0
Mixed tall shrubs	2	0	0	0	0	0	0	0	20	0	3	0	0	0	5	0	0	0	0	0
<i>Osmunda cinnamomea</i> seep	0	0	0	0	0	0	0	0	0	0	0	0	0	0	0	39	1	0	0	0
<i>Rubus allegheniensis</i> - <i>Morella pensylvanica</i> coastal vegetation	0	0	0	0	0	0	0	0	6	0	0	0	3	0	5	3	3	0	0	0
<i>Spartina patens</i> salt marsh	0	0	0	0	0	0	0	0	0	0	0	0	0	0	0	0	0	20	0	0
<i>Thalictrum pubescens</i> coastal vegetation	0	0	0	0	0	0	0	0	0	0	0	0	0	0	0	0	0	0	10	0
<i>Trichophorum caespitosum</i> bog	0	0	0	0	0	0	0	0	0	13	0	0	2	0	0	0	0	3	0	22

## Figures

Figure A2.1. Elevation above sea-level at A) Chebucto Head, B) Prospect Bay, and C) Polly's Cove.

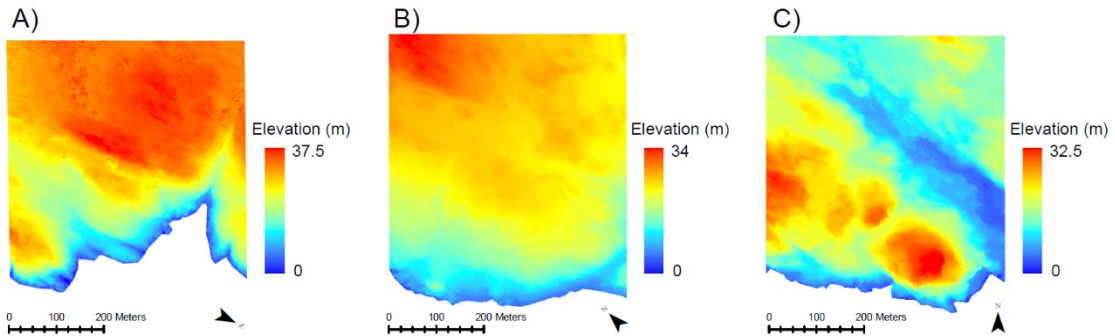


Figure A2.2. Distance from the coastline at A) Chebucto Head, B) Prospect Bay, and C) Polly's Cove.

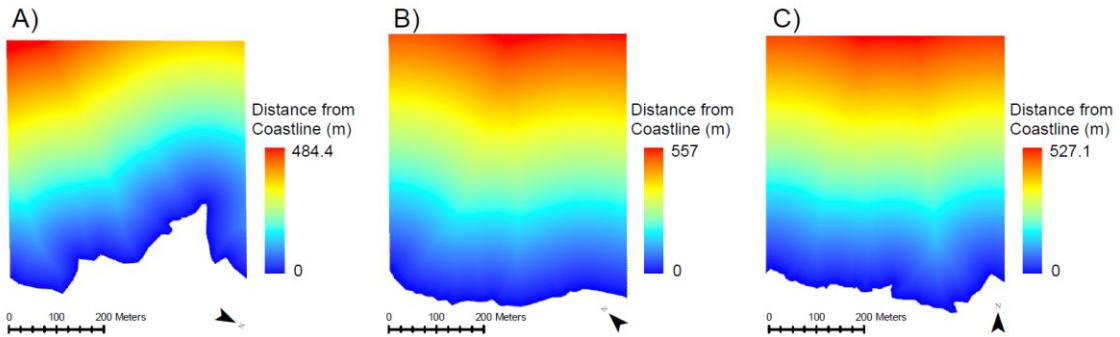


Figure A2.3. Wind exposure at A) Chebucto Head, B) Prospect Bay, and C) Polly's Cove.

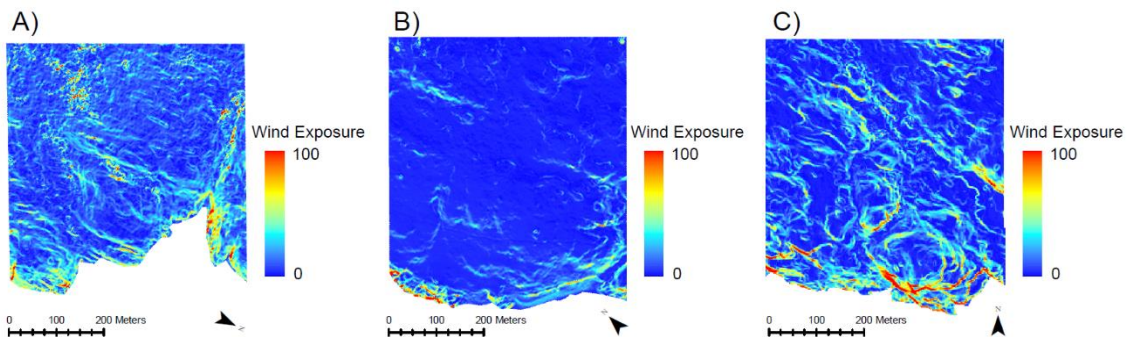




Figure A2.4. Stream orders of stream networks at A) Chebucto Head, B) Prospect Bay, and C) Polly's Cove.

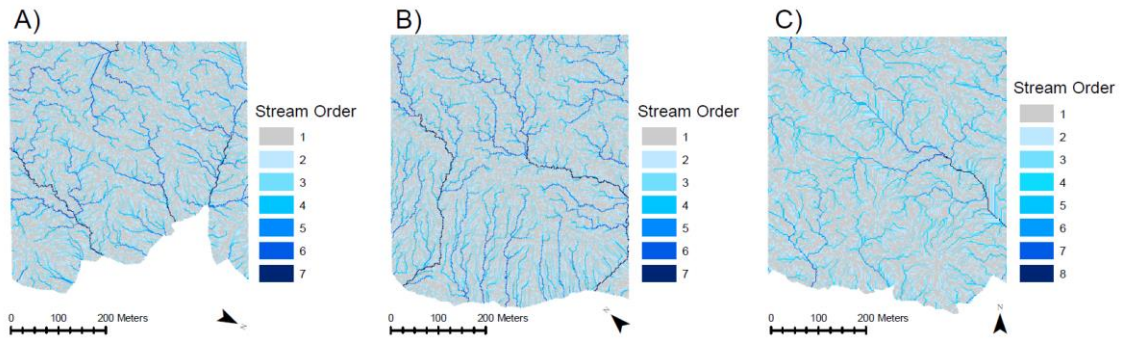


Figure A2.5. Incoming solar radiation at A) Chebucto Head, B) Prospect Bay, and C) Polly's Cove.

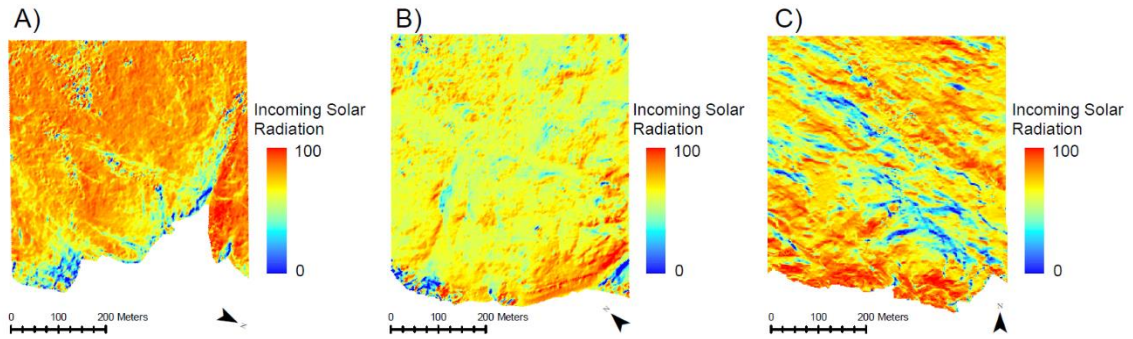


Figure A2.6. Slope positions at A) Chebucto Head, B) Prospect Bay, and C) Polly's Cove.

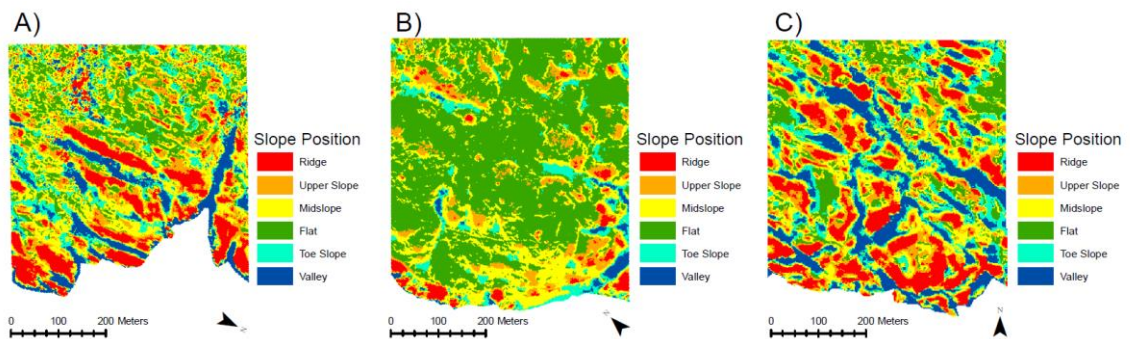


Figure A2.7. Local surface ruggedness at A) Chebucto Head, B) Prospect Bay, and C) Polly's Cove.

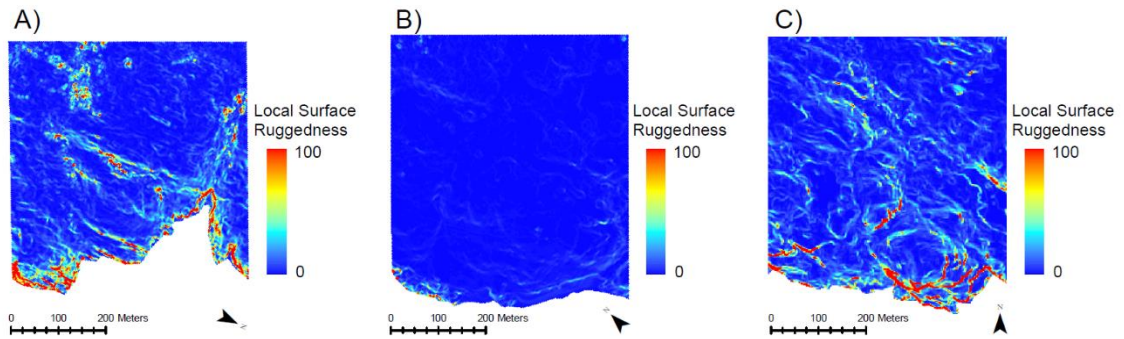


Figure A2.8. Global surface ruggedness at A) Chebucto Head, B) Prospect Bay, and C) Polly's Cove.

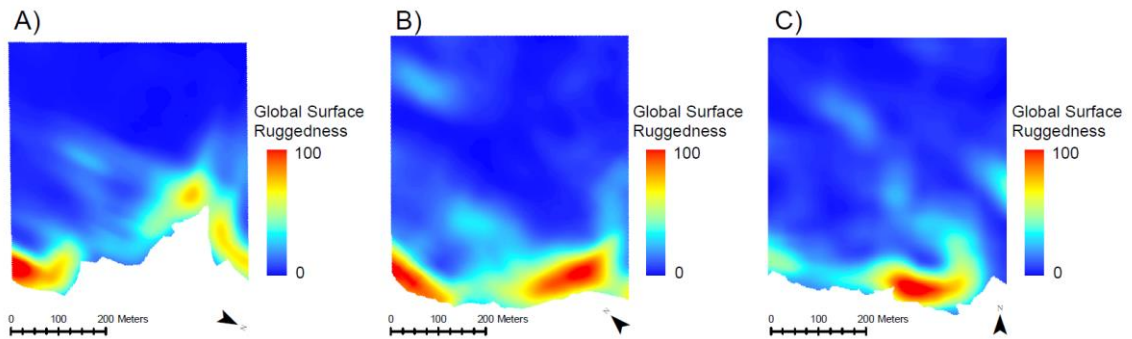


Figure A2.9. 95% confidence intervals for the area-weighted mean elevation of plant communities at Chebucto Head.

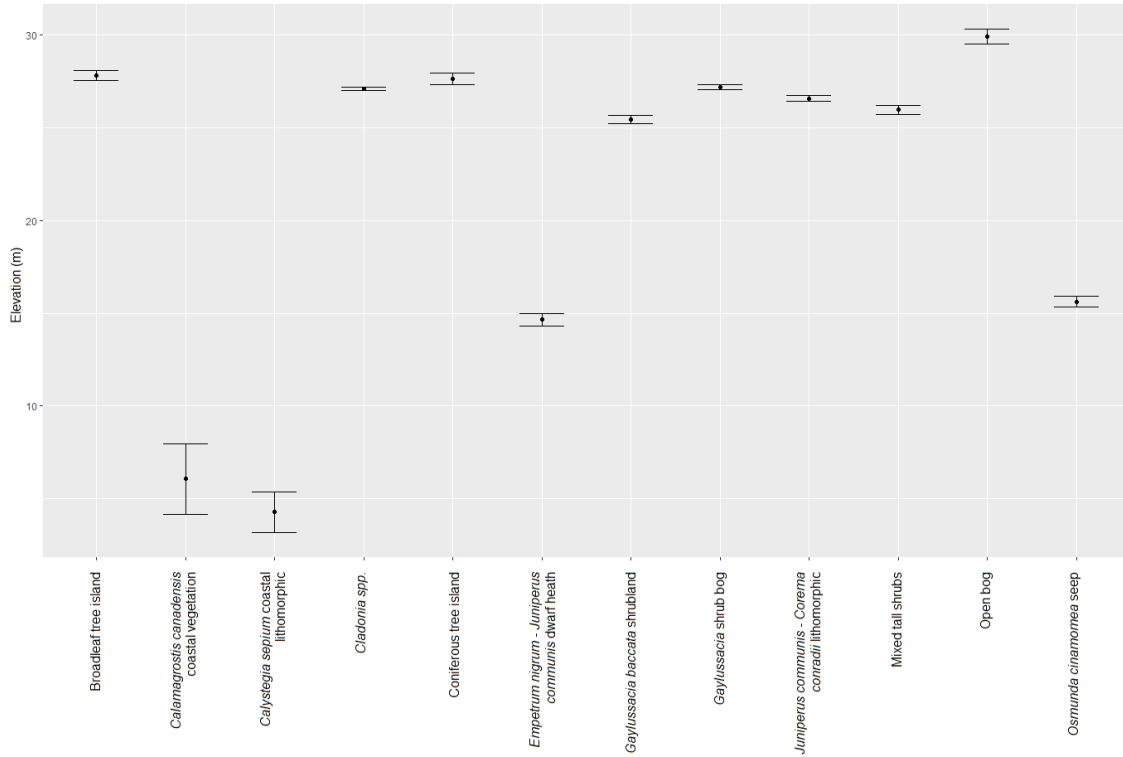


Figure A2.10. 95% confidence intervals for the area-weighted mean distance from the coastline for plant communities at Chebucto Head.

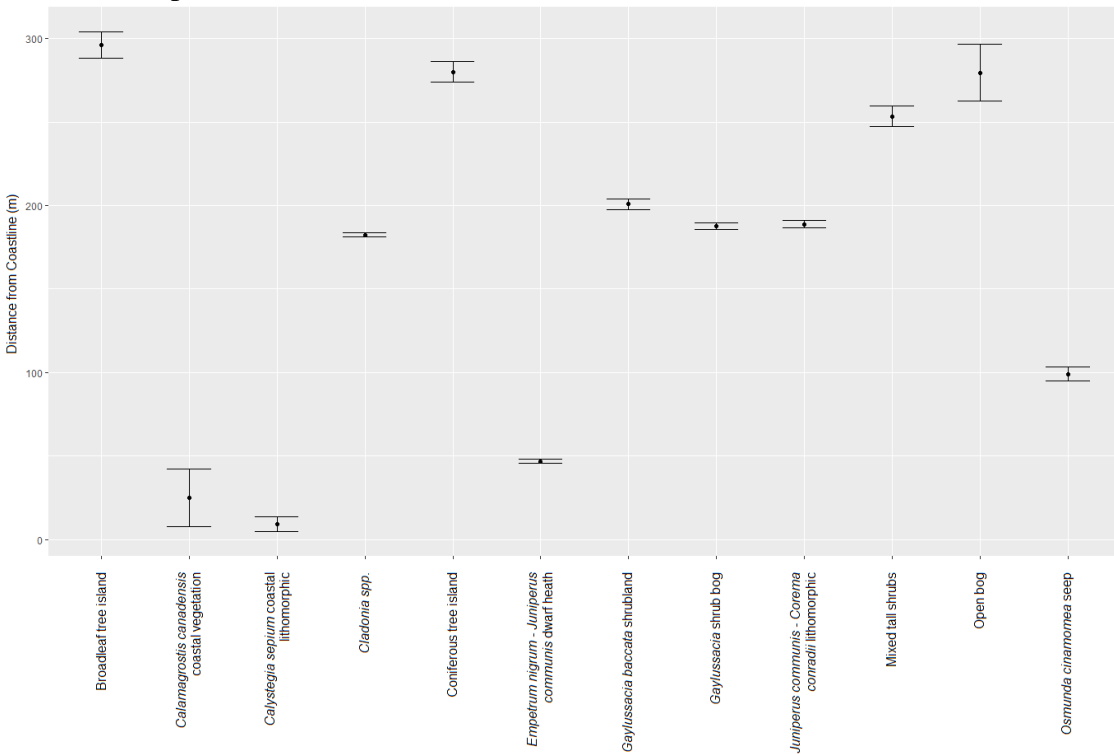


Figure A2.11. 95% confidence intervals for the area-weighted mean wind exposure of plant communities at Chebucto Head.

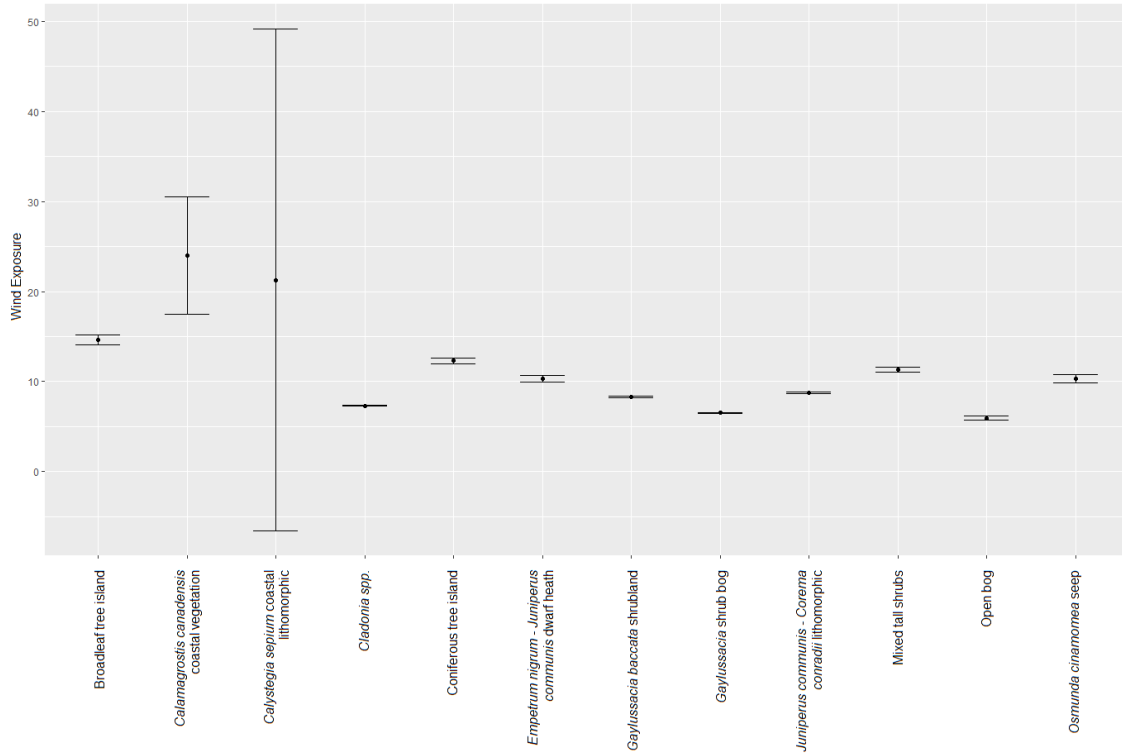


Figure A2.12. Most frequent (area-weighted) stream order for plant communities at Chebucto Head.

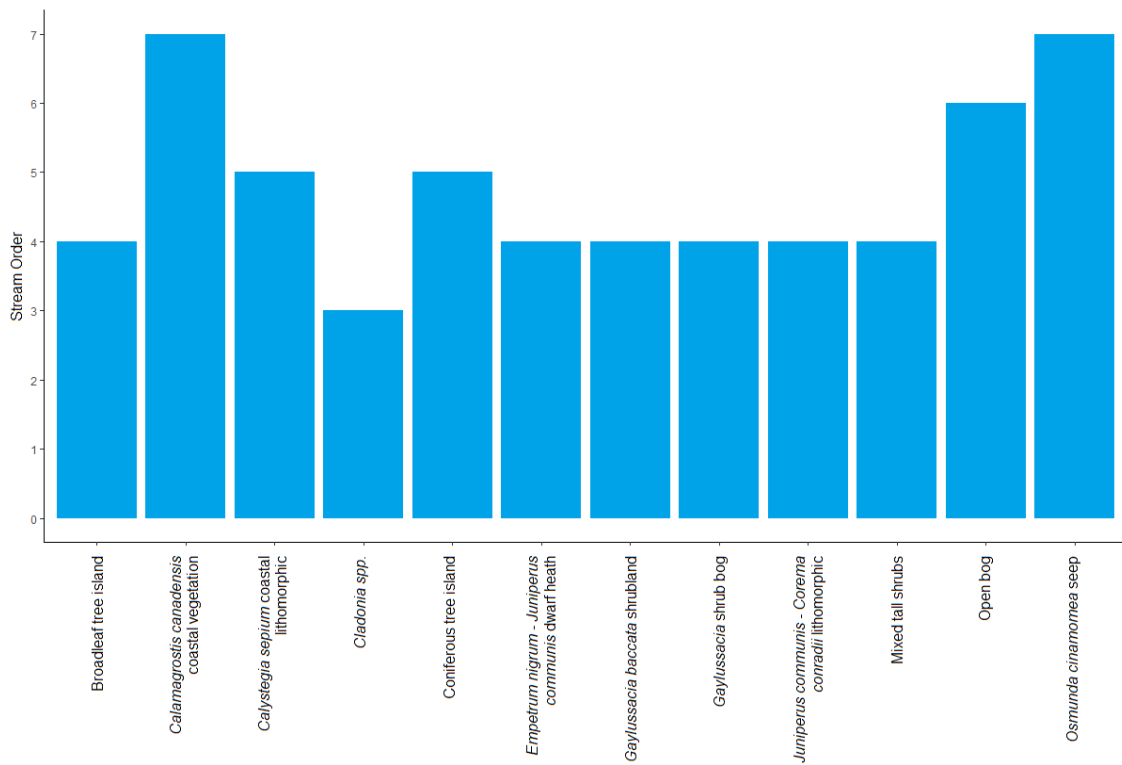


Figure A2.13. 95% confidence intervals for the area-weighted mean incoming solar radiation received by plant communities at Chebucto Head.

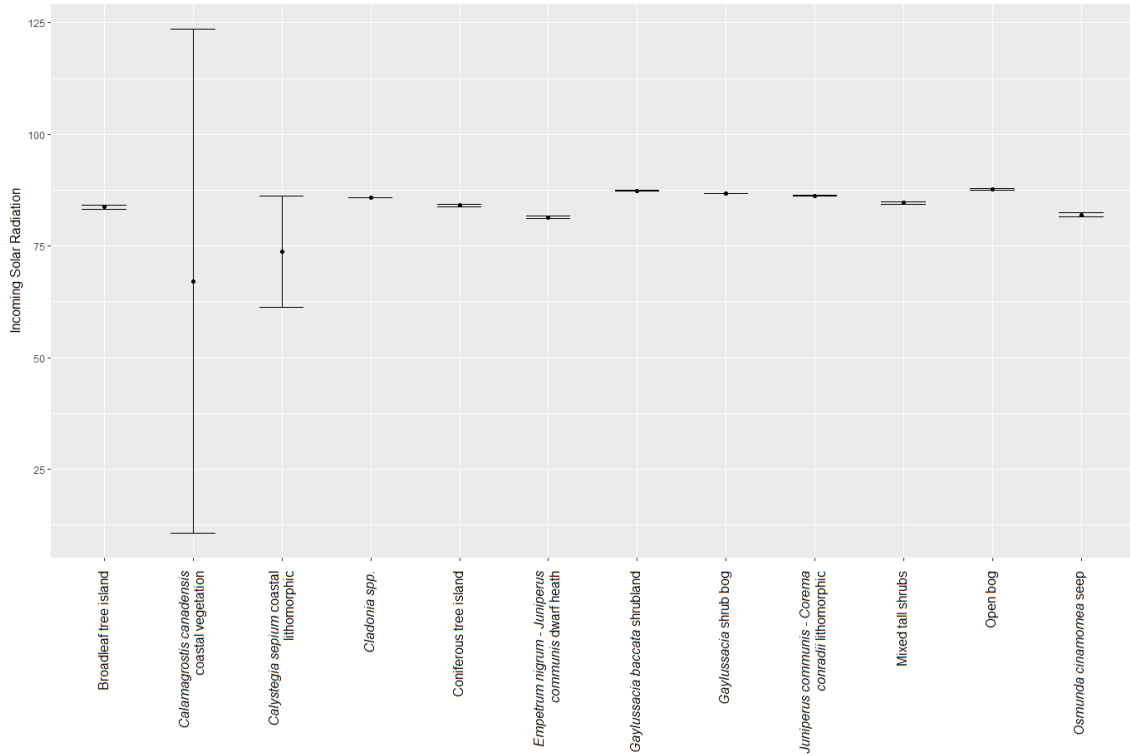


Figure A2.14. Most frequent (area-weighted) slope position classifications for plant communities at Chebucto Head.

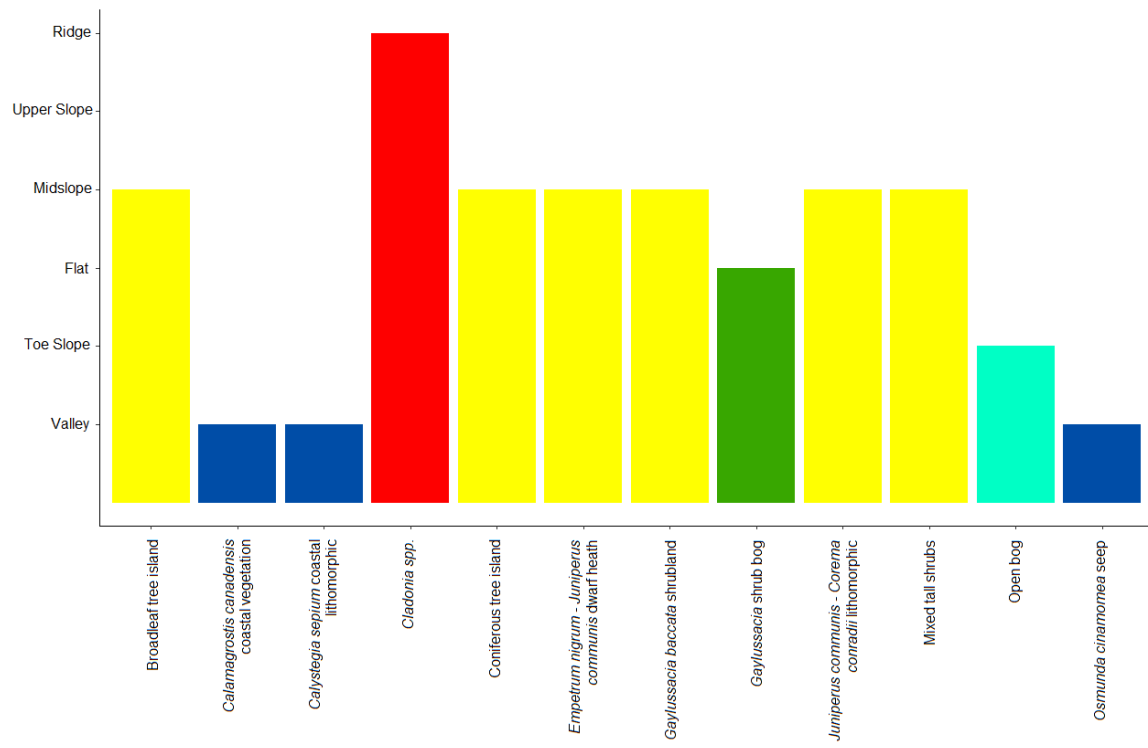


Figure A2.15. 95% confidence intervals for the area-weighted mean local surface ruggedness of plant communities at Chebucto Head.

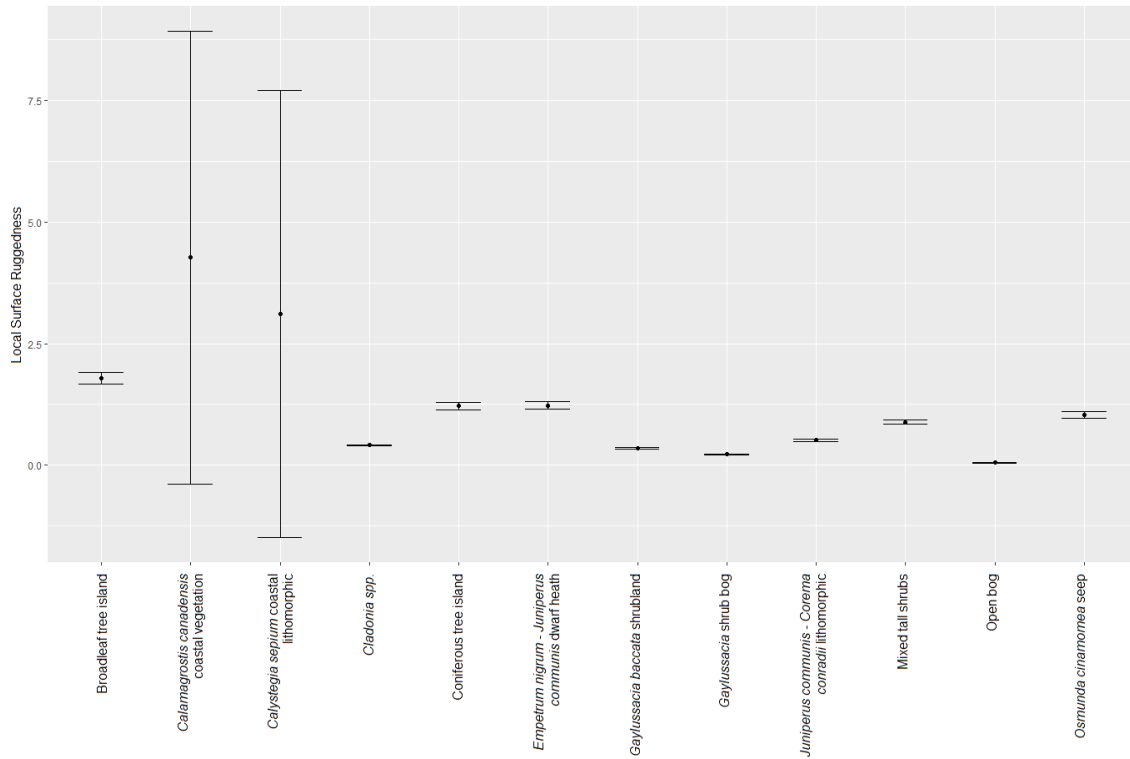


Figure A2.16. 95% confidence intervals for the area-weighted mean global surface ruggedness of plant communities at Chebucto Head.

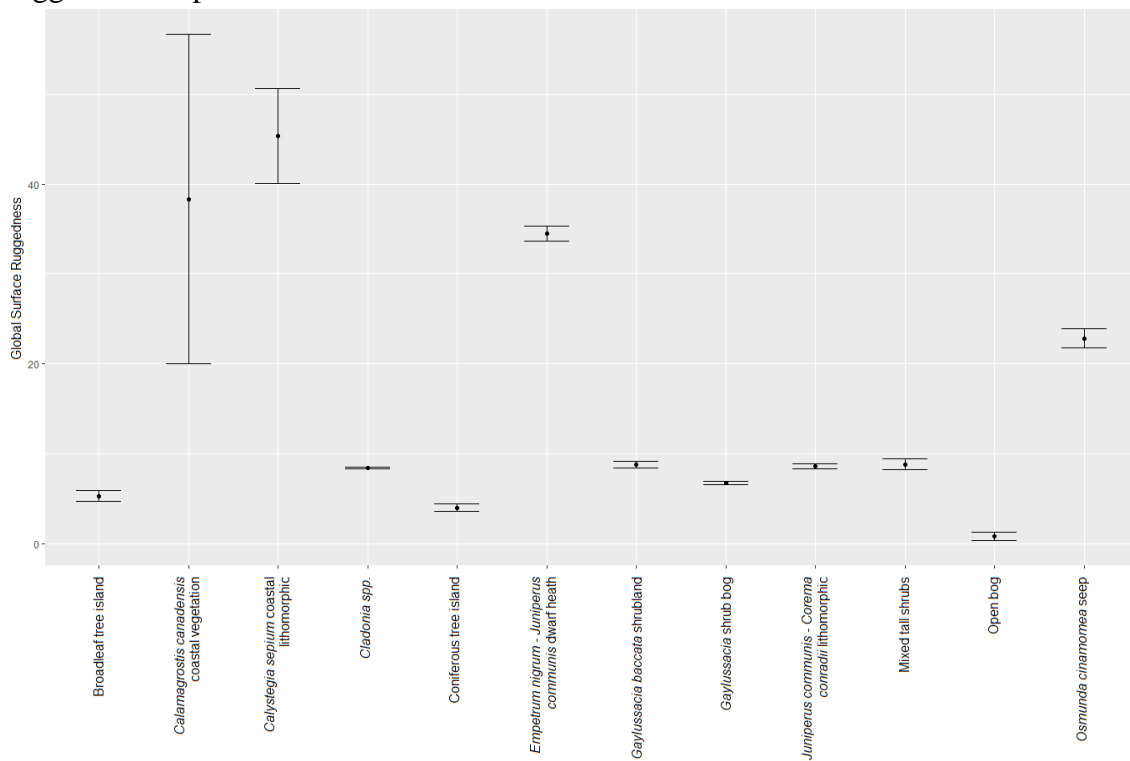


Figure A2.17. 95% confidence intervals for the area-weighted mean elevation of plant communities at Prospect Bay.

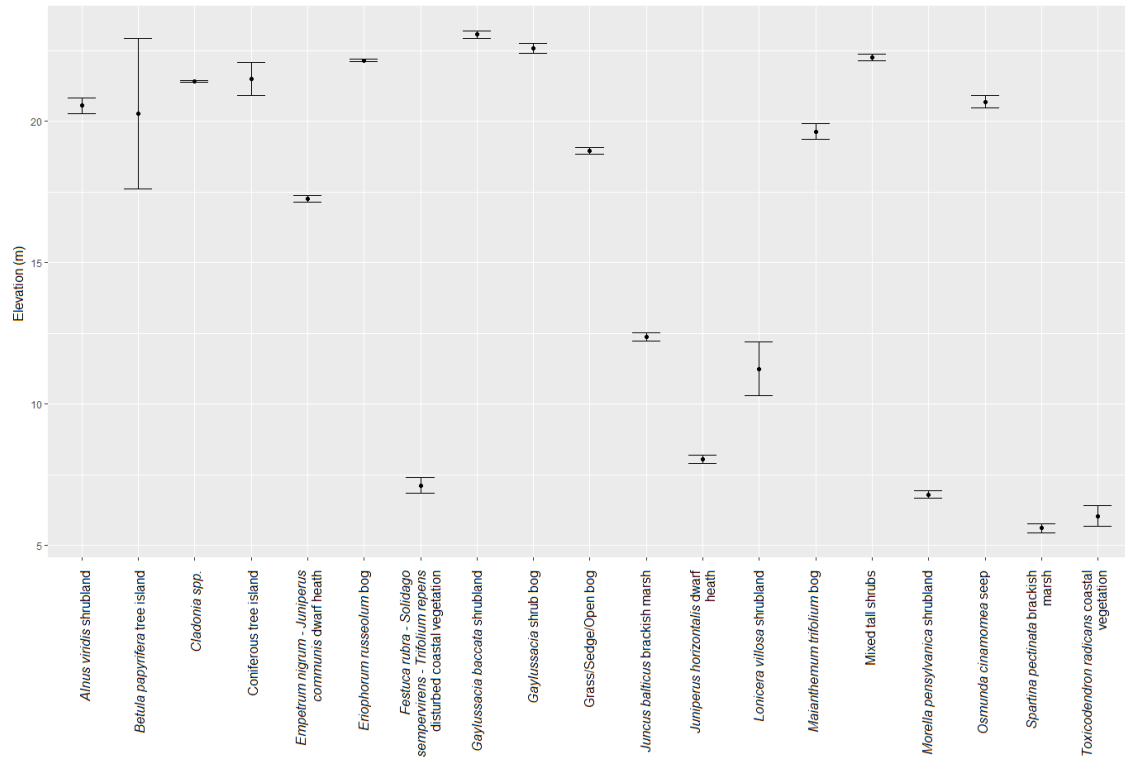


Figure A2.18. 95% confidence intervals for the area-weighted mean distance from the coastline for plant communities at Prospect Bay.

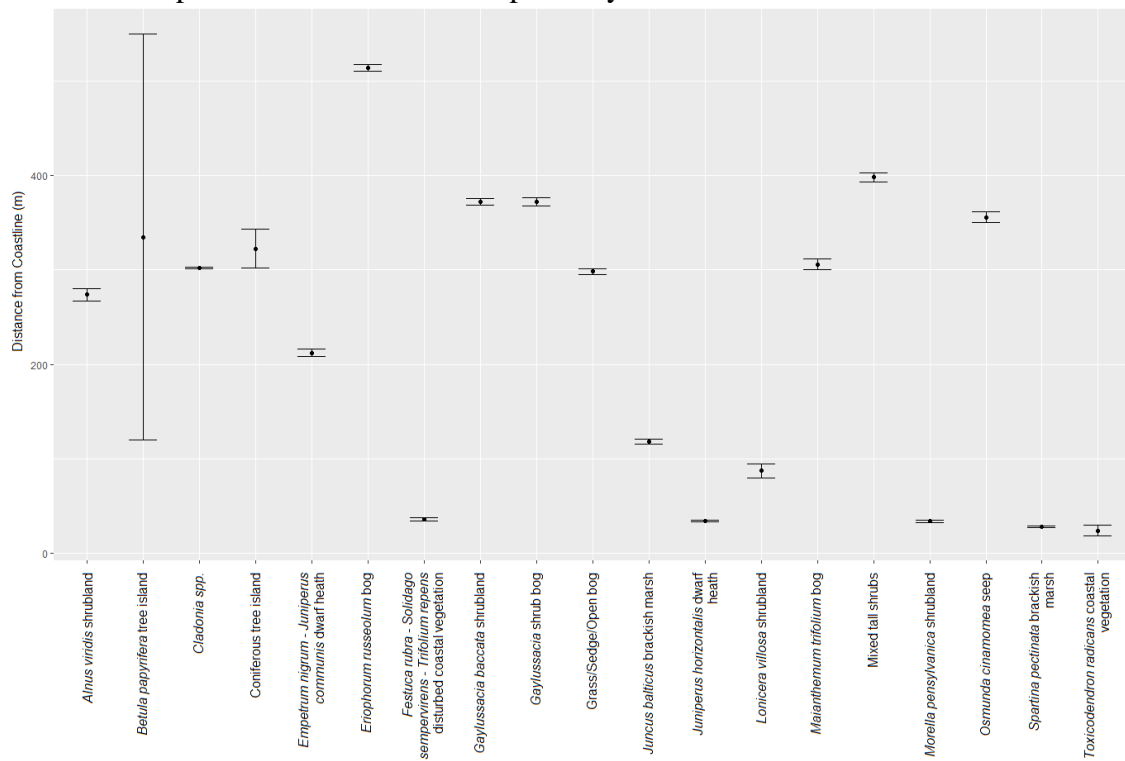


Figure A2.19. 95% confidence intervals for area-weighted the mean wind exposure of plant communities at Prospect Bay.

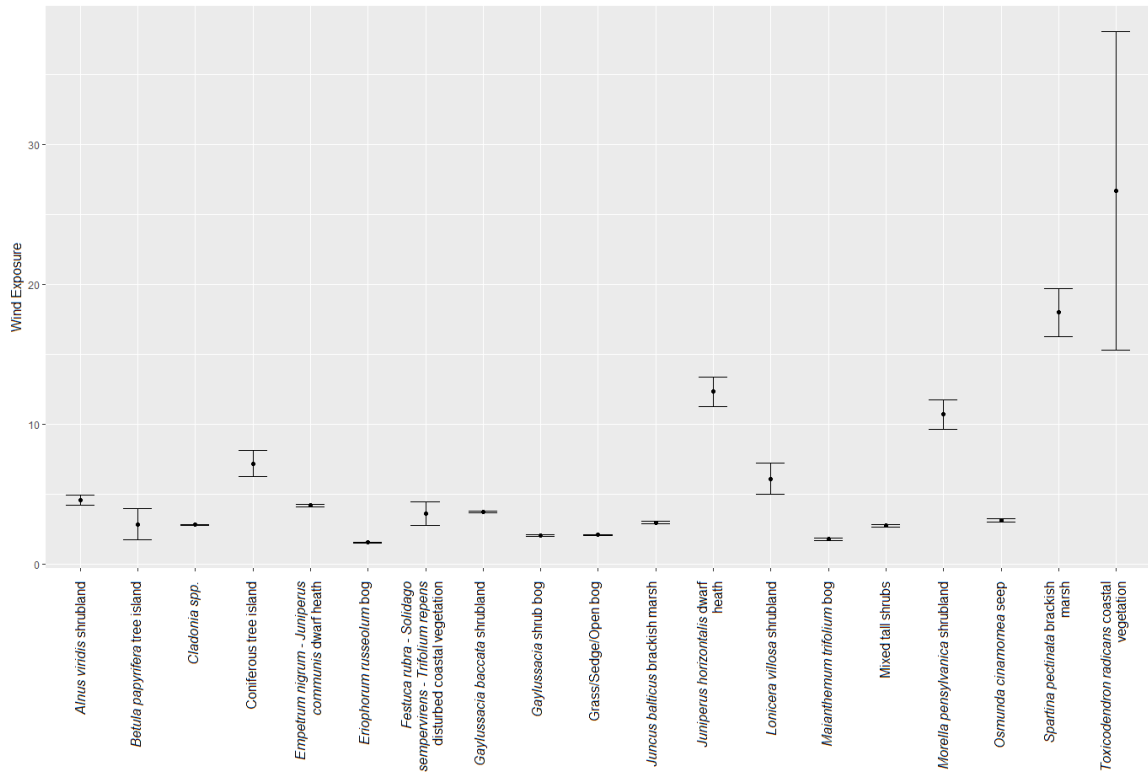


Figure A2.20. Most frequent (area-weighted) stream order for plant communities at Prospect Bay.

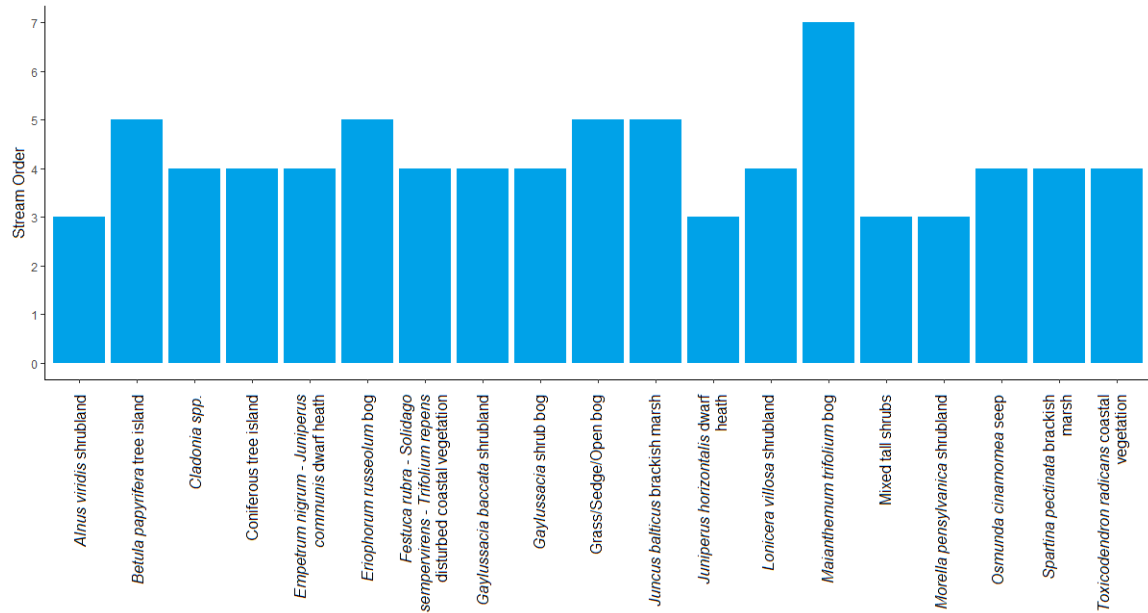




Figure A2.21. 95% confidence intervals for the area-weighted mean incoming solar radiation received by plant communities at Prospect Bay.

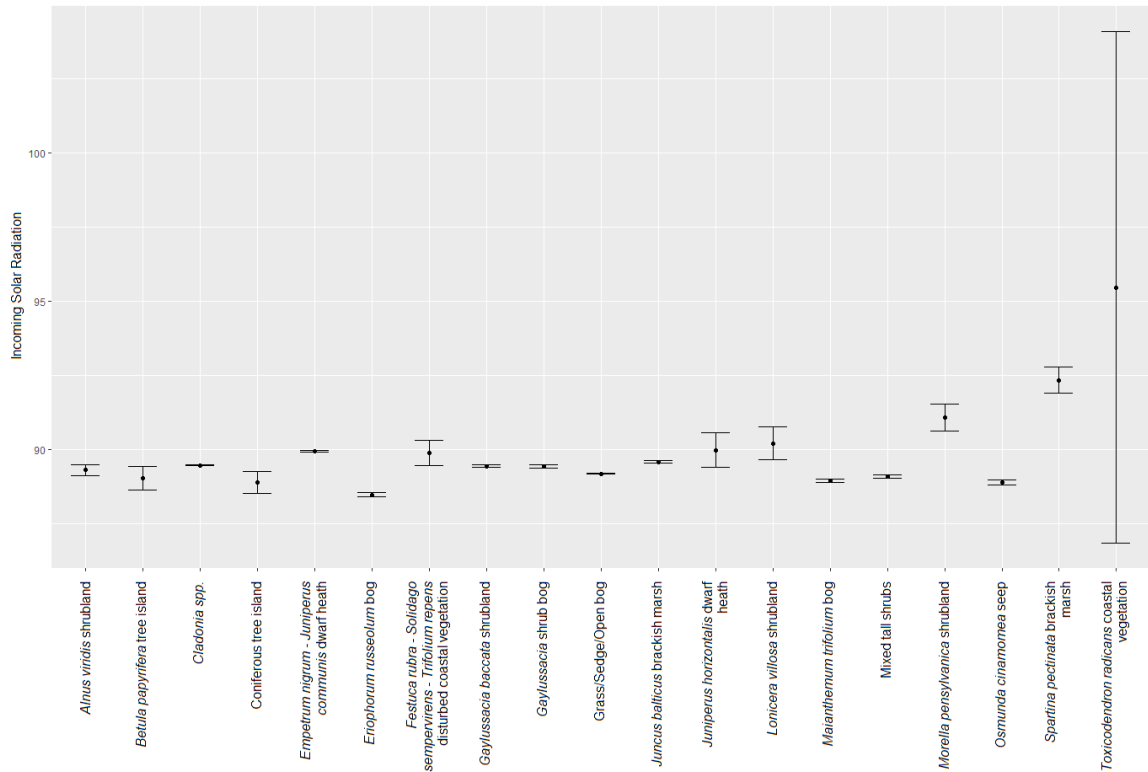


Figure A2.22. Most frequent (area-weighted) slope position classifications for plant communities at Prospect Bay.

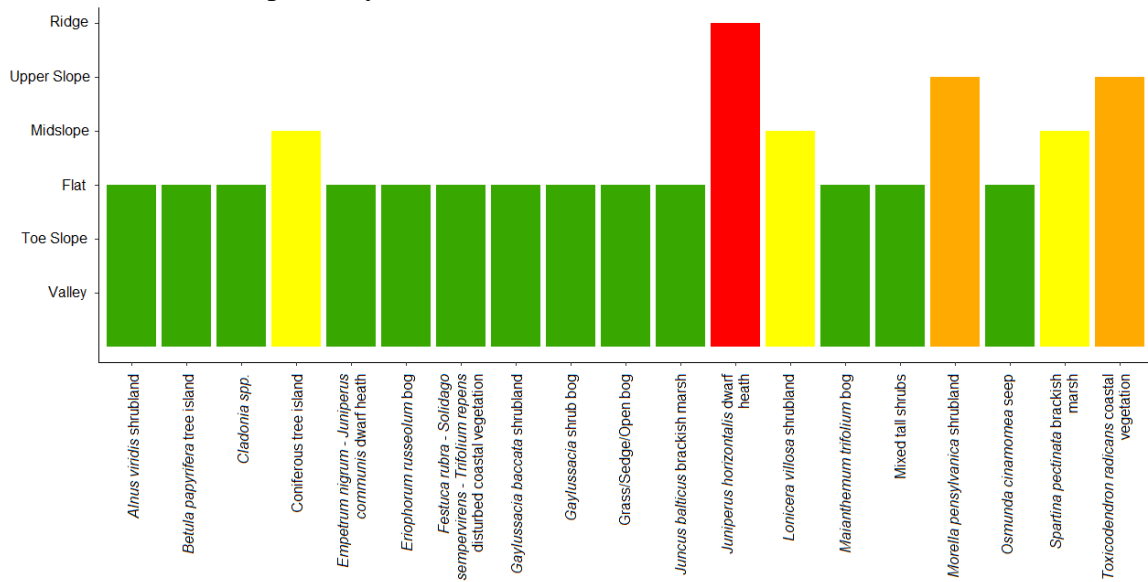


Figure A2.23. 95% confidence intervals for the area-weighted mean local surface ruggedness of plant communities at Prospect Bay.

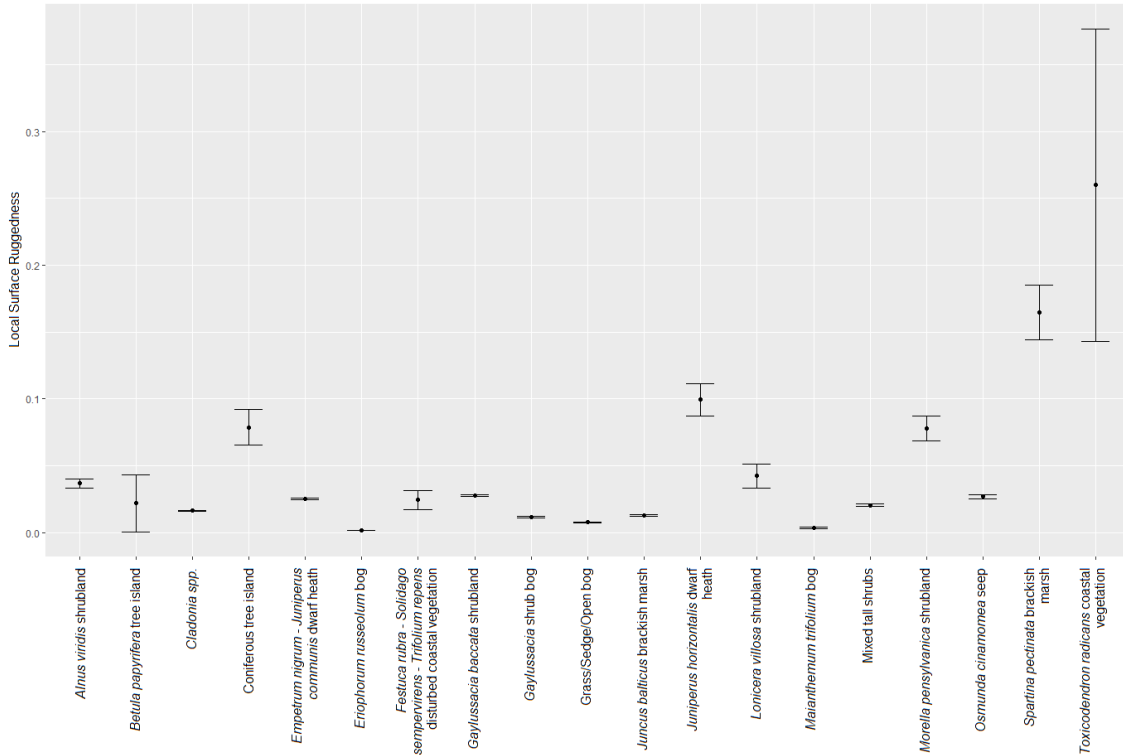


Figure A2.24. 95% confidence intervals for the area-weighted mean global surface ruggedness of plant communities at Prospect Bay.

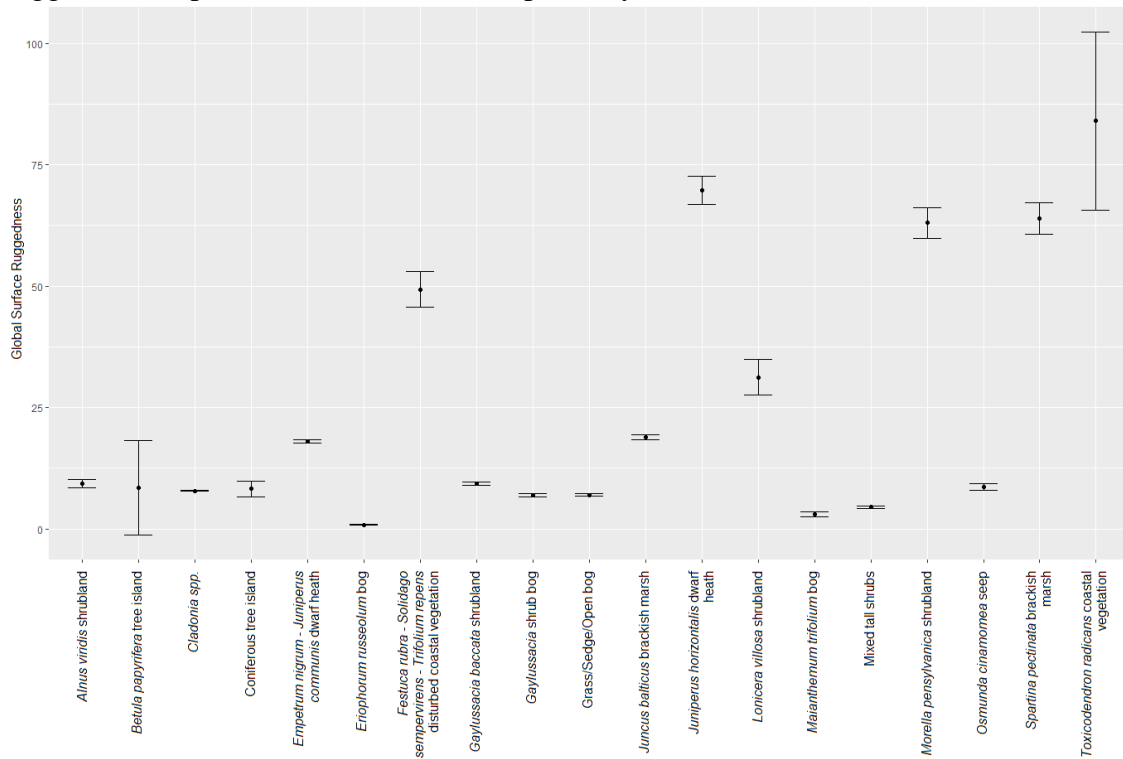


Figure A2.25. 95% confidence intervals for the area-weighted mean elevation of plant communities at Polly's Cove.

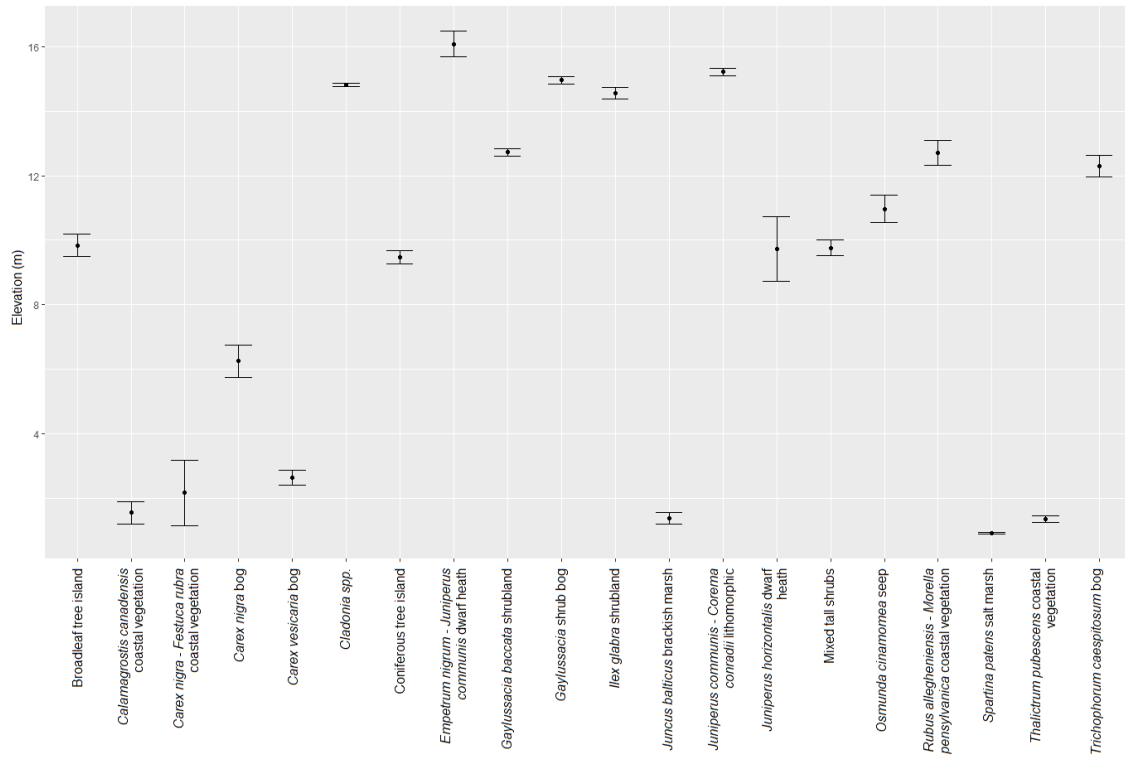


Figure A2.26. 95% confidence intervals for the area-weighted mean distance from the coastline for plant communities at Polly's Cove.

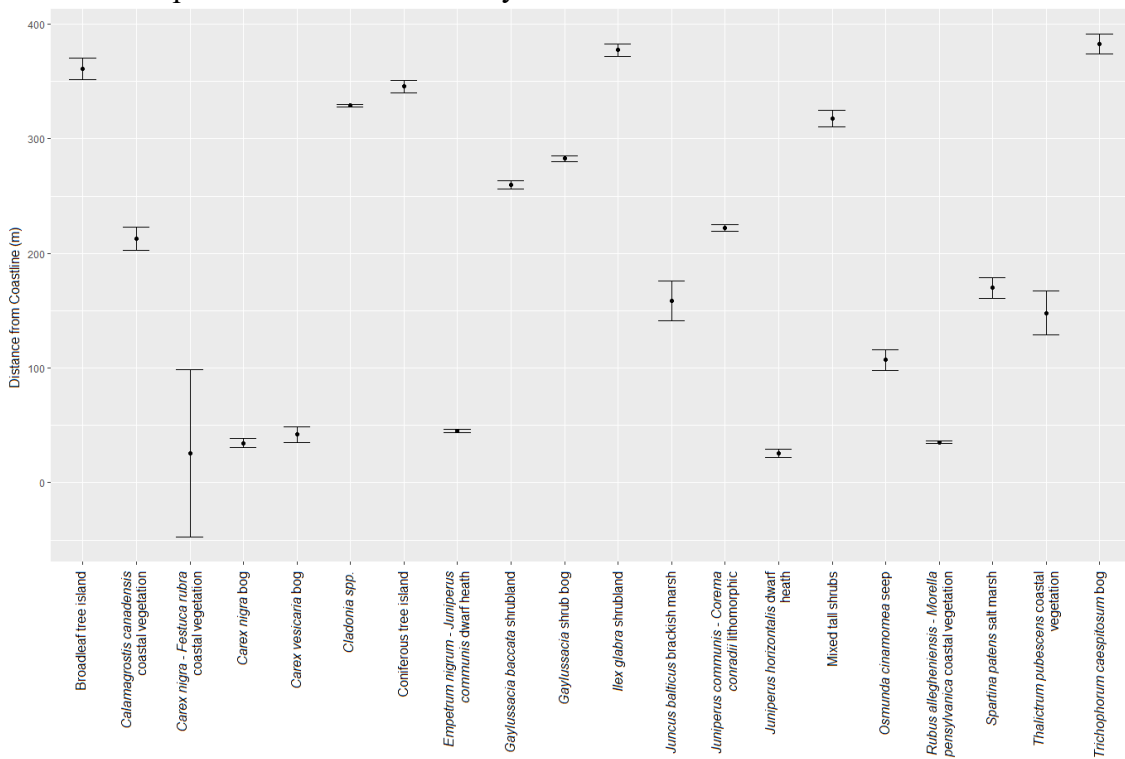


Figure A2.27. 95% confidence intervals for the area-weighted mean wind exposure of plant communities at Polly's Cove.

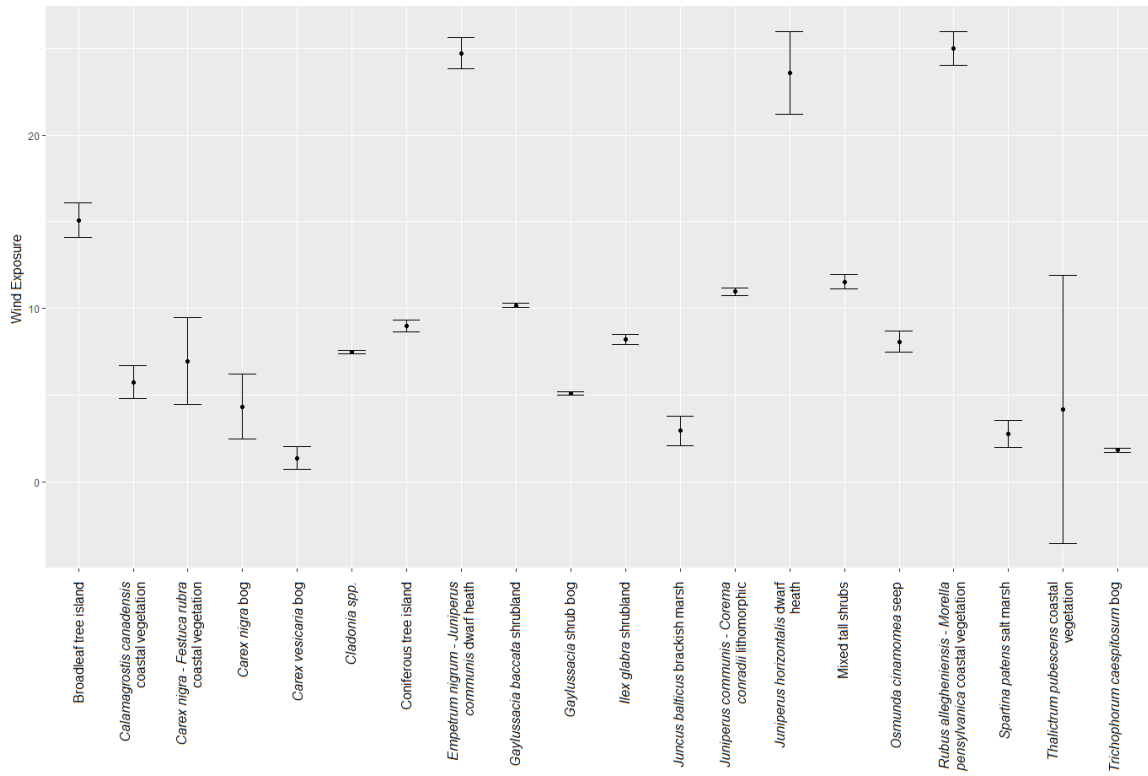


Figure A2.28. Most frequent (area-weighted) stream order for plant communities at Polly's Cove.

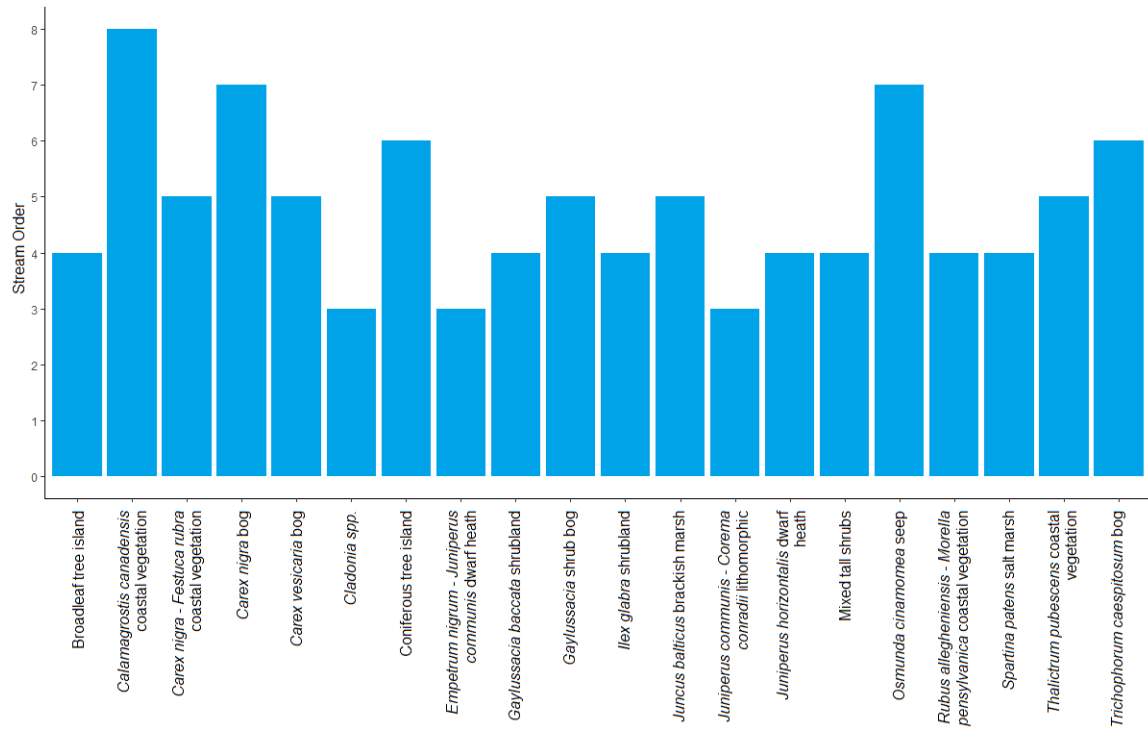


Figure A2.29. 95% confidence intervals for the area-weighted mean incoming solar radiation received by plant communities at Polly's Cove.

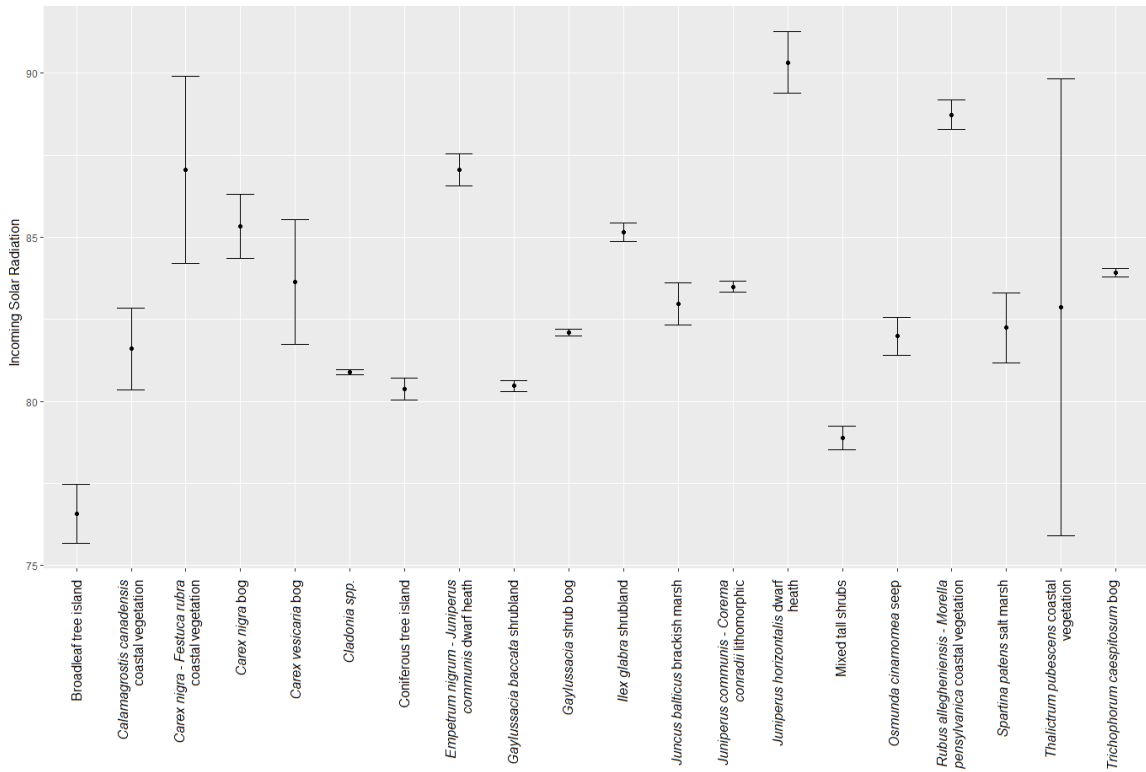


Figure A2.30. Most frequent (area-weighted) slope position classifications for plant communities at Polly's Cove.

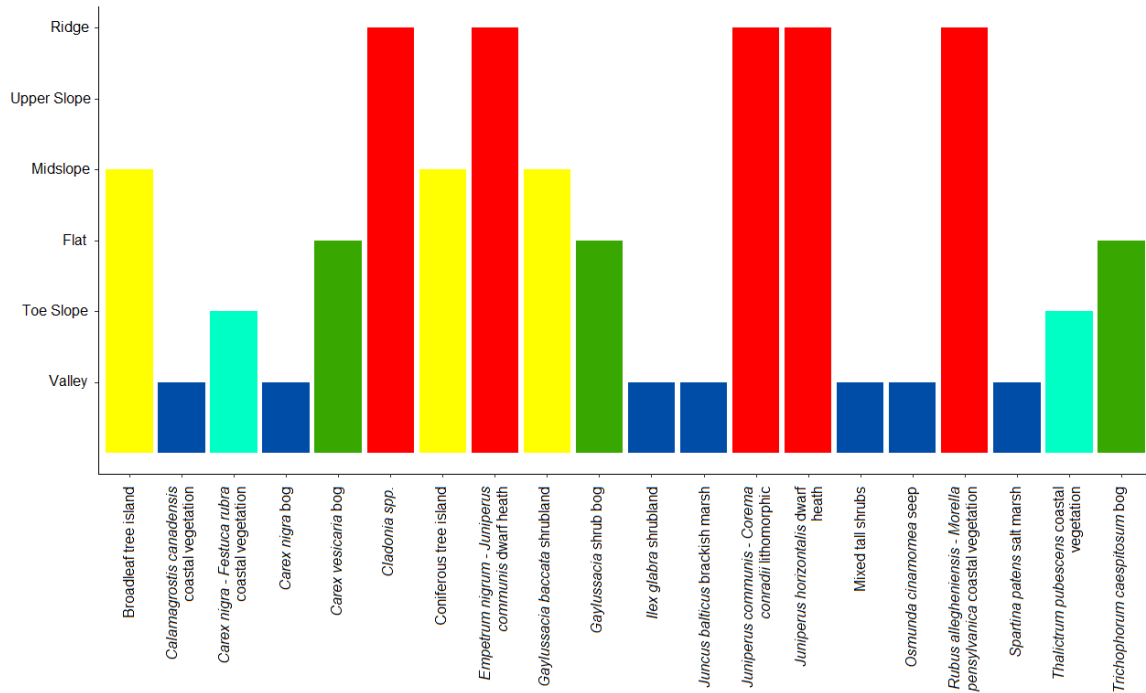


Figure A2.31. 95% confidence intervals for the area-weighted mean local surface ruggedness of plant communities at Polly's Cove.

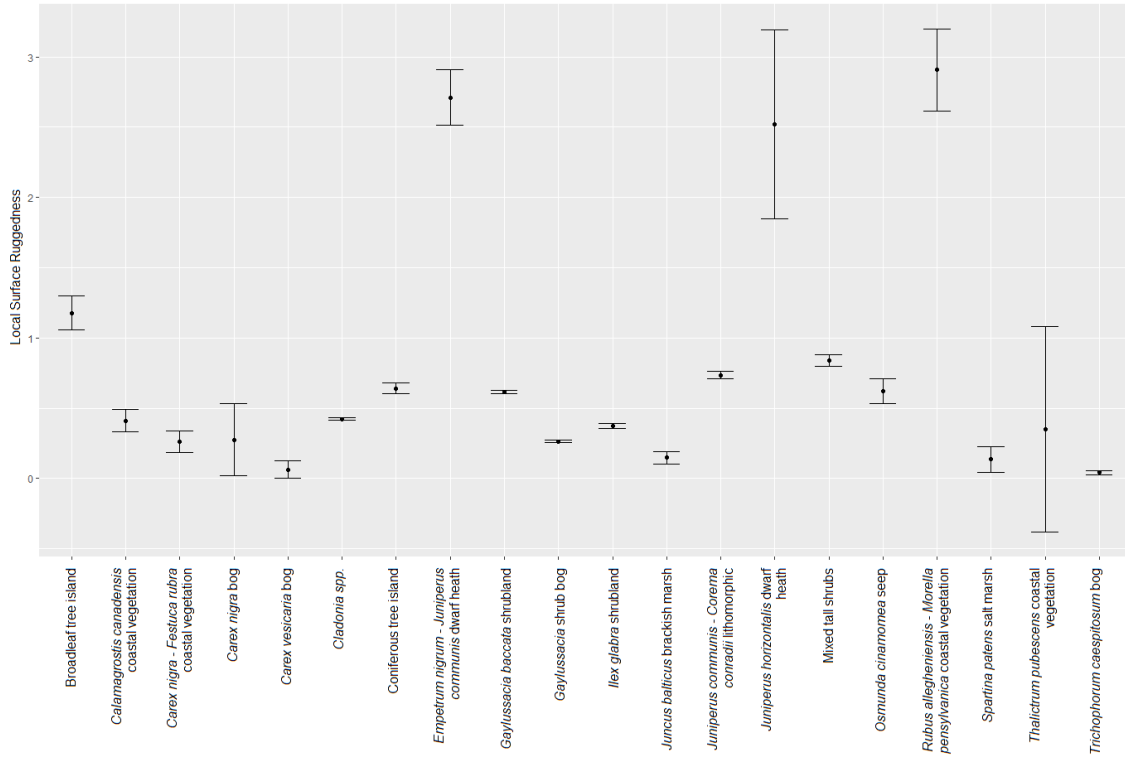


Figure A2.32. 95% confidence intervals for the area-weighted mean global surface ruggedness of plant communities at Polly's Cove.

